The Evolution of Star Clusters in Tidal Fields

THE SCALE SIZE AND DYNAMICAL EVOLUTION OF STAR CLUSTERS IN TIDAL FIELDS

By

JEREMY J. WEBB, M.Sc.

A Thesis
Submitted to the School of Graduate Studies
in Partial Fulfillment of the Requirements
for the Degree of

Doctor of Philosophy

McMaster University

DOCTOR OF PHILOSOPHY (2015)	McMaster University
(Physics and Astronomy)	Hamilton, Ontario

TITLE: The Scale Size and Evolution of Star Clusters in Tidal Fields

AUTHOR: Jeremy J. Webb, M.Sc. (McMaster University)

SUPERVISORS: Professor William E. Harris and Professor Alison Sills

NUMBER OF PAGES: xxi, 231

Abstract

Globular clusters are found in the halos of all types of galaxies, and have been shown to play major roles in the formation of stars and galaxies. The purpose of this thesis is to advance our level of understanding of the dynamical evolution of globular clusters through N-body simulations of clusters with a range of circular, eccentric, and inclined orbits. Theoretical studies have historically assumed that globular clusters experience a static tidal field, however the orbits of globular clusters are all non-circular and the tidal field of most galaxies is not symmetric. Understanding how clusters evolve in realistic potentials allows for them to be used to constrain the formation, merger history, and evolution of a host galaxy and even map out the current size, shape, and strength of a galaxy's gravitational field.

We find that dense and compact clusters evolve as if they are in isolation, despite being subject to a non-static tidal field. For larger clusters, tidal shocks and heating inject energy into the cluster and significantly alter its evolution compared to previous studies. We describe how a non-static field alters the mass loss rate and relaxation time of a cluster, and propose methods for calculating a cluster's size and orbit.

We then apply our work to clusters in the giant galaxies M87, NGC 1399, and NGC 5128. We consider each cluster population to be a collection of metal poor and metal rich clusters and generate models with a range of orbital distributions. From our models we constrain the orbital anisotropy profile of each galaxy, place constraints on their formation and merger histories, and explore the effects of nearby galaxies on cluster evolution.

By advancing studies of globular cluster evolution to include the effects of a non-static tidal field, we have made an important step towards accurately modelling globular clusters from birth to dissolution. Our work opens the door for globular clusters to be used as tools to study galaxy formation, evolution, and structure. Future studies will explore how galaxy formation and growth via the hierarchical merger of smaller galaxies will affect cluster evolution.

Co-Authorship

Chapters 2-6 are original papers written by myself, Jeremy Webb, and have been re-formatted to conform to the specifications of the McMaster thesis style.

Chapter 2 was published in *The Astrophysical Journal*, with reference Webb, Jeremy J.; Harris, William E.; Sills, Alison; Hurley, Jarrod R., Volume 764, Issue 2, pages 124-136, Bib. Code: 2013ApJ...764..124W, DOI: 10.1088/0004-637X/764/2/124. Chapter 3 was published in *Monthly Notices of the Royal Astronomical Society*, with reference Webb, Jeremy J.; Leigh, Nathan; Sills, Alison; Harris, William E.; Hurley, Jarrod R., Volume 442, Issue 2, pages 1569-1577, Bib. Code: 2014MNRAS.442.1569W, DOI: 10.1093/mnras/stu961. Chapter 4 was published in *Monthly Notices of the Royal Astronomical Society*, with reference Webb, Jeremy J.; Sills, Alison; Harris, William E.; Hurley, Jarrod R., Volume 442, Issue 2, pages 1569-1577, Bib. Code: 2014MNRAS.442.1569W, DOI: 10.1093/mnras/stu961. Chapter 5 was published in *The Astrophysical Journal*, with reference Webb, Jeremy J.; Sills, Alison; Harris, William E., Volume 779, Issue 2, pages 94-103, Bib. Code: 2013ApJ...779...94W, DOI: 0.1088/0004-637X/779/2/94. Chapter 6 has been recently submitted to *Monthly Notices of the Royal Astronomical Society*, and is currently under the review process. It will have co-authors Alison Sills, William E. Harris, Matías Gómez, Thomas H. Puzia, Maurizio Paolillo, and Kristin A. Woodley.

Chapter 1 (Introduction) and Chapter 7 (Summary) are also my original work, with the exception of Figures 1 and 2 which have been cited.

Acknowledgements

Arguably the hardest part of writing both a Master's and PhD thesis is writing two sets of acknowledgements. First time through I did my best to thank everyone who played a role in helping me not just get a Master's Degree, but get through public school, undergrad, and life. So can I simply say ditto for the PhD and be done with it? Do I just focus on the four year gap between the two degrees? A person could go mad trying to sort through all the possibilities.

Chances are if you read the Master's acknowledgement section and are also reading this, then you are most definitely somebody to whom I owe my gratitude. Despite there being just one name on the front of this thesis, and the degree for that matter, there are a whole lot of co-authors without which none of this would be possible. I am going to take a cue from one of my supervisors and thank Megan first, as opposed to last. You have been there every step of the way, helped me through so many different things in so many different ways. I couldn't imagine doing any of this alone. Frankly I do not think I would have made it. And without you, I may not have even wanted to. You inspire me, surprise me, push me, and when I need it take care of me. I owe you one. Just one though. Let's face it, I read a lot of flash cards!

Of course, a PhD is not really possible without one or more supervisors. And not just any supervisors. You need people who have the amazing ability to be administrators, teachers, and mentors all at the same time. People who know to push when you need to be pushed and when to sit back when you are ready to go it alone. I am truly grateful to have Alison Sills and Bill Harris as such people. You have been the best two supervisors, colleagues, and friends a student could ask for. And thanks to my committee member James Wadsley, for his helpful suggestions and comments throughout my PhD. I would also like to express my thanks to all of my collaborators who helped make this work possible. Especially Jarrod Hurley, Matias Gomez, and Thomas Puzia who all welcomed me for extended research visits and have contributed to much of the work within this thesis. An acknowledgement to Nathan Leigh is purposefully absent. And a big thanks to everyone that is part of the McMaster Physics Department for making the last 6 years an extremely enjoyable experience. Except you Rory, except you. You made it worse.

You can't just breeze through graduate school without a little help from your friends and family. Because as those of you who are reading this can likely attest to, its not easy being acquainted with a graduate student. We travel randomly, keep weird hours, and can go from being completely flexible to out of communication at the drop of hat. And no matter if you are a Webb, MacIver, Vercaigne, Darrach, Owen, MacDonald, a boyo/lady from one the Barrie, Everett, Guelph or Waterloo branches, or one of my 3/4 legged study buddies, you experienced all of this first hand. And not only have you put up with it, you have helped me out so much along the way and helped me stay sane throughout this whole process. In order to avoid plagiarism and repeating myself extensively, I refer the reader to my Master's thesis for further details. However I will say to Mom, Dad, Emily and Andy - thanks for being there for me every step of the way. You have all helped me out in more ways than I can count, and more times than I can count. And as someone with a few degrees in physics and astronomy, I can count pretty high. Thanks for being you guys. To Greg, Nancy, Jon, and Jamie - you have all welcomed me into your family and been very supportive and understanding along the way. I hope you know how much I appreciate everything you have done for me and Megan. I can't say thank you enough.

And while I would love to thank everybody else who is reading this individually, please cut me some slack. I just wrote a PhD thesis. I am tired. Ill buy you a beer (or some crazy pink drink) sometime and then all will be even right? I mean seriously, there is no way I can thank every last one of you for all the baked goods, whole meals of food, triple p's, summer jobs, late nights on the box, letters of reference, proof readings, boat rescues, road trips, advice, permanent roster positions, counter attacks, wallet repair and the endless get-togethers / visits. I could not convey to each of you how much I appreciate you being a sounding board or a test audience, for keeping me in the loop when I am far away (physically or mentally), and for the many, many, good times in between. Or maybe, hopefully, I just did?

And one more time just because it can never be said enough, thanks Peg. But mostly, deep down from the bottom of heart, what I really want to say to you is.... you're not the ONLY doctor meow! In your face!

Table of Contents

List of Figures

List of Tables

List of Acronyms

ACS	Advanced Camera for Surveys
CMD	Colour-magnitude diagram
FWHM	Full-width half-maximum
GC	Globular cluster
HST	Hubble Space Telescope
IMF	Initial Mass Function
IRAF	Image Reduction and Analysis Facility
MCMC	Monte Carlo Markov Chain
MF	Mass Function
MW	Milky Way
NSERC	(Canadian) Natural Sciences and Engineering Research Council
PSF	Point-spread function
SHARCNET	Shared Hierarchical Academic Research Computing Network
WFC3	Wide Field Camera 3

Chapter 1

Introduction

1.1 Globular Clusters

In our Universe, matter is found to be concentrated in large structures called galaxies. Galaxies are massive collections of stars and gas orbiting within a halo of dark matter that can be found in isolation, within small groups, or in large galaxy clusters. Galaxies form via the hierarchical merging of smaller dwarf-like galaxies and haloes, with many minor mergers initially leading to the formation of the most massive galaxies in a group. Major mergers in large galaxy clusters, where the masses of the two galaxies differ by less than a factor of 10, can lead to the formation of a massive central host galaxy (Kravtsov & Gnedin, 2005; Tonini , 2013; Li & Gnedin, 2014; Kruijssen, 2014). The final picture is then a central host galaxy that is surrounded by dwarf satellites that have yet to merge. Within each galaxy, stars are also found both in isolation and within clusters. Star clusters of all masses have been observed, ranging from lower masses of $\sim 300 M_{\odot}$ to masses greater than $\sim 10^6 M_{\odot}$. Star clusters also range in size, with lower mass clusters having limiting radii r_L (radius

Figure 1.1 The Galactic globular cluster M80 (Image Credit: F.R. Ferraro, M. Shara et al. and the Hubble Heritage Team).

at which stellar density drops to zero) on the order of 10 pc while high mass clusters can have values of r_L greater than ~ 35 pc (Binney & Tremaine, 2008). An example of a high-mass cluster (also known as a globular cluster) can be found in Figure 1.1, which is a Hubble Space Telescope (HST) image of the Milky Way globular cluster M80.

The key difference between low-mass clusters and high-mass clusters is that high-mass clusters can survive as bound clusters for longer periods of time. Lower mass clusters, typically referred to as open clusters, are known to be sites of recent star formation (within a few 100 Myr), as they are typically found in the disks of galaxies where there is plenty of gas and star formation is currently on-going. Furthermore, their metallicities reflect the current metallicity of their host galaxy and they contain high mass stars with notably short lifetimes (Binney & Tremaine, 2008). Due to their low mass and density, low-mass clusters will quickly dissolve and lose their stars to the host galaxy. Globular clusters, which are primarily found in galaxy halos where no star formation is occurring, are believed to be so old (10 - 12 Gyr) that they must form as part of the galaxy formation process (Marín-Franch et al., 2009; VandenBerg et al., 2013). Hence globular clusters have significantly lower metallicities than open clusters and are comprised of low-mass stars with long lifetimes. Similar to open clusters, globular clusters are also in the process of slowly dissolving as stars are lost to the galaxy. However their high mass and density has allowed for many globular clusters to survive until the present day, with the majority of clusters having dissolution times greater than the age of the Universe.

It is believed that the very first globular cluster ever discovered was M22, found in 1665 by Johann Abraham Ihle (Jones, 1991). In the 350 years since, we have found 157 globular clusters in the Milky Way (Harris, 1996) and countless globular clusters in distant galaxies. The giant elliptical galaxy M87 alone has over 13,000 globular clusters (McLaughlin et al., 1994; Strader et al., 2011). The discovery of globular clusters in almost all galaxies has led to them being considered one of main the building blocks of our Universe, as they represent the first structures which form during galaxy formation and the first sites of star formation. The general picture that emerges from star cluster studies is that the majority of stars ($70 - 90\%$) form in a clustered environment, with approximately 5% of stars populating bound stellar clusters (Lada & Lada, 2003). Galaxies first form via the hierarchical mergers of small galaxies, so the galaxies in which globular clusters first form are small, have low metallicities, high gas surface densities, and turbulent velocity dispersions. All of these factors result in the formation of massive globular cluster like objects. As smaller galaxies continue to merge to form a massive host galaxy, the tidal forces experienced by gas during the merger process can result in the formation of new globular clusters. Furthermore, tidal forces experienced by clusters during mergers serve to push globular cluster orbits out into the halo of the central host galaxy (Kruijssen, 2014). Over time, as these clusters evolve they slowly dissolve such that only the most massive and most dense globular clusters have survived to reach the present day. As less and less gas became available for star formation, stars could only be formed in low-mass clusters with short dissolution times. Hence only the most recently formed open clusters are observable today. The resulting stellar population within a galaxy is then made up of stars in star clusters and stars that have escaped star clusters.

Understanding how globular clusters initially form and evolve provides us with a road map linking observations of present day globular clusters and cluster populations to constrain the present day and past properties of a host galaxy. The general purpose of this thesis is to use theoretical models of globular cluster evolution to explain the observed properties of globular clusters today. Linking observable cluster parameters to the dynamical history and present day properties of host galaxies allows astronomers to use globular clusters as tools to study the Universe.

1.2 Observations of Globular Clusters

As observations of cluster populations in more and more galaxies have become available, an observational trend that has emerged is that globular cluster populations share many of the same global characteristics. Shared characteristics between cluster populations over a range of galaxies suggest that either globular clusters undergo similar formation and evolution mechanisms that are independent of the host galaxy or that galaxies undergo similar phases of formation and evolution which result in nearly identical globular cluster populations.

1.2.1 The Universal Globular Cluster Luminosity Function

The brightness or luminosity of a globular cluster is referred to as its absolute magnitude. Studies of globular clusters in the Milky Way have revealed the distribution of cluster luminosities is approximately Gaussian, centred on a absolute magnitude of -7.3 and a standard deviation of 1.3 (Figure 1.2). Studies of extragalactic cluster populations have revealed similar luminosity distributions, suggesting the globular cluster luminosity function is near-Universal (Brodie & Strader, 2006). Within stellar populations, light is considered to be a tracer of mass, with brighter stars being more massive than fainter stars. With Galactic globular clusters having a mean measured mass to light ratio of $(\frac{M}{L})_V = 2$ (McLaughlin & van der Marel, 2005), the luminosity function can be converted to a mass function centred around $\sim 10^5 M_{\odot}$. Studies have also shown that the luminosity function is the same throughout a given galaxy. A universal present day mass function immediately suggests that the portion

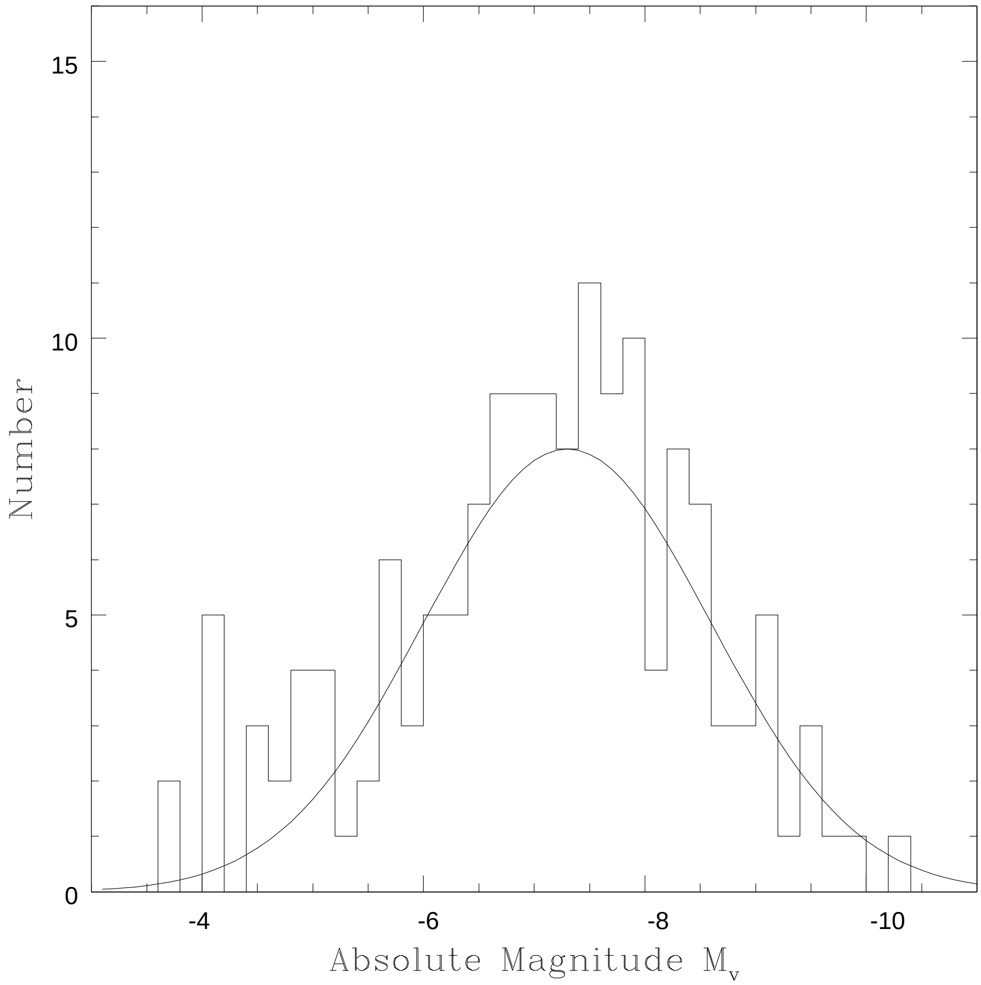

Figure 1.2 Globular cluster luminosity function for Milky Way globular clusters. The solid line is a Gaussian centered at -7.3 with a standard deviation of 1.3 (Brodie & Strader, 2006). Data taken from Harris (1996) (2010 Edition).

of the initial (or primordial) distribution of cluster masses which survives to reach the present day is also universal, and that these clusters must undergo similar evolutionary phases.

1.2.2 The Structure and Scale Size of Globular Clusters

Models of the density and surface brightness profiles of globular clusters date back to King (1962), and have continued to received attention in the over 50 years since (e.g. King , 1966; Sérsic , 1968; Wilson , 1975; Gunn & Griffin, 1979; Gebhardt & Fischer, 1995; van de Ven et al., 2006). Globular clusters can generally be modelled as a distribution of stars that gradually becomes less dense as you get farther from the centre. At a given clustercentric distance, stellar velocities follow a Maxwellian-like distribution which extends out to the escape velocity at that distance. An example of a standard King (1966) profile is illustrated in Figure1.3, and can be constrained by the core radius r_c (radius at which the stellar density drops to half the central density), effective radius r_h (also known as the half-light radius, the radius which contains half the cluster's total light) and r_L. The central density can be used in place of r_h to constrain a cluster's density profile. Differences between different cluster models are due to different choices for the cluster's distribution function and how exactly cluster density decreases to zero at r_L.

Unfortunately r_L is a very difficult quantity to measure. In the Milky Way, it is difficult to distinguish between stars that are gravitationally bound to a cluster and ones that have either recently escaped or are in the foreground/background. For extragalactic globular clusters, individual stars cannot be resolved and globular clusters appear as star like objects, as seen in Figure 1.4 of the Sombrero galaxy. The size of an extragalactic globular cluster can only be measured from its surface brightness profile which quickly transitions to background near r_L. Therefore astronomers instead use the r_h as a tracer of cluster size. Studies have shown the determination of r_h is quite

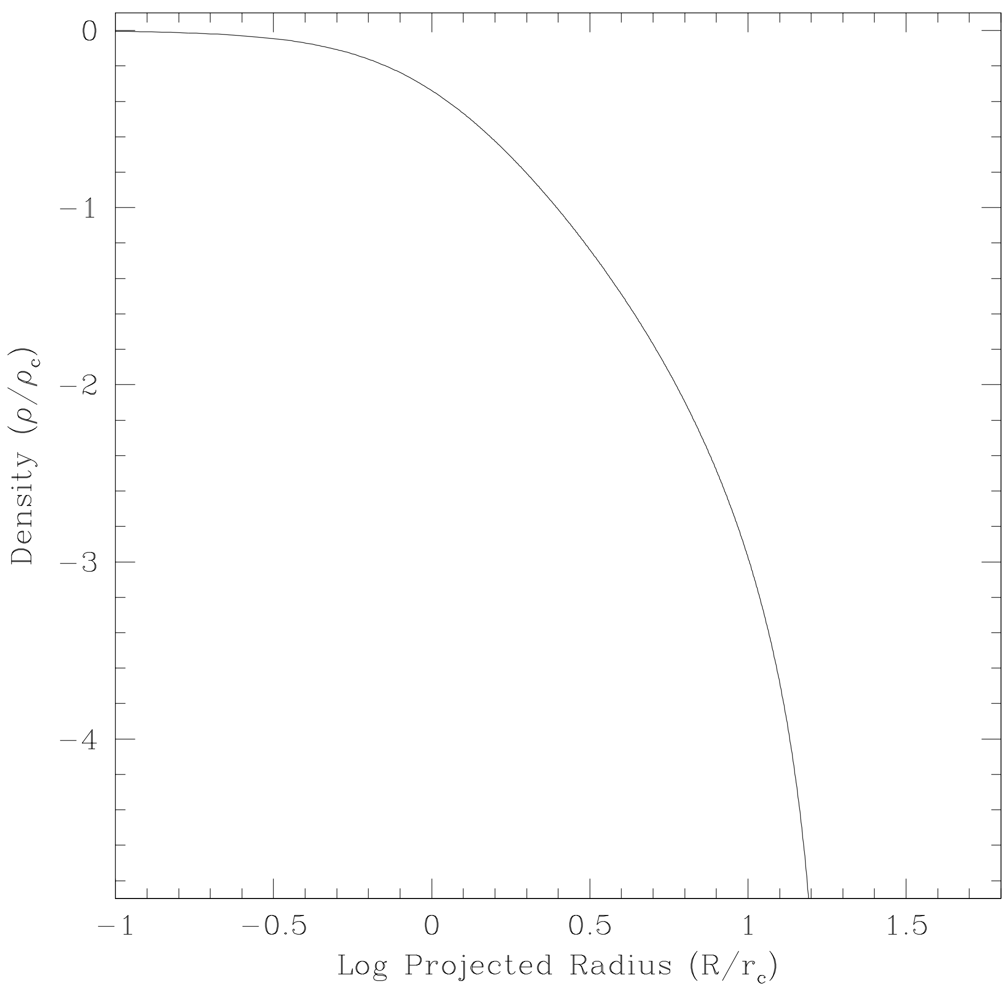

Figure 1.3 King 1966 globular cluster density profile (normalized by core density) as a function projected distance (normalized by core radius).

Figure 1.4 The Sombrero Galaxy. Almost all star-like objects in this image are actually globular clusters. (Image Credit: NASA, ESA and the Hubble Heritage Team).

robust and independent of the measurement technique used (e.g. Webb, Sills, & Harris, 2012a).

Surprisingly, like the universal globular cluster luminosity function, the distribution of cluster sizes also appears very similar between galaxies. The distribution of cluster sizes in all galaxies is centred around a mean r_h of approximately 2.5 pc, and has been illustrated for the Milky Way and the giant galaxies M87, NGC 1399, and NGC 5128 in Figure 1.5. Unlike the universal luminosity function, the distribution of globular cluster sizes does have some dependence on galactocentric distance as illustrated in Figure 1.6 again for the Milky Way, M87, NGC 1399, and NGC 5128. For comparison purposes, three dimensional galactocentric distances r_{gc} in the Milky Way have been converted to projected galactocentric distances R_{gc} assuming one is viewing the Milky Way face-on. In all cases, globular clusters near the centre

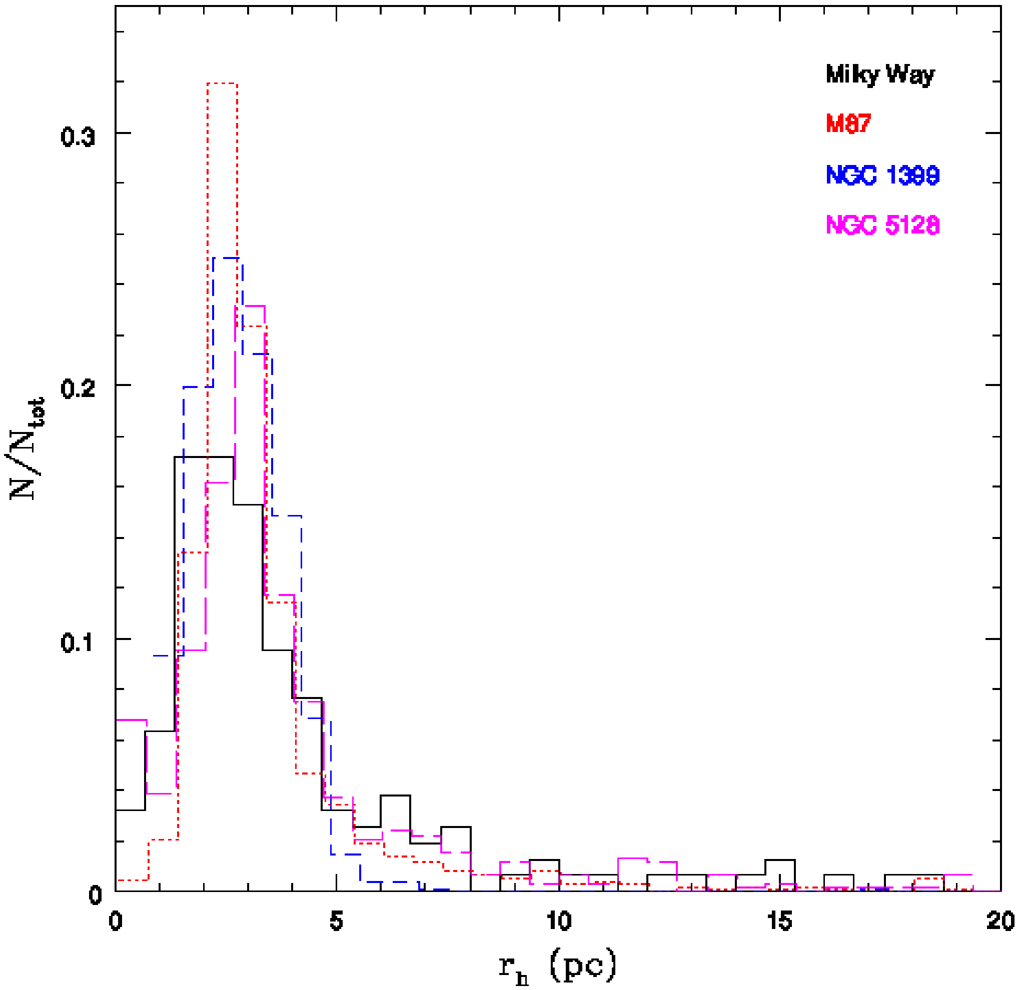

Figure 1.5 Distribution of globular cluster effective radii in the Milky Way (black), M87 (red), NGC 1399 (blue) and NGC 5128 (magenta).

of a galaxy are quite small with mean cluster size initially increasing with R_{gc}. Eventually, mean cluster size stops increasing with R_{gc} and even flattens out such that the mean r_h stays at ~ 2.5 pc. This trend is observed in almost all extragalactic cluster populations (Spitler et al., 2006; Gómez & Woodley, 2007; Harris , 2009a; Harris et al., 2010; Puzia et al., 2014).

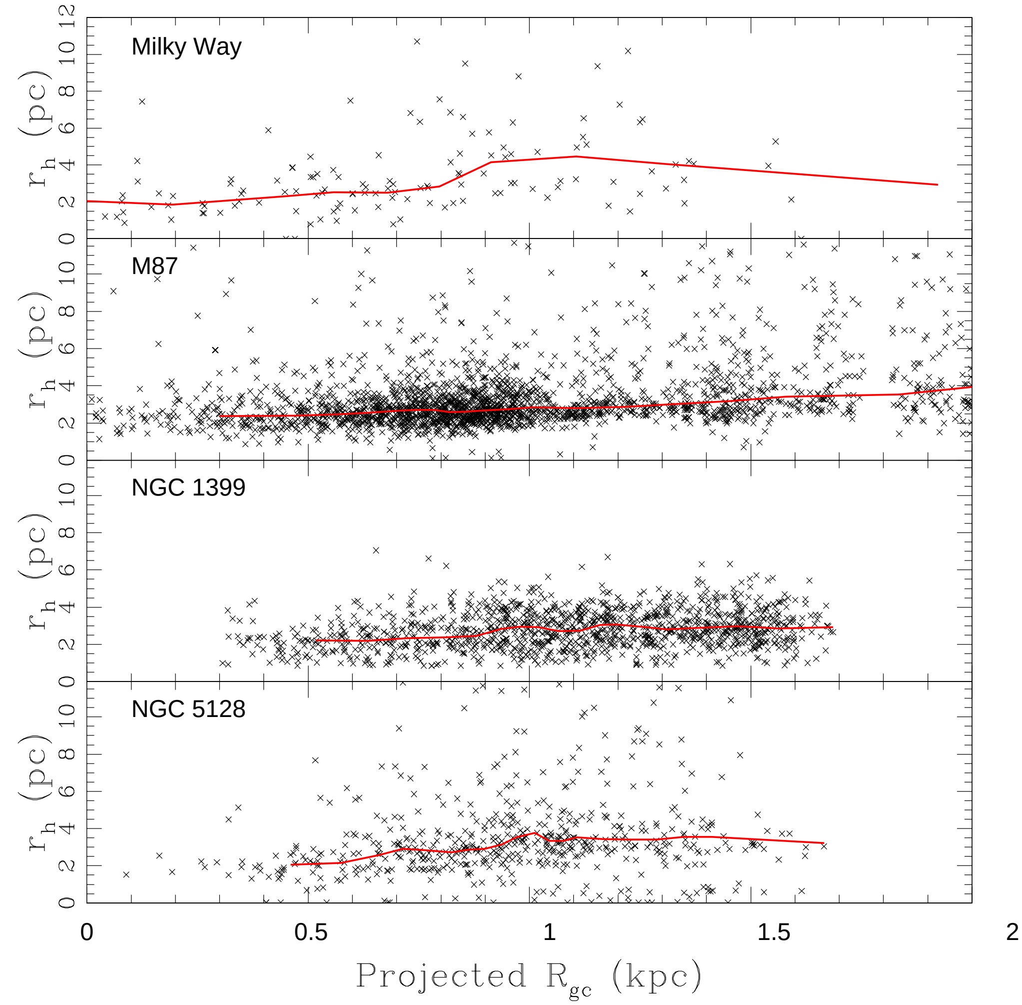

Figure 1.6 Effective radii r_h and log projected galactocentric distance LOG R_{gc} of globular clusters in the Milky Way, M87, NGC 1399 and NGC 5128. The solid lines represent the median r_h calculated with radial bins containing 5% (10% for the Milky Way) of the total cluster population each.

1.2.3 Color Bimodality in Globular Cluster Populations

Photometric studies of globular cluster populations have revealed that in almost all galaxies cluster populations are bi-modal in colour (e.g. Zepf & Ashman, 1993; Larsen et al., 2001; Harris , 2009b; Peng et al., 2006). This colour bimodality has been attributed to cluster populations consisting of metal poor and metal rich sub-populations, with metal poor clusters commonly referred to as the blue population and metal rich clusters referred to as the red population (e.g. Zepf & Ashman, 1993; Brodie & Strader, 2006). Many structural and kinematic differences have been identified between these two sub-populations that are surprisingly consistent between galaxies. Most applicable to this study is the common observation that blue globular clusters are on average 20% ($\sim$ 0.4 pc) larger than red clusters (e.g. Kundu & Whitmore, 1998; Kundu et al., 1999; Larsen et al., 2001; Jordán et al., 2005; Harris , 2009a; Harris et al., 2010; Paolillo et al., 2011; Blom et al., 2012; Strader et al., 2012; Woodley, 2012; Usher et al., 2013). While various studies have been able to show that the size difference can be attributed to different formation, dynamical and stellar evolution histories (e.g. Kundu & Whitmore, 1998; Jordán, 2004; Jordán et al., 2005; Harris , 2009a; Sippel et al., 2012; Schulman et al., 2012), the fact that the size difference is consistent between galaxies suggests cluster formation and evolution is galaxy independent.

Since the properties of the galaxies which host globular cluster populations are quite different, the fact that we observed such similar characteristics between cluster populations is surprising. These similarities suggest that we need to explore how and when the similar properties are established, as well as the subsequent role that environment plays on globular cluster evolution. We therefore turn to theoretical models of globular clusters to study the effects of environment and attempt to reproduce the observations discussed above.

1.3 Theoretical Studies of Globular Clusters

Pioneering work by von Hoerner (1957), Henon (1961), and King (1962) have helped set the stage for future studies on globular evolution. Through purely analytic techniques, these studies were able to model the evolution of a globular cluster from birth, both in isolation and in the presence of an external gravitational potential, and make strong predictions regarding the structure and kinematics of present day globular clusters. The majority of studies which focus on the dynamical evolution of globular clusters assume that the cluster has already formed and consists of a gravitationally bound population of stars with a range of initial positions, velocities, and stellar masses. At this stage globular clusters consist of almost no gas, with the exception of gas lost from stars via stellar evolution, and zero dark matter.

If we first consider a cluster in isolation, stellar evolution will be the initially dominant mechanism behind cluster evolution as the most massive stars in the cluster undergo mass loss and eventually go supernovae. After $\sim$ 100 Myr, once this early phase of mass loss is complete, energy transfer between stars via long-range two-body interactions begin altering the stellar orbits within the cluster (Henon, 1961, 1973; Spitzer, 1987; Heggie & Hut, 2003; Gieles, Heggie & Zhao, 2011). This mechanism, known as two-body relaxation, results in an overall cluster expansion as massive stars fall inwards and low mass stars are pushed to wider orbits. Some stars may even get energized to velocities greater than the escape velocity of the cluster, resulting in a decrease in total cluster mass. Given enough time, a cluster will completely dissolve via two-body relaxation. For any Milky Way-like globular cluster in isolation, dissolution time scales are much greater than the age of the Universe. Only extremely low mass ($M \sim 10^3 M_\odot$) or compact ($r_h \sim 0.5pc$) globular clusters will reach dissolution within a Hubble time.

For a cluster orbiting within the gravitational potential (tidal field) of a galaxy, the situation becomes quite a bit more complicated. The external tidal field of the host galaxy sets a boundary around a globular cluster that marks the distance where stars within a globular cluster feel a stronger acceleration toward the host galaxy than the cluster (von Hoerner, 1957). This distance is commonly referred to as the tidal radius r_t of the cluster, but is also known as the Jacobi radius or the Roche lobe of the cluster. If we simply consider a star on a circular orbit around a point-mass cluster of mass M, which in turn is orbiting around a more massive point mass galaxy (M_g) at a galactocentric distance r_{gc}, von Hoerner (1957) finds that the clustercentric distance the star must have in order to feel equal and opposite gravitational forces from the cluster and the galaxy is:

$$r_t = r_{gc}(\frac{M}{2M_g})^{1/3} \tag{1.1}$$

Equation 1.1 provides us with a first order approximation of how cluster size is related to cluster mass and the strength of the host galaxy's gravitational field. However, before a direct comparison can be made between theory and observations, a more rigorous derivation of r_t is necessary that does not constrain the gravitational potential of the host galaxy to be a point mass. Bertin & Varri (2008) consider a globular cluster on a circular orbit with radius r_{gc} and orbital frequency Ω in a galactic potential $\Phi_G(r)$. Assuming the galactic potential is spherically symmetric, r_t can be written as:

$$r_t = (\frac{GM}{\Omega^2 \upsilon})^{1/3} \tag{1.2}$$

Where Ω, κ and υ are defined as:

$$\Omega^2 = (d\Phi_G(r)/dr)_{r_{gc}}/r_{gc} \tag{1.3}$$

$$\kappa^2 = 3\Omega^2 + (d^2\Phi_G(r)/dr^2)_{r_{gc}} \tag{1.4}$$

$$\upsilon = 4 - \kappa^2/\Omega^2 \tag{1.5}$$

Equation 1.2 directly illustrates how an external tidal field primarily serves to restrict cluster sizes. However it also implies that an external tidal field will also strongly influence globular cluster dissolution times as two-body interactions only have to energize stars out to distances comparable to r_t. At a given r_{gc}, if a cluster is large enough to have stars orbiting near r_t (tidally filling) then the dissolution process will be accelerated as stars are more easily tidally stripped from the cluster. However, if a globular cluster is sufficiently small and compact, such that its size is much less than r_t (tidally underfilling), then it will evolve as if it were in complete isolation (unaffected by the surrounding galactic potential). Ultimately, the r_t of a cluster provides us with multiple theoretical predictions regarding cluster structure that can be compared to observations. Equation 1.2 predicts that:

- Within a given galaxy, cluster size should increase with r_{gc} as the tidal field weakens

- Cluster size should increase with cluster mass, as more massive clusters are able to retain stars out to larger distances

- For clusters at the same r_{gc} in different galaxies, clusters in the more massive galaxies will be smaller due to the strength of the tidal field.

1.4 Comparing Theory and Observations

With a thorough understanding of r_t, and its dependence on a cluster's location in a tidal field, the observational results from Section 1.2 can be further explored. It becomes surprising that observations of clusters in different galaxies suggest they all evolve in a similar manner, as clusters in different galaxies will all orbit within dramatically different gravitational potentials. Tidal fields will vary in both shape and strength, and should alter the sizes, dissolution timescales and orbital decay times of their respective cluster populations. All of a sudden, a universal globular cluster luminosity function, especially one that is the same at all r_{gc}, becomes difficult to explain. Galaxies with stronger tidal fields should more easily destroy low mass clusters and tidally strip high mass clusters than weaker galaxies. Even within a given galaxy, where the tidal field changes as a function of r_{gc}, the distribution of cluster masses would also be expected to change with r_t.

Even more difficult to explain is the distribution of cluster sizes, which we can directly link to tidal field strength, being the same from galaxy to galaxy. Since no correlation exists between cluster density and r_{gc}, r_h will scale with r_{gc} in the same way as r_t. Hence all cluster populations having a similar distribution in size about 2.5 pc is puzzling. Additionally, having mean cluster sizes initially increase with R_{gc} and then remain constant near

$r_h = 2.5$ pc also lacks a clear understanding. In the outskirts of a galaxy where the tidal field is weak, one may expect clusters in different galaxies to have similar ranges in size as most clusters will be tidally under-filling. Only the most extended clusters will be tidally affected. However moving towards the centre of the galaxy, where tidal field strength increases at different rates for different galaxies, the distribution of cluster sizes should also be different.

Tidal theory does however provide a possible explanation of why red and blue clusters have different mean sizes. Observational studies of globular cluster systems indicate that the blue sub-population is less centrally concentrated in the host galaxy than the red sub-population (e.g. Larsen et al., 2001; Forbes et al., 2006; Harris , 2009a,b). Given Equations 1.1 and 1.2, it is straightforward to conclude that red clusters are on average smaller than blue clusters because they will be subject to increased tidal stripping and decreased tidal radii since they orbit in a stronger tidal field. Larsen & Brodie (2003) then suggest the perceived size difference is simply due to the projection of two different spatial distributions, with blue clusters having larger r_{gc}. An observational prediction that stems from this argument is that the size difference between red and blue clusters should decrease with R_{gc}, and that the two sub-populations should have similar mean sizes when projection effects are minimized. This has been shown not to be the case by Harris (2009b), where the ratio between mean blue cluster size and mean red cluster size remains constant with R_{gc} in six different giant elliptical galaxies. Similar results were found in studies of NGC 1399 (Paolillo et al., 2011; Puzia et al., 2014), NGC 4365 (Blom et al., 2012), and M87 (Webb, Sills, & Harris, 2012b). So while these studies argue against the size difference being a result of projection, the question of why red and blue clusters in different galaxies are affected in the same way remains. As previously mentioned, differences between red and blue clusters are likely a result of differences in either their formation mechanisms and formation environments or their dynamical and stellar evolution histories. However for clusters that have expanded to the point of being affected by the surrounding tidal field, one should still expect the size difference between the two sub-populations to vary based on tidal field strength.

1.4.1 Advancing Tidal Theory

The simplest explanation for the discrepancies between observations and theory mentioned above is that all clusters must be tidally under-filling, such that they evolve effectively in isolation. This explanation in turn suggests that globular cluster populations are unaware of their surrounding tidal field. Alexander & Gieles (2013) was able to reproduce the current distribution of cluster sizes in the Milky Way by first assuming all clusters form extremely compact before expanding naturally due to two-body interactions. However, after 12 Gyr of evolution many clusters had expanded to the point of filling their tidal radius. That fact that not all clusters are under-filling is also supported by Gieles, Heggie & Zhao (2011), who finds that $\frac{1}{3}$ of the Milky Way's cluster population has expanded to the point of being tidally filling. So while a fraction of cluster populations are expected to look the same from one galaxy to the next, assuming of course they all form with similar properties, at least $\frac{1}{3}$ (if not more in galaxies with stronger tidal fields) of a globular cluster population will be tidally affected and should serve to alter the population's luminosity function and size distribution.

A second possible explanation, from Kruijssen (2014), suggests that the majority of cluster evolution occurs early during the galaxy formation stage when clusters are forming within the molecular clouds of dwarf galaxies. Since the high-pressure / high density environment of the molecular cloud subjects the cluster to impulsive shocks, clusters must quickly migrate to the halo of the galaxy in order to survive. Kruijssen (2014) suggests that this will happen naturally as galaxies undergo repeated mergers, as a merger event will help push clusters out into the halo. Once the migration is complete, the cluster will then effectively evolve in isolation as the tidal field is much weaker than its formation environment. However as previously mentioned, some clusters have had time to expand and fill their r_t with at least $\frac{1}{3}$ of the Milky Way cluster population is tidally affected.

To explore these apparent discrepancies between observations and theory further, we need to take a closer look at the definition of r_t. All derivations of Equation 1.2, including Innanen, Harris, & Webbink (1983), Jordán et al. (2005), Binney & Tremaine (2008), and Bertin & Varri (2008), make a few very important assumptions:

- The tidal field of the galaxy is spherically symmetric
- The tidal field of the galaxy is constant in time
- Globular cluster orbits are circular

All assumptions are made in order for the tidal field experienced by the cluster to be taken to be static. However there exist many situations under which this assumption breaks down, including:

- Globular cluster orbits are non-circular (Galactic clusters with solved orbits have a mean orbital eccentricity of ~ 0.6)

- The host galaxy is not spherically symmetric (e.g. elongated elliptical galaxies and spiral galaxies)

- The mass profile of the host galaxy changes as a function of time (e.g. accretion of satellites or the accretion of a globular cluster)

- Globular clusters undergo close encounters with sub-structure (e.g. giant molecular clouds, dark matter sub-halos)

If the tidal field that a cluster experiences is not static, then an analytic determination of r_t is no longer possible (Renaud et al., 2011). The main goal of this thesis is to remove these assumptions and still be able to quantify r_t for any cluster in an arbitrary tidal field. For clusters with eccentric orbits in a spherically symmetric potential, it has historically been assumed that r_t is set at the cluster's perigalactic distance R_p (King , 1962). The reasoning behind this assumption is that stars are stripped from the cluster at R_p where the tidal field experienced by the cluster is the strongest, and the cluster does not have time to significantly expand over the course of its orbit before returning to R_p again.

Secondary effects also begin to play important roles when a cluster has an eccentric orbit. For abrupt changes in the local gravitational field, such as when a cluster is undergoing a perigalactic pass or a close encounter with a molecular cloud, the cluster receives what is known as a tidal shock. When a cluster undergoes a tidal shock, individual stars within the cluster receive additional energy which in turn increases the size of their orbit. For stars already orbiting near r_t, a tidal shock can result in an episode of enhanced mass loss (Spitzer, 1958; Gnedin & Ostriker, 1997; Gieles et al., 2007; D'Onghia et al., 2010; Madrid et al., 2014). For slower changes in the local gravitational field that occur over the course of the cluster's entire orbit, this process is called tidal heating. Even though the effects of tidal heating are small compared to a tidal shock, over the course of a cluster's lifetime energy injection via tidal heating will still have a significant effect on the cluster evolution by redistributing stellar orbits and accelerating the mass loss process (Baumgardt & Makino, 2003; Renaud et al., 2011; Brockamp et al., 2014; Madrid et al., 2014).

The long term effects of tidal shocks and tidal heating need to be further explored in order to determine how the effects will be reflected in studies of globular cluster population. Furthermore, prior to the work presented in this thesis recent studies had begun finding that assuming r_t is imposed at R_p is likely incorrect. These studies instead suggest that an orbit average distance better reflects the cluster's size and evolution (e.g. Brosche, Odenkirchen, & Geffert, 1999; Baumgardt & Makino, 2003; Kupper et al., 2010). Unfortunately, a formal definition of the r_t for a cluster with an eccentric orbit is lacking. With proper motion measurements of Galactic globular clusters revealing that no clusters in our galaxy actually have a circular orbit (e.g. Dinescu et al., 1999; Casetti-Dinescu et al., 2007, 2013), and galaxy formation models suggesting that the distribution of cluster orbits will differ from galaxy to galaxy (e.g. Côté et al., 2001; Prieto & Gnedin, 2008; Zait, Hoffman, & Shlosman, 2008; Weijmans et al., 2009; Gnedin & Prieto, 2009; Ludlow et al., 2010; Kruijssen et al., 2012) it is clear that we need to develop an understanding of how orbital eccentricity affects globular cluster evolution.

In non-spherically symmetric potentials, like disk galaxies or tri-axial elliptical galaxies, even clusters with circular orbits will undergo tidal heating and tidal shocks during disk passages if their orbit is inclined relative to the non-spherically symmetric component of the galaxy. While the effects of disk shocking on individual globular clusters have been well studied (Gnedin & Ostriker, 1997; Madrid et al., 2014), a calculation of a cluster's size in a non-spherically symmetric potential does not exist. Furthermore, the long term evolution of a globular cluster population in a non-spherically symmetric tidal field has not been explored.

Finally, the effects of a time dependent potential on cluster evolution are not well understood. Since galaxies are built up via the hierarchical merger of dwarf galaxies, the early tidal field of a galaxy will be in a constant state of flux. Globular clusters which form in the central host galaxy will undergo repeated dynamical interactions as a galaxy is assembled. Furthermore, clusters which form in dwarf galaxies that are then accreted by a central host will also be subject to a variable tidal field. Previous studies attempt to replicate a time dependent tidal field by treating a merger event as a step process, where the mass of the central galaxy is increased at specific time intervals (Madrid et al., 2014) or a cluster is instantaneously moved from a dwarf galaxy potential to a more massive central host (Miholics et al., 2014). Only recently have studies begun looking at the effects of a truly time dependent tidal field on globular cluster evolution (Bianchini et al., 2015; Renaud & Gieles, 2015). Preliminary results from these studies suggest cluster structure is only dependent on the present day tidal field, however more detail simulations are required with a more accurate treatment of the tidal field's evolution. In order to better quantify and understand the effects of orbital eccentricity, inclination, and time dependent tidal fields on globular cluster evolution, specifically tidal heating and tidal shocks, we must abandon the analytic approach and turn to computational N-body simulations of star clusters.

1.4.2 *N-Body Simulations of Star Clusters*

N-body simulations are effective tools for studying problems for which an analytic approach is either difficult or not possible. In an N-body star cluster simulation, each star within the model is treated as a point particle. Each particle can be given a position, velocity, mass, and metallically generated from a distribution of the user's choosing. Hence we can set the initial conditions under which a star cluster forms. N-body codes also typically allow for binary stars to be included within the stellar population as well. Once the initial system is setup, the simulation calculates the gravitational force on each star due to all the other stars in the cluster and the external tidal field. From the gravitational force, the equation of motion for each star can be determined and the future position and velocity of each star at the next specified time step can be predicted. This process can then be repeated in order to study cluster evolution for long periods of time. Since N-body simulations utilize Newtonian gravity (which is well understood) to calculate gravitational forces, the output of these models is quite realistic.

The publicly available code used in this thesis, NBODY6 (Aarseth et al., 1974; Aarseth , 2003), has two key advantages that make it ideal for realistically modelling star clusters. The first, is that the code keeps track of stellar evolution throughout the simulation. So not only can the future positions and velocities of each star be predicted, but the mass of each star at the next time step is predicted based on stellar evolution tracks for both single stars and binary stars (Hurley, 2008a,b). The second advantage is the code's ability to incorporate a realistic gravitational field into the simulation. While previous studies simply invoke a maximum radius that stars can reach in order to mimic the existence of a gravitational field, NBODY6 allows for the formal definition of a galactic potential which contributes to the net gravitational force acting on each star within the cluster. The form of the galactic potential is also flexible, with NBODY6 allowing for a three component potential consisting of a galactic bulge, disk, and halo that mimics the Milky Way. Therefore the effects of tidal heating and shocking, which are difficult to model analytically, are automatically taken into consideration as the model cluster orbits within a gravitational field. NBODY6 serves as the best tool for studying the effects of orbital eccentricity and inclination on globular cluster evolution, as it allows the user to study and quantity the various mechanisms at play in a non-static tidal field.

1.5 The Evolution of Star Clusters in Tidal Fields

The purpose of this thesis is to establish an understanding of how cluster evolution is related to the local environment, specifically the gravitational field of the host galaxy, and to extend dynamical evolution theory to a more advanced and general level of understanding. As previously discussed, many of the observed properties of globular cluster populations are identical from one galaxy to the next, suggesting cluster evolution is independent of environment. Tidal theory on the other hand indicates that an external gravitational field should have a significant effect on cluster evolution, assuming the cluster is sufficiently large (tidally filling).

The key drawback to previous theoretical studies of globular clusters is that they assume clusters have circular orbits in spherically symmetric potentials, in order for an analytic calculating of cluster size and mass loss rate to be determined. When a cluster has an eccentric orbit, previous studies have always assumed that cluster size is imposed at R_p. Based on these assumptions, the only way cluster evolution could be independent of environment is if all clusters are tidally under-filling, which has been shown to not be true for a significant number of clusters in the Milky Way. Furthermore, globular clusters with proper motion measurements have revealed that no Galactic clusters have circular orbits and theoretical studies have begun to show that assuming size is imposed at R_p is incorrect (e.g. Dinescu et al., 1999; Brosche, Odenkirchen, & Geffert, 1999; Baumgardt & Makino, 2003; Casetti-Dinescu et al., 2007; Kupper et al., 2010; Casetti-Dinescu et al., 2013). Taking into consideration that assuming any galaxy is spherically symmetric is likely incorrect, especially disk galaxies like the Milky Way, there is no surprise that theoretical cluster studies cannot reproduce observed cluster populations.

For my Master's thesis, we attempted to reproduce the distribution of cluster sizes in the giant elliptical galaxy M87 by allowing clusters to have different orbital distributions. We assumed that cluster size is imposed at R_p when orbits are eccentric and that all clusters tidally filling. The best fit model that reproduced the relationship between cluster size and R_{gc} out to 12 kpc assumes that cluster orbits are preferentially radial. While this finding is in line with galaxy formation models, the mean orbital eccentricity of clusters in our model is much higher than observations of M87 suggest (Côté et al., 2001; Strader et al., 2011). We proposed that a more in-depth study on the effects of orbital eccentricity, allowing cluster orbits to become more radial with R_{gc}, incorporating the existence of under-filling clusters, and extending our observational dataset out to larger R_{gc} will allow for more accurate models to be used to reproduce the observed characteristics of globular cluster populations (Webb, Sills, & Harris, 2012a).

Establishing a clear relationship between cluster evolution and galaxy environment will help introduce a new era of globular cluster studies. Linking a cluster's size to its orbit within a tidal field opens the door to use observations of cluster populations to map out the size, shape, and strength of a galaxy's gravitational field. This approach is especially useful for mapping dark matter halos, which is a very difficult thing to do. Cluster sizes could even be used to search for evidence of sub-structure within dark matter halo's, a theoretical prediction that has yet to be observationally confirmed, as repeated dynamical interactions with sub-structure will tidally heat a cluster and help stars escape. In galaxies with well studied tidal fields, clusters sizes could even be used to constrain the orbital anisotropy profile of a galaxy. Understanding how these galaxies must have evolved over time also means that we can constrain the initial size and mass of both individual clusters and the global cluster population. The latter point is extremely useful for models of galaxy formation. Clusters which appear to have evolved irregularly given their local environment will also be of interest, as they may represent a population that has been recently accreted by a galaxy via a minor or major merger. Hence globular clusters could also be used to constrain the merger history of a particular galaxy.

This work first explores how the orbit of a cluster in a gravitational field affects the evolution of its mass, scale size, and stellar mass function. In Chapter 2, N-body simulations of globular clusters with a range of initial sizes and orbits in a Milky Way-like potential are used to explore how orbital eccentricity affects the evolution of cluster structure. We include simulations of both tidally filling and under-filling star clusters. From this study we introduce a correction factor for calculating r_h and r_t for tidally filling clusters with eccentric orbits. In Chapter 3, we use a similar set of N-body simulations to explore how mass loss due to orbital eccentricity influence the stellar mass function of a globular cluster, and propose a method for constraining cluster orbits using a cluster's stellar mass function. Similar to our study of orbital eccentricity on globular cluster sizes, we also use N-body simulations of star clusters in Chapter 4 to determine how tidal heating and tidal shocks experienced by clusters on inclined orbits in the Milky Way influence their evolution. From our models, we suggest the best method for theoretically calculating r_h and r_t when a cluster's orbit is inclined.

In the subsequent chapters, we take what we have learned regarding the effects of environment on cluster evolution from N-body studies and apply the results to observations of globular cluster populations. In Chapter 5, we were able to build on our study of globular clusters in M87 from Webb, Sills, & Harris (2012a) out to 120 kpc thanks to an accepted HST proposal. With an improved calculation for the size of a cluster with an eccentric orbit from our N-body studies, we again search for the distribution of cluster orbits which reproduces the relationship between cluster size and R_{gc} in M87. We also explore the possibility of cluster populations having orbital anisotropy profiles such that orbits become more radial with distance, allow for the existence of tidally under-filling clusters, and study the metal-poor and metal-rich sub-populations separately in M87. In Chapter 6, we take our work with the M87 cluster population and apply it to the cluster populations of NGC 1399 and NGC 5128. We improve on our previous work by allowing cluster orbits to become preferentially radial with r_{gc} and allow clusters to become more and more tidally under-filling with r_{gc} as the tidal field weakens. By studying the distribution of cluster sizes in each galaxy, we are able to constrain the orbital anisotropy and tidally filling profiles of each cluster population. While an isotropic distribution of orbits suggests a cluster population has not undergone any recent dynamical disruptions, a high degree of radial anisotropy serves as an indicator of recent or on-going merger events as a significant amount of clusters still have highly eccentric orbits. The tidal filling profile of a galaxy indicates what the initial structural properties of a globular cluster population was at formation, which in turn allows us to place constraints on the surrounding birth environment of globular clusters. Hence we can use the results to make conclusions regarding the formation and merger histories of each galaxy. We also explore the differences between the metal-poor and metal-rich sub-populations in each galaxy, and find evidence for the distribution of cluster orbits being different between the two sub-populations which would help explain the observed size difference. Finally, in Chapter 7 we summarize our findings and identify future studies which will be based on the results of this thesis.

Bibliography

Aarseth, S.J. 2003, Gravitational N-body Simulations: Tools and Algorithms (Cambridge Monographs on Mathematical Physics). Cambridge University Press, Cambridge

Aarseth, S., Hénon, M., Wielen, R., 1974, A&A, 37, 183

Alexander, P. E. R. & Gieles, M. 2013, MNRAS, 432L, 1

Baumgardt H., Makino J. 2003, MNRAS, 340, 227

Bertin, G. & Varri, A. L. 2008, ApJ, 689, 1005

Bianchini, P., Renaud, F., Gieles, M., Varri, A.L. 2015, MNRAS, 447, 40

Binney, J. & Tremaine, S. 2008, Galactic dynamics second edition (Princeton, NJ, Princeton University Press, 1987, 747 p.)

Blom, C., Spitler, L. R., Forbes, D. 2012, MNRAS, 420, 37

Brockamp, M., Küpper, A. H. W, Ties, I., Baumgardt, H., Kroupa, P, 2014, MNRAS, 441, 150

Brodie, J. P. & Strader, J. 2006, ARAA, 44, 193

Brosche, P., Odenkirchen, M., Geffert, M. 1999, New Astron., 4, 133

Casetti-Dinescu, D.I., Girard, T.M., Herrera, D., van Altena, W.E., López, C.E., Castillo, D.J. 2007, AJ, 134, 195

Casetti-Dinescu, D.I., Girard, T.M., Jíková, L., van Altena, W.F., Podestá, F., López, C.E. 2013, AJ, 146, 33

Côté, P., McLaughlin, D.E., Hanes, D.A., Bridges, T.J., Geisler, D., Merrid, D., Hesser, J.E., Harris, G.L.H., Lee, M.G., 2001, ApJ, 559, 828, 257B

Dinescu, D.I., Girard, T.M., van Altena, W.E. 1999, AJ, 117, 1792

D'Onghia, E., Springel, V., Hernsquist, L., & Keres, D. 2010, ApJ, 709, 1138

Forbes, D.A., Sánchez-Blázquez, P., Phan, A.T.T., Brodie, J.P., Strader, J., Spitler, L. 2006, MNRAS, 366, 1230

Gebhardt, K. & Fischer, P. 1995, AJ, 109, 209

Georgiev, I.Y., Puzia, T.H., Hilker, M., Goudfrooij, P. 2010, MNRAS, 409, 447

Gieles, M., Athanassoula, E., Portegies Zwart, S. F., 2007, MNRAS, 376, 809

Gieles M., Heggie D., Zhao H. 2011, MNRAS, 413, 2509

Gnedin, O.Y. & Ostriker, J.P. 1997, ApJ, 474, 223

Gnedin, O. Y., & Prieto, J. L. 2009, in ESO Astrophysics Symp.: Globular Clusters-Guides to Galaxies (Berlin: Springer), 323

Gómez, M. & Woodley, K.A. 2007, ApJ, 670, L105

Gunn, J.E. & Griffin, R.F. 1979, AJ, 84, 752

Harris, W. E. 1996, AJ, 112, 1487, 2010 Edition

Harris, W.E. 2009a, ApJ, 703, 939

Harris, W.E. 2009b, ApJ, 699, 254

Harris, W.E., Spitler, L.R., Forbes, D.A., Bailin, J. 2010, MNRAS, 401, 1965

Heggie D. C., Hut P. 2003, The Gravitational Million-Body Problem: A Multidisciplinary Approach to Star Cluster Dynamics (Cambridge: Cambridge University Press)

Henon M. 1961, Annales d'Astrophysique, 24, 369

Henon M. 1973, Dynamical Structure and Evolution of Dense Stellar Systems, ed. L. Martinet & M. Mayor (Geneva Obs.)

Hurley, J.R. 2008a, Lecture Notes in Physics, 760, The Cambridge N-body Lectures. Springer-Verlag, Berlin, p.283

Hurley, J.R. 2008b, Lecture Notes in Physics, 760, The Cambridge N-body Lectures. Springer-Verlag, Berlin, p.321

Innanen, K. A., Harris, W.E., Webbink, R.F. 1983, AJ, 88, 338

Jones, K.G. 1991, Messier's Nebulae and Star Clusters, 2nd ed, Cambridge University Press

Jórdan, A. 2004, ApJ, 613, L117

Jórdan, A., Côté, P., Blakeslee, J. P., Ferrarese, L., McLaughlin, D. E. , Mei, S., Peng, E. W., Tonry, J. L., Merrit, D., Milosavljević, M., Sarazin, C. L., Sivakoff, G. R., West, M. J., 2005, ApJ, 634, 1002

King, I. R. 1962, AJ, 67, 471

King, I. R. 1966, AJ, 71, 64

Kravtsov, A.V. & Gnedin, O.Y. 2005, ApJ, 623, 650

Kruijssen, J.M.D., Pelupessy, F.I., Lamers, H.J.G.L.M., Portegies Zwart, S.F., Bastian, N., Icke, V. 2012, MNRAS, 421, 1927

Kruijssen, J.M.D. 2014, Classical and Quantum Gravity, 31, 244006

Kundu, A. & Whitmore, B. C. 1998, AJ, 116, 2841

Kundu, A., Whitmore, B. C., Sparks, W. B., Macchetto, F. D., Zepf, S. E., Ashman, K. M. 1999, ApJ, 513, 733

Kupper, A. H. W, Kroupa, P, Baumgardt, H., Heggie , D. C., 2010, MNRAS, 407, 2260

Lada, C.J. & Lada, E.A. 2003, ARA&A, 41, 57

Larsen, S. S., Brodie, J. P., Huchra, J. P., Forbes, D. A., Grillmair, C. J., 2001, AJ, 121, 2974

Larsen, S. S. & Brodie, J. P. 2003, ApJ, 593, 340

Li, H. & Gnedin, O.Y. 2014, ApJ, 796, 10

Ludlow, A. D., Navarro, J. F., Springler, V., Vogelsberger, M., Wang , J., White, S. D. M., Jenkins, A., & Frenk, C. S. 2010, MNRAS, 406, 137

Madrid, J.P., Hurley, J.R., Martig, M., 2014, ApJ, 784, 95

Marín-Franch, A., Aparicio, A., Piotto, G., Rosenberg, A., Chaboyer, B., Sarajedini, A., Siegel, M., Anderson, J., Bedin, L. R., Dotter, A., Hempel, M., King, I., Majewski, S., Milone, A. P., Paust, N., Reid, I. N. 2009, ApJ, 694, 1498

McLaughlin, D.E., Harris, W.E., & Hanes, D.A. 1994, ApJ, 422, 486

McLaughlin, D. E. & van der Marel, R. P. 2005, ApJs, 161, 304

Miholics, M., Webb, J., Sills, A., 2014, MNRAS, 445, 2872

Paolillo, M., Puzia, T. H., Goudfrooij, P., Zepf, S. E., Maccarone, T. J., Kundu, A., Fabbiano, G., Angelini, L. 2011, ApJ, 736, 90

Peng, E.W., Jórdan, A., Côté, P., Blakeslee, S., Ferrarese, L., Mei, S., West, M. J., Merritt, D., Milosavljević, M., Tonry, J. L. 2006, ApJ, 639, 95

Prieto, J. L. & Gnedin, O. Y. 2008, ApJ, 689, 919

Puzia, T.H., Paolillo, M., Goudfrooij, P., Maccarone, T.J., Fabbiano, G., Angelini, L. 2014, ApJ, 786, 78

Renaud, F., Gieles, M., Christian, M. 2011, MNRAS, 418, 759

Renaud, F. & Gieles, M. 2015, MNRAS, accepted, arXiv:1503.04815

Schulman, R. D., Glebbeek, E., Sills, A. 2012, MNRAS, 420, 651

Sérsic, J. L. 1968, Atlas de galaxias australes. Observatorio Astronomico, Cordoba

Sippel, A.C., Hurley, J.R., Madrid, J.P., Harris, W.E. 2012, MNRAS, 427, 167

Spitler, L.R., Larsen, S.S., Strader, J., Brodie, J.P., Forbes, D.A., Beasley, M.A. 2006, AJ, 132, 1593

Spitzer L. Jr. 1958, ApJ, 127, 17

Spitzer L. Jr. 1987, Dynamical Evolution of GCs (Princeton, NJ: Princeton Univ. Press)

Strader, J., Romanowsky, A.J., Brodie, J.P., Spitler, L.R., Beasley, M.A., Arnold, J.A., Tamura, N., Sharples, R.M., Arimoto, N. 2011,APJS, 197, 33

Strader, J., Fabbiano, G., Luo, B., Kim, D., Brodie, J.P., Fragos, T., Gallagher, J.S., Kalogera, V., King, A., Zezas, A. 2012, ApJ, 760, 87

Tonini, C. 2013, ApJ, 762, 39

Usher, C., Forbes, D.A., Spitler, L.R., Brodie, J.P., Romanowsky, A.J., Strader, J., Woodley, K.A. 2013, MNRAS, 436, 1172

van de Ven, G., van den Bosch, R. C. E., Verolme, E. K., de Zeeuw, P. T. 2006, A&A, 445, 513

VandenBerg, D.A., Brogaard, K., Leaman, R., Casagrande, L. 2013, ApJ, 775, 134

von Hoerner, S. 1957, ApJ, 125, 451

Webb, J. J., Sills, A., Harris, W.E. 2012a, ApJ, 746, 93

Webb, J. J., Harris, W.E., Sills, A. 2012b, ApJ, 759, 39

Weijmans, A., Cappellari, M., Bacon, R., de Zeeuw, P. T., Emsellem, E., Falcon-Barroso, J., Kuntschner, H., McDermid, R. M., van den Bosch, R. C. E., and van de Ven, G., 2009, MNRAS, 398, 561

Wilson, C. P. 1975, AJ, 80, 175

Woodley, K. 2012, AAS Meeting #220, #438.07

Zait, A., Hoffman, Y. & Shlosman, I. 2008, ApJ, 682, 835

Zepf, S. E. & Ashman, K. M. 1993, MNRAS, 264, 611

Chapter 2

The Influence of Orbital Eccentricity on Tidal Radii of Star Clusters

Jeremy J. Webb, William E. Harris, Alison Sills, Jarrod R. Hurley

The Astrophysical Journal, Volume 764, Issue 2, pages 124-136,

Bib. Code: 2013ApJ...764..124W, DOI: 10.1088/0004-637X/764/2/124

2.1 Introduction

Theoretical calculations of the radius of a star cluster, or *tidal radius*, usually assume that the gravitational field of the host galaxy regulates cluster size. In most previous treatments, for simplicity it is further assumed that the gravitational field in which the cluster orbits is constant, i.e. the cluster has a circular orbit in a spherically symmetric galactic potential (e.g. von Hoerner, 1957; King, 1962; Innanen, Harris, & Webbink, 1983; Jordán et al., 2005; Binney & Tremaine, 2008; Bertin & Varri, 2008). The tidal radius is then assumed to be equal to the *Jacobi radius* (r_J), the distance beyond which the acceleration a star feels towards the galaxy center is greater than the acceleration it feels towards the cluster center, and the star is able to escape. First-order tidal theory determines the tidal radius (von Hoerner, 1957) via:

$$r_t = R_{gc}(\frac{M_{cl}}{2M_g})^{1/3} \tag{2.1}$$

where R_{gc} is the galactocentric distance of the cluster, M_{cl} is cluster mass, and M_g is the mass of the galaxy (assumed in early studies to be a point mass).

For a cluster with a non-circular orbit, the fact that the tidal field is no longer static makes an analytic approach very difficult (see Renaud et al. (2011) for another approach). Historically it has been assumed that for a globular cluster on an eccentric orbit, its tidal radius is imposed at perigalacticon (R_p) where the tidal field of the host galaxy is the strongest. This assumption was initially suggested by von Hoerner (1957) and later King (1962), and follows from the fact that the internal relaxation time (t_{r_h}) of the cluster is greater than its orbital period for almost all observed globular clusters. Therefore after stars outside the tidal radius at perigalacticon escape, the cluster would not be able to relax and expand before it returns to perigalacticon. Thus in Equation 6.1, R_{gc} is usually replaced with R_p to calculate the tidal radius of a cluster with an eccentric orbit (e.g. Innanen, Harris, & Webbink, 1983; Fall & Zhang, 2001; Read et al., 2006; Webb, Sills, & Harris, 2012).

However, recent studies are showing with increasingly strong evidence that the actual sizes of observed clusters are not imposed at perigalacticon in this simple way. The actual size of an observed cluster is known as its limiting radius r_L, which marks the point where the cluster density falls to zero (Binney & Tremaine, 2008). Using the solved orbits of 15 Galactic globular clusters, Odenkirchen et al. (1997) demonstrated that cluster limiting radii are not solely dependent on perigalactic distance. Brosche, Odenkirchen, & Geffert (1999) suggested some sort of orbit-averaged tidal radius is more appropriate when predicting limiting radii. Even with the orbits of an additional 29 Milky Way globular clusters currently known (Dinescu et al., 1999; Casetti-Dinescu et al., 2007), there is still no clear relationship between limiting radii and perigalactic distance, and the conclusions of Odenkirchen et al. (1997) still hold.

With the Galactic potential as given by Johnston et al. (1995) (the same Galactic potential Casetti-Dinescu et al. used to solve cluster orbits), we calculated the *theoretical* tidal radius r_t at perigalacticon (that is, the Jacobi radius at $R = R_p$) of each of the 44 Galactic clusters with known orbits. The r_t values were calculated with the formalism of Bertin & Varri (2008) (as outlined in Section 3.0). The main uncertainty in the theoretical tidal radius is due to the uncertainty in R_p quoted in Dinescu et al. (1999) and Casetti-Dinescu et al. (2007). To compare theory and observations for individual clusters, we take cluster limiting radii as determined from direct King (1966) model fits

r_k to the observed cluster profiles as listed in Harris (1996) (2010 edition). We then calculate the ratio of the difference $(r_k - r_t)$ between observed and theoretically predicted values to their average $((r_k + r_t)/2)$. An uncertainty of 10% was assigned to values of r_k. If theory and observations are in agreement, the ratio will be approximately zero. Clusters which have a ratio greater than zero will be ones which overfill their predicted tidal radius, while clusters with ratios less than zero will be tidally under-filling. The comparison between theory and observations is illustrated in Figure 2.1.

While it is not expected that all clusters are tidally filling (Gieles et al., 2010), the fact that the majority of clusters appear to be tidally overfilling is a strong signal that the simple assumptions built into the model need investigation. The known presence of tidal tails around observed (e.g. Odenkirchen et al., 2001) and simulated (e.g. Montuori et al., 2007; Küpper et al., 2012; Lane et al., 2012) globular clusters is not sufficient to explain the cases of apparent overfilling. The observed r_k values are determined from King-model profile fits that are heavily dominated by the inner populations of stars, out to a few half-light radii. In almost all cases the extremely low densities of stars in the tails, at or beyond the nominal tidal radius, exert little leverage on these fits. Furthermore, King (1966) models are known to underestimate cluster sizes in general as they require a sharp tidal cutoff which is not observed in all clusters (McLaughlin & van der Marel, 2005). Only in the most extreme cases (e.g. Pal 5 (Odenkirchen et al., 2003)), will large and extended tidal tails influence model fits to the cluster surface brightness profile.

Theoretical calculations may also underestimate r_k because the assumption that the tidal radius is imposed at perigalacticon implies that the shape of the tidal field and the cluster orbit are not important. Hence factors such as

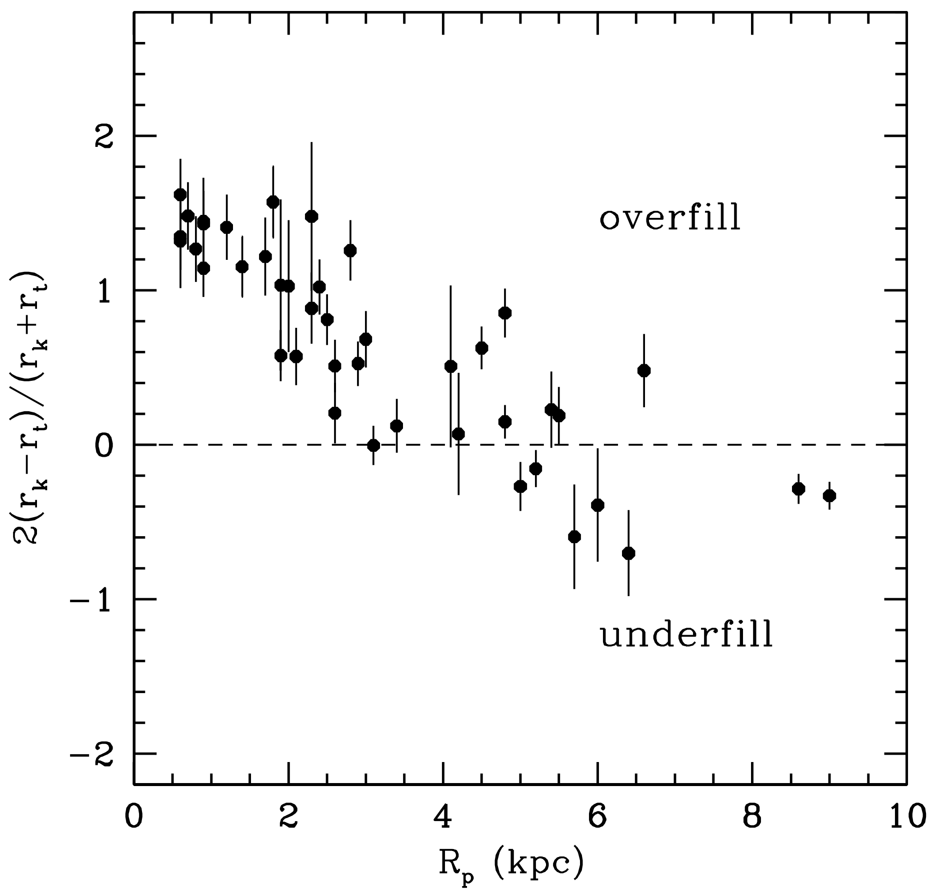

Figure 2.1 Ratio of difference between observed (r_k) and theoretical (r_t) tidal radius at perigalacticon to the average ($(r_t+r_k)/2$) versus perigalactic distance for Galactic globular clusters.

tidal heating and disk shocking due to a varying symmetric galactic potential are not taken into consideration. However, despite these potential inaccuracies we still expect to see some sort of correlation between r_k and perigalactic distance, if tidal radii are imposed at perigalacticon. The Milky Way cluster data therefore suggest that something is wrong with basic tidal theory.

Recent N-body simulations by Küpper et al. (2010), find that their fitted King (1962) radius was better represented by the time averaged mean tidal radius of the cluster and not the perigalactic tidal radius. In a later study on the structure of tidal tails, Küpper et al. (2012) found that while stars outside the tidal radius as calculated at perigalacticon will likely become unbound at perigalacticon, some are able to be re-captured by the cluster as it moves away from perigalacticon and the instantaneous tidal radius of the cluster increases. That is, the limiting radius of a cluster will be greater than the tidal radius calculated at perigalacticon. This discrepancy is expected to be amplified for clusters on very eccentric orbits, as they make quick perigalactic passes and spend the majority of their time near apogalacticon (R_a). In fact, N-body simulations by Madrid et al. (2012) suggest that the half-mass radius of a globular cluster is more likely imposed at R_a than R_p.

The purpose of this study is to explore more thoroughly the influence of orbital eccentricity on cluster size. Model N-body clusters with different initial half-mass radii are evolved from zero age to 10 Gyr over a range of orbital eccentricities in the disk of a Milky Way-like potential. The models and their initial conditions are described in Section 2. In Section 3 we focus on the influence of orbital eccentricity on the mass (M), half-mass radius (r_m), limiting radius, and tidal radius of each model cluster over time. In Section 4 we explore the influence of initial cluster half-mass radius on our results. In

Section 5 we discuss the results of all our N-body models and the influence of orbital eccentricity not only on cluster radii, but on individual stars within the cluster as well. Based on our findings, in Section 6 we suggest a correction factor that can be applied to the perigalactic tidal radius of a cluster to better match its observed limiting radius. This correction factor is then applied to the Galactic globular clusters shown in Figure 2.1. Finally in Section 7 we summarize our conclusions.

2.2 The Models

We use the NBODY6 direct N-body code (Aarseth , 2003) to evolve model star clusters from zero age to a Hubble time, over a range of both initial cluster half-mass radii and orbital eccentricity. All models in this study begin with 48000 single stars and 2000 binaries.

As long as we use one particle to represent one real star, clusters of this size correspond physically to either a very massive open cluster, or a low-mass globular cluster in the Milky Way. Ideally, we would like to follow more "average" globular clusters, which will typically have 200,000 stars or more. However, to this point in the history of the subject, direct N-body integrations with N-values that large have only been carried out for special, specific purposes (for example, see Hurley & Shara (2012) for a 200,000-star simulation in the tidal field of a point-mass Galactic potential and a circular orbit; Zonoozi et al. (2011) for $N \leq 100,000-$star simulations directed at modelling Pal 14, again on a circular orbit; or Heggie & Giersz (2009) for a 105,000-star simulation of NGC 6397 over 1 Gyr). Encouragingly, however, these high-N models generally confirm the trends obtained from earlier, small-

N simulations (see Hurley et al. for additional discussion).

The purpose of our suite of 50,000-star models is instead to survey a wide parameter space of initial cluster half-mass radii and orbital type. Our chosen ranges (see below) match real Milky Way star clusters moving in a realistic time-varying potential. Eventually, with advances in computational capabilities this type of survey work can be extended to higher N values (up to 10^6) that will cover almost the entire known range of globular clusters. However, as will be seen below, the models summarized here already prove to be highly informative in revealing important physical effects of orbital eccentricity on the internal dynamical evolution in a direct way that does not rely on analytical approximations.

Since we are only concerned with the influence of orbital eccentricity on clusters of different initial half mass radii, our choice of initial parameters such as cluster metallicity, the stellar initial mass function (IMF), and binary fraction are of little consequence as long as they remain consistent between models. However, we note that binary fractions of a few per cent are typical for globular clusters (e.g. Davis et al., 2008).

The masses of single stars are drawn from a Kroupa, Tout, & Gilmore (1993) IMF between 0.1 and 30 $M_{\odot}$. For binary stars, the masses of two randomly selected single stars are combined to equal the total mass of the binary, with the primary and secondary masses determined by a mass-ratio randomly drawn from a uniform distribution. The initial total mass of each model is $3 \times 10^4 M_{\odot}$. The initial period of each binary is drawn from the distribution of Duquennoy & Mayor (1991) and their orbital eccentricities are assumed to follow a thermal distribution (Heggie , 1975). All stars were given a metallicity of $Z = 0.001$. The initial positions and velocities of the stars are generated based on a Plummer density profile (Plummer , 1911; Aarseth et al., 1974). We note that the Plummer model extends to an infinite radius so we impose a cut-off at $\sim 10\ r_m$ to avoid rare cases of large cluster-centric distances. A description of the algorithms for stellar and binary evolution can be found in Hurley (2008a,b).

The model clusters orbit in a three-dimensional Galactic potential, which consists of a point-mass bulge, a Miyamoto & Nagai (1975) disk (with $a = 4.5$ kpc and $b = 0.5$ kpc), and a logarithmic halo potential. The combined mass profiles of all three potentials result in a circular velocity of 220 km/s at a galactocentric distance of 8.5 kpc. The bulge and disk have masses of 1.5×10^{10} and $5 \times 10^{10} M_{\odot}$ respectively (Xue et al., 2008). Aarseth (2003) and Praagman, Hurley, & Power (2010) describe the incorporation of the Galactic potential into NBODY6. All models were set to orbit in the plane of the disk such that a cluster on a circular orbit experiences a static tidal field, and will not be subject to factors such as tidal heating or disk shocking.

For the purposes of our study, the only parameters which are important and change from model to model are initial cluster half-mass radius, initial cluster position, and initial cluster velocity which determine the shape of the orbit. Our first models were for clusters with orbital eccentricities of 0.25, 0.5, 0.75, and 0.9, where eccentricity is defined as $e = \frac{R_a - R_p}{R_a + R_p}$. All of these have the same perigalactic distances of 6 kpc and initial half-mass radii $r_{m,i}$ of 6 pc. These clusters are located at perigalacticon at time zero. For comparison purposes a model was simulated with a circular orbit at perigalacticon (6 kpc) and four more with circular orbits at the apogalactic distance of each eccentric cluster (10 kpc, 18 kpc, 43 kpc, and 104 kpc). These simulations allow us to directly compare the properties of a globular cluster on an eccentric orbit to clusters on circular orbits at both perigalacticon and apogalacticon.

Our set of models also included re-simulations of the cluster with an orbital eccentricity of 0.5, and the corresponding e = 0 perigalactic and apogalactic simulations, but with initial half-mass radii of 4 pc, 2 pc, 1 pc, and 0.5 pc. This range allows us to study the influence of initial cluster half-mass radius. Both sets of models are summarized in Table 4.1. Model names are based on orbital eccentricity (e.g. e05), circular radius at apogalacticon (e.g. r18), and initial half mass radius (rm6). Hence a model cluster with a perigalactic distance of 6 kpc, apogalactic distance of 18 kpc (orbital eccentricity of 0.5), and an initial half-mass radius of 6 pc would be labeled e05r18rm6.

Table 2.1: Model Input Parameters

Model Name	$r_{m,i}$ pc	R_p kpc	v_p km/s	e
e0r6rm6	6	6	212	0
e025r10rm6	6	6	280	0.25
e0r10rm6	6	10	224.5	0
e05r18rm6	6	6	351.5	0.5
e0r18rm6	6	18	232	0
e075r43rm6	6	6	455	0.75
e0r43rm6	6	43	229.95	0
e09r104rm6	6	6	543.5	0.9
e0r104rm6	6	104	225.25	0
e0r6rm4	4	6	212	0
e05r18rm4	4	6	351.5	0.5
e0r18rm4	4	18	232	0
e0r6rm2	2	6	212	0
e05r18rm2	2	6	351.5	0.5

e0r18rm2	2	18	232	0
e0r6rm1	1	6	212	0
e05r18rm1	1	6	351.5	0.5
e0r18rm1	1	18	232	0
e0r6rm05	0.5	6	212	0
e05r18rm05	0.5	6	351.5	0.5
e0r18rm05	0.5	18	232	0

2.3 Influence of Orbital Eccentricity

The first portion of this study will focus solely on models with an initial r_m equal to 6 pc, with the only difference between each model being their Galactic orbits. However, we first need to determine whether any given star is bound to the cluster. In a cluster-centric coordinate system, we define the x-axis as pointing away from the galactic center, the y-axis pointing in the direction of motion of the cluster, and the z-axis pointing perpendicular to the orbital plane. In this coordinate system the energy of an individual star can be written as:

$$E = \frac{1}{2}(\dot{x}^2 + \dot{y}^2 + \dot{z}^2) - \sum_{i=1}^{N-1} \frac{Gm_i}{\|r - r_i\|} - \frac{1}{2}\Omega^2(z^2 - \upsilon x^2) \tag{2.2}$$

where the second term is the potential energy due to the remaining N-1 stars in the simulation, each with mass m_i and located a distance r_i from the star. The third term is the tidal potential with Ω^2 equal to the orbital frequency of the cluster. Here υ is a dimensionless positive coefficient defined below in Equation 4.5. The tidal potential, taken from Bertin & Varri (2008), results in a stretching of the cluster in the x-direction, no change in the y-direction, and a compression in the z-direction. If the resultant energy is less than zero the star is bound, otherwise it is considered unbound.

We considered additional criteria for determining whether a star is bound or unbound in addition to the energy calculation. Other studies have invoked a distance cutoff such that the stars' cluster-centric distance must be greater than the cluster perigalactic or instantaneous tidal radius for it to be unbound (e.g. Takahashi & Baumgardt, 2012). It has also been suggested that a star's velocity plays a role in whether or not it can be considered unbound (e.g. Küpper et al., 2010, 2012). However, we found these additional criteria did not change any of the results found in Section 3 as they only effected a small percentage of simulated stars. Therefore, we only require that a star's energy as given by Equation 2.2 to be greater than zero for the star to be considered unbound.

Figure 2.2 shows a model cluster at a representative timestep. The tidal tails formed by escaping stars are clearly visible in our simulations. The densely populated spherical collection of stars marked in red are those that satisfy our boundedness criterion and are considered cluster members. The unbound stars that appear close to the centre of the cluster are foreground stars with a large z coordinate and are simply projected onto the cluster in the x-y plane. These tails have no effect on our determination of theoretical tidal radii or observed limiting radii as we only consider stars that are bound to the cluster.

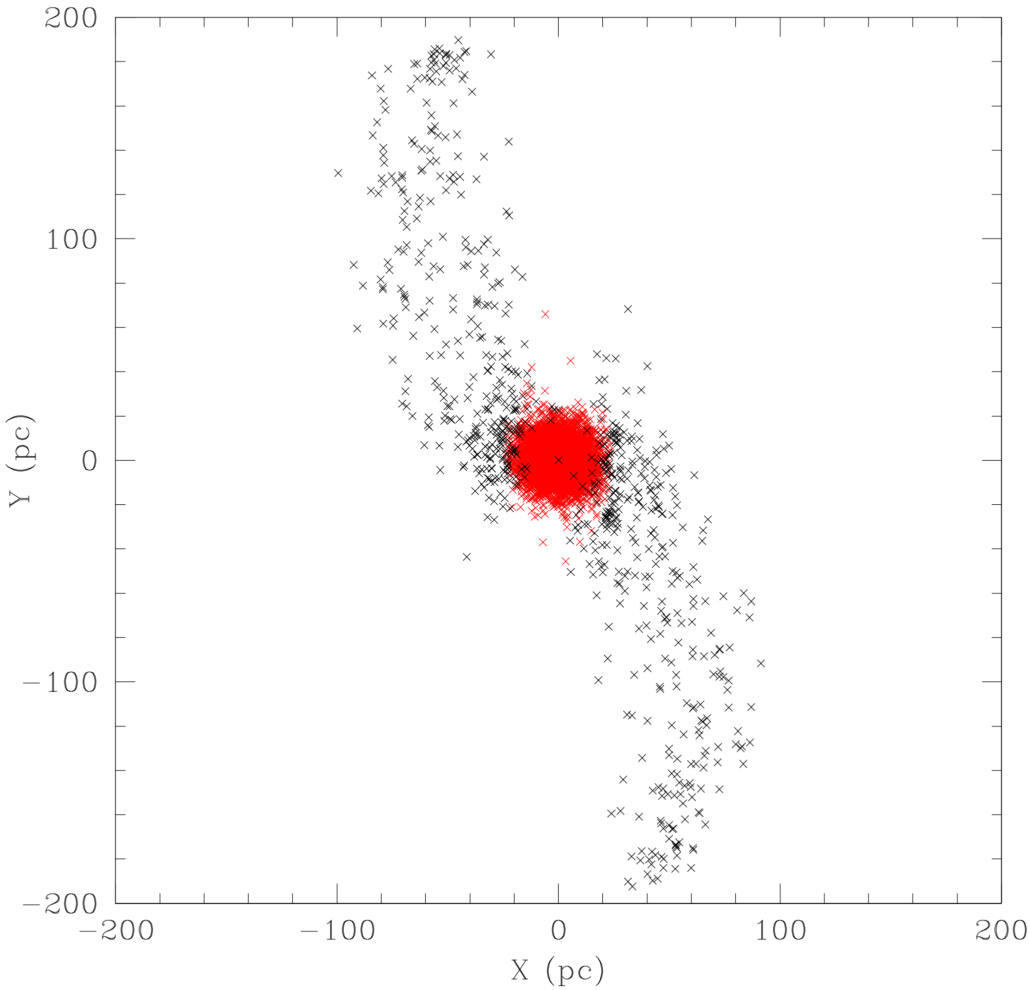

Figure 2.2 Snapshot of a model cluster on a circular orbit at 6 kpc after 32 orbits (5680 Myr). Bound stars are marked in red.

2.3.1 Mass

We first wish to study how orbital eccentricity influences the total mass, or more specifically the mass loss, of a star cluster over time, which then plays an important role in determining tidal radii ($r_t \propto M^{\frac{1}{3}}$). The total mass of stars bound to the cluster in each model is illustrated in Figure 2.3. In general, mass loss is due to stellar evolution, evaporation due to two-body interactions, and tidal stripping. For clusters with circular orbits, in all cases the apogalactic cluster loses mass at a lower rate than the perigalactic case as a result of less tidal stripping.

The e=0.25 case loses mass at almost the same rate as if it had a circular orbit at its perigalactic distance, but the final mass is still notably larger than the perigalactic case. Since eccentric clusters spend the majority of their time away from perigalacticon, they too will be subject to less tidal stripping than an ideal cluster that spends all its time at perigalacticon. As eccentricity increases, the mass-loss profile shifts further away from the perigalactic case and closer to a cluster with a circular orbit at apogalacticon.

At higher eccentricities the mass no longer smoothly decreases, in contrast to the circular orbit cases. Instead periodic fluctuations are present. The minima of these fluctuations correspond to perigalactic passes, where the rapid increase in tidal field strength results in episodes of significant mass loss. These fluctuations suggest that a greater change in tidal field strength between apogalacticon and perigalacticon results in stars gaining more energy at or near perigalacticon.

Especially interesting in the lower right panel of Figure 2.3 is the fact that once a cluster undergoes significant mass loss during a perigalactic pass,

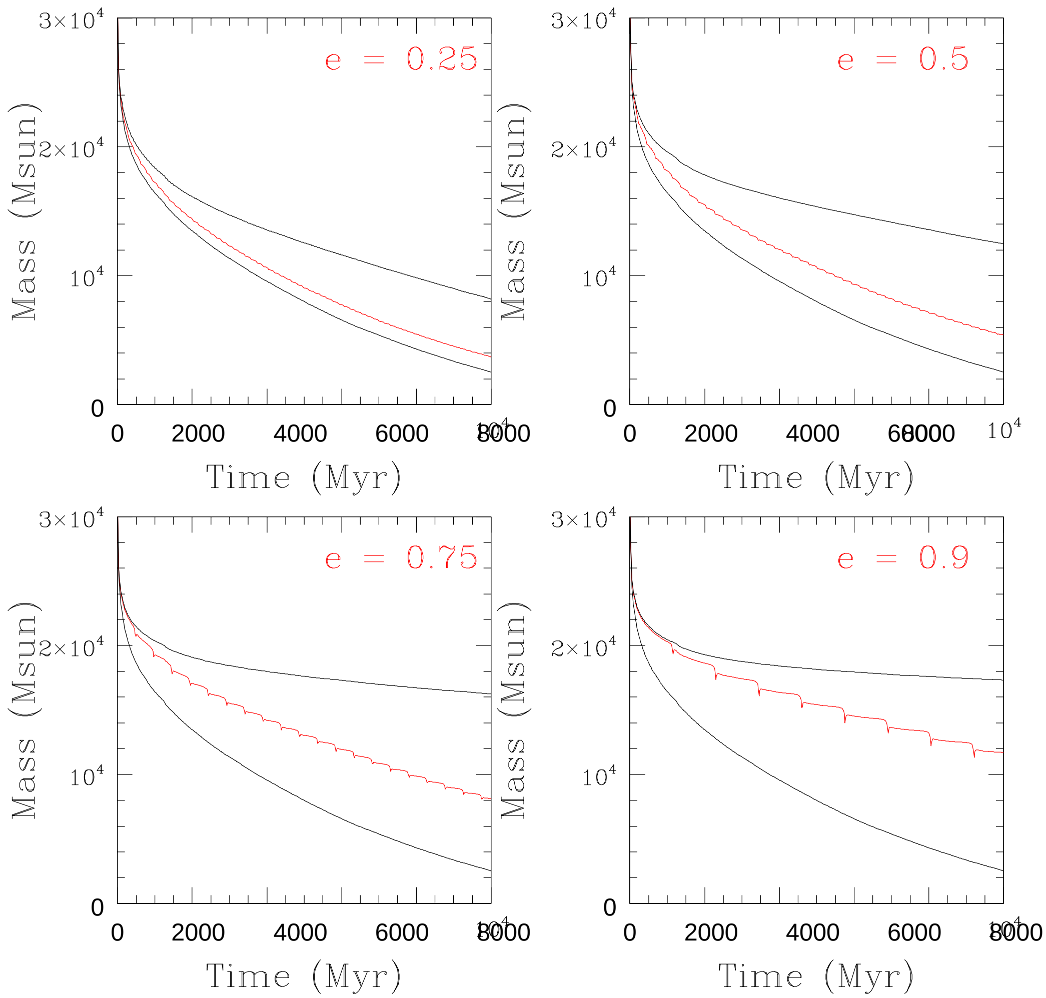

Figure 2.3 The evolution of total cluster mass over time. The red lines correspond to models with orbital eccentricities as labelled in each panel. In each plot, the lower black line corresponds to a cluster with a circular orbit at perigalacticon (6 kpc), while the upper black line corresponds to a cluster with a circular orbit at apogalacticon.

the cluster starts to regain mass before resuming its mean mass loss rate. In these intervals just after perigalacticon, the cluster is re-capturing some of the stars which were previously unbound. Stated differently, many of the stars that were formally unbound at R_p drift away slowly enough that they are recaptured as the cluster moves back outward and its instantaneous tidal radius expands again. Furthermore, these fluctuations suggest that while a perigalactic pass does have a strong effect on an eccentric cluster, the cluster cannot be treated as if it had a circular orbit at R_p. These results are in agreement with the findings of Küpper et al. (2012) discussed earlier.

2.3.2 Half-mass Radius

We next consider how orbital eccentricity can influence the half-mass radius r_m of bound stars within a globular cluster. It should be noted that r_m is not the same as the *half-light radius* r_h (also known as the effective radius), which is a directly observable parameter. In our simulations, the half-mass radius is always slightly larger than the half-light radius.

The results of our simulations are illustrated in Figure 2.4. The initial increase in r_m during the first ~ 2000 Myr in all cases is driven by two-body relaxation and stellar evolution mass-loss. However once the cluster is relaxed, tidal stripping becomes the dominant dynamical process.

The r_m profiles of the apogalactic cases in the lower panels do not begin to decrease after 2000 Myr, but instead continue to increase up to 10 Gyr. As discussed in the next section this trend is due to the fact that these clusters are barely tidally filling, so can still expand and not be subject to tidal stripping.

Similar to the results of Section 3.1, for low eccentricities the r_m pro-

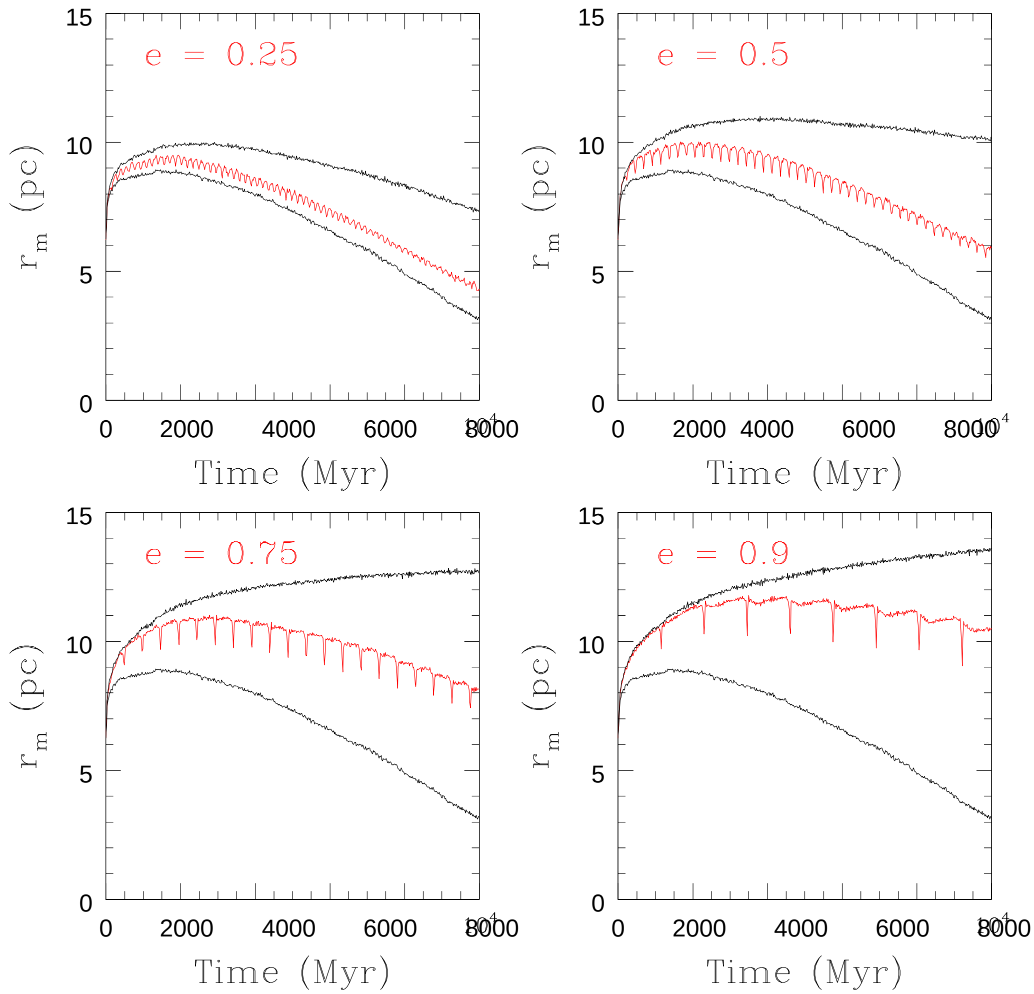

Figure 2.4 The evolution of half mass radius over time. The red lines correspond to models with orbital eccentricities as labelled in each panel. In each plot, the lower black line corresponds to a cluster with a circular orbit at perigalacticon (6 kpc), while the upper black line corresponds to a cluster with a circular orbit at apogalacticon.

file of the eccentric model cluster is comparable to the circular orbit case at perigalacticon. Increasing eccentricity brings the r_m profile closer to the apogalactic case on the average, but increasing eccentricity again results in sharp fluctuations in the r_m profile which correspond to perigalactic passes. The trends shown in Figure 2.4 reveal what is perhaps the most striking difference between clusters on static circular orbits (the classically assumed case) and ones on more realistic eccentric orbits. If cluster limiting radii are imposed at perigalacticon, we would expect the minima of the eccentric r_m profile to be equal to the r_m profile of a cluster orbiting at R_p. While a high-e cluster may briefly expand after a perigalactic pass, the next perigalactic pass would restore r_m to a size equal to the perigalactic case. But not even at perigalacticon does the r_m of the eccentric cluster equal the perigalactic case. Instead, the time averaged r_m is reflective of a tidal field weaker than the field at perigalacticon, in agreement with Küpper et al. (2010).

After a perigalactic pass, Figure 2.4 illustrates again that the cluster is able to increase in size. Especially apparent in the lower right panel of Figure 2.4 is the fact that the cluster is able to increase to a size greater than its mean r_m. Inspection of our N-body models shows that this increase in size is due to a combination of re-capturing some of the previously unbound stars (Küpper et al., 2012) and the stars in the inner region of the cluster gaining enough energy to move outward and repopulate the halo of the cluster. These statements are discussed in further detail in Section 5.0.

2.3.3 Tidal and Limiting Radii

The Jacobi radius represents a theoretical surface around a cluster past which a star cannot pass and still remain bound. The Jacobi radius allows for the calculation of the instantaneous tidal radius of each model cluster as a function of time. To calculate the instantaneous tidal radius of each model cluster, we require a derivation of cluster tidal radius which takes into consideration the tidal field of the host galaxy. Assuming only that the tidal field must be spherically symmetric, the theoretical tidal radius as derived by Bertin & Varri (2008) is:

$$r_t = (\frac{GM}{\Omega^2 \upsilon})^{1/3} \tag{2.3}$$

where Ω, κ and υ are defined as:

$$\Omega^2 = (d\Phi_G(R)/dR)_{R_p}/R_p \tag{2.4}$$

$$\kappa^2 = 3\Omega^2 + (d^2\Phi_G(R)/dR^2)_{R_p} \tag{2.5}$$

$$\upsilon = 4 - \kappa^2/\Omega^2 \tag{2.6}$$

Φ_G is the galactic potential, R_p is the perigalactic distance, Ω is the orbital frequency of the cluster, κ is the epicyclic frequency of the cluster at R_p, and υ is a positive dimensionless coefficient. Using the tidal field of the Milky Way discussed in Section 2.0 and the mass and galactocentric distance of the model clusters at each time step, we calculate the instantaneous tidal radius of each model. The results of these calculations are shown in Figure 2.5. Here the instantaneous r_t increases and decreases periodically along the orbit, but

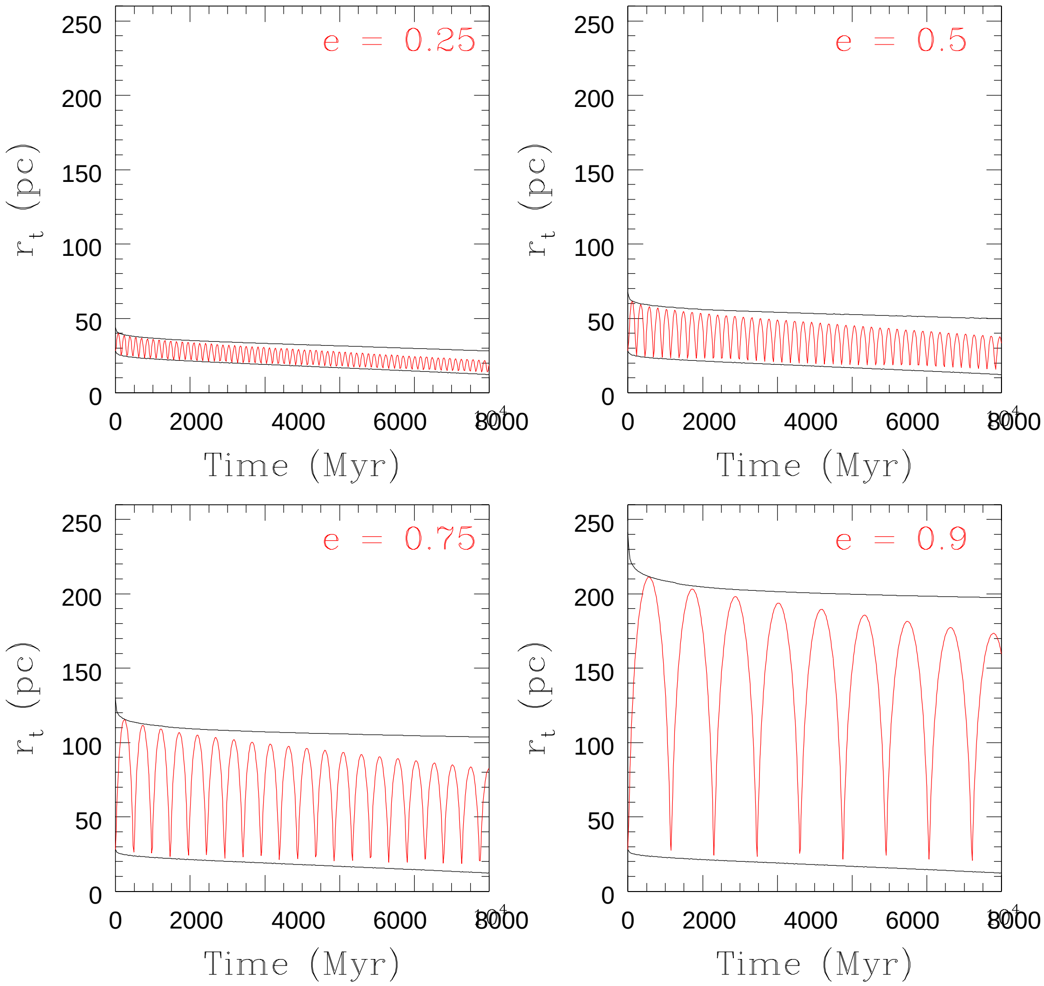

Figure 2.5 The evolution of the instantaneous tidal radius over time. The red lines correspond to models with orbital eccentricities as labelled in each panel. In each plot, the lower black line corresponds to a cluster with a circular orbit at perigalacticon (6 kpc), while the upper black line corresponds to a cluster with a circular orbit at apogalacticon.

never quite reaches the perigalactic and apogalactic cases due to differences in mass loss rates among all three cases.

Next we compare the tidal radius to the limiting radius. For a simulated cluster, since we know which stars are bound or unbound, we could call the limiting radius of the cluster the distance to the farthest bound star, but this approach introduces some significant problems. First, since cluster tidal radii are calculated for stars with *circular prograde orbits*, any star with a retrograde and/or eccentric orbit within its cluster can remain bound beyond the nominal tidal radius (Read et al., 2006). Second, any star in the process of escaping the cluster can reach large clustercentric distances before becoming energetically unbound. Third, the stars along the y-axis of the cluster (the direction of motion) are unaffected by the tidal potential in Equation 2.2, allowing them to also remain bound at larger clustercentric distances. These three issues cause the true limiting radius of the cluster to change dramatically from time-step to time-step. To gain a more stable indication of cluster size, we instead focus on the x-axis of the cluster, the axis along which the tidal radius is calculated, and define the limiting radius as the average x-coordinate of all stars with $\|x\| > r_t$. This calculation typically involves less than 1% of the total cluster population. While this is not the true limiting radius of the cluster and will always be slightly larger than the true tidal radius, it acts as a tracer of the outer region that is less affected by individual extreme outliers. If a cluster is tidally over-filling, the limiting radius will still be significantly larger than the tidal radius. For a cluster that is tidally under-filling, the limiting radius is simply the distance to the outermost bound star.

In Figure 2.6 we show this empirically determined r_L for each model as a function of time. For circular orbits, on average the limiting radius of the cluster decreases smoothly as a result of mass loss. For eccentric orbits, the small fluctuations with perigalactic passes in Figures 2.3 and 2.4 are much more prevalent in Figure 2.6. Comparing Figure 2.5 to Figure 2.6, the fluctuations in both figures indicate that the limiting radius behaves the same as the instantaneous tidal radius.

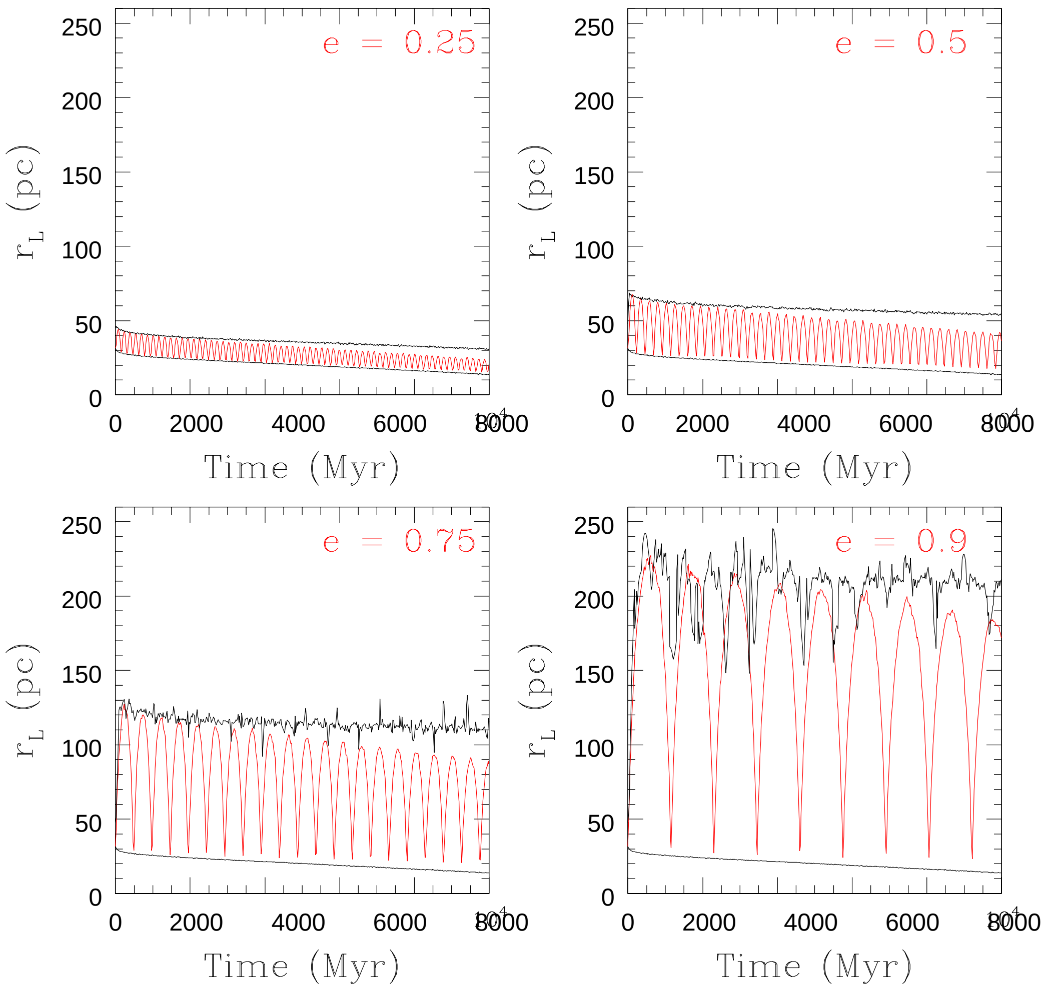

Figure 2.6 The evolution of the limiting radius over time. The red lines correspond to models with orbital eccentricities as labelled in each panel. In each plot, the lower black line corresponds to a cluster with a circular orbit at perigalacticon (6 kpc), while the upper black line corresponds to a cluster with a circular orbit at apogalacticon.

It should be noted that the apogalactic cases for e = 0.75 and 0.9 in Figure 2.6 are not smooth due to the fact that these clusters are barely tidally filling and their limiting radii are easily influenced by individual escaping stars.

Directly comparing limiting radii in Figure 2.6 and tidal radii in Figure 2.5, all circular orbits have a relatively constant ratio at approximately $\frac{r_L}{r_t} = 1.1$. Since we expect r_L to slightly overestimate r_t, a ratio of 1.1 suggests that these clusters are approximately tidally filling. For eccentric clusters the ratio is in general also 1.1, suggesting the clusters come close to filling their instantaneous tidal radius at all times. Fluctuations in the ratio for the e = 0.75 and 0.9 cases indicate that after a perigalactic pass the cluster is slightly tidally under-filling and works to fill its instantaneous tidal radius on the way to apogalacticon. When travelling back in from apogalacticon to perigalacticon, the cluster will remain tidally filled and lose stars to tidal stripping as the instantaneous tidal radius shrinks.

2.4 Influence of Initial Cluster Half-Mass Radius

Up until this point we have only considered clusters with initial half-mass radii of 6 pc. This initial half-mass radius was chosen simply to ensure that the model clusters with $R_p = 6$ kpc would be tidally filling. As seen in Figure 2.4 this produces clusters with sizes at 10 Gyr ranging from 3 to 14 pc, which are larger than most (but not all) real globular clusters. In an attempt to produce Milky Way-like clusters which have a mean effective radius of 2.5 pc, we re-simulated the e0r6rm6, e05r18rm6, and e0r18rm6 models with initial

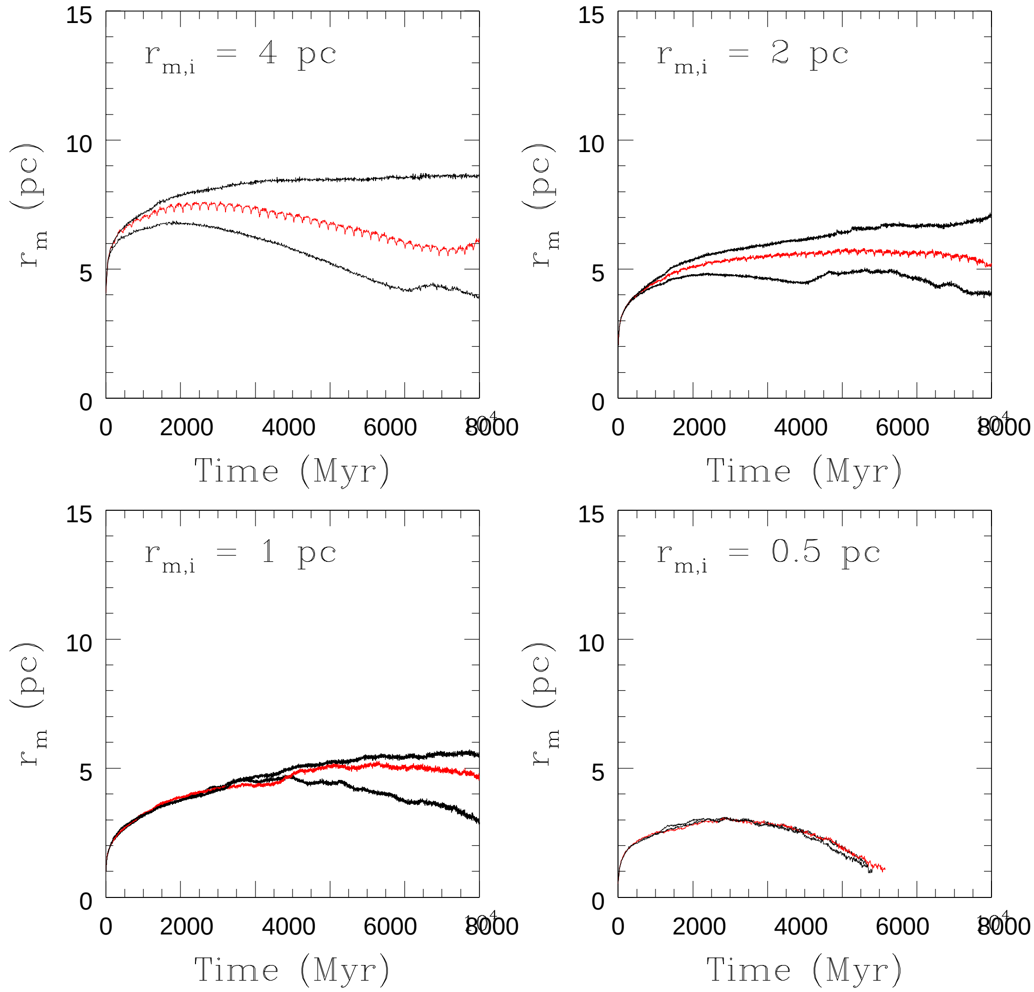

Figure 2.7 The evolution of half mass radius over time. The upper left, upper right, lower left, and lower right panels are for simulations with initial half mass radii of 4 pc, 2 pc, 1 pc, and 0.5 pc respectively. The red lines correspond to models with orbital eccentricities of 0.5, while the lower black lines correspond to a cluster with a circular orbit at perigalacticon (6 kpc) and the upper black lines correspond to a cluster with a circular orbit at apogalacticon (18 kpc).

half-mass radii of 4 pc, 2 pc, 1 pc, and 0.5 pc. The results are shown in plots of half mass radius versus time in Figure 2.7.

The rm4 clusters closely resemble the rm6 clusters, with similar periodic fluctuations with perigalactic passes and the final r_m values for the perigalactic, eccentric, and apogalactic cases. However, the rm4 clusters undergo smaller initial expansion due to two-body interactions than the rm6 clusters, and thus when outer region stars are being removed through tidal stripping, since the majority of the mass is concentrated in the inner region, the mass-loss profile is less affected.

This issue of initial size becomes even more significant in the rm2, rm1, and rm05 cases. The periodic fluctuations on the eccentric orbit are barely visible in the rm2 cluster, and non-existent in the rm1 and rm05 clusters. The rm1 cases are significantly smaller at 10 Gyr, approaching the typical ~ 2 - 3 pc size that match the majority of real globular clusters. The rm05 models have completely dissolved by 10 Gyr.

These small clusters are only tidally filling in the sense that two-body interactions have pushed *some* bound stars to orbits that take them out to the instantaneous tidal radius. With the majority of the bound stars located in the inner regions of the cluster, tidal stripping is not the dominant form of mass loss and the influence of the galactic potential and cluster orbit are minimized. Instead, stellar evolution and two-body interactions are the dominant forms of mass loss. These clusters would be classified as "tidally unaffected" (Carballo-Bello et al., 2012). For the rm1 case, the r_m profiles of the perigalactic, eccentric, and apogalactic cases begin to split only after ~ 5 Gyr, when stars have been finally pushed to the outer regions of the cluster and tidal stripping is beginning to play an important role. While this is true, it is not due to two-body interactions but instead a result of core collapse. For the rm05 case, not even core collapse can push stars to the outer region of the cluster in order for tidal stripping to occur. In fact, the rm05 clusters all have the same r_m up until the complete evaporation of the cluster at approximately

7 Gyr.

Producing Milky Way-like globular cluster effective radii of 2 - 3 pc for clusters on circular orbits at 6 kpc or greater appears to require initial r_m size less than 1 pc. The N-body models reveal that either clusters originally are extremely compact and tidally unaffected, or present-day cluster orbits have changed significantly from the orbit along which the clusters originally formed. Some observational support for this view can be found in recent measurements of very young, massive clusters (e.g. Bastian et al., 2008, 2012; Portegies Zwart et al., 2010; Marks & Kroupa, 2010). However, recent N-body simulations by Sippel et al. (2012) showed that r_h and r_m can be very different because of stellar mass segregation, and produce clusters with final r_h values near 3 pc despite large $r_{m,i}$. These issues will be explored in future studies.

2.5 Discussion

A perigalactic pass has three effects on a globular cluster, which we illustrate in Figure 2.8 for the e=0.9 model e09r104rm6. In this figure, we plot the energy per unit mass of individual stars (as per Equation 2.2) as a function of radial distance from the cluster center at 9 points in the orbit. Beginning in Panel A of Figure 2.8, for a given time between apogalacticon and perigalacticon there are a few stars that are within close proximity of the cluster but remain unbound (marked in red). As the cluster moves towards R_p and the instantaneous tidal radius shrinks (Panel B), more and more stars become temporarily unbound. As predicted in Section 3.0, even stars in the inner region of the cluster are provided with a significant increase in energy by the tidal shock and can become unbound. Just after the cluster reaches perigalacticon (Panel

C), a large number of stars are no longer bound to the cluster. As the cluster moves away from perigalacticon (Panels D to I):

- some stars that became unbound escape the cluster (which causes the initial decrease in r_m and r_L);
- some of the stars that are unbound in Panel C return to energies below zero and are recaptured (see Figure 2.9);
- the tidal shock gives stars initially found in the inner region enough additional energy to move outward and fill the orbits vacated by stars which permanently escaped the cluster (see Figure 2.10).

It is even possible for inner region stars to become temporarily or permanently unbound if they move outward at a rate faster than the instantaneous tidal radius increases.

2.6 Predicting Cluster Limiting Radii

Now that we have shown that limiting radii are not imposed at perigalacticon, it is useful to know how to calculate a meaningful number that predicts the limiting radius of a globular cluster on an eccentric orbit. As we saw in Figures 2.5 and 2.6, the limiting radius essentially traces the instantaneous tidal radius. However the ratio between cluster limiting radius and instantaneous tidal radius undergoes small periodic variations as a function of the location of a cluster along its orbit.

Orbital phase is defined as:

$$F = \frac{R_{gc} - R_p}{R_a - R_p} \tag{2.7}$$

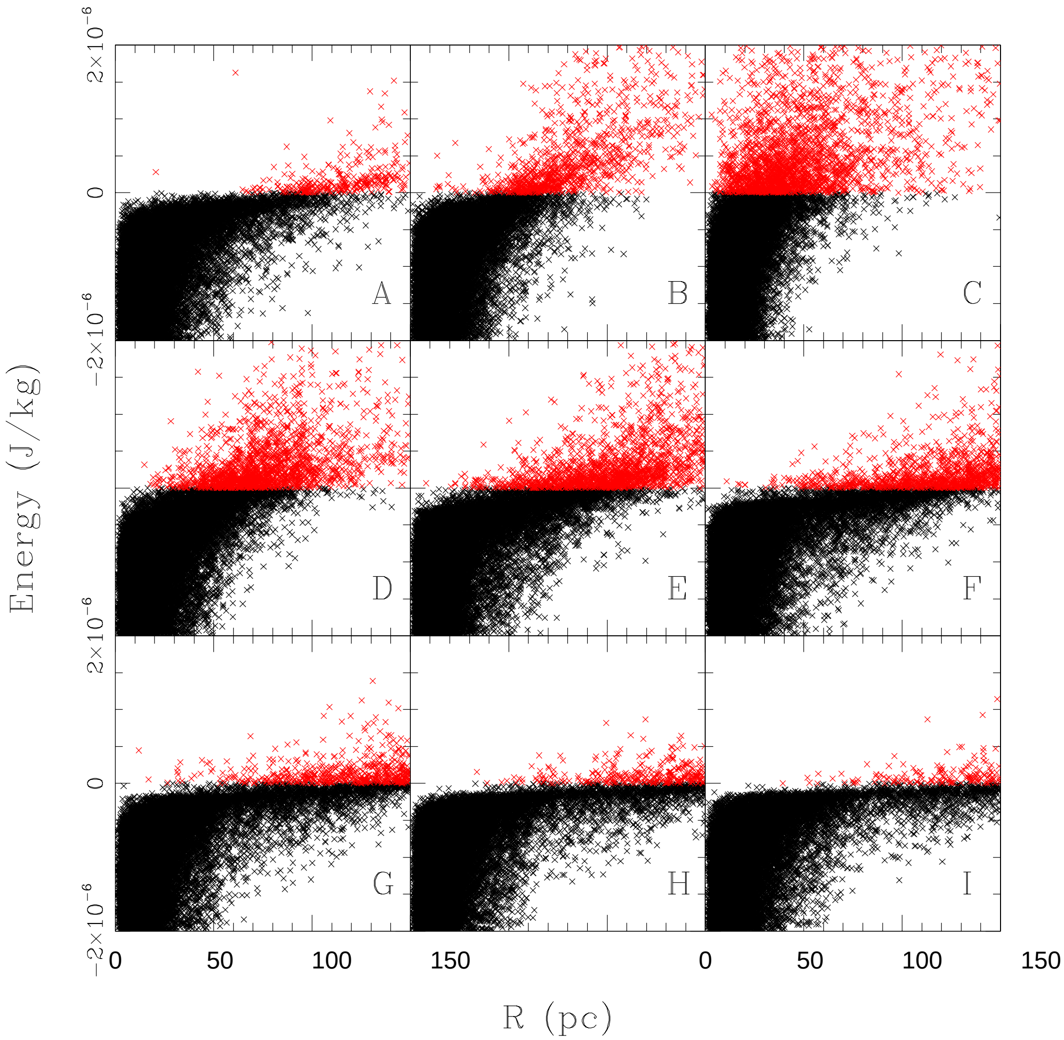

Figure 2.8 The radial distance and energy of stars within model cluster e09r104rm6 for different time steps. Beginning in Panels A and B the cluster is travelling towards perigalacticon. In Panel C the cluster has just left perigalacticon. In Panels D to I the cluster is moving away from perigalacticon. Bound stars are marked as black and unbound stars are marked as red.

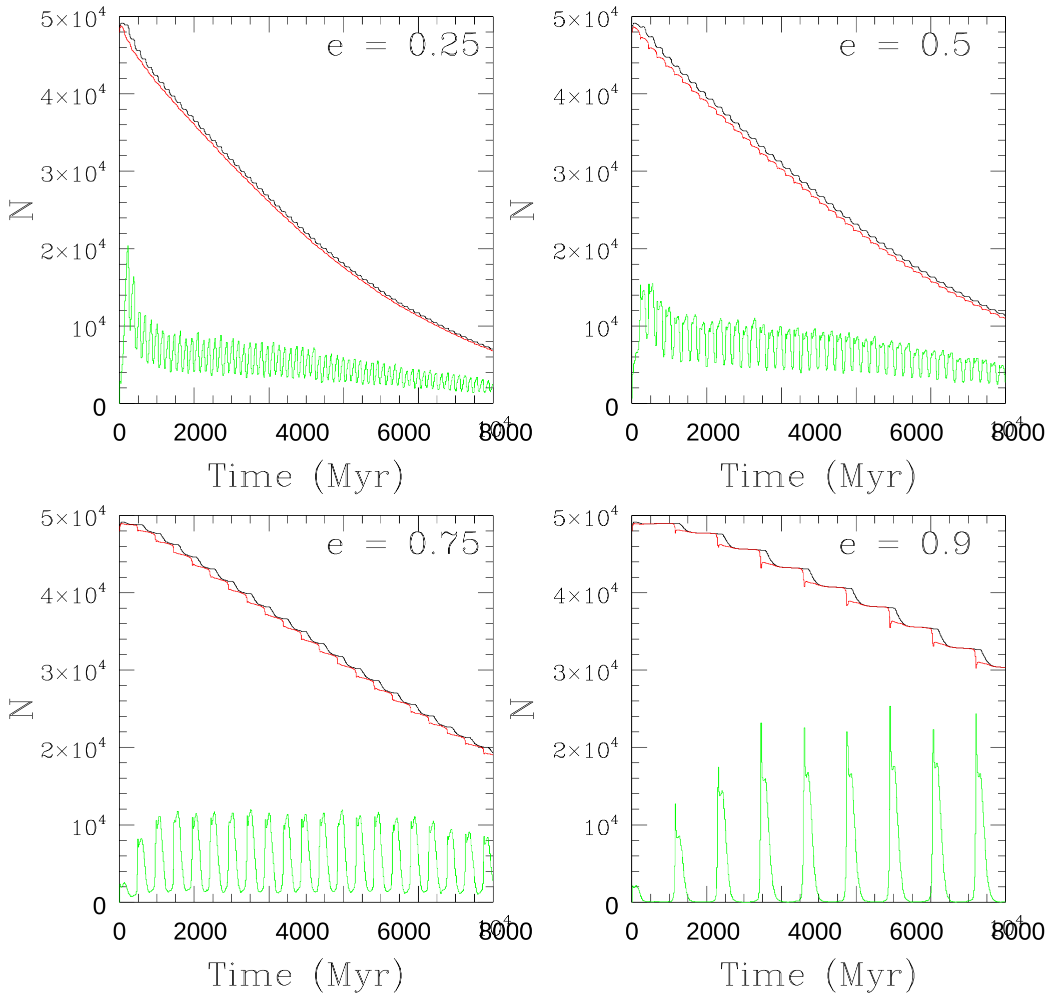

Figure 2.9 The total number of bound (red) and unbound (green) stars in a cluster as a function of time. The black line corresponds to the total number of stars and the orbital eccentricity of the model is labelled in each panel. For comparison purposes, the number of unbound stars has been increased by a factor of 10.

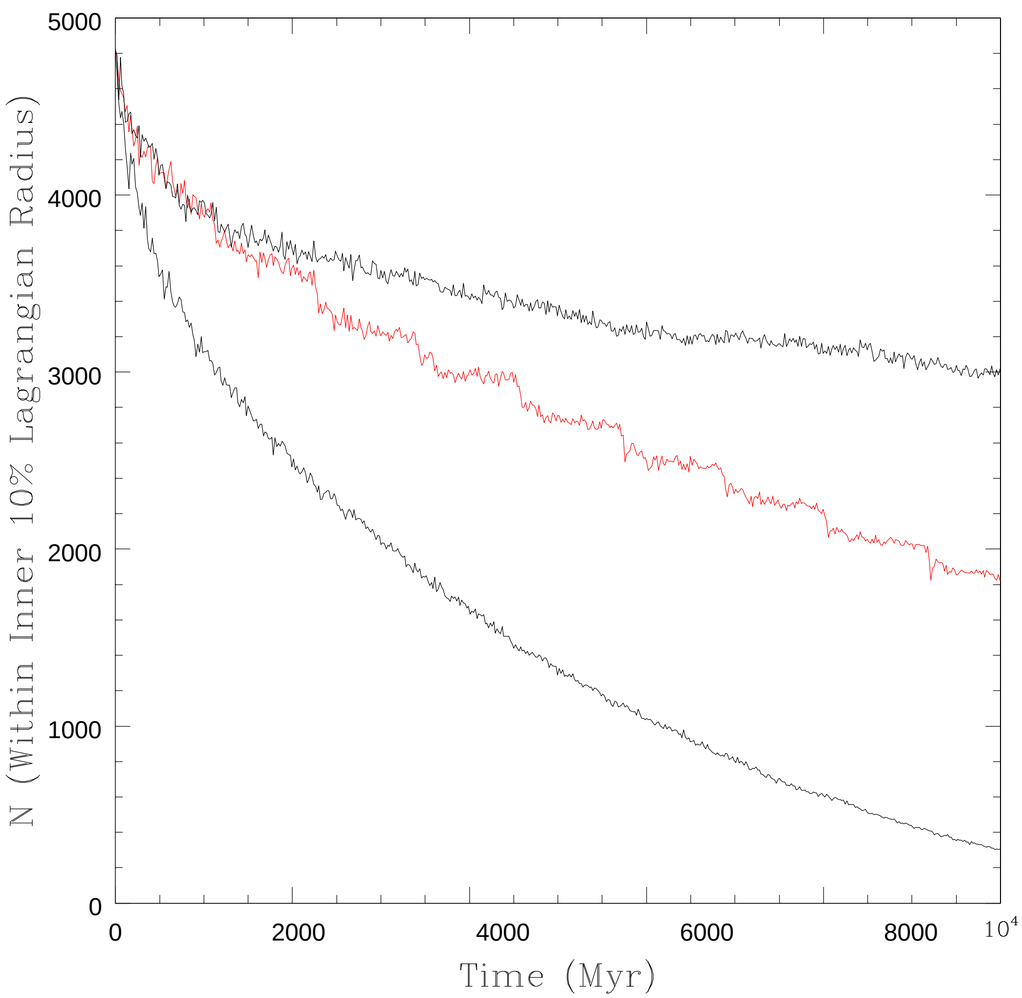

Figure 2.10 The evolution of the number of stars within the inner 10 % Lagrangian radius over time. The red line correspond to the e=0.9 model (e09r104b). The lower black line corresponds to a cluster with a circular orbit at perigalacticon (6 kpc), while the upper black line corresponds to a cluster with a circular orbit at apogalacticon (104 kpc). The number of stars within the inner 10 % Lagrangian radius will naturally decrease over time due to two-body encounters, however the eccentric case (red line) illustrates that with each perigalactic pass a significant number of stars move beyond the inner 10 % Lagrangian radius.

such that the cluster has $F = 0$ at perigalacticon and $F = 1$ at apogalacticon. A cluster with a circular orbit will always have $F = 0$. The median limiting radius of the eccentric cluster as a function of orbital phase is then determined in order to calculate the ratio of the instantaneous limiting radius to the limiting radius of the e = 0 perigalactic case ($\frac{r_L(e)}{r_L(e=0)}$), both normalized by mass. This ratio is plotted as a function of phase in Figure 2.11. It is important to note that we have ignored the first 2000 Myr of evolution for each model cluster when evaporation due to two-body relaxation is the dominant source of mass loss.

For a given orbital eccentricity, $\frac{r_L(e)}{r_L(e=0)}$ changes almost linearly with phase F. It is interesting to note that we observed a second order effect that the rate at which the cluster expands is lower than the rate at which it contracts. When the cluster is moving away from perigalacticon, it works to fill its expanding tidal radius. Conversely a cluster moving towards perigalacticon would be larger as it is always tidally filling on the way inward.

The *rate* at which the limiting radius of the cluster increases and decreases as a function of orbital phase is a strong function of orbital eccentricity. These rates were determined explicitly by finding the slopes of each line, where the y-intercept is forced to equal one. The slopes are listed in Table 2.2, along with the associated uncertainty (1σ).

Table 2.2: Lines of Best Fit

Orbital Eccentricity	Slope	Uncertainty
0.25	0.512	0.007
0.5	1.29	0.04
0.75	3.37	0.07

0.9	7.84	0.07

A smooth relationship between slope and eccentricity emerges, that can be fit with an exponential, and allows us to propose a purely analytical correction to the calculation of the tidal radius of a globular cluster. For a globular cluster on an orbit with eccentricity E, with a tidal radius at perigalacticon $r_t(R_p)$ and located at a phase F in its orbit, its limiting radius is equal to

$$r_L(F) = r_t(R_p)(1 + a\ F\ e^{b\ E}) \tag{2.8}$$

where $a = 0.17 \pm 0.03$ and $b = 4.1 \pm 0.2$. Note that since this calculation involves a single cluster over the course of a single orbit, the mass normalization is no longer necessary as cluster mass will not have changed significantly over a fraction of one orbit.

The next step is to simulate a larger suite of model clusters ranging in initial cluster mass and half-mass radii to determine if these parameters play a role in the correction factor suggested above. However, regardless of the influence of cluster mass or initial half-mass radius, all tidally affected simulations follow the rule that the limiting radius traces the instantaneous tidal radius rather well. Thus if full orbital information or phase F is unknown, the calculation of the instantaneous tidal radius is a reasonable estimate of the limiting radius of a cluster. For globular clusters in other galaxies, in which only their projected galactocentric distances are known, it may be possible to determine their theoretical tidal radius based on their present King radius r_k. Future work will explore this possibility.

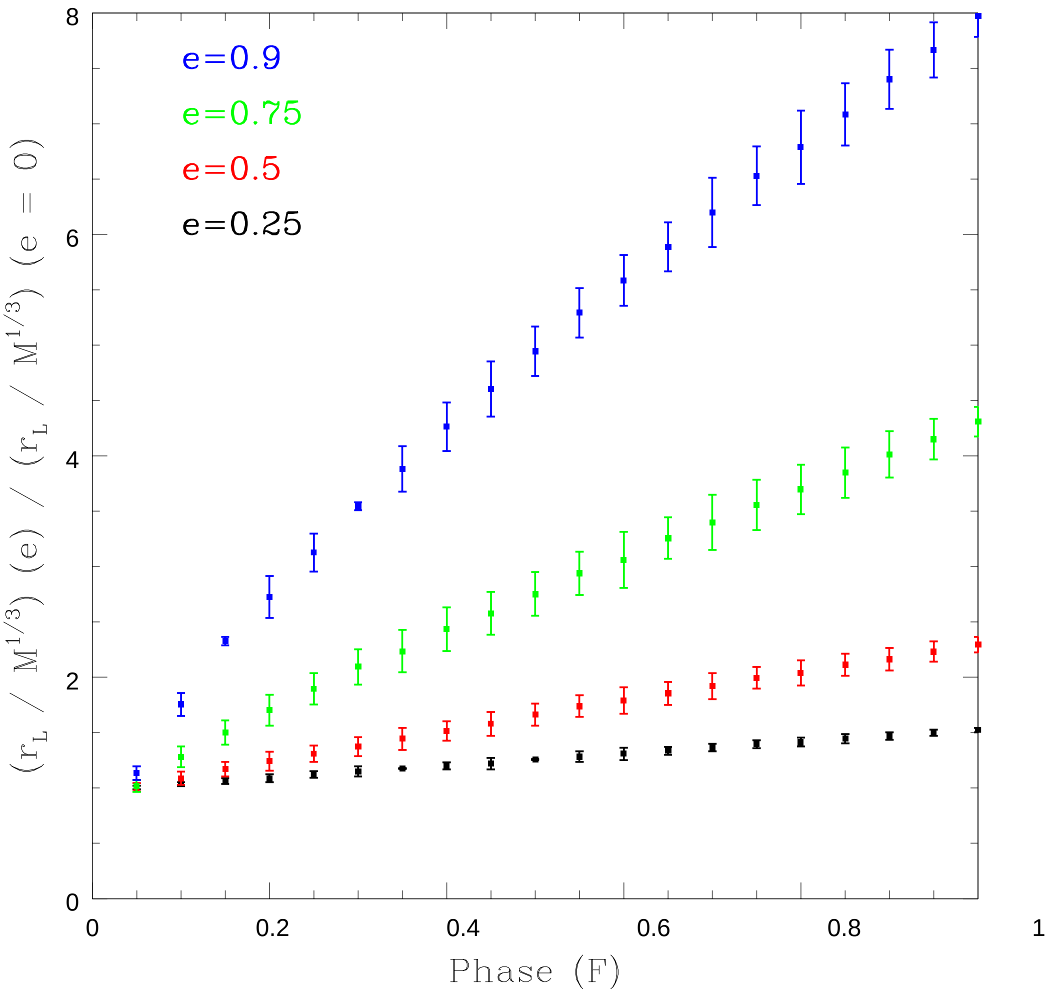

Figure 2.11 The ratio of the mass normalized limiting radius of model clusters with eccentric orbits to the mass normalized limiting radius of a cluster with a circular orbit at perigalacticon as a function of orbital phase as defined in Equation 2.7. Error bars represent an uncertainty of 1σ.

2.6.1 Application to the Milky Way

For many Milky Way globular clusters, their current galactocentric distance, orbital eccentricity and orbital phase are known. In Figure 2.12 the revised, fully corrected version of Figure 2.1 is illustrated, where r_L is now the phase-corrected value from Equation 2.8. We now see more tidally under-filling clusters and the scatter of points more nearly around zero. A stronger agreement between theory and observations emerges. Correcting for using a non-spherically symmetric potential in calculating tidal radii and improved methods for determining observational limiting radii will likely strengthen this comparison further.

2.7 Conclusions and Future Work

Globular clusters have been simulated with a range of both circular and eccentric orbits. After determining which stars are bound to the cluster at a given time, we show that while eccentric clusters undergo episodes of significant mass loss during a perigalactic pass, their time averaged mass loss rate reflects a tidal field less than the tidal field at perigalacticon. Additionally it was found that clusters are able to re-capture unbound stars after a perigalactic pass as their instantaneous tidal radius increases.

Second, we show that the half-mass radius of a globular cluster increases and decreases about a mean value over the course of an orbit. These fluctuations suggest that the perigalactic pass also has the effect of energizing inner region stars to larger orbits. Finally, we find that the limiting radius of a cluster traces its instantaneous tidal radius at all times.

These findings argue against the historical assumption that globular

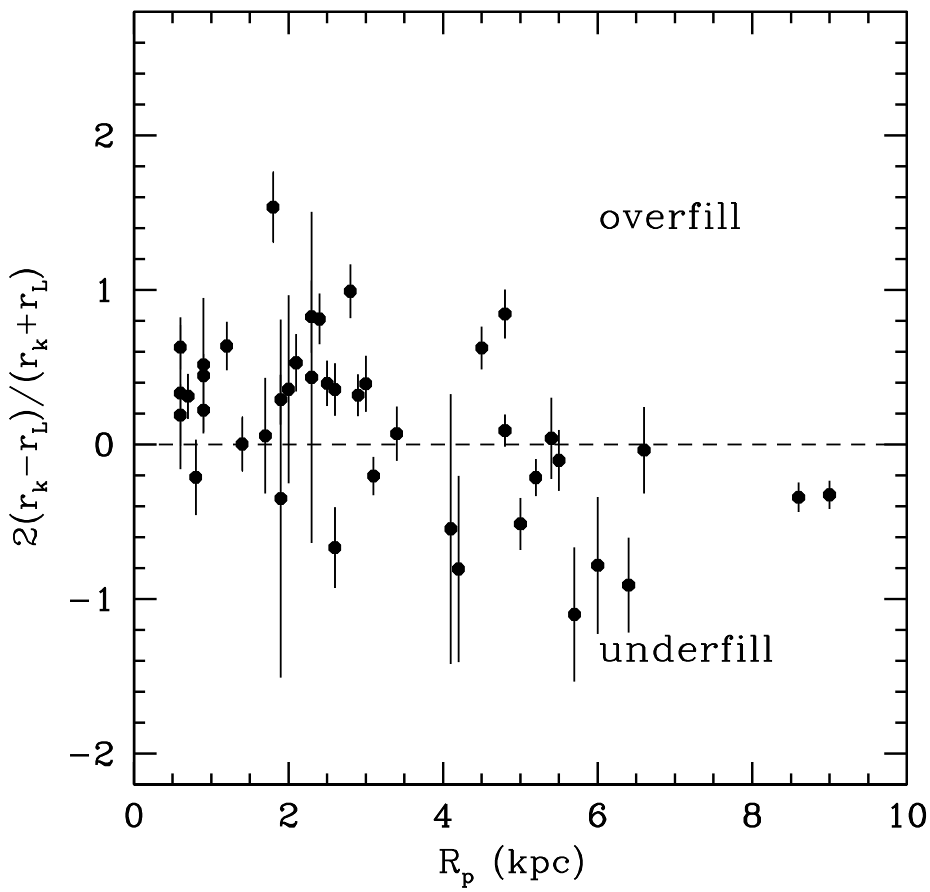

Figure 2.12 Ratio of difference between fitted King (1962) radius (r_k) and limiting radius (r_L) to the average of the two radii versus perigalactic distance for Galactic globular clusters. Limiting radii have been calculated based on the orbital eccentricity and phase of a cluster as given by Equation 2.8.

cluster tidal radii, and by extension limiting radii, are imposed at perigalacticon for clusters that do not have circular orbits. While it remains true that the half-mass relaxation time is greater than one orbital period, the cluster does not need to fully relax in order to expand. The eccentric orbit introduces an effect of tidal shocking that is not experienced by clusters in a static potential (circular orbit).

While the instantaneous tidal radius is a useful first approximation of the limiting radius, we have proposed an analytically determined correction factor that is a function of orbital eccentricity and phase. This correction leads to a much stronger agreement between the predicted limiting radii and observational King (1962) radii of Milky Way globular clusters. Future studies will explore how the correction factor depends on initial mass or initial half-mass radius and how corrected limiting radii are related to King radii.

Since the tidal field of the Milky Way is not spherically symmetric, correcting limiting radii based on eccentricity and orbital phase is not the final step. We still need to correct for orbital inclination to account for factors like disk shocking and tidal heating, which may reveal important effects for the Milky Way and other disk galaxies. However, the present results already have clear applicability to elliptical galaxies, which have more nearly spherical potentials. We are currently investigating N-body simulations in these directions. The ultimate goal is to be able to predict the limiting radius of any tidally affected globular cluster, given its orbit, galactocentric position and the galactic potential of the host galaxy.

2.8 Acknowledgements

JW would like to acknowledge funding through the A. Boyd McLay Ontario Graduate Scholarship. JW would also like to thank Juan P. Madrid and Anna Sippel for valuable discussions and correspondence. AS and WEH acknowledge financial support through research grants from the Natural Sciences and Engineering Research Council of Canada.

Bibliography

Aarseth, S.J. 2003, Gravitational N-body Simulations: Tools and Algorithms (Cambridge Monographs on Mathematical Physics). Cambridge University Press, Cambridge

Aarseth, S., Hénon, M., Wielen, R., 1974, å, 37, 183

Bastian, N., Gieles, M., Goodwin, S. P., Trancho, G., Smith, L. J., Konstantopoulos, I., Efremov, Y, MNRAS, 389, 223

Bastian, N., Adamo, A., Gieles, M., Silva-Villa, E., Lamers, H. J. G. L. M., Larsen, S. S., Smith, L. J., Konstantopoulos, I., Zackrisson, E., MNRAS, 419, 2606

Bertin, G. & Varri, A. L. 2008, ApJ, 689, 1005

Binney, J. & Tremaine, S. 2008, Galactic dynamics second edition (Princeton, NJ, Princeton University Press, 1987, 747 p.)

Brosche, P., Odenkirchen, M., Geffert, M. 1999, New Astron., 4, 133

Carballo-Bello, J.A., Gieles, M., Sollima, A., Koposov, S., Martnez-Delgado, D. & Penarrubia, J. 2012, MNRAS, 419, 14

Casetti-Dinescu, D.I., Girard, T.M., Herrera, D., van Altena, W.E., López, C.E., Castillo, D.J. 2007, AJ, 134, 195

Davis, D. S., Richer, H. B., Anderson, J., Brewer, J., Hurley, J., Kalirai, J. S., Rich, R. M., Stetson, P. B. 2008, AJ, 135, 2155

Dinescu, D.I., Girard, T.M., van Altena, W.E. 1999, AJ, 117, 1792

Duquennoy, A. & Mayor, M. 1991, å, 248, 485

Fall, S. M. & Zhang, Q., 2001, ApJ, 561, 751

Gieles, M., Baumgardt, H., Heggie , D. C., Lamers, H.J.G.L.M. 2010, MNRAS, 408, L16

Harris, W. E. 1996, AJ, 112, 1487, 2010 Edition

Hegie, D.C. 1975, MNRAS, 173, 729

Heggie, D. C. & Giersz, M. 2012, MNRAS, 397, 46

Hurley, J.R. 2008a, Lecture Notes in Physics, 760, The Cambridge N-body Lectures. Springer-Verlag, Berlin, p.283

Hurley, J.R. 2008b, Lecture Notes in Physics, 760, The Cambridge N-body Lectures. Springer-Verlag, Berlin, p.321

Hurley, J. R. & Shara, M. M. 2012, MNRAS, 425, 2872

Innanen, K. A., Harris, W.E., Webbink, R.F. 1983, AJ, 88, 338

Johnston, K.V., Spergel, D.N., Hernquist, L. 1995, ApJ, 451, 598

Jórdan, A., Côté, P., Blakeslee, J. P., Ferrarese, L., McLaughlin, D. E. , Mei, S., Peng, E. W., Tonry, J. L., Merrit, D., Milosavljević, M., Sarazin, C. L., Sivakoff, G. R., West, M. J., 2005, ApJ, 634, 1002

King, I. R. 1962, AJ, 67, 471

King, I. R. 1966, AJ, 71, 64

Kroupa, P., Tout C.A., Gilmore, G. 1993, MNRAS, 262, 545

Küpper, A. H. W, Kroupa, P, Baumgardt, H., Heggie , D. C., 2010, MNRAS, 407, 2241

Küpper, A. H. W, Lane, R. R., Heggie , D. C., 2012, MNRAS, 420, 2700

Lane, R. R., Küpper, A. H. W, Heggie , D. C., 2012, MNRAS, 426, 797L

Madrid, J.P., Hurley, J.R., Sippel, A.C., 2012, ApJ, 756, 167

Marks, M. & Kroupa, P. 2010, MNRAS, 406, 2000

McLaughlin, D. E. & van der Marel, R. P. 2005, ApJS, 161, 304

Miyamoto, M. & Nagai, R. 1975, PASJ, 27, 533

Montuori, M., Capuzzo-Dolcetta, R., Di Matteo, P., Lepinette, A., & Miochhi, P., 2007, ApJ, 659, 1212

Odenkirchen, M., Grebel, E. K., Dehnen, W., Rix, H., Yanny, B., Newberg, H. J., Rockosi, C. M., Martínez-Delgado, D., Brinkmann, J., Pier, J.R. 2003, AJ, 126, 2385

Odenkirchen, M., Grebel, E. K., Rockosi, C. M., Dehnen, W., Ibata, R., Rix, H., Stolte, A., Wolf, C., Anderson, J. E., Bahcall, N., et al. 2001, ApJ, 548L, 165

Odenkirchen, M., Brosche, P., Geffert, M., Tucholke, H. -J. 1997, New Astron., 2, 477

Plummer, H.C. 1911, MNRAS, 71, 460

Portegies Zwart, S. F., McMillan, S. L. W., Gieles, M., 2010, ARA&A, 48, 431

Praagman, A., Hurley, J., Power C. 2010, New Astron., 15, 46

Read, J. I., Wilkinson, M. I., Evans, N. W., Gilmore, G., Kleyna, J. T., 2006, MNRAS, 366, 429

Renaud, F., Gieles, M., Christian, M. 2011, MNRAS, 418, 759

Sippel, A.C., Hurley, J.R., Madrid, J.P., Harris, W.E. 2012, MNRAS, 427, 167

Takahashi, K. & Baumgardt, H. 2012, MNRAS, 420, 1799

von Hoerner, S. 1957, ApJ, 125, 451

Webb, J. J., Sills, A., Harris, W.E. 2012, ApJ, 746, 93

Xue, X.X. et al., 2008, ApJ, 684, 1143

Zonoozi, A. H., Küpper, A. H. W, Baumgardt, H., Haghi, H., Kroupa, P., Hilker, M. 2011, MNRAS, 411, 1989

Chapter 3

The Effect of Orbital Eccentricity on the Dynamical Evolution of Star Clusters

Jeremy J. Webb, Nathan Leigh, Alison Sills, William E. Harris, Jarrod R. Hurley

Monthly Notices of the Royal Astronomical Society, Volume 442, Issue 2, pages 1569-1577,

Bib. Code: 2014MNRAS.442.1569W, DOI: 10.1093/mnras/stu961

3.1 Introduction

Massive star clusters in the Milky Way (MW), called globular clusters (GCs), have typical total masses and ages ranging from $\sim 10^4$ - 10^6 $M_\odot$ and $\sim$ 10-

12 Gyrs, respectively (Harris, 1996, 2010 update; Marín-Franch et al., 2009). They have had time for their structural properties and stellar mass functions (MFs) to have been modified from their primordial forms due to both stellar evolution and stellar dynamics. Thus, in order to constrain the initial cluster conditions and mass function, simulations are needed to rewind their dynamical clocks.

The dominant mechanisms which drive the dynamical evolution of star clusters are:

- Stellar Evolution
- Two-body Relaxation
- Tidal Stripping
- Tidal Heating
- Disk Shocking

Stellar evolution is initially the main driver of dynamical evolution in a cluster as significant mass loss occurs when massive stars quickly evolve off the main sequence and go supernova. After 2-3 Gyr, two-body relaxation, the cumulative effects of long-range gravitational interactions between stars acting to alter stellar orbits within the cluster, becomes dominant (e.g. Henon, 1961, 1973; Spitzer, 1987; Heggie & Hut, 2003; Gieles, Heggie & Zhao, 2011). The most massive stars accumulate in the central cluster regions, and the lowest mass stars are dispersed to wider orbits. The re-distribution of low and high mass stars, known as mass segregation, is also a source of mass loss with the probability of ejection past the tidal boundary increasing with decreasing stellar mass. Therefore, two-body relaxation will slowly modify the distribution of stellar masses within clusters, and can cause very dynamically evolved clusters to appear severely depleted of their low-mass stars (e.g. von Hippel & Sarajedini, 1998; Koch et al., 2004; De Marchi, Paresce & Portegies Zwart, 2010).

Tidal stripping is the removal of stars from a cluster by the host galaxy. The galactic potential imposes a theoretical boundary around a globular cluster, known as the tidal radius r_t or the Jacobi radius r_J. Beyond r_t, a star will feel a greater acceleration towards the galaxy center than it feels towards the center of the cluster, and will therefore escape (Binney & Tremaine, 2008). For clusters subject to a strong tidal field, stripping serves to both accelerate mass loss and minimize cluster size.

Tidal heating is an effect only experienced by clusters which experience a non-static tidal field, and so only applies to clusters with eccentric orbits or circular orbits in non-spherically symmetric potentials. The non-static tidal field injects energy into the stellar population of a globular cluster and the kinetic energy of individual stars increases. Energy injection leads to both the energization of stars to larger orbits and the ejection of stars that would otherwise remain bound to the cluster. The effects of energy injection are strongest during a perigalactic pass where the cluster experiences a sudden and dramatic increase in the local potential (Spitzer, 1987; Webb et al., 2013). Disk shocking is a specific and extreme form of tidal heating, similar to a perigalactic pass, as the local potential changes dramatically when the cluster passes through the Galactic disk.

While stellar evolution, two-body relaxation and tidal stripping have all been well studied for GCs in isolation and on circular orbits in realistic potentials, how these mechanisms change as a function of orbital eccentricity remains unclear. The purpose of this study is to determine how tidal heating, due to a non-circular orbit in a disk potential, and energy injection during perigalactic passes can influence both relaxation and mass loss due to tidal stripping. All of the Galactic GCs with solved orbits are non-circular (Dinescu et al., 1999; Casetti-Dinescu et al., 2007, 2013), therefore understanding the effects of orbital eccentricity are key to any future studies of GCs.

We evolve model N-body clusters for 12 Gyr with a range of orbits in a Milky Way-like potential. Clusters with different orbits experience different degrees of tidal stripping and tidal heating, which can have significant effects on both the low-mass stellar population in the outer regions of the cluster and cluster density. In Section 3.2 we discuss the N-body models used in this paper. To study how orbital eccentricity can alter the dynamical evolution of a cluster, we investigate the effect that tidal heating has on cluster mass loss rate (Section 3.3), velocity dispersion (Section 3.4), relaxation time (Section 3.5), and the stellar MF (Section 3.6). Within Section 3.6, the evolution of the MF in different regions of the cluster is also discussed. Finally in Section 3.7, we illustrate how present day characteristics of GCs can be used to provide constraints on cluster orbits. We then place constraints on the orbits of specific GCs that remain unsolved. We summarize our results in Section 3.8.

3.2 N-body models

We use the NBODY6 direct N-body code (Aarseth , 2003) to study the evolution of model star clusters over 12 Gyr. The models in this study begin with 96000 single stars and 4000 binaries and have a total initial mass of $6 \times 10^4 M_\odot$.

Since we are only concerned with the influence of orbital eccentricity on cluster evolution, only the initial position and initial velocity vary from model to model while all other parameters remain unchanged.

A Kroupa, Tout, & Gilmore (1993) IMF between 0.1 and 30 $M_\odot$ is used to assign masses to individual stars, all with a metallicity of $Z = 0.001$. For binary stars, the total mass of the binary is set equal to the mass of two randomly selected stars. The mass-ratio between the primary and secondary masses is then randomly selected from a uniform distribution. The distribution of Duquennoy & Mayor (1991) is used to set the initial period of each binary and orbital eccentricities are assumed to follow a thermal distribution (Heggie , 1975). Initial positions and velocities of the stars are based on a Plummer density profile (Plummer , 1911; Aarseth et al., 1974) with a cut-off at $\sim 10\ r_m$ to avoid the rare case of stars positioned at large cluster-centric distances. The initial half-mass radius $r_{m,i}$ of each model is 6 pc. The algorithms for stellar and binary evolution are described in Hurley (2008a,b).

The Galactic potential is made up of a $1.5 \times 10^{10} M_\odot$ point-mass bulge, a $5 \times 10^{10} M_\odot$ Miyamoto & Nagai (1975) disk (with $a = 4.5\,\mathrm{kpc}$ and $b = 0.5\,\mathrm{kpc}$), and a logarithmic halo potential (Xue et al., 2008). The combined mass profiles of all three components force a circular velocity of 220 km/s at a galactocentric distance of 8.5 kpc. The incorporation of the Galactic potential into NBODY6 is described by Aarseth (2003) and Praagman, Hurley, & Power (2010). In order for the model clusters to experience a spherically symmetric tidal field they were set to orbit in the plane of the disk, eliminating factors such as disk shocking or tidal heating due to a non-spherically symmetric potential.

Since we are only focussed on stars that are energetically bound to the cluster, the simulation eliminates stars with $r > 2\ r_t$, where r_t is the King

(1962) tidal radius. We then calculate the total energy of each star given its kinetic energy, the potential energy due to all other stars in the cluster, and the tidal potential (Bertin & Varri, 2008; Webb et al., 2013). Stars with $E > 0$ are considered to be unbound, and are not included in calculations of cluster parameters. It should be noted that a star with $E > 0$ can be recaptured at a later time if it does not travel beyond 2 r_t.

We first simulate three clusters with orbital eccentricities of 0 (circular orbit), 0.5, and 0.9, where eccentricity is defined as $e = \frac{R_a - R_p}{R_a + R_p}$. R_a and R_p are the apogalactic and perigalactic distance of the orbit, respectively. All three models have an R_p equal to 6 kpc and are located at R_p at time zero. For comparison purposes we also simulate two additional models with circular orbits at the apogalacticon of the $e = 0.5$ and $e = 0.9$ models, corresponding to orbits at 18 kpc and 104 kpc, respectively. Therefore we can directly compare the properties of a cluster on an eccentric orbit to clusters on circular orbits at both R_p and R_a.

The initial model parameters are summarized in Table 4.1, with model names based on orbital eccentricity (e.g. e05) and either circular radius or radius at apogalacticon (e.g. r18).

Table 3.1: Model Input Parameters

Model Name	$r_{m,i}$	R_p	v_p	e
	pc	kpc	km/s	
e0r6	6	6	212	0
e05r18	6	6	351.5	0.5
e0r18	6	18	232	0
e09r104	6	6	543.5	0.9

e0r104	6	104	225.25	0

3.3 Mass Loss Rate

The most important characteristic of a globular cluster is its total mass, as it sets r_t, the relaxation time t_{rh} and velocity dispersion σ_V of the cluster. Since our models all start with the same initial mass, the key feature which sets the models apart is their mass loss rate. Mass loss due to stellar evolution will be identical from model to model, however mass loss due to tidal stripping is orbit dependent since r_t is a function of the instantaneous galactocentric distance R_{gc} of a cluster. The total mass (left panel) and mass loss rate (right panel) of each model is plotted in Figure 3.1.

In Figure 3.1, the mass loss rate of a GC on a circular orbit increases with decreasing R_{gc}, resulting in the present day mass of inner clusters (e0r6) to be much less than outer clusters (e0r104). The relationship between mass loss rate and R_{gc} is expected as r_t decreases linearly with R_{gc}. A stronger tidal field and smaller r_t results in outer stars being easily removed from the cluster. The only exception to this rule is when a cluster is not tidally filling.

As shown in Webb et al. (2013), clusters fill their instantaneous tidal radius at all times, independent of their orbital phase. That is to say there will always be energetically bound stars at or near r_t. However the degree to which a cluster is tidally filling depends on the ratio $\frac{r_h}{r_t}$, where a cluster can be approximated to be tidally filling if $\frac{r_h}{r_t} > 0.145$ (Henon, 1961). The fraction $\frac{r_h}{r_t}$ indicates whether the bulk of the cluster is centrally concentrated and only a

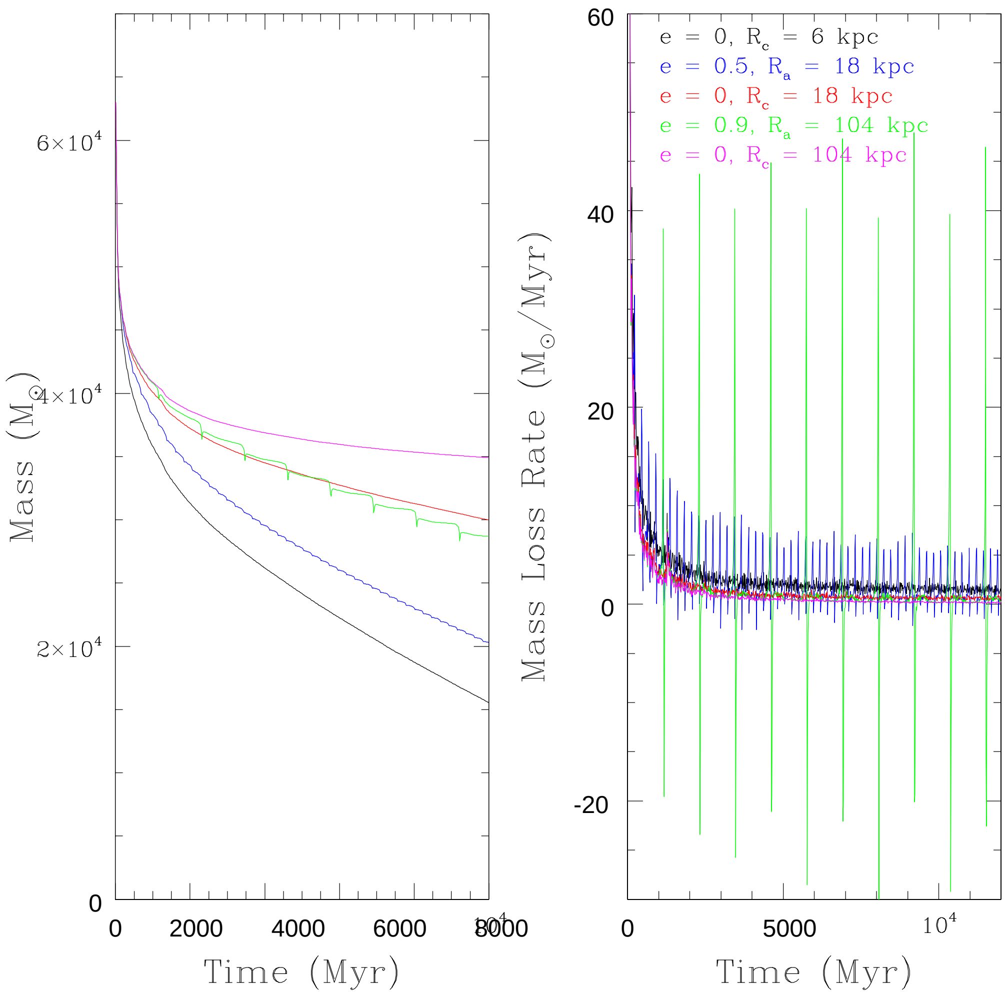

Figure 3.1 Mass (left) and mass loss rate (right) of each model cluster as a function of time. Models are separated by colour as indicated.

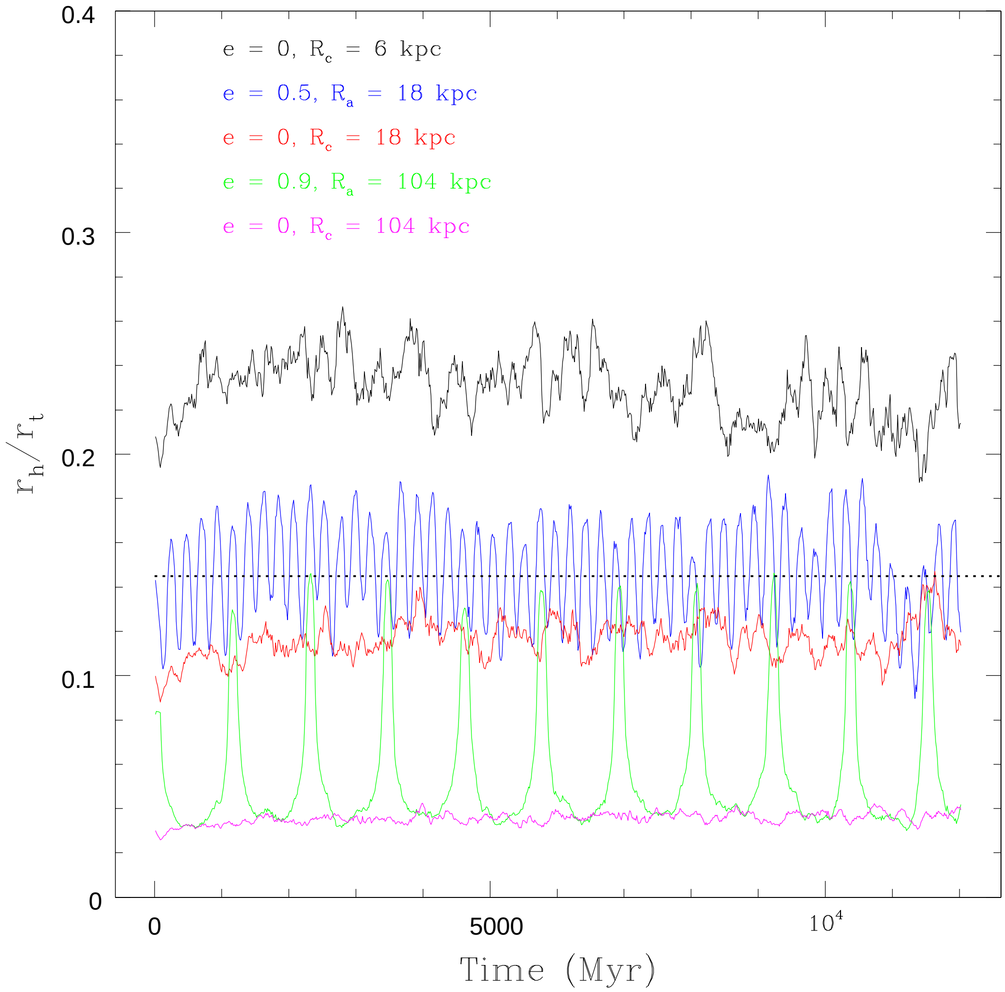

Figure 3.2 Ratio of $\frac{r_h}{r_t}$ as a function of time. Models are separated by colour as indicated. The dotted line indicates a value of 0.145.

few outer stars are affected by the tidal field (tidally under-filling) or if stars are more uniformly spread out between the cluster center and r_t. $\frac{r_h}{r_t}$ is plotted as a function of time for each model cluster in Figure 3.2.

Tidally under-filling clusters, like e0r014, will therefore have a lower mass loss rate at a given R_{gc} than if $\frac{r_h}{r_t} > 0.145$. Mass loss in under-filling GCs is primarily driven by stellar evolution and close two-body interactions occurring primarily in the dense cluster core.

The mass loss rate of a GC on an eccentric orbit can be much higher than if it had a circular orbit where it is currently observed, which is most likely near R_a. For example, in the left panel of Figure 3.1 the final masses of e05r18 and e09r104 are significantly less than the apogalactic cases of e0r18 and e0r104 respectively. So despite spending the majority of its lifetime near R_a, an eccentric cluster will be lower in mass than a cluster with a circular orbit at R_a. Periodic episodes of enhanced mass loss (right panel of Figure 3.1) during a perigalactic pass are greater than the mass gained from recapturing stars as the instantaneous r_t increases while the GC travels to R_a.

It is interesting to note that e09r104 has a lower mass loss rate than e0r18 during the majority of its orbit, but e09r104 undergoes periodic episodes of mass loss at R_p that results in similar mass profiles during the first 12 Gyr of their lifetime. e0r18 and e09r104 having similar mass profiles is in disagreement with the relationship between dissolution time and cluster orbit given by Baumgardt & Makino (2003). The results of Baumgardt & Makino (2003) suggest that a cluster with an orbital eccentricity of 0.9 and perigalactic distance of 6 kpc would behave as if it had a circular orbit between 10.5 and 11.5 kpc and that e0r18 will take between 1.4 and 1.7 times longer to reach dissolution than e09r104. However, evolving our model clusters beyond 12 Gyr and defining the dissolution time as the time it takes for clusters to reach 35% of their initial mass, we find that the mass profiles eventually diverge and e0r18 takes 1.35 times longer to reach dissolution than e09r104. The slight discrepancy between our models and the results of Baumgardt & Makino (2003) can easily be attributed to our clusters having different initial conditions and orbiting in a different tidal field than those presented in Baumgardt & Makino (2003). e09r104 having a similar mass profile to e0r18 can be attributed to the clusters undergoing non-linear mass loss rates which result in both models losing similar amounts of mass over the first 12 Gyr of cluster evolution and different amounts of mass beyond 12 Gyr. Therefore we consider e09r104 to have an *effective circular orbit* R_e near 18 kpc. R_e can be thought of qualitatively as the circular orbit distance that an eccentric cluster could have and undergo the same dynamical evolution. [1]

e09r104 has a semi-major axis of 60 kpc and a time average galactocentric distance ($< R_{gc} >= \frac{1}{12Gyr} \int_0^{12Gyr} R_{gc}(t)dt$) of 73 kpc, both significantly larger than R_e. Even the time averaged galactic potential experienced by e09r104 ($< \Psi >= \frac{1}{12Gyr} \int_0^{12Gyr} \Psi(t)dt$), which is the exact same as a cluster with a circular orbit at 62 kpc, is larger than R_e. The circular orbit distance which experiences the same $< \Psi >$ as an eccentric cluster will be referred to as R_Ψ, such that $\Psi(R_\Psi) =< \Psi >$. Hence perigalactic mass loss leads to the mass loss rate of an eccentric cluster being higher than if the cluster had a circular orbit at $< R_{gc} >$, R_Ψ or with the same semi-major axis.

It should be noted that we consider e0r6 and e05r18 to be tidally filling, while e09r104 is only tidally filling near R_p. e0r18 is marginally filling, so while it is still subject to the effects of the tidal field, tidal heating and stripping will be less efficient than in tidally filling clusters. e0r104 is the only cluster that can be considered to be truly tidally under-filling over 12 Gyr, and its evolution independent of the tidal field.

[1]Unfortunately, no quantitative relationship between the orbit of e09r104 and its apparent R_e of 18 kpc could be established.

3.4 Velocity Dispersion

An observable parameter that is commonly used to study the dynamical state of a globular cluster is its global line of sight velocity dispersion σ_V (Equation 3.1)

$$\sigma_V = \sqrt{\frac{\sum\limits_{i=1}^{N} v_i^2}{N}} \tag{3.1}$$

where v_i is the line of sight velocity of individual stars. We have plotted the evolution of the global line of sight velocity dispersion of each model as a function of both time (left panel) and fraction of initial mass $\frac{M}{M_0}$ (right panel) in Figure 3.3. The velocity dispersion was calculated along a random line of sight at each time step. Comparing model clusters as a function of fraction of initial mass is equivalent to comparing clusters on the same evolutionary timescale, as the fraction of initial mass lost from the system per relaxation time due to energy equipartition-driven dynamical evolution should be approximately the same for all clusters independent of their mass, as shown by Lamers et al. (2013). It should be noted that since the model clusters are only simulated to 12 Gyr and not to dissolution, each model cluster will have lost a different fraction of its initial mass by the end of the simulation.

The trend is for the velocity dispersion of all models to decrease as they evolve, primarily due to mass loss over time. Since velocity dispersion is proportional to cluster mass and inversely proportional to size, both of which are dependent on orbit, it is difficult to relate velocity dispersion to cluster orbit when plotted as a function of time (Figure 3.3 left panel). However, if we plot velocity dispersion versus the fraction of initial mass (Figure 3.3 right

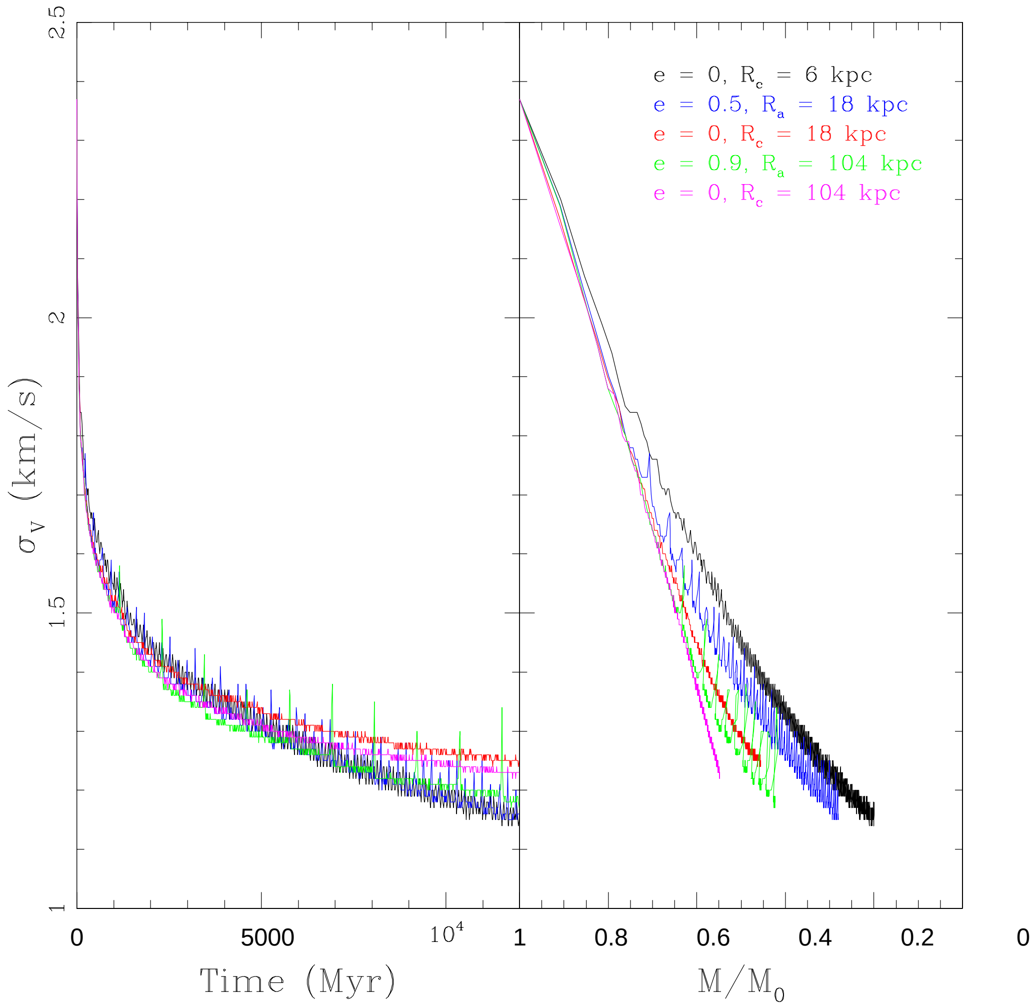

Figure 3.3 Velocity dispersion as a function of time (left panel) and fraction of initial mass (right panel). Models are separated by colour as indicated.

panel) we are comparing clusters at the same mass. Since GC r_h decreases with decreasing R_{gc}, we expectedly see a higher σ_V for clusters with circular orbits that experience a stronger tidal field for a given fraction of initial mass.

While stronger Galactic tides increase the velocity dispersion of a GC on a circular orbit, tidal heating due to a non-circular orbit can play a secondary role. In Figure 3.3 we see that the velocity dispersion of GCs with eccentric orbits spikes during perigalactic passes as tidal heating injects all stars with additional energy (Spitzer, 1987; Gnedin et al., 1999), with the line of sight velocity dispersion deviating by up to 0.15 km/s and the three dimensional velocity dispersion deviating by up to 0.3 km/s. When this energy is injected into the cluster, the acceleration (and hence energy) imparted to these stars will push them outwards as they move closer to being energetically unbound and can even strip outer low-mass stars from the cluster if their initial binding energy is low enough, in agreement with Webb et al. (2013).

Even though the majority of the high velocity stars will escape the cluster and not be recaptured, some stars will remain bound. The periodic process of increasing the velocity dispersion during a perigalactic pass acts to slow the decrease in σ_V compared to if it had a circular orbit at $< R_{gc} >$, R_Ψ, the semi-major axis of the eccentric cluster, or R_a. Therefore for two given clusters that are equal in mass at the same R_{gc}, a higher velocity dispersion will indicate an eccentric orbit assuming the eccentric cluster is located near apogalacticon.

3.5 Relaxation

We next wish to examine how cluster orbit affects the timescale over which the distribution of stellar energies approaches equilibrium, known as the relaxation time t_{rh} (Heggie & Hut, 2003; Trenti & van der Marel, 2013). t_{rh} is given by Equation 3.2 (Meylan et al., 2001), where M is the total GC mass, $\bar{m}$ is the mean stellar mass, and r_h is the half-light radius.

$$t_{rh}[yr] = (8.92 \times 10^5)\frac{(M/M_\odot)^{\frac{1}{2}}}{(\bar{m}/M_\odot)}\frac{(r_h/1pc)^{\frac{3}{2}}}{log(0.4M/\bar{m})} \tag{3.2}$$

The relaxation time, plotted as a function of time (left panel) and fraction of initial mass (right panel) in Figure 3.4, is dependent on all three of the previously discussed cluster characteristics; mass, r_h, and velocity dispersion.

As previously discussed, a cluster which experiences a strong tidal field will have a higher mass loss rate, higher velocity dispersion and be smaller in size than a cluster which experiences a weaker tidal field. While a larger velocity dispersion will increase the relaxation time of a GC, differences in σ_V due to cluster orbit are minimal compared to the differences in mass and size of clusters in different tidal fields. Therefore the relaxation and segregation times of a cluster are primarily dependent on cluster size and density, both of which are proportional to R_{gc}. With the exception of e0r104, t_{rh} decreases with time after its initial expansion while each cluster loses mass and contracts. Since e0r104 is undergoing a near-zero mass loss rate and still expanding, t_{rh} continues to increase.

Figure 3.4 indicates that a cluster with an eccentric orbit relaxes on a timescale between that of GCs with circular orbits at R_p and R_a. Increasing eccentricity increases t_{rh} relative to the R_p case, primarily due to the eccentric

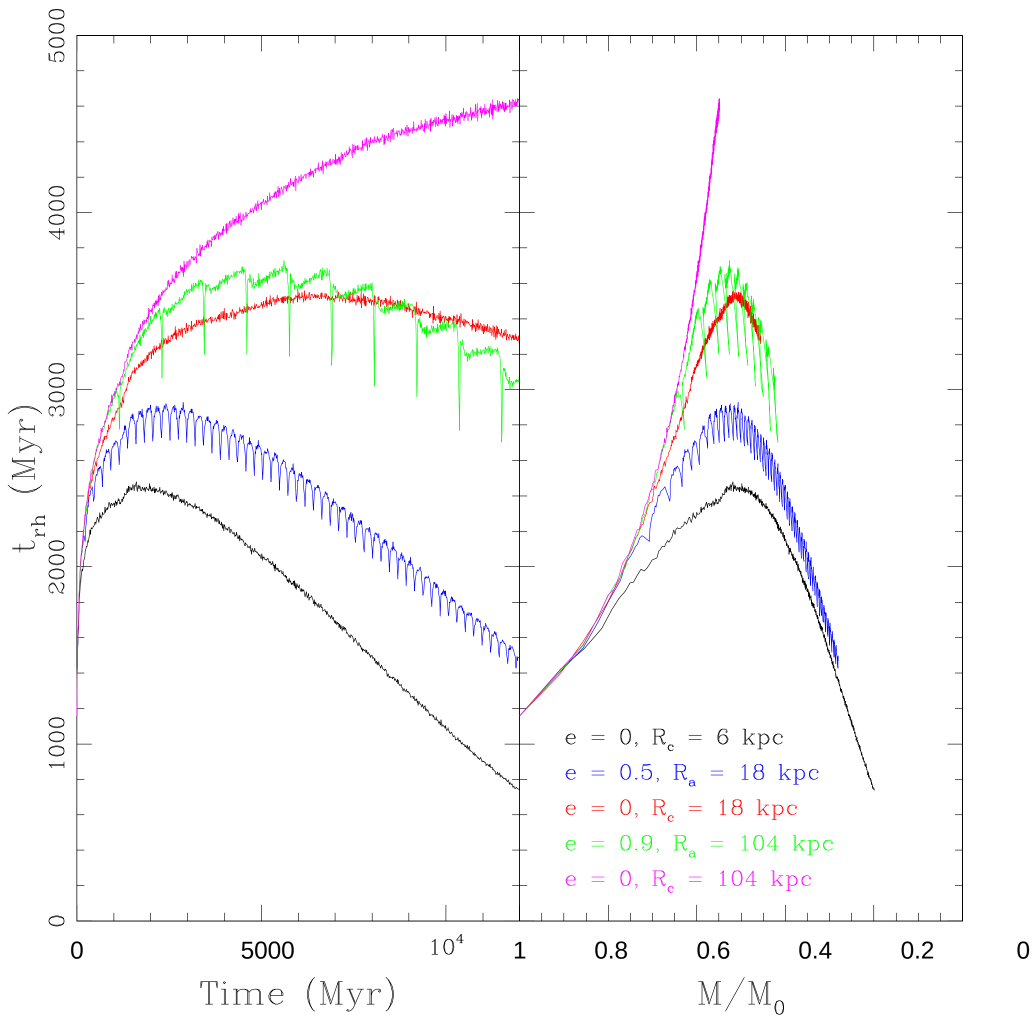

Figure 3.4 Half-mass relaxation time of each model cluster as a function of time (left panel) and fraction of initial mass (right panel). Models are separated by colour as indicated.

cluster having a larger r_h. Therefore for two clusters at the same R_{gc}, the cluster with a more eccentric orbit which brings it deeper into the galactic potential will have a shorter relaxation time and be more mass segregated than a cluster with a near-circular orbit. Similar to the evolution of total mass and σ_V in Figures 3.1 and 3.3, model e09r104 has a relaxation time profile that overlaps with e0r18.

3.6 Evolution of the Mass Function

The overall effect of orbital eccentricity on the dynamical evolution of GCs is observed in the stellar MF. Increased tidal stripping results in eccentric clusters being severely depleted of mass segregated low-mass stars compared to clusters with circular orbits near the same R_{gc}. Hence studying the stellar MF of a GC allows for constraints to be placed on its orbital eccentricity.

3.6.1 Evolution of α

We quantify the evolution of the MF by calculating the exponent α, where α is defined in Equation 3.3.

$$\frac{dN}{dm} \propto m^{\alpha} \tag{3.3}$$

In this form, the traditional Salpeter initial MF has α = -2.35 (Salpeter , 1955). For each model, α is the best fit slope to a plot of $log(\frac{dN}{dm})$ versus $log(m)$, calculated over mass bins greater than $0.15 M_{\odot}$ and less than the main sequence turn-off. The evolution of the global α for each of our models is plotted in Figure 3.5 as a function of time (left panel) and fraction of initial

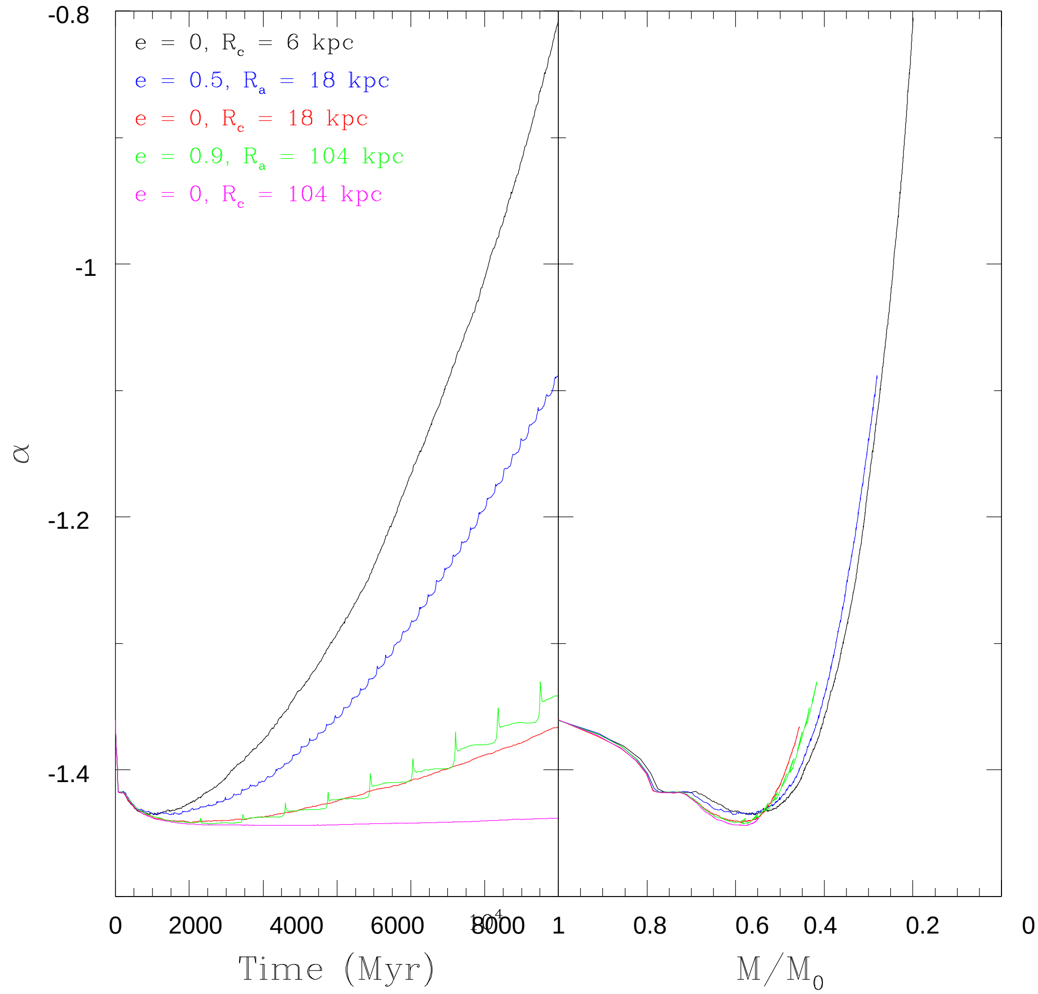

Figure 3.5 The evolution of the global α is plotted as a function of time (left panel) and fraction of initial mass (right panel). Models are separated by colour as indicated.

mass (right panel).

Almost immediately, α decreases from its initial value due to both stellar evolution and the breaking up of binaries which are assumed to be unresolved. After 1000-2000 Myr α begins to increase as a function of time at a faster rate for GCs which experience a stronger tidal field. The accelerated evolution of α is a direct result of increased mass loss due to tidal stripping producing a lower mass cluster with a shorter relaxation time and a smaller scale size ($r_t \propto M^{\frac{1}{3}} R_{gc}^{\frac{2}{3}}$). As a function of fraction of initial mass, all models again undergo a similar initial evolution in α. It is not until after the first 1000 Myr and each cluster has completed multiple orbits and experienced the combined effects of the galactic potential that the evolution of α becomes orbit dependent. For a given fraction of initial mass, α will then be higher for a cluster with a large $< R_{gc} >$ as the weaker tidal field can only remove the least massive of the low mass stars. A stronger tidal field can remove stars over a larger mass range, slowing the evolution of α.

We have already shown that tidal heating, on top of the lower mass and smaller scale size of an eccentric cluster, accelerates its dynamical evolution compared to a GC with a circular orbit and either the same semi-major axis, the same $< R_{gc} >$ or the same R_{Ψ}. Comparing GCs as a function of initial mass, α increases at a faster rate with increasing eccentricity (for a given R_p) because the weaker tidal field again can only remove the lowest of low mass stars. Since clusters with higher orbital eccentricities are subject to increased tidal heating and a tidal shock at R_p, a larger fraction of low-mass stars populating the outer regions have the potential to be tidally stripped.

3.6.2 Radial Dependence of the Mass Function

It is often the case that the slope of the mass function for a given GC is measured in a specific region of the GC (e.g. De Marchi, Paresce & Portegies Zwart, 2010). Therefore, to properly compare with observable parameters we consider the evolution of α for stars in different radial regions of the cluster. Specifically we focus on stars within the 10% Lagrangian radius (r_{10}), stars between r_{10} and the half mass radius (r_m), and bound stars beyond r_m. For our purposes, r_m is used as a substitute for r_h because it undergoes a smoother evolution from time step to time step than r_h.

The slope of the mass function in all radial bins (Figure 3.6) follows the same trend as the global mass function, however within observational uncertainties the inner mass function appears to be independent of orbit. The orbital independence is due to two-body interactions being the dominant physical process in the core of a GC relative to tidal stripping. Assuming a Universal IMF, the nearly orbit independent evolution of α for $r < r_{10}$ could be used to solve for the initial MF and hence total initial mass of MW GCs given their core mass function (Leigh et al., 2012).

For the intermediate mass function, we begin to see a clear separation in the evolution of α for GCs with different orbits. α increases at a slower rate than the inner region, primarily because both two-body relaxation and tidal stripping are in effect. The removal of low mass stars via tidal stripping slows the evolution of α compared to if just two-body relaxation was occurring.

In the outer region we see an initial decrease in α as mass segregation results in high mass stars migrating to the inner region of the GC. However, α quickly begins to increase for tidally filling clusters (e0r6, e05r18) as they lose mass. Unlike the inner region of the cluster, tidal stripping is now the dominant mechanism and can produce significantly different values of α based on cluster orbit. Specifically the difference between e0r6 and e05r18 is larger in the outer region than the intermediate region. With observational uncertainties in α typically ranging from 2 to 15% (De Marchi, Paresce & Portegies Zwart, 2010; Paust et al., 2010), discrepancies of this magnitude should be measurable in high quality observations. For the outer regions of clusters e0r18, e09r104,

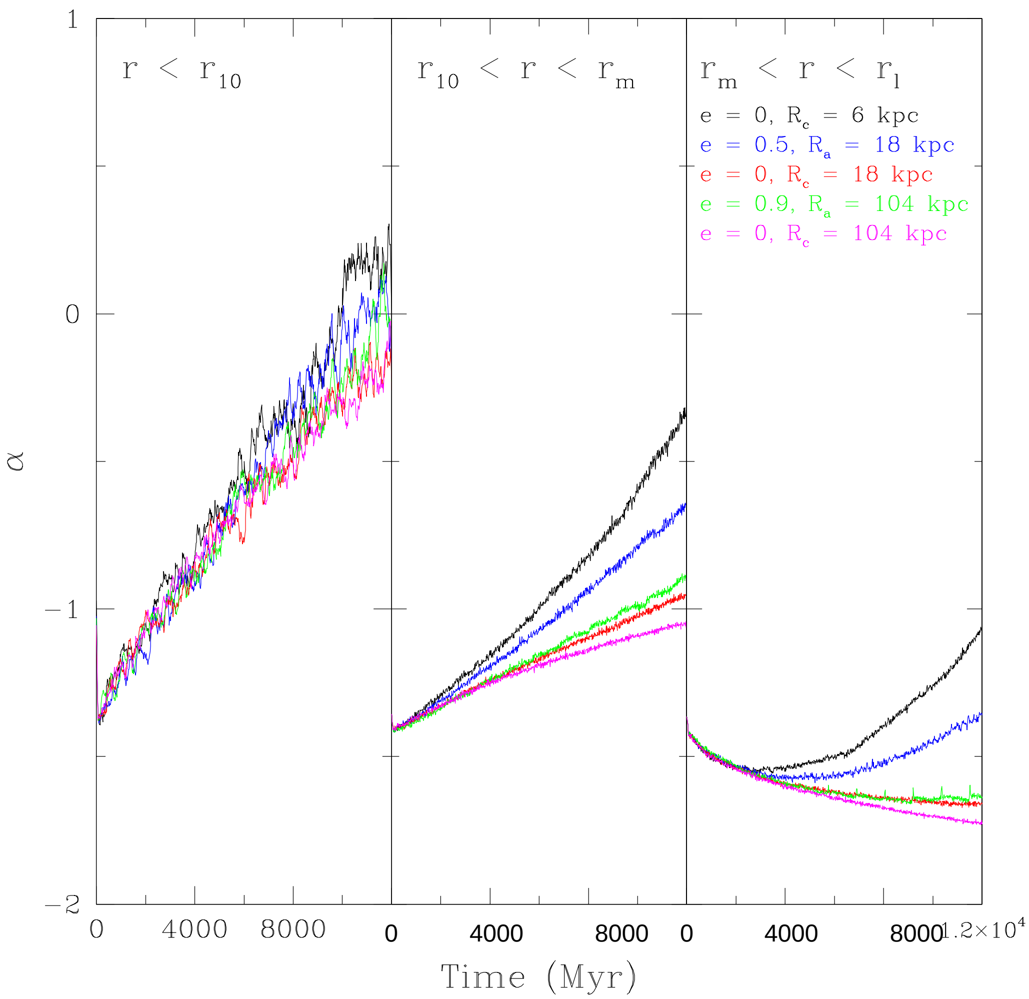

Figure 3.6 Slope of the mass function (α) for stars within r_{10} (left), stars between r_{10} and r_m (center), and bound stars beyond r_m (right). Models are separated by colour, as indicated in the right panel.

and e0r104, α is still decreasing as the cluster relaxes. Since outer clusters are either barely tidally filling or not at all (see Figure 3.2), two-body interaction is the only mechanism affecting the outer region of the GC and the evolution of α is not accelerated due to tidal stripping. Unfortunately, the outer mass functions of Galactic GCs are difficult to measure due to low number statistics and field contamination, and we are forced to rely on mass functions measured near r_h.

In principle, the ratio of α in the core to α in the outskirts could put very tight constraints on orbital eccentricity. Consider two clusters with the exact same mass, r_h, R_{gc} and value of α in their outskirts. While one may conclude these two clusters must have similar orbits, this conclusion would be incorrect if the clusters had different sizes or masses at birth. The evolution of α in the core on the other hand is independent of cluster orbit, and only depends on the initial mass and size of the cluster of birth as these properties are what govern the time it takes for the core to relax. Therefore normalizing by the value of α in the core is analagous to normalizing by the initial cluster conditions. In the current example, the cluster with the smaller core α was likely more massive and larger than the other cluster at birth and took longer to relax. To have the same value of α in the outskirts, the cluster with the higher initial mass and size must have an eccentric orbit and be near R_a in order to have lost a higher fraction of its initial mass. Additional simulations of clusters with different initial conditions are required to further explore the usefulness of the ratio of α in the core to α in the outskirts.

3.7 Application to Milky Way Globular Clusters

Our models demonstrate that the periodic perigalactic passes and tidal heating experienced by GCs with eccentric orbits can lead to enhanced mass loss, increased velocity dispersions, and shorter relaxation times than if the cluster had a circular orbit at R_a, $< R_{gc} >$, R_Ψ, or with the same semi-major axis. All of these effects combine to alter the stellar MF of a GC in a predictable manner. Assuming a universal IMF, which is consistent with the results of Leigh et al. (2012), the possibility then arises to relate the observationally determined MF of GCs to the tidal field, and thereby constrain GC orbits. A universal IMF is consistent with results of Leigh et al. (2012). Below, we use our model results and the MFs of GCs with solved orbits to illustrate how GC orbits can be constrained given α and R_{gc}.

In Figure 3.7, we plot α from De Marchi, Paresce & Portegies Zwart (2010) versus current R_{gc}, R_p, orbital eccentricity, and the ratio $\frac{r_h}{r_t}$ (Harris, 1996, 2010 update) for Galactic GCs with solved orbits (Dinescu et al., 1999; Casetti-Dinescu et al., 2007, 2013). Cluster tidal radii are calculated at their current R_{gc} given the formalism of Bertin & Varri (2008). The vertical dotted line in the bottom right panel corresponds to $\frac{r_h}{r_t} = 0.145$, where clusters with $\frac{r_h}{r_t} > 0.145$ are considered to be tidally filling and clusters with $\frac{r_h}{r_t} < 0.145$ are considered to be tidally under-filling (Henon, 1961). Clusters in the De Marchi, Paresce & Portegies Zwart (2010) dataset with unsolved orbits are plotted in Panels A and D as large green crosses. For comparison purposes, NGC 7078 (black triangle), NGC 6809 (blue filled circle) and NGC 2298 (red filled squares) have been singled out as they cover the full range in R_{gc}, eccentricity, and α. It should be noted that values of α taken from De Marchi, Paresce & Portegies Zwart (2010) were measured near the effective radius of the cluster. Therefore differences between eccentric and non-eccentric clusters should follow the behaviour described in the centre panel of Figure 3.6.

3.7.1 Clusters with Solved Orbits

3.7.1.1 NGC 7078 (M15)

NGC 7078 (black triangle) has the steepest mass function (most negative α) of all the GCs with solved orbits, suggesting it is the least dynamically evolved. Without any prior knowledge about the orbit, this cluster appears at face-value to represent an anomaly as its present day R_{gc} is approximately the mean R_{gc} of all clusters in the dataset. We conclude, based solely on the mass function of NGC 7078, that it has a low orbital eccentricity and a correspondingly large perigalactic distance. Taking into consideration the cluster's known orbital parameters, NGC 7078 actually has one of the largest perigalactic distances of all clusters with solved orbits. Therefore, it experiences a weaker mean tidal field than the majority of GCs. Compared to other clusters with large values of R_p, NGC 7078 is very tidally under-filling. Being smaller in size and tidally under-filling, combined with experiencing a weaker mean tidal field, means that NGC 7078 has a very low mass loss rate and has likely retained the majority of its stars. Furthermore, its lower orbital eccentricity means that tidal heating plays a near negligible role.

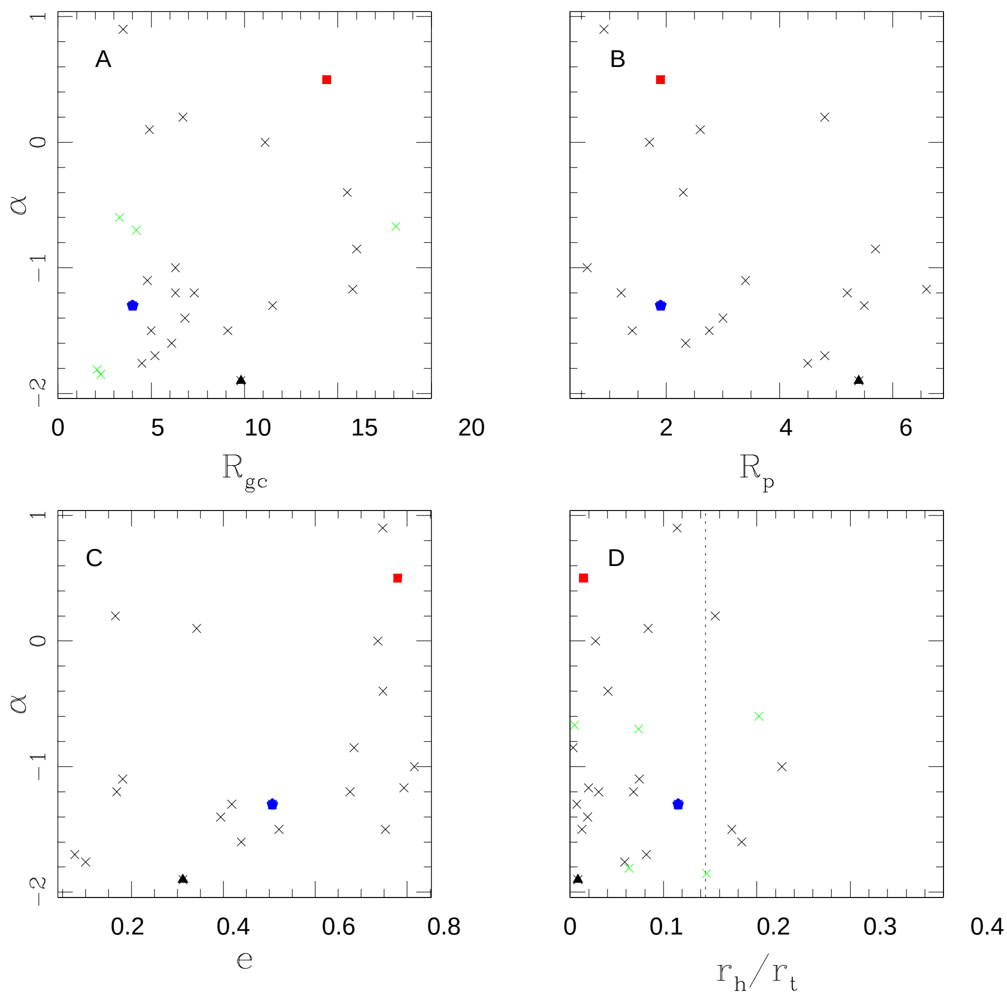

Figure 3.7 Slope of the mass function (α) compared to the present R_{gc} (Panel A), R_p (Panel B), orbital eccentricity (Panel C), and $\frac{r_h}{r_t}$ (Panel D) for Galactic GCs with solved orbits. In Panel D, the vertical line corresponds to $\frac{r_h}{r_t} = 0.145$. NGC 7078 (black triangle), NGC 6809 (blue filled circle) and NGC 2298 (red filled squares) have been highlighted. In Panels A and D, large green crosses mark the clusters in the De Marchi, Paresce & Portegies Zwart (2010) dataset with unsolved orbits.

3.7.1.2 NGC 6809 (M55)

NGC 6809 (blue filled circle) represents the inner most cluster in the dataset with a present day R_{gc} of 4 kpc, however it is less dynamically evolved than one would expect given the strong tidal forces it must experience. Its tidal and effective radii suggest that the cluster has expanded enough such that it is almost tidally filling and stars should be able to be stripped from the outskirts. Therefore we would conclude that the cluster must actually spend more time beyond 4 kpc than within 4 kpc, so it must have a moderate to high orbital eccentricity and be located near R_p. This statement is consistent with the solved orbit for this cluster. The cluster has an orbital eccentricity near 0.5 and an R_p of approximately 2 kpc, meaning that the cluster is currently closer to R_p than R_a, such that its current position does not represent the mean tidal field it experiences. The weaker than expected tidal forces experienced by NGC 6809 result in a lower mass loss rate and larger relaxation time, both of which help to account for the relatively unevolved (i.e. steep) slope of the MF.

3.7.1.3 NGC 2298

Finally, NGC 2298 (red filled squares) is very dynamically evolved as it has an inverted mass function with a large positive value of α. Again, without prior orbital information, this cluster would appear to be too dynamically evolved as the weak tidal forces it experiences at its current R_{gc} should not have been able to remove enough stars to invert the mass function. Panel D suggests that NGC 2298 is also very tidally under-filling, so one would expect that it would not be strongly affected by tidal forces. Hence the only way NGC

2298 can be so dynamically evolved given its current R_{gc} would be if it has a highly eccentric orbit that brings it deep into the tidal field of the galaxy. Furthermore, NGC 2298 must be near R_a to explain its extremely low $\frac{r_h}{r_t}$. Our conclusion is confirmed by noting NGC 2298 has an orbital eccentricity of 0.78 (Figure 3.7), a R_a of 15.3 kpc, and a current R_{gc} of 14.4 kpc. Periodic episodes of enhanced mass loss during each perigalactic passes have stripped the majority of low mass stars from the outer regions of NGC 2298 leaving it to appear tidally under-filling when near R_a.

Note that a similar argument can be made for NGC 288 and Pal5, which despite having R_{gc}'s greater than 10 kpc, both appear to be quite dynamically evolved with an α of 0. With orbital eccentricities greater than 0.68, perigalactic passes bring both clusters deep into the Galactic potential to R_p's less than 2 kpc. Enhanced mass loss and energy injection have accelerated each cluster's evolution compared to if they had circular orbits at their current R_{gc}'s.

3.7.2 Clusters with Unsolved Orbits

We have demonstrated that an understanding of how orbital eccentricity can influence the dynamical evolution of GCs can be used to make predictions of a GC's orbit based on its R_{gc} and α. While it is difficult to predict cluster orbit based solely on R_{gc} and α without additional simulations to explore possible degeneracies between orbit, initial size, and initial mass, we can make some general statements about the remaining clusters in the De Marchi, Paresce & Portegies Zwart (2010) dataset with unsolved orbits (plotted as green crosses in Figure 3.7):

- NGC 1261 is tidally under- filling, has the largest R_{gc}, and has one of the least negative values of α of the remaining clusters suggesting it is similar in nature to NGC 2298. Therefore NGC 1261 is likely located near R_a and has a large (e $>$ 0.7) orbital eccentricity. Its high-e orbit causes NGC 1261 to be subject to significant tidal heating and large injections of energy during perigalactic passes, accelerating its dynamical evolution compared to if it had a circular orbit at its current R_{gc}.

- NGC 6352 and NGC 6496 both have similar values of α to NGC 1261 but are located in the inner region of the MW (3 kpc $< R_{gc} <$ 5 kpc). Therefore their orbital eccentricities are likely less than NGC 2298 or NGC 6809 (e $<$ 0.5), and are currently located somewhere between R_p and R_a. Since NGC 6352 is tidally filling, it is likely closer to R_p. Similarly since NGC 6496 is tidally under-filling it is likely closer to R_a.

- NGC 6304 is tidally filling, but has an extremely negative α considering it is located deep in the galactic potential of the MW ($R_{gc} \sim$ 2 kpc). NGC 6304 is comparable to the previously discussed NGC 6809, and likely has a moderate to high (e $\sim$ 0.5) orbital eccentricity and is currently located near R_p. Hence its very negative α can be explained by the fact that NGC 6304 spends the majority of its time beyond its current R_{gc}.

- Unfortunately no firm conclusions can be made regarding the orbit of NGC 6541 as it is both extremely tidally under-filling and located at a small R_{gc}. Hence the evolution of its mass function is likely independent of its orbit. Its extremely negative α suggests the cluster has retained the majority of its stars over its lifetime and likely formed extremely compact relative to other GCs. Due to its low R_{gc}, it is also possible that the cluster is near R_p and has a low eccentricity orbit which brings the cluster slightly farther out in the galactic potential. However the fact that it is so tidally under-filling is surprising given its low R_{gc}. It may instead be the case that NGC 6541 is a recently accreted GC or the nucleus of a dwarf galaxy, and did not evolve at its current location in the Milky Way . Further simulations of tidally under-filling clusters on eccentric orbits are required to explore these hypotheses.

3.8 Summary

Our simulations show that orbital eccentricity can play an important role in the dynamical evolution of a star cluster. Our models demonstrate that for two GCs located at the same R_{gc}, one with a circular orbit and one with an eccentric orbit and $R_a = R_{gc}$, the GC with an eccentric orbit will have:

- increased mass loss rate
- smaller size
- increased velocity dispersion
- shorter relaxation time
- shallower mass function

The same conclusion would be reached by comparing a cluster with a circular orbit at a smaller R_{gc} to the cluster with a circular orbit at R_a. However, the non-static tidal field and periodic perigalactic passes experienced by a cluster with an eccentric orbit produce second order effects.

The first effect of an eccentric orbit is periodic episodes of enhanced mass loss during perigalactic passes. So while the mass loss rate that an eccentric cluster experiences for most of its lifetime may correspond to $< R_{gc} >$, the enhanced episodes of mass loss produce a higher overall mass loss rate. The second effect of perigalactic passes is the energization of inner region stars to larger orbits, as first discussed in Webb et al. (2013). The periodic injection of energy into the cluster, combined with additional energy due to tidal heating from a non-static tidal field, increases the kinetic energy of individual stars. Therefore inner region stars will be pushed to larger orbits and stars in the outskirts will be able to escape, decreasing the relaxation time and mass segregation time of the cluster. The combined effects of orbital eccentricity serve to partially balance the decreased tidal field strength the eccentric cluster experiences during the majority of its orbit, such that its evolution is comparable to a cluster with a circular orbit at a distance much less than R_{Ψ}, $< R_{gc} >$, or with the semi-major axis of the eccentric cluster. The recurring example discussed in this paper involves model e09r104, which undergoes a similar dynamical evolution as a cluster with a circular orbit at 18 kpc.

The influence of tidal heating and perigalactic passes are reflected in the global mass function of eccentric GCs, as it will be flatter (less negative slope) than would be expected given the clusters current R_{gc}. A flatter mass function is the direct result of increased tidal stripping of outer region stars that are preferentially low in mass due to mass segregation. Conversely, the inner mass function appears to be independent of cluster orbit as the effects of tidal heating are negligible compared to two-body relaxation. Hence the inner mass functions of Galactic GCs may instead be used to constrain the initial mass and size of the GC, and the ratio of α in the core to α in the outskirts could serve as a tracer of orbital eccentricity.

We make use of the measured mass functions of 33 GCs by De Marchi, Paresce & Portegies Zwart (2010), 28 of which have solved orbits (Dinescu et al., 1999; Casetti-Dinescu et al., 2007, 2013), to demonstrate how α and R_{gc} can be used to constrain cluster orbit. We then put constraints on the orbital eccentricity of the remaining clusters with unsolved orbits based on their α and R_{gc}:

- NGC 1261 has $e > 0.7$, and is currently located near R_a
- NGC 6352 has $e < 0.5$, and is currently located near R_p
- NGC 6496 has $e < 0.5$, and is currently located near R_a
- NGC 6304 has $e \sim 0.5$, and is currently located near R_p
- NGC 6541 is extremely under-filling with a low R_{gc}, so its α must be orbit independent. To be under-filling with such a small R_{gc}, it is likely that NGC 6541 either formed extremely compact and is currently located near R_p with a low e, is a captured GC, or is a dwarf galaxy remnant.

Additional simulations, specifically exploring the influence of orbital inclination, initial size, and initial mass on the dynamical evolution of GCs, will help explain the current dynamical state of all Galactic GCs. Isolating the effects of orbital eccentricity, however, is an important first step towards understanding the different ways tidal heating and periodic perigalactic passes can influence cluster evolution. A complete suite of simulations will allow for specific constraints to be placed on the orbits of GCs that have yet to be solved.

Acknowledgments

We would like to thank the referee for constructive comments and suggestions regarding the presentation of the paper. JW, AS, and WEH acknowledge financial support through research grants and scholarships from the Natural Sciences and Engineering Research Council of Canada. JW also acknowledges support from the Dawes Memorial Fellowship for Graduate Studies in Physics.

Bibliography

Aarseth, S.J. 2003, Gravitational N-body Simulations: Tools and Algorithms (Cambridge Monographs on Mathematical Physics). Cambridge University Press, Cambridge

Aarseth, S., Hénon, M., Wielen, R., 1974, A&A, 37, 183

Baumgardt H., Makino J. 2003, MNRAS, 340, 227

Bertin, G. & Varri, A. L. 2008, ApJ, 689, 1005

Binney, J. & Tremaine, S. 2008, Galactic dynamics second edition (Princeton, NJ, Princeton University Press, 1987, 747 p.)

Casetti-Dinescu, D.I., Girard, T.M., Herrera, D., van Altena, W.F., López, C.E., Castillo, D.J. 2007, AJ, 134, 195

Casetti-Dinescu, D.I., Girard, T.M., Jíková, L., van Altena, W.F., Podestá, F., López, C.E. 2013, AJ, 146, 33

De Marchi G., Paresce F., Portegies Zwart S. 2010, ApJ, 718, 105

Dinescu, D.I., Girard, T.M., van Altena, W.E. 1999, AJ, 117, 1792

Duquennoy, A. & Mayor, M. 1991, A&A, 248, 485

Gieles M., Heggie D., Zhao H. 2011, MNRAS, 413, 2509

Gnedin, O.Y., Lee, H. M., Ostriker, J. P., 1999, ApJ, 522, 935

Harris, W. E. 1996, AJ, 112, 1487 (2010 update)

Heggie, D.C. 1975, MNRAS, 173, 729

Heggie D. C., Hut P. 2003, The Gravitational Million-Body Problem: A Multidisciplinary Approach to Star Cluster Dynamics (Cambridge: Cambridge University Press)

Henon M. 1961, Annales d'Astrophysique, 24, 369

Henon M. 1973, Dynamical Structure and Evolution of Dense Stellar Systems, ed. L. Martinet & M. Mayor (Geneva Obs.)

Hurley, J.R. 2008a, Lecture Notes in Physics, 760, The Cambridge *N*-body Lectures. Springer-Verlag, Berlin, p.283

Hurley, J.R. 2008b, Lecture Notes in Physics, 760, The Cambridge *N*-body Lectures. Springer-Verlag, Berlin, p.321

King, I. R. 1962, AJ, 67, 471

Koch, A., Grebel, E. K., Odenkirchen, M., Martínez-Delgado, D., Caldwell, J. A. R., 2004, AJ, 128. 2274

Kroupa, P., Tout C.A., Gilmore, G. 1993,MNRAS, 262, 545

Lamers, H. J. G. L. M., Baumgardt, H., Gieles, M., 2013, MNRAS, 433, 1378

Leigh N. W., Umbreit S., Sills A., Knigge C., de Marchi G., Glebbeek E., Sarajedini A. 2012, MNRAS, 422, 1592

Marín-Franch, A., Aparicio, A., Piotto, G., Rosenberg, A., Chaboyer, B., Sarajedini, A., Siegel, M., Anderson, J., Bedin, L. R., Dotter, A., Hempel, M., King, I., Majewski, S., Milone, A. P., Paust, N., Reid, I. N. 2009, ApJ, 694, 1498

Meylan, G., Sarajedini, A., Jablonka, P., Djorgovski, S.G., Bridges, T., Rich, R.M., 2001, AJ, 122, 830

Miyamoto, M. & Nagai, R. 1975, PASJ, 27, 533

Paust, N. E. Q., Reid, I. N., Piotto, G., et al. 2010, AJ, 139, 476

Plummer, H.C. 1911, MNRAS, 71, 460

Praagman, A., Hurley, J., Power C. 2010, New Astron., 15, 46

Salpeter, E.E. 1955, ApJ, 121, 161

Spitzer L. Jr. 1987, Dynamical Evolution of GCs (Princeton, NJ: Princeton Univ. Press)

Tremaine S. D., Ostriker J. P., Spitzer L. Jr. 1975, ApJ, 196, 407

Trenti M., van der Marel, R. 2013, MNRAS, 435, 3272

Tutukov A. V. 1978, A&A, 70, 57

von Hippel T., Sarajedini A. 1998, AJ, 116, 1789

Webb, J.J., Harris, W.E., Sills, A., Hurley, J.R. 2013, ApJ, 764, 124

Xue, X.X. et al., 2008, ApJ, 684, 1143

Chapter 4

The Effects of Orbital Inclination on the Scale Size and Evolution of Tidally Filling Star Clusters

Jeremy J. Webb, Alison Sills, William E. Harris, Jarrod R. Hurley

Monthly Notices of the Royal Astronomical Society, Volume 445, Issue 1, pages 1048-1555,

Bib. Code: 2014MNRAS.445.1048W, DOI: 10.1093/mnras/stu1763

4.1 Introduction

The gravitational dynamics of a three-body system which consists of a star orbiting in the combined potential of a star cluster and its host galaxy becomes increasingly complicated as one attempts to make the system more realistic.

By treating all three members of the system (star, cluster, galaxy) as point masses, one can easily determine the tidal radius r_t (or Jacobi radius r_J) of the cluster, which is defined as the distance beyond which a star feels a stronger acceleration towards the host galaxy than the cluster itself (von Hoerner, 1957). A straightforward derivation of r_t yields a function that depends on cluster mass M_{cl}, galaxy mass M_g, and the cluster's galactocentric distance R_{gc}:

$$r_t \simeq R_{gc}(\frac{M_{cl}}{2M_g})^{1/3} \tag{4.1}$$

Allowing the host galaxy to have a non-point-mass potential introduces significant complexity that has led to multiple analytic definitions of r_t (e.g. King, 1962; Innanen, Harris, & Webbink, 1983; Jordán et al., 2005; Binney & Tremaine, 2008; Bertin & Varri, 2008). However all analytic expressions of r_t, no matter how complex the tidal field, are limited by the assumptions that the host galaxy has a spherically symmetric potential and the cluster has a circular orbit. Under these assumptions the tidal field experienced by the cluster can be taken to be static. The derivation by Bertin & Varri (2008) is likely the most generalized derivation of r_t, as spherical symmetry is the only assumption it makes. In that work, r_t is defined as:

$$r_t = (\frac{GM_{cl}}{\Omega^2 \upsilon})^{1/3} \tag{4.2}$$

where Ω, κ and υ are:

$$\Omega^2 = (d\Phi_G(R)/dR)_{R_{gc}}/R_{gc} \tag{4.3}$$

$$\kappa^2 = 3\Omega^2 + (d^2\Phi_G(R)/dR^2)_{R_{gc}} \tag{4.4}$$

$$\upsilon = 4 - \kappa^2/\Omega^2 \tag{4.5}$$

Here Φ_G is the galactic potential, M and R_{gc} are the mass and galactocentric distance of the cluster respectively, Ω is its orbital frequency, κ is the epicyclic frequency of the cluster at R_{gc}, and υ is a positive dimensionless coefficient.

Since disk and triaxial elliptical galaxies have non-spherically symmetric potentials, and most Galactic globular clusters have non-circular orbits (Dinescu et al., 1999; Casetti-Dinescu et al., 2007, 2013), assuming that a cluster experiences a static tidal field as it evolves is clearly incorrect. Various works have studied the evolution of clusters in non-static tidal fields (Baumgardt & Makino, 2003; Giersz & Heggie, 2009, 2011; Renaud et al., 2011; Webb et al., 2013; Brockamp et al., 2014; Madrid et al., 2014), where the easiest approach is to first consider clusters with eccentric orbits in a spherically symmetric tidal field. These studies have shown that a cluster on an eccentric orbit will lose mass faster than if it has a circular orbit at apogalacticon R_a, but slower than if it has a circular orbit at perigalacticon R_p. The increased mass loss rate is attributed to tidal shocks during perigalactic passes and tidal heating.

Tidal heating and tidal shocks occur when a cluster experiences a time varying gravitational force. A tidal shock refers to a highly varying gravitational force experienced over a short period of time (e.g. perigalactic pass or passage through a disk). During a tidal shock, individual stars undergo an increase in energy that is dependent on their location within the cluster, and the cluster's binding energy is reduced. The orbits of stars during a shock can receive a significant kick, which can push loosely bound stars outside r_t (Gnedin & Ostriker, 1997). Tidal heating on the other hand refers to a slowly varying gravitational force experienced over a long period of time (e.g. eccentric orbit or non-spherically symmetric potential). While the amount of energy injected into the cluster per unit time is much smaller than a tidal shock, over significant periods of time tidal heating can also have a strong influence on a cluster's evolution. Both mechanisms can provide stars with additional energy to escape the cluster that otherwise would remain bound, accelerating mass loss (Webb et al., 2013; Brockamp et al., 2014).

For a cluster on an eccentric orbit in a spherically symmetric potential, Equation 4.2 represents the instantaneous r_t of the cluster, which fluctuates between a maximum at R_a and minimum at R_p. In Webb et al. (2013) we demonstrate that the limiting radius r_L of a tidally filling cluster (the radius at which the stellar density approaches zero) traces r_t at all phases of its orbit. The agreement between r_L and r_t can be attributed to the cluster recapturing stars as it moves away from R_p, as well as energy injection from tidal shocks and tidal heating energizing bound stars to larger orbits within the cluster.

To better reflect the globular cluster population of disk galaxies, including the Milky Way, orbits need to be considered that are both eccentric and inclined to the plane of the disk. Studies of the effects of an inclined orbit on star clusters have primarily been focused on the effects of disk shocking as the cluster passes through the plane of the disk, which accelerates accelerate mass loss (Gnedin & Ostriker, 1997; Gieles et al., 2007; D'Onghia et al., 2010; Madrid et al., 2014).

A cluster on an inclined orbit will not only undergo tidal shocks, but tidal heating as well even though its orbit is circular. If the cluster orbit is inclined *and* eccentric, which is the case for Galactic globular clusters, it will experience a third tidal shock at R_p. The overall effect on the mass loss rate and scale size of such a cluster has not been fully explored.

The purpose of this study is to both isolate and identify the effects of orbital inclination on the evolution of a star cluster and consider the combined effects of orbital inclination and eccentricity. Model N-body clusters with a range of orbital inclinations and eccentricities are evolved from t=0 to 12 Gyr in a Milky Way-like potential. In Section 2 we introduce the models and their initial conditions. In Section 3 we focus on how orbital inclination and eccentricity influence the evolution of cluster mass (M), r_t, velocity dispersion σ_V, r_L and half-mass radius r_m. We discuss the results of all our N-body models in Section 4. Specifically we suggest a method to correct both the dissolution time and the theoretical calculation of a cluster's scale size for inclination and/or eccentricity. We summarize our conclusions in Section 5.

Model clusters are evolved from t=0 to 12 Gyr with the NBODY6 direct N-body code (Aarseth 2003). The initial mass of each model is $6 \times 10^4 M_\odot$ and has 96000 single stars and 4000 binaries. Stellar masses are drawn from a Kroupa, Tout, & Gilmore (1993) initial mass function between $0.1 M_\odot$ and $30 M_\odot$, with each star assigned a metallicity of $Z = 0.001$. The distribution of stellar positions and velocities follow a Plummer density profile with a cutoff at $10 r_m$ (Plummer , 1911; Aarseth et al., 1974). The initial half mass radius of each model is set to 6 pc, which ensures that all models exhibit bound stars at or beyond r_t and can be considered tidally filling.

To first study the effects of orbital inclination on star clusters, we simulate model clusters with circular orbits at 6 kpc and 18 kpc that have orbital inclinations of 0°, 22°, and 44°. We then study the combined effects of orbital eccentricity and inclination by simulating a cluster with an orbital eccentricity of 0.5, orbiting between R_p of 6 kpc and R_a of 18 kpc, with the same orbital inclinations. We selected these orbital parameters to allow us to compare a cluster with an eccentric orbit to clusters with circular orbits at R_p and R_a over a range of inclinations. The models with orbital inclinations of $0°$ were first introduced in Webb et al. (2014), hence we refer the reader to that study for additional details on the input parameters used in our models.

The clusters orbit within a Milky Way-like potential made up of a $1.5 \times 10^{10} M_\odot$ point mass bulge (Equation 4.6), a Miyamoto & Nagai (1975) disk (Equation 4.7 with $M_d = 5 \times 10^{10} M_\odot$, a= 4.5 kpc, and b = 0.5 kpc), and a logarithmic halo potential (Equation 4.8 (Xue et al., 2008)). The halo is scaled such that the three potentials combine to give a circular velocity (v_C) of 220 km/s at a galactocentric distance of 8.5 kpc in the plane of the disk (Aarseth , 2003). Therefore R_C in Equation 4.8 is 8.8 kpc. The initial radius in the plane of the disk (R_{xy}), initial height above disk (Z_i), R_p, eccentricity and orbital inclination of each cluster is given in Table 4.1. Note that model names are based on orbital eccentricity (e.g. e05), circular orbit distance or apogalactic distance (e.g. r18) and orbital inclination (e.g. i22).

$$\Phi_{bulge}(R_{gc}) = \frac{-GM_b}{R_{gc}} \tag{4.6}$$

$$\Phi_{disk}(R_{xy}, z) = \frac{-GM_d}{\sqrt{R_{xy}^2 + [a + \sqrt{b^2 + z^2}]^2}} \tag{4.7}$$

$$\Phi_{halo}(R_{gc}) = \frac{1}{2}(v_C^2)LOG(R_{gc}^2 + R_C^2) \tag{4.8}$$

Table 4.1: Model Input Parameters

Model Name	R_{xy} kpc	Z_i kpc	R_p kpc	e	i degrees
e0r6i0	6	0	6	0	0
e0r6i22	5.56	2.25	6	0	22
e0r6i44	4.32	4.17	6	0	44
e05r18i0	6	0	6	0.5	0
e05r18i22	5.56	2.25	6	0.5	22
e05r18i44	4.32	4.17	6	0.5	44
e0r18i0	18	0	18	0	0
e0r18i22	16.69	6.74	18	0	22
e0r18i44	12.73	12.73	18	0	44

In order to better visualize the orbits of each model cluster, specifically how they evolve with time, we have plotted the x and z coordinates at each time step for each cluster in Figure 4.1. The orbital eccentricity, circular orbit distance or apogalactic distance, and orbital inclination are marked in each panel.

4.2 Influence of Orbital Inclination

To study the effects of orbital inclination on the scale sizes of clusters, we focus on the evolution of the mass, tidal radius, velocity dispersion, limiting radius and half-mass radius of all bound stars in each model cluster. A star is considered to be bound if the difference between its kinetic energy and the potential energy due to all other stars in the simulation is less than 0.

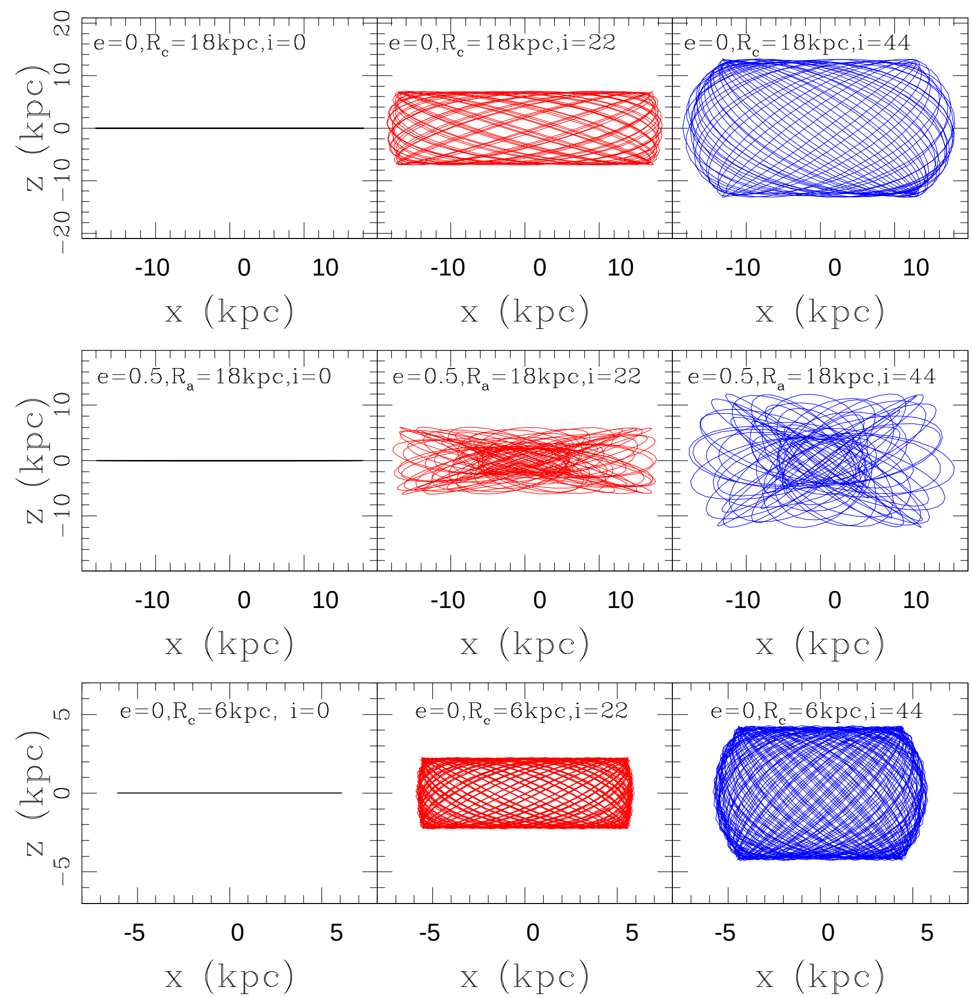

Figure 4.1 Orbits of all model clusters. Clusters with circular orbits at 6 kpc are in the lower row, with orbital eccentricities of 0.5 and perigalactic distances of 6 kpc in the middle row, and circular orbits at 18 kpc in the top row. Orbital inclination changes from 0° in the left column, to 22° in the middle column, to 44° in the right column.

4.2.1 Mass

The total bound mass of each cluster is plotted in Figure 4.2 as a function of time. For any cluster, mass loss is driven by stellar evolution and the tidal stripping of stars pushed beyond r_t. For clusters with circular orbits in the plane of the disk, the mean mass loss rate increases with decreasing R_{gc} due to the increased strength of the tidal field. For clusters which experience non-static tidal fields (those with eccentric and/or inclined orbits) tidal heating and tidal shocks due to a sudden increase in the local gravitational potential (passage through a galactic disk or near R_p) are additional sources of mass loss. For example, clusters with circular orbits at 6 kpc that are inclined lose mass at a higher rate than the $i = 0$ case, with e0r6i22 losing mass the fastest.

Model e0r6i22 (22° inclination) loses more mass than e0r6i44 (44° inclination) over 12 Gyr for two reasons. First, e0r6i22 passes through the disk more often, thus experiencing more frequent disk shocking. Secondly, the tidal field of the disk is proportional to z^{-1} for a given R_{xy} (see Equation 4.7, so the cluster e0r6i22 spends the majority of its time in a stronger tidal field. e0r6i44 is far enough from the plane of the disk that when at its maximum height z_{max} it experiences a weaker and nearly spherically symmetric tidal field such that tidal heating is less of a contributing factor. Model clusters with higher inclinations, like those performed by Madrid et al. (2014), are also in agreement with our findings. Clusters with extremely high inclinations not only pass through the disk more frequently due to shorter orbital periods, but also pass through the disk perpendicular to the Galactic plane. Crossing the disk at such a high inclination increases the amount of energy imparted to cluster stars. Stronger and more frequent disk shocks experienced by high inclina-

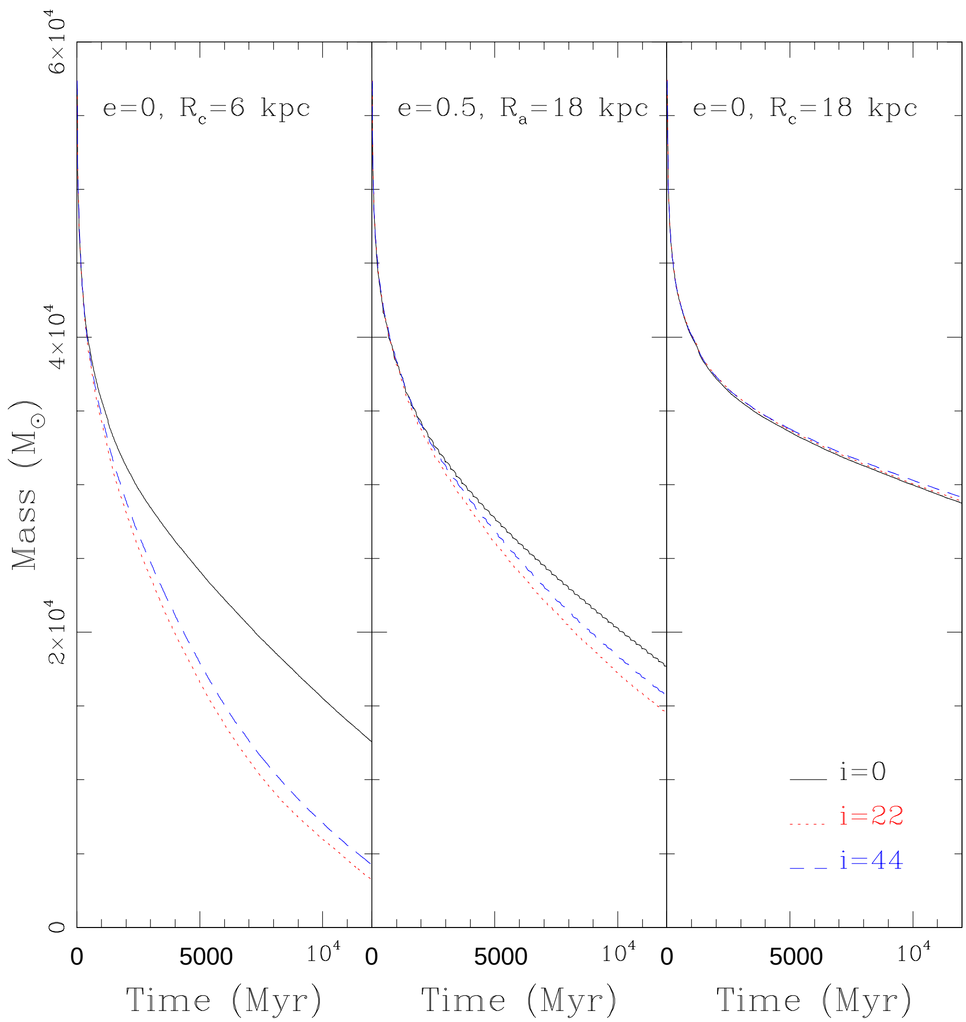

Figure 4.2 The evolution of total cluster mass over time for clusters with a circular orbit at 6 kpc (left panel), an orbital eccentricity of 0.5 and an apogalactic distance of 18 kpc (center panel) and a circular orbit at 18 kpc (right panel). The black solid lines, red dotted lines, and blue dashed lines correspond to models with orbital inclinations of 0°, 22°, and 44° respectively.

tion clusters result in an accelerated mass loss rate compared to the models presented here.

For circular orbits at 18 kpc, there is very little difference between the mass profiles of the inclined and non-inclined cases. The strength of a Miyamoto & Nagai (1975) disk decreases as R_{xy}^{-1} (Equation 4.7). Hence for clusters orbiting at similarly large distances, the majority of the disk's mass is within their orbit, and the clusters evolve more as if they are in a spherically symmetric potential. However it is surprising that the clusters on inclined orbits are actually more massive at all times than the $i = 0$ case since we expect these clusters to undergo some degree of disk shocking and tidal heating. This will be addressed in Section 4.2.

For clusters with eccentric orbits, periodic episodes of enhanced mass loss due to perigalactic passes are present in all three cases. In the case of a cluster with orbital eccentricity e in the plane of the disk (e05r180), the cluster takes (1+e) times longer to reach dissolution than a cluster with a circular orbit at R_p, or (1-e) times shorter than a cluster with a circular orbit at R_a. The dissolution time scaling is in agreement with Baumgardt & Makino (2003), who defines the dissolution time as the time it takes for the cluster to reach $100 M_\odot$. Given that the behaviour of collisional N-body simulations can become noisy at late times when only a small number of stars remain, we have checked the results of Figure 4.2 against an alternative definition of the dissolution time (when the cluster reaches 10% of its original mass) and find no noticeable change.

The amount of mass lost during a perigalactic pass decreases with increasing inclination because the tidal field is weaker at R_p when the cluster is above or below the plane of the disk. However, the inclined and eccentric clusters still lose more mass than e05r18i0 because they undergo additional mass loss via disk shocking and increased tidal heating. While tidal heating has been shown to be a factor for clusters with eccentric orbits in the plane of the disk (Webb et al., 2013), it is even more effective for clusters with inclined orbits as the rate of change of the local potential is higher. The rate of change of the local potential is reflected in plots of r_t versus time and the cluster's height above the disk as discussed in Sections 3.2 and 4.1 respectively. Disk shocking, while still an additional source of mass loss, is less effective than if the cluster had a circular orbit at R_p because disk passages occur at larger galactocentric radii. The combined effects result in the (1-e) scaling factor from the perigalactic case remaining an accurate indicator of dissolution time (within 9%) for a given orbital inclination, while the R_a case does not (greater than 30%).

4.2.2 Tidal Radii

Tidal shocks and tidal heating can be traced by the evolution of r_t over the course of a cluster's orbit and lifetime. Any correlation between r_t and orbital phase indicates that tidal heating is occurring, while a tidal shock occurs when r_t suddenly goes from decreasing to increasing. To illustrate events of tidal shocking and heating, we plot the instantaneous r_t of the models with circular orbits at 6 kpc in Figure 4.3. Model e0r6i22 is plotted in the lower panel (red) and e0r6i44 in the upper panel (blue). The non-inclined case, e0r6, has been plotted in black in both panels. The instantaneous r_t has been calculated via Equation 4.2 given each cluster's mass and instantaneous location in the Galactic potential. To remove any dependence of r_t on the mass loss rate

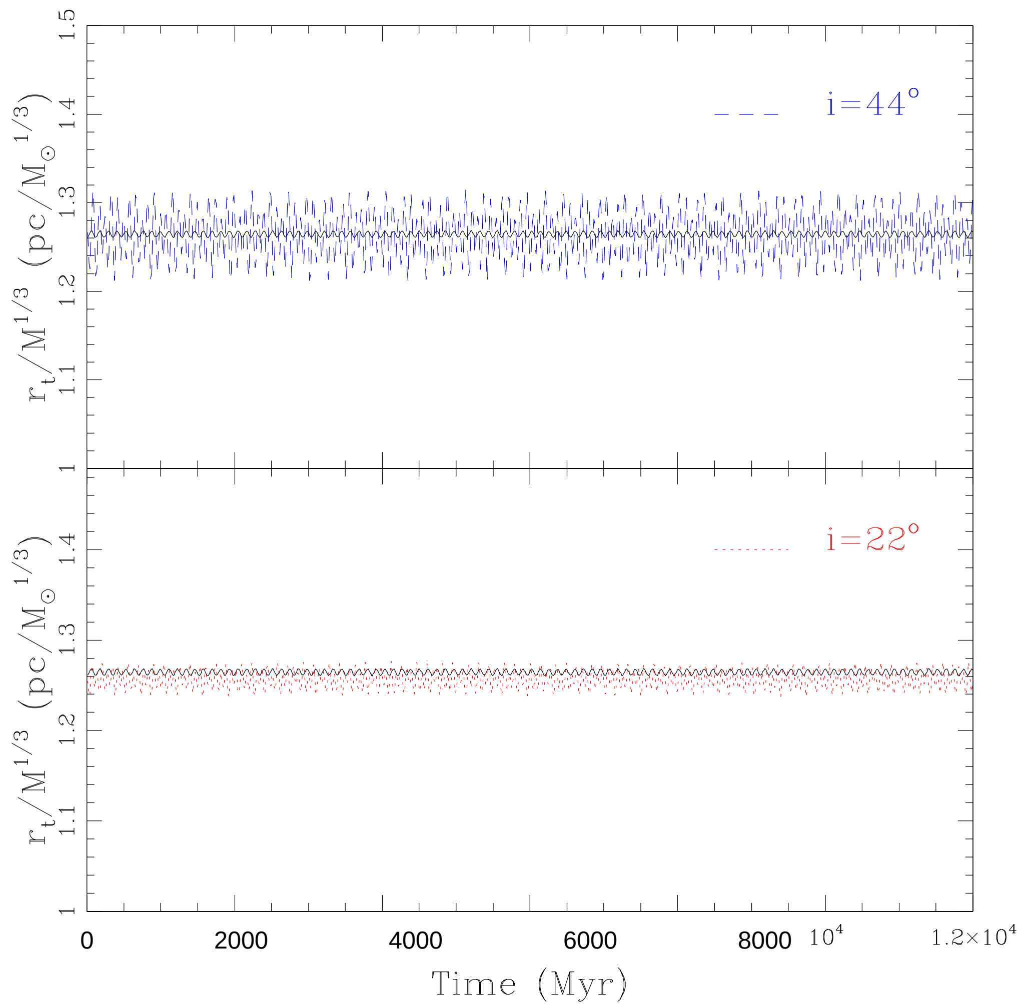

Figure 4.3 The evolution of the mass normalized tidal radius over time for clusters with a circular orbit at 6 kpc. The black solid lines, red dotted lines, and blue dashed lines correspond to models with orbital inclinations of 0°, 22°, and 44° respectively.

and focus on effects due to cluster orbit, r_t has been normalized by $M^{\frac{1}{3}}$ (See Equation 6.1). Hence for clusters with circular orbits in the plane of the disk, their mass normalized r_t never changes.

Figure 4.3 indicates that the r_t of clusters with inclined orbits fluctuates by ±5% over the course of a single inclined orbit. The fluctuations in r_t can be

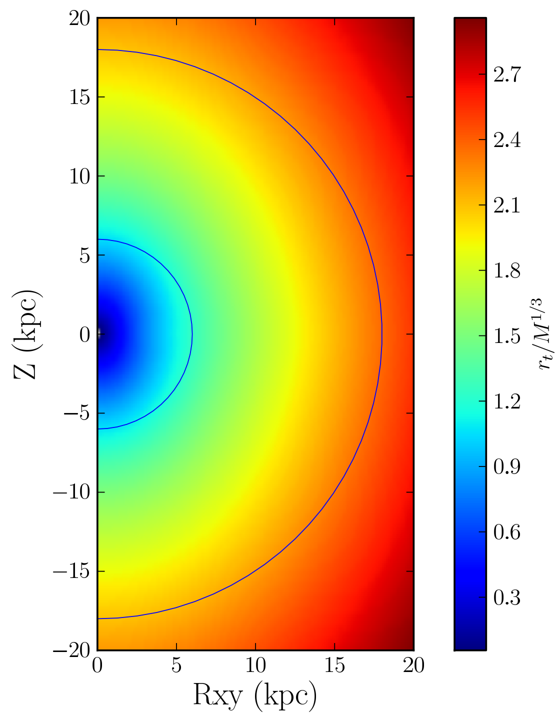

Figure 4.4 The mass normalized instantaneous tidal radius at all points in the $R_{xy} - z$ plane. Solid lines mark galactocentric distances of 6 kpc and 18 kpc.

understood by plotting the mass normalized r_t at all locations in the Galactic potential with $R_{xy} < 20$ kpc and $|z| < 20$ kpc in Figure 4.4. A cluster will have its largest r_t when at its maximum height above the disk, with r_t decreasing as the cluster approaches the disk. The process is then reversed as the cluster leaves the disk again on its way to its maximum distance below the disk.

For clusters orbiting at 18 kpc we see that the tidal field is essentially spherically symmetric. The tidal field imposed by the Galactic disk alone, and its gradient, become independent of z at approximately 15 kpc. Therefore a possible cut-off radius for the influence of orbital inclination may exist. Future studies on how this cut-off radius may depend on initial cluster conditions or the assumed structure of the Galactic disk are planned.

For a cluster on an inclined *and* eccentric orbit, r_t will also be growing and shrinking as it moves towards and away from R_p. With the distance above or below the disk at R_p and R_a changing from one orbit to the next, a cluster with such a complicated orbit cannot be considered to be in any form of equilibrium, but is instead in a constant state of flux.

4.2.3 Velocity Dispersion

The clearest demonstration of how these model clusters are affected by tidal shocks and tidal heating is in the evolution of the global three dimensional velocity dispersion σ_V of all bound stars in Figure 4.5. The general trend in all cases is for σ_V to decrease with time as mass segregated low-mass stars with higher velocities escape and the cluster loses mass. For a cluster on a circular orbit in the plane of the disk, the decrease in σ_V is smooth. Periodic spikes in σ_V, that are only present in the inclined and eccentric clusters, are points where a sudden injection of energy (a tidal shock) has occurred. A sudden increase in energy can cause a significant increase in stellar velocities (Webb et al., 2014).

For models on circular inclined orbits, each peak in σ_V signifies a disk shock. The peak is followed by a sharp decrease in σ_V as r_t decreases and stars with lower binding energies (and high velocities) escape. σ_V then slowly increases due to both the recapturing of temporarily unbound stars as r_t begins to re-expand, and tidal heating as the cluster moves through a non-static tidal field. Hence the cluster expands as it moves towards z_{max}. The process then repeats itself when the clusters moves through the disk during the second half of its orbit. The strength of the shock decreases with R_{gc} as the disk's

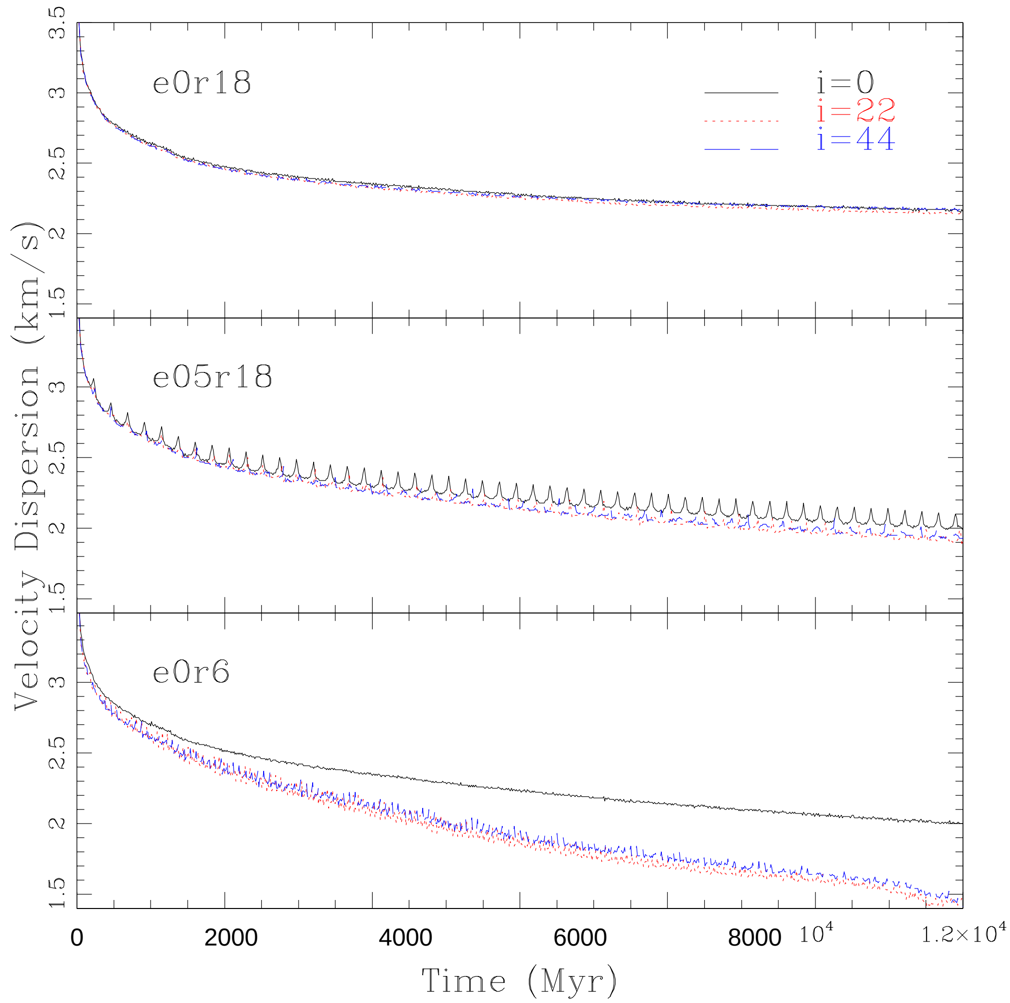

Figure 4.5 The evolution of the velocity dispersion of all bound stars over time for clusters with a circular orbit at 6 kpc (bottom panel), an orbital eccentricity of 0.5 and an apogalactic distance of 18 kpc (center panel) and a circular orbit at 18 kpc (top panel). The black solid lines, red dotted lines, and blue dashed lines correspond to models with orbital inclinations of 0°, 22°, and 44° respectively.

contribution to the Galactic potential decreases.

The situation is slightly more complicated for models with eccentric *and* inclined orbits like e05r18i22 and e05r18i44 . The cluster still crosses the disk twice per orbit, but since the orbit is non-circular the disk passages occur at different galactocentric radii. The disk shock that occurs nearest R_p will be much stronger than the shock occurring near R_a. The weaker second shock results in the mass loss rate of inclined and eccentric clusters being only marginally higher than the non-inclined case. It is also important to note that when a cluster has a circular and inclined orbit, tidal heating and the recapturing of unbound stars is able to increase σ_V between shocks. But when the cluster has an eccentric and inclined orbit, the weaker tidal field experienced as the cluster moves towards R_a only injects enough energy to keep σ_V constant between shocks. Therefore clusters on eccentric and inclined orbits do not expand in size as efficiently as clusters on inclined and circular orbits near R_p while the cluster moves towards z_{max}.

4.2.4 Limiting Radii

We next consider the effect of inclination on the [limiting radius]. For the purposes of this study, the limiting radius is defined as the average cluster-centric distance of all bound stars located beyond the instantaneous r_t (Webb et al., 2013). The interplay between a changing theoretical r_t and the actual size of the cluster r_L is illustrated in Figure 4.6 where we plot the ratio of $\frac{r_L}{r_t}$ as a function of time. Based on our definition of r_L, the ratio will always be slightly larger than 1.0.

How a cluster responds to its instantaneous r_t is indicated by how much

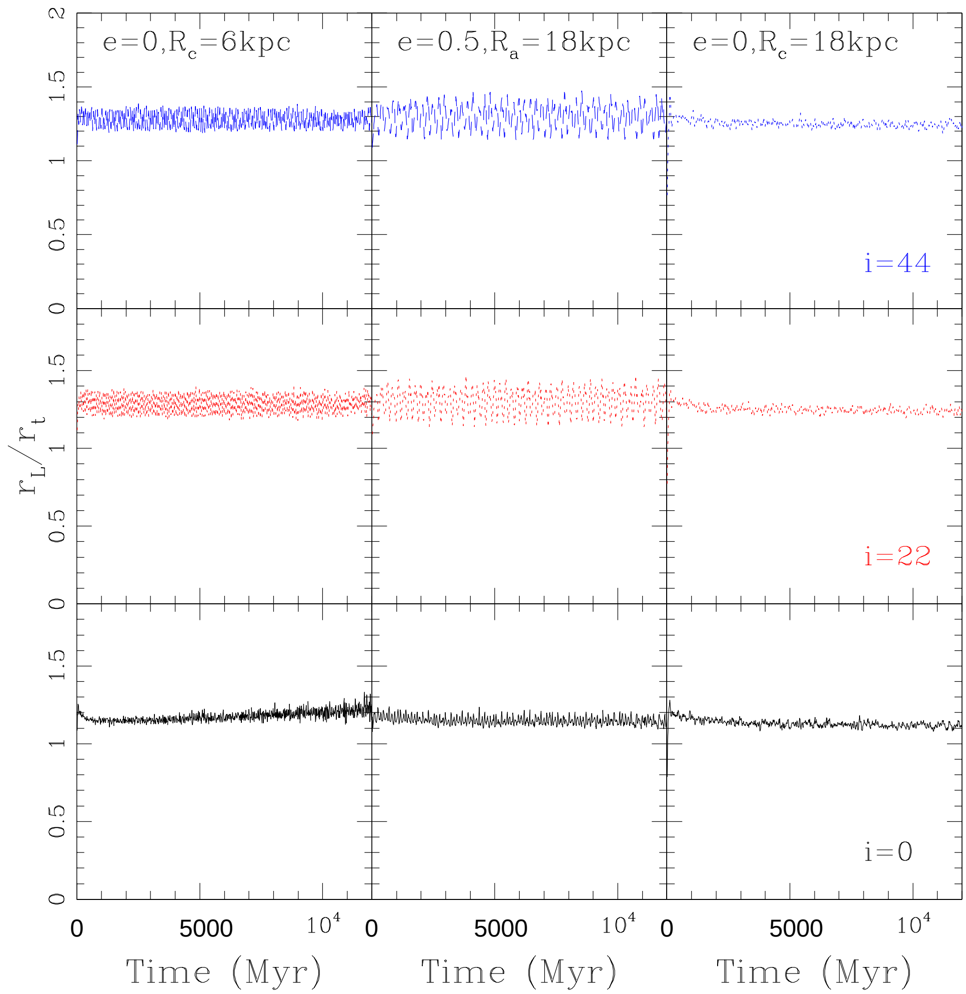

Figure 4.6 The ratio of the limiting radius of each cluster to its tidal radius as a function of time for clusters with a circular orbit at 6 kpc (left panels), an orbital eccentricity of 0.5 and an apogalactic distance of 18 kpc (center panels) and a circular orbit at 18 kpc (right panels). The black (bottom panels), red (middle panels), and blue (top panels) lines correspond to models with orbital inclinations of 0°, 22°, and 44° respectively.

the ratio fluctuates around its mean value. For example, it has been shown that clusters which orbit in the plane of the disk fill their instantaneous r_t at all times (Webb et al., 2013), which is why the ratio is nearly constant as a function of time for the non-inclined cases. The inclined cases, however all fluctuate around the mean $\frac{r_L}{r_t}$ value of the non-inclined case. The fluctuations are not the result of a non-static field, as e05r18 has a nearly constant ratio despite orbiting between 6 kpc and 18 kpc in the plane of the disk. The oscillations are due to inclined clusters being subject to increased tidal heating and additional shocking events per orbit compared to clusters in the plane of the disk. Before the cluster even has a chance to respond to its new local potential, which takes approximately one crossing time (Madrid et al., 2014), the local potential has already changed so quickly that the cluster never comes to equilibrium.

During each orbit, when the cluster is moving away from the disk and towards z_{max} it will be slightly underfilling as r_t expands. As the cluster approaches z_{max} it slows down and therefore has time to respond to its local potential and fill r_t. As the cluster moves away from z_{max} and towards the plane of the disk, the cluster is slightly overfilling since r_t is now decreasing. As the cluster passes through the plane of the disk and undergoes a disk shock, outer stars can become permanently or temporarily unbound, and the cluster becomes briefly tidally filling before r_t begins to increase again.

4.2.5 Half-mass Radius

The inner structure of globular clusters, observationally traced by the effective radius r_h, is far more robust and less model dependent than r_L (e.g. McLaughlin & van der Marel, 2005; Webb, Sills, & Harris, 2012; Puzia et al., 2014). For N-body simulations, the half-mass radius r_m is more commonly used to probe the inner regions of globular clusters (e.g. Gieles et al., 2010; Madrid et al., 2012; Webb et al., 2013). The three-dimensional half mass radius is taken to be the radius enclosing half of the total bound mass, including both bound objects orbiting beyond r_t and stellar remnants. The latter points resulting in r_m being on average slightly larger than r_h.

The half-mass radius and the mass normalized half-mass radius of each cluster as a function of time are plotted in Figure 4.7. It should be noted that our clusters all have final half-mass radii 2-3 times greater than most actual globular clusters. Future studies will explore the influence of inclined orbits in disk potentials on a wider range of initial r_m.

Figure 4.7 suggests that the inner structure of a star cluster is less affected by changes in orbital inclination than r_L. If we first consider the models orbiting at 6 kpc, the inclined clusters are smaller because they lose mass at a faster rate than the non-inclined case. However if we normalize by mass, the mass normalized r_m of all three cases are nearly identical for almost 7 Gyr. At 7 Gyr, the inclined clusters are approximately $1 \times 10^4 M_\odot$ in mass, and are in the process of dissolving. The eccentric clusters only differ in r_m by 1 pc after 12 Gyr and the clusters orbiting at 18 kpc differ by less than 0.5 pc. After normalizing by cluster mass, the eccentric and 18 kpc clusters are nearly always identical in size.

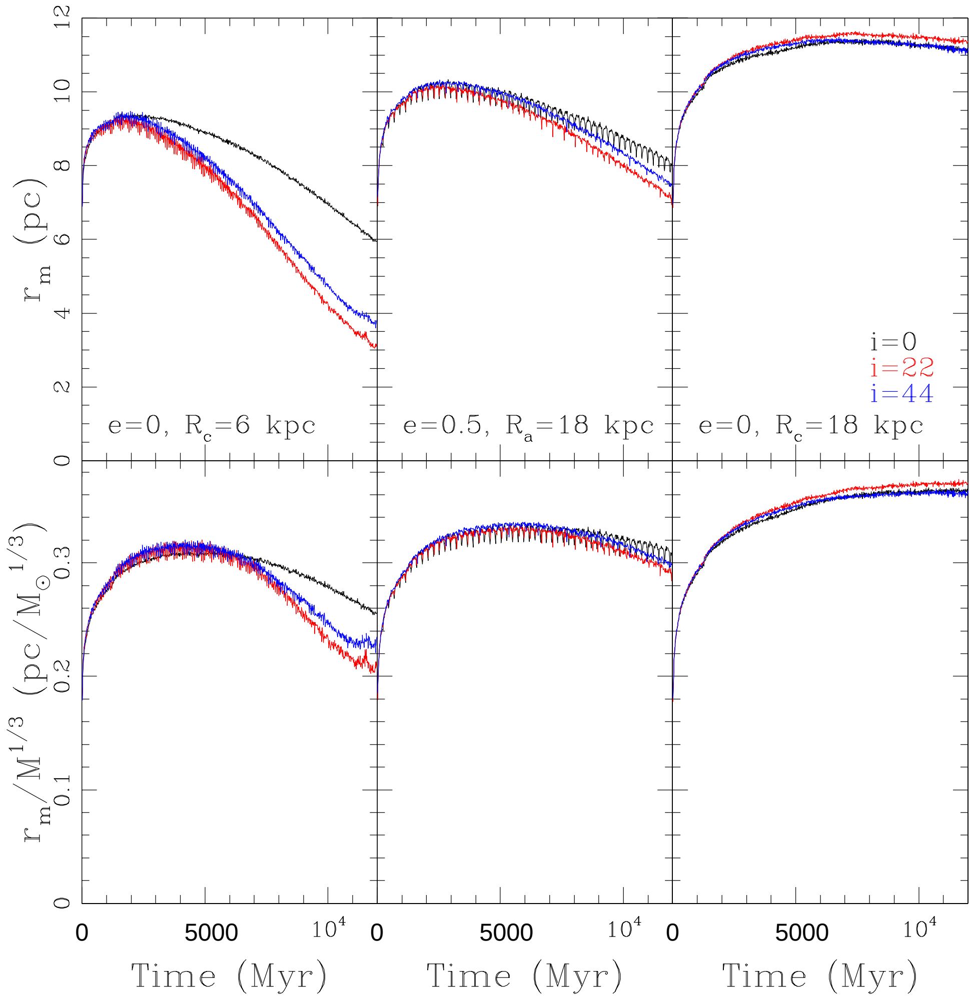

Figure 4.7 The evolution of the half mass radius (top panels) and the half mass radius normalized by mass (bottom pannels) over time for clusters with a circular orbit at 6 kpc (left panels), an orbital eccentricity of 0.5 and an apogalactic distance of 18 kpc (center panels) and a circular orbit at 18 kpc (right panels). The black solid lines, red dotted lines, and blue dashed lines correspond to models with orbital inclinations of 0°, 22°, and 44° respectively.

4.3 Discussion

Our simulations indicate that the primary effect of an inclined orbit in a non-spherically symmetric potential is an increased mass loss rate due to tidal heating and shocking. To apply these findings to observations of star clusters, we need to know how tidal shocks and heating depend on cluster orbit and how they would influence the calculated size of a cluster.

4.3.1 Tidal Heating and Shocks

The increased mass loss rate experienced by clusters on inclined orbits is a direct result of them being subject to both tidal heating and tidal shocks, neither of which clusters on non-inclined circular orbits experience. We examine both of these effects further by plotting the mass normalized r_t of each model cluster as a function of its height z over 12 Gyrs (Figure 4.8). Since data points are equally spaced in time, the density of points reflects the proportion of its lifetime a cluster spends at a given z.

In Figure 4.8, episodes of tidal heating are indicated by gradual changes in r_t. All model clusters experience some degree of tidal heating as r_t decreases while the cluster moves inward from z_{max}. Tidal shocks are seen in Figure 4.8 when the mass normalized r_t goes from decreasing to increasing. For an inclined orbit that is perfectly circular (e=0), a disk shock would be a singular event as r_t reaches a minimum at $z = 0$. However, since the orbits of our model clusters at 6 kpc and 18 kpc are not perfectly circular ($e \leq 0.05$), the situation is slightly more complicated. At smaller R_{xy} (6 kpc) the *disk shock* appears to consist of two shocking events, just before and just after the cluster passes through the plane of the disk, unless the disk passage actually

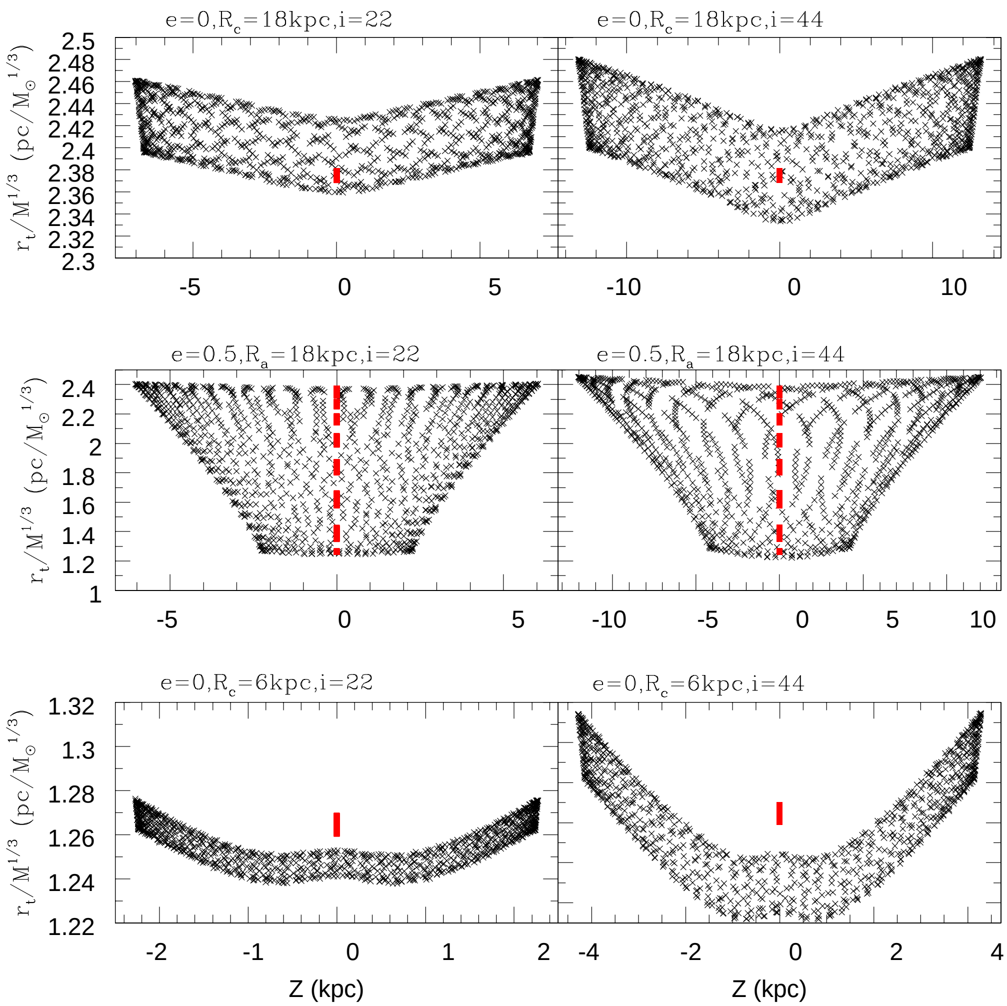

Figure 4.8 Mass normalized tidal radius as a function of height above the disk z for all inclined model clusters (black crosses). Data points are equally spaced in time and cover 12 Gyrs of evolution, so the density of points reflects the amount of time the cluster spends at a given z. Red squares mark model clusters with orbits in the plane of the disk.

occurs at R_p. The increase in r_t to a local maximum between the shocks lets the cluster temporarily expand freely. The dual shocks are what separates a disk shocking event from a more simple tidal shock, like a perigalactic pass, and make it more efficient at removing stars from the cluster. However, since the shape of the disk potential changes and strength of the disk decreases with R_{xy}, both shocks are not necessarily equal in magnitude, with one of the shocks sometimes being weaker and even negligible when orbits are near circular. At larger R_{xy} (18 kpc), the decreased strength of the disk results in the disk shock being a singular event. Inclined *and* truly eccentric clusters (middle row of Figure 4.8) experience a strong dual tidal shock during its innermost disk passage, a weaker single shock during its outermost disk passage, and a third shock during each perigalactic pass.

Figure 4.8 indicates that inclined, eccentric clusters experience varying amounts of tidal heating from one orbit to another. While some orbits keep the cluster at a high z until just before crossing the disk (minimizing tidal heating), other orbits gradually bring the cluster in from z_{max} to z=0 (maximizing tidal heating). The complex orbits of clusters that are inclined and eccentric makes quantifying the effects of tidal heating or shocking difficult. However this study suggests that the evolution of a cluster with an eccentric and inclined orbit is more similar to a cluster with the same eccentricity and $i = 0°$ rather than a cluster with the same i orbiting at R_p with e=0.

4.3.2 The Effective Tidal Radius of an Inclined Orbit

Because of the chaotic evolution of the instantaneous r_t of a cluster with an inclined orbit, and because r_L does not precisely trace r_t as in a spherically symmetric potential, it is difficult to define what exactly the *size* of a star cluster is. While an inclined cluster may appear to have an r_L greater than its current r_t, this could simply be a function of its current orbital phase and not accurately indicate its current dynamical state. As we saw in Figure 4.6, an inclined cluster ranges between being tidally over-filling and under-filling, except at z_{max} and $z = 0$ when r_L and r_t are near equal.

We wish to define an *effective* r_t for a cluster with an inclined orbit, in order to get a sense of its dynamical state and whether or not the cluster is tidally filling. When defining an *effective* r_t, it should ideally represent a stable state during the cluster's orbit at which the cluster spends the majority of its orbit. We consider the rate of change in the mass normalized tidal radius as a function of height above the disk in Figure 4.9. The r_t of a cluster near the plane of the disk fluctuates dramatically during the disk passage, and only represents a brief portion of the total orbit. Setting the *effective* r_t equal to the r_t near $z = 0$ would be equivalent to setting the r_t of a cluster on an eccentric orbit equal to its r_t at R_p, which we know to be incorrect (Webb et al., 2013). The clear choice is to let the *effective* r_t of a cluster with an inclined orbit be equal to its instantaneous r_t at z_{max}. Not only is the rate of change in r_t is at its minimum when the cluster is both approaching and leaving z_{max}, but inclined clusters also spend the majority of their lifetime near z_{max}. Therefore the time averaged r_t of each model also corresponds to r_t at z_{max}.

4.4 Summary

In this paper, we simulated the evolution of star clusters orbiting in a Milky Way-like potential with a range of orbital inclinations in order to study the

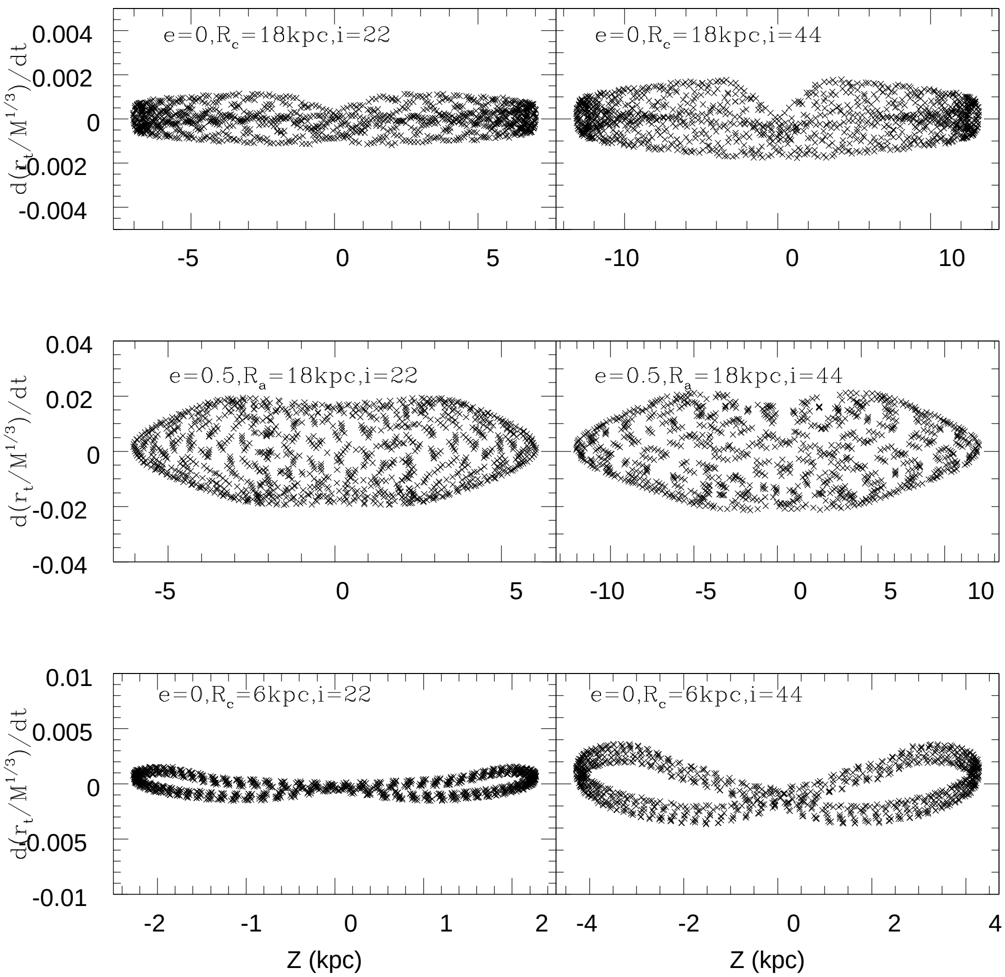

Figure 4.9 The rate of change in the mass normalized tidal radius ($pc/M_{\odot}s^{-1}$ as a function of height above the disk z for all inclined model clusters. Data points are equally spaced in time and cover 12 Gyrs of evolution, so the density of points reflects the amount of time the cluster spends at a given z.

effects of orbital inclination on their dynamical and structural evolution. The main factors which separate star clusters on inclined orbits are tidal heating and tidal shocking. While clusters on eccentric orbits in a spherically symmetric potential do experience tidal heating and tidal shocking at perigalacticon, both inclination and eccentricity are more dominant when the orbit is inclined and a galactic disk is present. The strength of both tidal heating and shocking due to an inclined orbit however weakens with R_{gc}. By 18 kpc, the Galactic potential is nearly spherically symmetric and orbit inclination is nearly negligible. When performing N-body simulations of remote halo clusters, such as Pal 4 and Pal 14 (Zonoozi et al., 2011, 2014), unless their orbits are highly eccentric and bring them deep into the inner regions of the Milky Way it can be safely assumed that they orbit in a spherically symmetric potential.

We have simulated model clusters with identical initial conditions with both circular and eccentric orbits over a range of orbital inclinations to determine the main effects of tidal heating and tidal shocking. Our main conclusions are as follows:

- For clusters with small R_{gc}, inclined clusters experience an enhanced mass loss rate due to increased tidal heating and two tidal shocking events during a disk passage. Clusters with small orbital inclinations are more strongly affected since they spend a longer time in the stronger disk potential.

- At higher R_{gc}, the strength of the galactic disk is weaker, minimizing the effects of tidal heating and disk shocking. Furthermore, r_t at z_{max} is larger than in the plane of the disk, so inclined clusters will actually lose mass at a lower rate than non-inclined clusters.

- Disk shocking causes a temporary increase in σ_V, followed by a sharp drop as stars that have been energized to higher velocities escape the cluster.

- Between shocking events, σ_V can remain constant or even increase due to tidal heating.

- The local potential around a cluster with an inclined orbit is in a constant state of flux, so an inclined cluster is not able respond to its instantaneous r_t except at z_{max}. The r_L of the cluster instead fluctuates around r_t at z_{max}, ranging between being tidally under-filling and over-filling as it travels away from or towards the disk respectively.

- Tidal heating and shocking have a negligible effect on the inner region of the cluster ($r < r_m$).

- The tidal radius of a cluster on an inclined (or inclined and eccentric) orbit is best approximated by assuming it has a circular orbit at its maximum height above the disk: $r_t(R_{xy}, z, e, i) = r_t(R_{xy}, z_{max})_{z_{max}}$

The final point that r_m is unaffected by orbital inclination is helpful when studying globular clusters in other galaxies. More specifically in disk galaxies or elliptical galaxies that are triaxial, the commonly observed effected radius is independent of the orientation of the clusters orbit in the galactic potential, which would be difficult to determine. Therefore the effective radius is solely dependent on the cluster's three dimensional position and orbital eccentricity.

The combined effects of orbital inclination and eccentricity on a cluster are complex. The cluster experiences a strong disk shock when it crosses the disk near R_p, a weak disk shock when crossing near R_a, and a tidal shock during its perigalactic pass. Furthermore, the cluster does not cross the disk at the same R_{gc} or reach R_p at the same z from one orbit to the next. The cluster is also constantly subjected to tidal heating since both the R_{gc} and z coordinate of the cluster change with time. Ultimately, predicting the evolution of a cluster with an inclined and eccentric orbit is difficult, although the effects of orbital inclination clearly decrease with increasing orbital eccentricity since high-e clusters spend the majority of their lifetime at large galactocentric radii. We do find that the dissolution time of such a cluster can be approximated to be (1+e) times longer than the dissolution time of a cluster with a circular orbit at R_p and the same orbital inclination, in agreement with the work of Baumgardt & Makino (2003) for clusters with non-inclined obits.

Exploring a large parameter space in both orbital inclination and eccentricity, and their subsequent effects on clusters, is necessary as the orbits of Galactic globular clusters are neither circular nor in the plane of the disk. As previously mentioned, we also wish to explore how the initial r_m of a cluster changes its dynamical evolution in a non-spherically symmetric potential. The ultimate goal is to be able to predict the size of any cluster no matter its position or orbit in an arbitrary tidal field. Any clusters whose theoretical and observational sizes do not match may indicate recently captured clusters that have not spent long in their current tidal field. When theory and observations do match, we will be able to predict other dynamical properties of a cluster, including its stellar mass function, and rewind the cluster's dynamical clock to determine its initial mass and initial size.

4.5 Acknowledgements

JW, WEH and AS acknowledge financial support through research grants and scholarships from the Natural Sciences and Engineering Research Council of Canada. This work was made possible by the facilities of the Shared Hierarchical Academic Research Computing Network (SHARCNET:www.sharcnet.ca) and Compute/Calcul Canada.

Bibliography

Aarseth, S.J. 2003, Gravitational N-body Simulations: Tools and Algorithms (Cambridge Monographs on Mathematical Physics). Cambridge University Press, Cambridge

Aarseth, S., Hénon, M., Wielen, R., 1974, A&A, 37, 183

Baumgardt H., Makino J. 2003, MNRAS, 340, 227

Bertin, G. & Varri, A. L. 2008, ApJ, 689, 1005

Binney, J. & Tremaine, S. 2008, Galactic dynamics second edition (Princeton, NJ, Princeton University Press, 1987, 747 p.)

Brockamp, M., Küpper, A. H. W, Ties, I., Baumgardt, H., Kroupa, P, 2014, MNRAS, 441, 150

Casetti-Dinescu, D.I., Girard, T.M., Herrera, D., van Altena, W.E., López, C.E., Castillo, D.J. 2007, AJ, 134, 195

Casetti-Dinescu, D.I., Girard, T.M., Jíková, L., van Altena, W.F., Podestá, F., López, C.E. 2013, AJ, 146, 33

D'Onghia, E., Springel, V., Hernsquist, L., & Keres, D. 2010, ApJ, 709, 1138

Dinescu, D.I., Girard, T.M., van Altena, W.E. 1999, AJ, 117, 1792

Gieles, M., Athanassoula, E., Portegies Zwart, S. F., 2007, MNRAS, 376, 809

Gieles, M., Baumgardt, H., Heggie , D. C., Lamers, H.J.G.L.M. 2010, MNRAS, 408, L16

Giersz, M. & Heggie, D. C. 2009, MNRAS, 395, 1173

Giersz, M. & Heggie, D. C. 2011, MNRAS, 410, 2698

Gnedin, O.Y. & Ostriker, J.P. 1997, ApJ, 474, 223

Henon M. 1961, Annales d'Astrophysique, 24, 369

Innanen, K. A., Harris, W.E., Webbink, R.F. 1983, AJ, 88, 338

Johnston, K.V., Spergel, D.N., Hernquist, L. 1995, ApJ, 451, 598

Jórdan, A., Côté, P., Blakeslee, J. P., Ferrarese, L., McLaughlin, D. E. , Mei, S., Peng, E. W., Tonry, J. L., Merrit, D., Milosavljević, M., Sarazin, C. L., Sivakoff, G. R., West, M. J., 2005, ApJ, 634, 1002

King, I. R. 1962, AJ, 67, 471

Kroupa, P., Tout C.A., Gilmore, G. 1993, MNRAS, 262, 545

Leigh, N., Giersz, M., Webb, J.J., Hypki, A., de Marchi, G., Kroupa, P., Sills, A. 2013, MNRAS, 436, 3399

Madrid, J.P., Hurley, J.R., Sippel, A.C., 2012, ApJ, 756, 167

Madrid, J.P., Hurley, J.R., Martig, M., 2014, ApJ, 784, 95

McLaughlin, D. E. & van der Marel, R. P. 2005, ApJs, 161, 304

Miyamoto, M. & Nagai, R. 1975, PASJ, 27, 533

Plummer, H.C. 1911, MNRAS, 71, 460

Praagman, A., Hurley, J., Power C. 2010, New Astron., 15, 46

Puzia, T.H., Paolillo, M., Goudfrooij, P., Maccarone, T.J., Fabbiano, G., Angelini, L. 2014, ApJ, 786, 78

Renaud, F., Gieles, M., Christian, M. 2011, MNRAS, 418, 759

von Hoerner, S. 1957, ApJ, 125, 451

Webb, J. J., Sills, A., Harris, W.E. 2012, ApJ, 746, 93

Webb, J.J., Harris, W.E., Sills, A., Hurley, J.R. 2013, ApJ, 764, 124

Webb, J.J., Leigh, N., Sills, A., Harris, W.E., Hurley, J.R. 2014, MNRAS, 442, 1569

Xue, X.X. et al., 2008, ApJ, 684, 1143

Zonoozi, A. H., Küpper, A. H. W, Baumgardt, H., Haghi, H., Kroupa, P., Hilker, M. 2011, MNRAS, 411, 1989

Zonoozi, A. H., Haghi, H., Küpper, A. H. W, Baumgardt, H., Frank, M.J., Kroupa, P 2014, MNRAS, 440, 3172

Chapter 5

Globular Cluster Scale Sizes in Giant Galaxies: The Case of M87 and the Role of Orbital Anisotropy and Tidal Filling

Jeremy J. Webb, Alison Sills, William E. Harris

The Astrophysical Journal, Volume 779, Issue 2, pages 94-103,
Bib. Code: 2013ApJ...779...94W, DOI: 10.1088/0004-637X/779/2/94

5.1 Introduction

Many globular cluster (GC) properties, even simple ones like scale size, lack fundamental explanations. It is typically assumed that the gravitational field of the host galaxy is responsible for limiting cluster size (e.g. von Hoerner, 1957; King, 1962; Innanen, Harris, & Webbink, 1983; Jordán et al., 2005; Binney & Tremaine, 2008; Bertin & Varri, 2008). The tidal field imposes a *tidal radius* r_t, also known as the Jacobi radius r_J, of the GC, beyond which a star feels a stronger acceleration towards the host galaxy than toward the cluster and can escape. It is often assumed that the observationally determined *limiting radius* r_L, which marks the point where cluster density drops to zero (Binney & Tremaine, 2008), represents r_t. But comparisons of the observational relationship between cluster size and galactocentric distance to theory are beginning to suggest otherwise.

First-order tidal theory suggests that the r_t of a GC on a circular orbit is related to its galactocentric distance (von Hoerner, 1957) via:

$$r_t = r_{gc}(\frac{M}{2M_g})^{1/3} \tag{5.1}$$

where r_{gc} is the three dimensional galactocentric distance of the cluster, M is the cluster's mass, and M_g is the mass of the galaxy. Assuming the mean cluster mass is independent of galactocentric distance and the host galaxy potential can be approximated by an isothermal sphere ($M_g(r_{gc}) \propto r_{gc}$), we expect $r_t \propto r_{gc}^{\frac{2}{3}}$. Furthermore, if central concentration c is also independent of r_{gc}, the mean effective (or half-mass) radius r_h will also be related to galactocentric distance by the same scaling.

Suppose we assume more generally that $r_h \propto R_{gc}^{\alpha}$, where now R_{gc} is the two-dimensional (projected) galactocentric distance. If $r_h \propto r_{gc}^{\frac{2}{3}}$, then the effects of projection from 3D to 2D would make $\alpha \sim 0.4-0.5$ for normal radial distributions. However, observations of GCs in different galaxies do not match this simple theoretical prediction. The Milky Way cluster population comes the closest with $\alpha = 0.46 \pm 0.05$ (data from Harris 1996 (2010 Edition)). The discrepancy in α can perhaps be attributed to the Milky Way's non-spherical potential, and to the fact that GCs do not have circular orbits (e.g. Dinescu et al., 1999; Casetti-Dinescu et al., 2007, 2013).

Issues due to a non-spherical potential can be minimized by focussing on giant elliptical galaxies. However recent measurements of α in giant elliptical galaxies present an even larger discrepancy between theoretical and observational values. Spitler et al. (2006) found $\alpha = 0.19 \pm 0.03$ for NGC 4594, as did Harris et al. (2010). Gomez & Woodley (2006) found relationships for the metal poor and metal rich GC populations of NGC 5128 separately, with $\alpha = 0.05 \pm 0.05$ for the metal poor clusters and $\alpha = 0.26 \pm 0.06$ for the metal rich clusters. Harris (2009a) found an extremely flat relationship $\alpha = 0.11$ for a sample of six massive gE galaxies. However, Blom et al. (2012) found that NGC 4365 has a rather steep value of α equal to 0.49 ± 0.04 compared to other giant ellipticals, in closer agreement with simple theory. Such a high value of α, along with the identification of three distinct GC sub-populations, may indicate NGC 4365 underwent unique stages of formation and evolution compared to the other galaxies mentioned above.

In summary, measurements of α in most galaxies so far yield an observed relationship between r_h and R_{gc} much shallower than predicted. Attempts to explain this disagreement have been inconclusive. Madrid et al. (2012) used N-body simulations to illustrate the relationship between r_h and R_{gc} is better represented by $r_h \propto tanh(R_{gc})$ for identical model clusters on a range of circular orbits in a Milky-Way like potential. They found that r_h increases steadily with galactocentric distance out to 40 kpc, beyond which r_h

stays relatively constant as the effect of tides becomes less and less important. However, their model clusters had larger effective radii than clusters seen in the outer regions of giant E galaxies. Application of this work to the potentials of giant E galaxies and including a larger range of non-circular orbits is promising.

It may instead be the case that outer halo clusters originally formed tidally under-filling, and are still in the process of expanding (e.g. Gieles et al., 2010; Webb et al., 2013). Strader et al. (2012) also found that clusters in NGC 4649 showed no relationship between r_h and R_{gc} beyond 15 kpc, indicating they are not tidally truncated. For tidally under-filling clusters, r_L would be distinctly less than the theoretically allowed r_t, and tidal theory would then over-estimate their size. It may also be possible that the current location of outer GCs is not indicative of their location when they formed; they may represent a captured population from smaller satellite galaxies. Therefore it would be the cluster's orbit in the potential of the satellite galaxy that first imposed cluster size, making any predictions with the potential of the current host galaxy inapplicable. The concept of GC populations consisting of one or more captured sub-populations has also been used to explain their observed bi-modal or even tri-modal distribution in colour, typically attributed to differences in cluster metallicity (e.g. Zepf & Ashman, 1993; Larsen et al., 2001; Brodie & Strader, 2006; Peng et al., 2006; Harris , 2009a; Blom et al., 2012).

In a previous paper (Webb, Sills, & Harris, 2012) we measured the size distribution of GCs with $R_{gc} \leq 10$ kpc in M87, and found a very shallow trend $\alpha = 0.08 \pm 0.02$. We explained the distribution by introducing an anisotropy gradient in the cluster orbits. If GC orbits become more and more radial with galactocentric distance, the mean cluster size will drop below the theoretical prediction as clusters will be subject to increased tidal stripping (Webb et al., 2013) and will thus flatten the relationship between r_h and R_{gc}. Unfortunately our work was limited by the range in R_{gc} of our observations. In this paper we present new Hubble Space Telescope (HST) observations of the outer regions of M87, extending cluster size measurements beyond 100 kpc. M87 contains the largest easily accessibly GC population, making it easiest to trace out to large R_{gc}. The larger range in R_{gc} allows for a much stronger test of how orbital anisotropy effects the size distribution of GCs.

In Section 2 we introduce our new observations and determine the effective radii of each cluster in order to extend the observed trend between cluster size and galactocentric distance. In Section 3 we discuss the model originally used in Webb, Sills, & Harris (2012) for simulating a theoretical M87 cluster population, and discuss in detail the improvements we have made. The model makes use of the known mass distribution of M87 (McLaughlin , 1999) and various cluster population parameters (set to match the observations) to establish a theoretical relationship between cluster size and R_{gc}. In Section 4 we discuss the comparison between between theory and observations, as well as planned future work.

5.2 Observations

We use a combination of archived and new HST images to study the GC population of M87. The new HST images presented in this study are from program GO-12532 (PI Harris), and consist of both Wide Field Camera 3 (WFC3) and Advanced Camera for Surveys (ACS) images of the outer regions ($R_{gc} > 10$

kpc) of M87, extending out to nearly 110 kpc. For each field, three WFC3 exposures totalling approximately 2600 seconds and three ACS exposures totalling approximately 2300 seconds were taken simultaneously with the F814W filter. The following orbit repeated the same observations with the F475W filter. The process was repeated for three additional ACS/WFC3 pairs for a total of 8 fields of view over 8 orbits. The final co-added composite exposures in each filter were constructed through use of the STSDAS/MULTIDRIZZLE routine within IRAF. The details of of each M87 image are summarized in Table 5.1 and the locations of our fields are illustrated in Figure 5.1.

Table 5.1: HST Image Information

Field	RA (J2000)	DEC (J2000)	Camera	Filter	Exposure Time (seconds)
F3WI	12 30 56.4865	+12 21 48.20	WFC3	F814W	2589
F3WB	12 30 56.4865	+12 21 48.20	WFC3	F475W	2729
F3AI	12 31 03.691	+12 27 29.47	ACS	F814W	2282
F3AB	12 31 03.691	+12 27 29.47	ACS	F475W	2351
F5WI	12 31 15.360	+12 21 48.30	WFC3	F814W	2589
F5WB	12 31 15.360	+12 21 48.30	WFC3	F475W	2729
F5AI	12 31 23.374	+12 27 25.58	ACS	F814W	2282
F5AB	12 31 23.374	+12 27 25.58	ACS	F475W	2351
F7WI	12 31 34.849	+12 21 48.20	WFC3	F814W	2589
F7WB	12 31 34.849	+12 21 48.20	WFC3	F475W	2729
F7AI	12 31 50.450	+12 17 13.94	ACS	F814W	2282
F7AB	12 31 50.450	+12 17 13.94	ACS	F475W	2351
F8WI	12 32 06.642	+12 21 25.08	WFC3	F814W	2589
F8WB	12 32 06.642	+12 21 25.08	WFC3	F475W	2729
F8AI	12 32 15.130	+12 15 50.32	ACS	F814W	2282

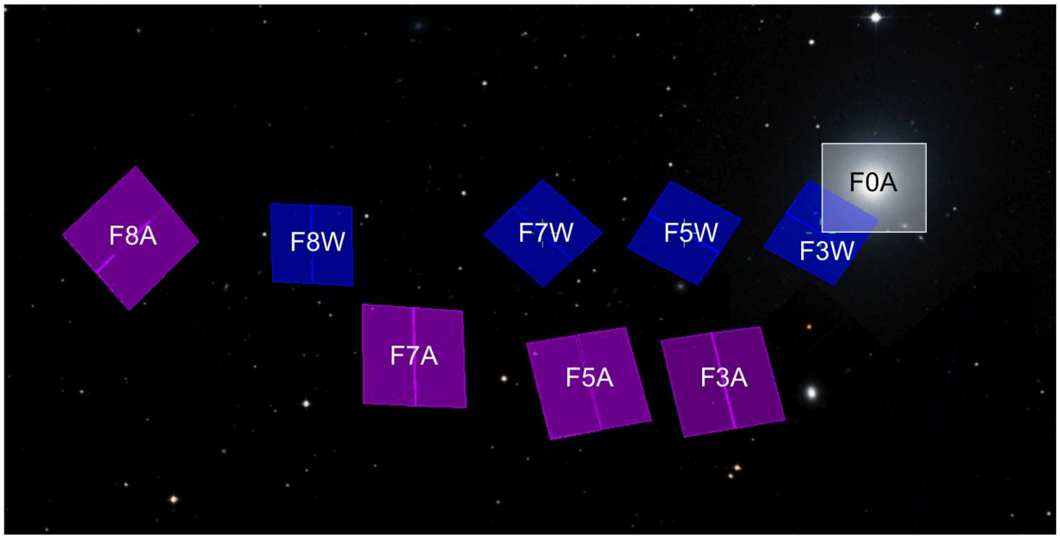

Figure 5.1 Fields of view for new HST images relative to the center of M87. WFC3 images (F3W, F5W, F7W, F8W) are marked in blue and ACS images (F3A, F5A, F7A, F8A) marked in purple. Field of view of archive ACS images (F0A) is marked in white.

F8AB	12 32 15.130	+12 15 50.32	ACS	F475W	2351

We combined our new HST data with archived HST ACS/WFC images of the central regions of M87 in the F814W (I) and F606W (V) filters (also illustrated in Figure 5.1), from program GO-10543 (PI Baltz). A detailed description of the co-added composite exposures in each filter can be found in Bird et al. (2010). The GCs in this central field have been studied in detail by Madrid et al. (2009), Peng et al. (2009), Waters et al. (2009) and Webb, Sills, & Harris (2012). To follow the nomenclature established in Table 5.1, these images will be referred to as F0AI and F0AV.

For consistency, our search for GC candidates was performed with the method described in Webb, Sills, & Harris (2012). All images were searched for GC candidates with thresholds set such that individual halo stars are rejected while the faintest of GCs are still included. Finally, only objects that were found in both the F814W and F475W filters were accepted, resulting in an initial candidate list of 3287 objects.

5.2.1 Globular Cluster Effective Radii

Before we can make any measurements of the structural parameters of our GC candidates, a point spread function (PSF) must first be modelled for each image, which we do empirically. The process is described in detail by Madrid et al. (2009). For a given image, stars were identified with SExtractor (Bertin & Arnouts, 2008) by approximately measuring the full width half maximum (FWHM) of all objects that are brighter than the background by a factor of 5 times the standard deviation of the background. Star-like objects with FWHMs of approximately 2.5 pixels for the WFC3 images and 2.0 pixels for the ACS images are easily identifiable that correspond to the expected $0\farcs01$ FWHM of stars. Stars were inspected for faint companions, bad pixels, or other anomalies before use of the standard DAOPHOT routines to build the PSF.

In Webb, Sills, & Harris (2012), the surface brightness distribution of each cluster was fit with PSF-convolved King (1962) models via the code GRIDFIT (e.g. Barmby et al., 2007; McLaughlin et al., 2008; Harris et al., 2010). Unfortunately, attempts to use GRIDFIT with the new HST dataset resulted in poor fits due to the lower resolution. Therefore we opted to measure the r_h of each cluster candidate with the software ISHAPE (Larsen, 1999) which has been successfully used many times on images with similar resolution (e.g. Madrid et al., 2009).

For consistency purposes, we also re-measured the GCs in the central field F0A with ISHAPE. We measured these clusters through both $0\farcs025\ px^{-1}$ and $0\farcs05\ px^{-1}$ versions of the F0A combined images. Then, since a portion of the F3W image overlaps with the F0A image, we explore the influence of measuring cluster sizes on images with different detectors by plotting the r_h of clusters found in both images in the left panel of Figure 5.2. From Figure 5.2 (left panel), images with lower resolution appear to result in underestimating cluster sizes by a mean value of 0.7 pc, or 0.2 pixels in the lower resolution image.

To determine whether the discrepancy of 0.7 pc can be attributed to differences in resolution, we compare the GCs in F3 in the right panel of Figure 5.2 with the same objects in F0A but now at $0\farcs05\ px^{-1}$. When measured at similar resolutions, the overlapping GCs in each field have comparable effective radii, with the scatter centered around a $1:1$ correlation. The scatter is expected due to the images having significantly different signal-to-noise ratios (F0AV and F0AI images have much longer exposure times equalling 24,500 and 73,800 seconds). Therefore, the mean difference of 0.7 pc in Figure 5.2 (left) can be attributed to differences in both resolution and signal-to-noise between the F0A and F3W images. To remain consistent with works of Madrid et al. (2009), Peng et al. (2009), Waters et al. (2009) and Webb, Sills, & Harris (2012) regarding F0A, cluster sizes measured with our new HST dataset in fields F3-F8 are increased by 0.7 pc.

Objects were then removed from the candidate list that were poorly fit by ISHAPE (χ^2 values greater than 10) or that had large differences between the measured r_h in the F814W and F475W bands. For the ACS images, true magnitudes were determined through aperture photometry extrapolated to

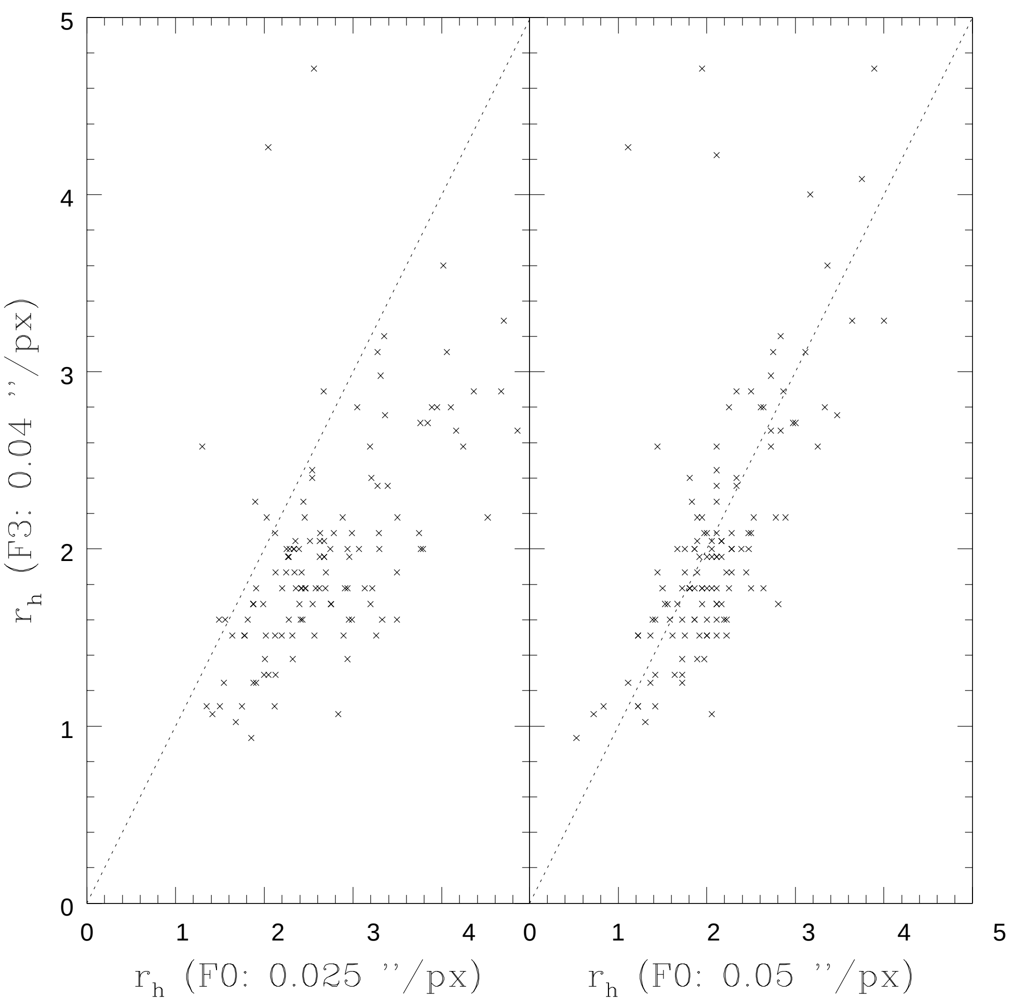

Figure 5.2 r_h of F3W GCs vs. the r_h of overlapping GCs in the high resolution ($0''.025$ px^{-1}) F0A images (left) and low resolution $0''.05$ px^{-1} F0A images (right). The dotted lines represent a 1:1 correlation.

large radius (Sirianni et al., 2005). The transformations of Saha et al. (2011) were then used to convert magnitudes to the standard B and I. However for the WFC3 images, only the filter-based magnitudes could be measured (F475W, F814W) since no well calibrated transformation to (B,I) is available at present.

The candidate list was trimmed further by cutting objects that were either extremely blue, extremely red, or extremely faint and could be visually identified as non-GCs. Colour-magnitude diagrams (CMDs) of the final 1047 candidates are shown in Figures 5.3 and 5.4. In both CMDs, the blue (metal-poor) and red (metal-rich) sequences are clearly visible. ACS objects with B-I < 1.8 and WFC3 objects with F475W-F814W < 1.5 were declared blue, with the remaining clusters declared red. The size, goodness of fit, colour, and magnitude cuts described above ensure none of the objects in Figures 5.3 and 5.4 are either foreground stars or background galaxies.

The F814W and F475W images of each field were then co-added to boost the signal to noise ratio, and ISHAPE was again used to measure the r_h of each of the final candidates. The r_h from these combined images as a function of R_{gc} for each candidate is illustrated in Figure 5.5. The median r_h is plotted in red, calculated with radial bins containing 50 GCs each. Finding the slope of the median line in log-log space allowed for the determination of α to be 0.14 ± 0.01, similar to the values found in other giant E galaxies discussed in Section 1.

While the relationship between the median r_h and R_{gc} is shallow, it is important to note that the scatter about the median increases with R_{gc}. The outer halo of M87 consists of extended ($r_h > 5$ pc) GCs at large R_{gc} and that have been projected to smaller R_{gc}. The extended clusters are more in line with what is expected from simple tidal theory, which indicates that the outer

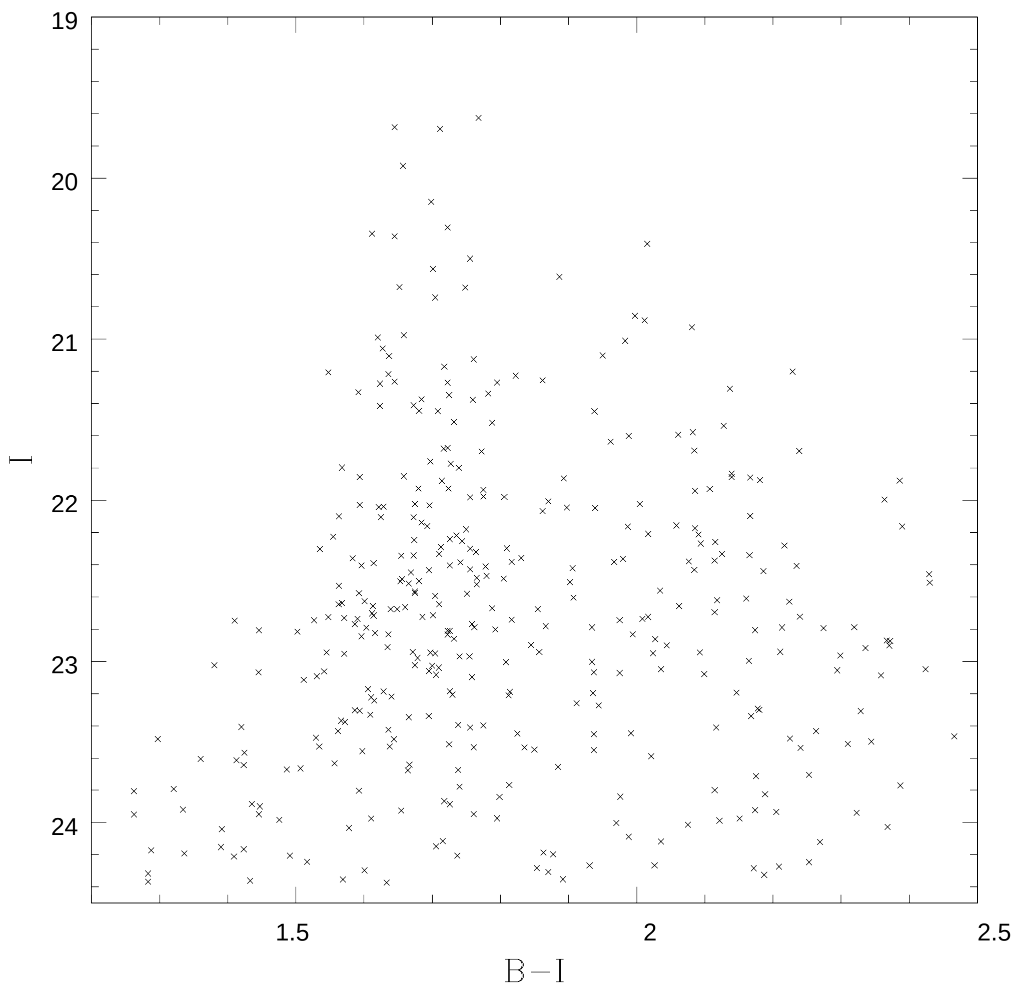

Figure 5.3 CMD of the GC candidates in ACS images of the outer regions M87.

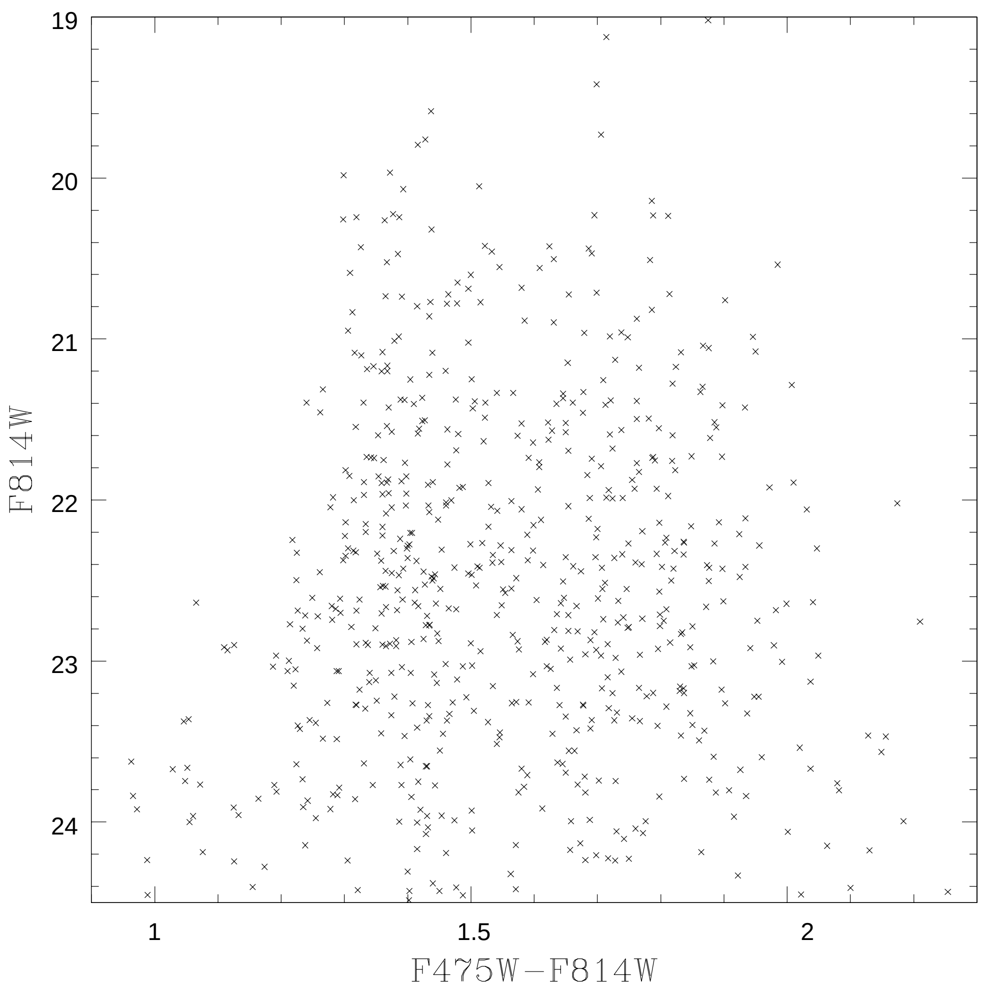

Figure 5.4 CMD of the GC candidates in WFC3 images of the outer regions M87.

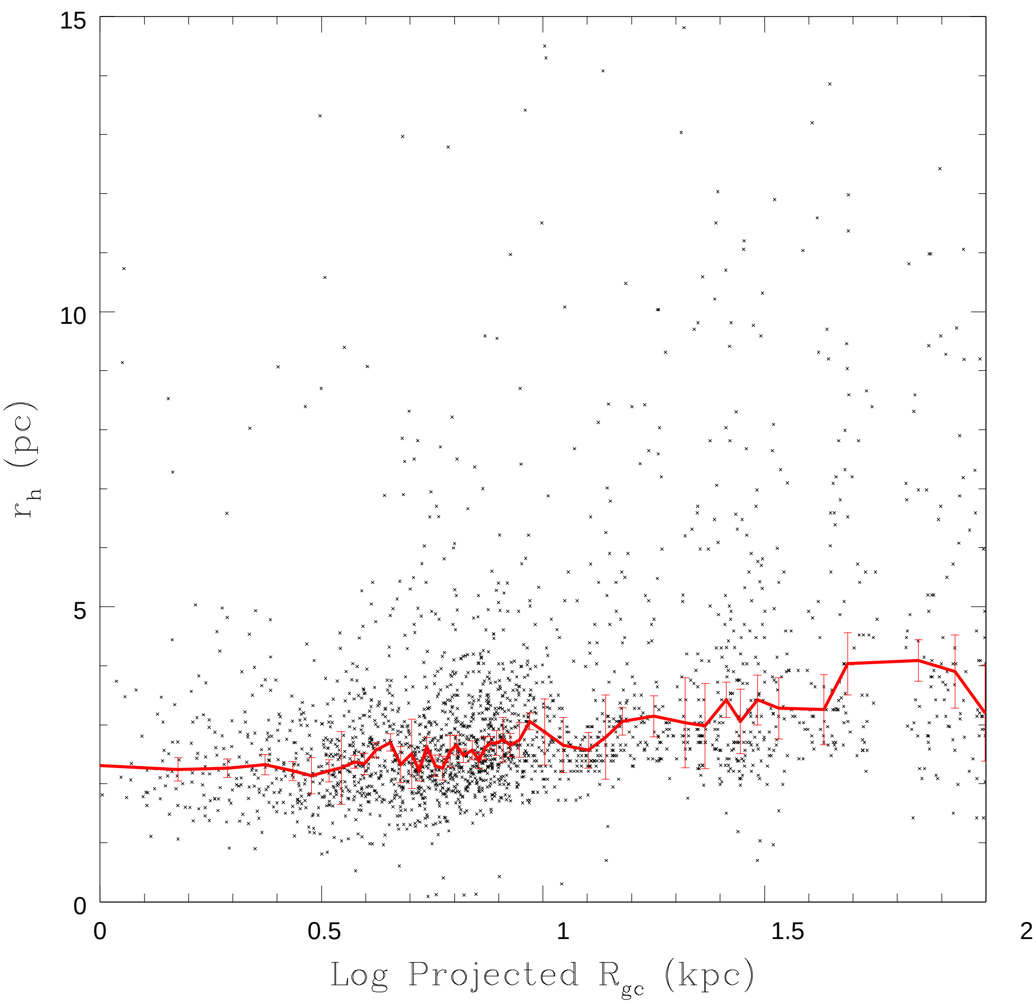

Figure 5.5 r_h vs. log R_{gc} for observed GCs. The solid red line indicates the median r_h calculated with radial bins containing 50 GCs each. Error bars represent the standard error $\sigma/\sqrt(n)$ as given by Harris et al. (2010).

halo may comprise a mixture of dynamical histories.

5.3 Simulation

The observational results shown in Figure 5.5 are next compared to models of GCs moving in the tidal field of M87, to constrain our understanding of their scale sizes. The simulation we use is described in detail in Webb, Sills, & Harris (2012), but we now extend it further.

5.3.1 Initial Conditions

We first set up a model cluster population with the same observational characteristics (radial profile, velocity dispersion, mass distribution, central concentration distribution) as the observed population of M87 clusters, and then use tidal theory to establish a theoretical relationship between cluster size and R_{gc} that can be compared to Figure 5.5. The simulation allows for separate red and blue populations to be modelled.

Each simulated GC is given a position in the halo (r, θ, ϕ), velocity (v_r, v_θ, v_ϕ), mass (M), and central concentration ($c = \frac{r_t}{r_c}$). The spatial distribution of the red and blue cluster subpopulations is taken from Harris (2009b), and we assume the angular distribution to be spherically symmetric. The luminosity function of the F0A GCs, a Gaussian with a mean visual magnitude of -7.3 and a standard deviation of 1.3 (Webb, Sills, & Harris, 2012), is used to establish the mass distribution of GCs with $(\frac{M}{L})_V = 2$ (e.g. McLaughlin & van der Marel (2005)). We adopt $(m-M)_0 = 30.95$ for M87 (Pierce et al., 1994; Tonry et al., 2001). The central concentration of each simulated GC was drawn from the observed distribution of Milky Way clusters from Harris 1996 (2010 Edition), a Gaussian with a mean of $c = 1.5$ and standard deviation of 0.4.

The observed line of sight velocity dispersion (σ) (Côté et al., 2001) is initially assumed to be identical for each spherical coordinate (R, θ, ϕ), such that $\sigma_R = \sigma_\theta = \sigma_\phi$. This assumption results in an isotropic distribution of orbits and the anisotropy parameter (β) equal to zero (Equation 6.3) (Binney & Tremaine, 2008),

$$\beta = 1 - \frac{\sigma_\theta^2 + \sigma_\phi^2}{2\sigma_R^2} \tag{5.2}$$

In our simulation β is kept as a free parameter, and can also change with galactocentric distance. All distribution parameters are summarized in Table 5.2.

Table 5.2: Simulated Globular Cluster Population Input Parameters

Parameter	Value
Radial Distribution	Hubble Profile
Blue Population	
σ_0	66 arcmin^{-2}
R_0	2.0'
a	1.8
Red Population	
σ_0	150 arcmin^{-2}
R_0	1.2'
a	2.1
Angular Distribution	Spherically Symmetric
Mass-To-Light Ratio	$(M/L)_V = 2$
Mass Distribution	Gaussian

$\langle log(M/M_0)\rangle$	5.5
$\sigma_{log(M/M_0)}$	0.52
Velocity Dispersion	Gaussian
$\langle v\rangle$	-19 km/s
σ_v	401 km/s
β	0
Central Concentration	Gaussian
$\langle c\rangle$	1.5
σ_c	0.4

While the initial setup of our model population is the same as in Webb, Sills, & Harris (2012), improvements have since been made towards making the model cluster population more realistic and representative of the observations we are trying to duplicate.

5.3.2 Calculating Tidal and Effective Radii

After a cluster has been assigned a position, velocity, mass, and central concentration the orbit of the cluster is then solved. Now we have all the ingredients necessary to calculate r_t and r_h,which is the first improvement made over the model presented in Webb, Sills, & Harris (2012). Recent N-body simulations by Webb et al. (2013) have shown that the historical assumption that tidal radii are imposed at perigalacticon is invalid because a GC is able to fill its instantaneous r_t at all times, independent of its orbital eccentricity. More specifically, the mass normalized limiting radius of a cluster ($r_{L,n} = \frac{r_L}{M^{\frac{1}{3}}}$) is the same at a given R_{gc}, independent of cluster orbit.

However, comparing the instantaneous r_t of a cluster to its observationally determined r_L is also incorrect. Küpper et al. (2010) found that the bulk of the cluster, and hence the surface brightness profile, is nearly constant over an orbital period and more accurately reflects the mean tidal field that the cluster experiences. So while the true r_L of a cluster changes with orbital phase (Webb et al., 2013), the observational limiting and effective radius as determined by a King (1962) model does not. To best compare with observations we need to calculate the effective radii of our simulated clusters, as the effective radius does not fluctuate as dramatically with orbital phase (Küpper et al., 2010; Webb et al., 2013) and will therefore be more comparable to observationally determined effective radii.

In Figure 5.6 we plot the mass normalized half-mass radii $r_{m,n} = \frac{r_m}{M^{\frac{1}{3}}}$ of various N-body model clusters as a function of time. A detailed discussion of the N-body models presented here is done in Webb et al. (2013). With the infinite resolution of our model clusters, r_h can fluctuate dramatically from time step to step. Therefore we use the half-mass radius r_m to trace the evolution of r_h as it remains consistent between time-steps. Even though r_m is always slightly larger than r_h, the two radii scale the same with respect to time (Webb et al., 2013). In each panel, the lower black line is for a model cluster with a circular orbit at 6 kpc. The red line is for a model cluster with an eccentric orbit that has a perigalactic distance of 6kpc. Clusters were modelled with eccentricities of 0.25, 0.5, 0.75, and 0.9, with the eccentricity marked in each panel. The upper black line in each panel is for a model cluster with a circular orbit at the apogalactic distance of the eccentric cluster, which in these cases are 10 kpc, 18 kpc, 43 kpc, and 104 kpc.

In Figure 5.6, the $r_{m,n}$ profile of clusters with circular orbits (black

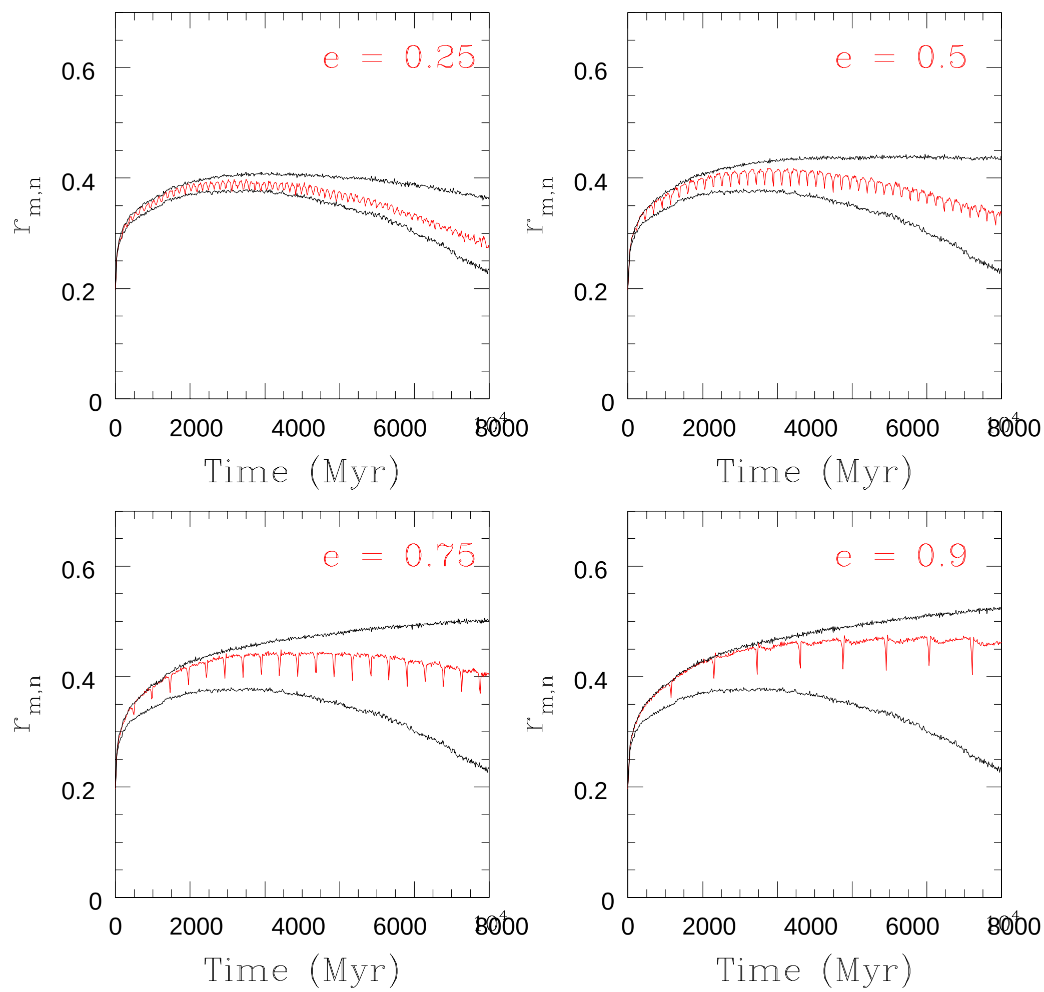

Figure 5.6 Mass normalized r_m of simulated star clusters on eccentric orbits (red) compared to clusters with circular orbits at R_p (lower black line, always 6 kpc) and R_{ap} (upper black line) as a function of time. Data taken from Webb et al. (2013).

lines) decreases smoothly over time. Clusters with eccentric orbits (red lines) only undergo a brief fluctuation at R_p, but are also more or less smooth from one time-step to the next. A smooth evolution in r_m is in agreement with the results of Küpper et al. (2010) discussed above. The effective radius also appears to be linked to the time-averaged tidal field that the cluster experiences: highly eccentric clusters are closer in size to clusters with orbits at R_a while clusters with low eccentricities are comparable to clusters with circular orbits at R_p.

In order to predict r_m or r_h given the orbit and limiting radius of a cluster, we note that $r_{m,n}$ increases strongly as a function of eccentricity in Figure 5.6. Hence the $r_{m,n}$ of two clusters with the same R_p and at the same R_{gc} will not be the same if they have different orbits. From the results of our N-body simulations in Webb et al. (2013) (Figure 5.6) as well as larger mass versions of each model (presented in Leigh et al. (2013)), we find that the ratio of $r_{m,n}$ for a cluster with an eccentric orbit to $r_{m,n}$ for a cluster with a circular orbit at R_p increases linearly with eccentricity after 10 Gyr. More specifically, clusters with eccentric orbits have effective radii that are a factor of $(1 + 0.31 \times e)$ larger than if they had circular orbits at R_p. The uncertainty in the correction factor of 0.31 is ± 0.01. The correction factor is applicable to old GCs, but further simulations are required to determine how it depends on a GCs evolutionary stage.

In order to determine the effective radius of each simulated cluster, we first calculate their tidal radii as if they had a circular orbit at R_p given the formalism of Bertin & Varri (2008). The derivation of r_t by Bertin & Varri (2008) is ideal as it makes no assumptions regarding the potential of the host galaxy except that it must be spherically symmetric. Therefore the mass profile of M87 determined by McLaughlin (1999) can be used to determine the galactic potential. We next assume that all clusters are tidally filling, such that r_L can be set equal to r_t at perigalacticon. We explore the effects of non-tidally filling clusters in Section 5.4.3. The perigalactic effective radius (r_h assuming a circular orbit at R_p) is then calculated given the central concentration of the cluster and assuming that it can be represented by a King (1962) model. The true r_h will be a factor of $(1.0 + 0.31 \times e)$ larger than the perigalactic case.

5.3.3 Including Orbital Anisotropy

The second major improvement to our model involves the anisotropy parameter β. In our previous work (Webb, Sills, & Harris, 2012), σ_θ and σ_ϕ were kept equal to the observed line of sight velocity dispersion when $\beta < 0$, while σ_R was decreased based on Equation 6.3. Similarly for $\beta > 0$, σ_R was kept equal to the observed line of sight velocity dispersion while σ_θ and σ_ϕ were decreased. This approach did have the desired effect of altering the distribution of cluster orbits, but the resulting velocity dispersion was no longer equal to the observed one. The improved simulation we use here now adjusts σ_R, σ_θ and σ_ϕ simultaneously such that Equation 6.3 is satisfied and the overall mean velocity dispersion equals the observed line of sight velocity dispersion.

5.3.4 The Effect of Tidally Under-filling Clusters

Previously we have assumed that all simulated clusters are *tidally filling*, as it allows for a straightforward calculation of r_L and r_h for each cluster. But not all observed GCs are expected to be tidally filling (Gieles et al., 2010). Therefore we added the filling parameter $R_F = \frac{r_L}{r_t}$ to the simulation, where

r_L is the limiting radius (essentially, the observed outer radius) and r_t is the theoretically permitted tidal radius. The simulation allows for all GCs to be tidally under-filling by the same amount ($R_F = constant$) in order to explore the effect that tidally under-filling GCs have on the exponent α. With the exception of Section 5.4.3 R_F is always set equal to 1.0.

5.3.5 Observational Constraints

Finally, we introduce a minimum r_h cut-off set equal to the smallest measurable value from the resolution limit of our observations. The simulation already includes a tidal dissolution time and dynamical friction infall time cutoff of 10 Gyr as described in Webb, Sills, & Harris (2012).

5.4 Comparing Theory and Observations

To match the observations, populations of 10000 clusters were simulated following the real spatial profile such that the total number of clusters within 10 kpc of M87 is the same as the observed dataset. The ratio of number of blue clusters to red clusters was set equal to 3 : 2, in agreement with the profiles in Harris (2009b). The only difference between red and blue clusters in our simulation is which radial distribution profile in Table 5.2 is used to determine cluster position.

5.4.1 The Isotropic Case

The first comparison between theory and observations was done for a model population with an isotropic distribution of orbits ($\beta = 0$) and $R_F = 1$. The

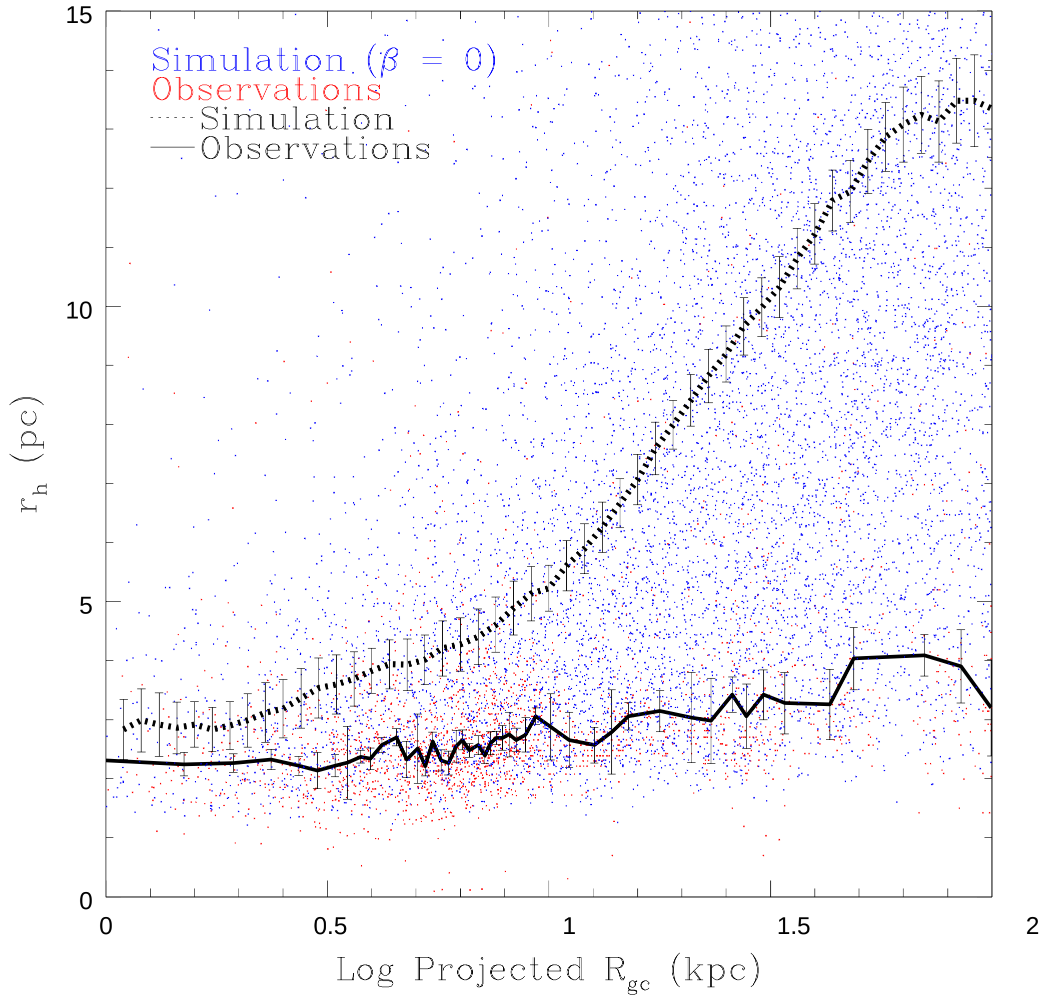

Figure 5.7 r_h and log R_{gc} of each simulated GC (blue) for $\beta = 0$. The dashed black line marks the median r_h calculated with radial bins containing 50 GCs each. For comparison purposes we also plot the observed clusters (red) and median (solid black line) from Figure 5.5. Error bars represent the standard error $\sigma/\sqrt(n)$ as given by Harris et al. (2010).

r_h of both model (blue) and observed (red) clusters are plotted in Figure 5.7 as functions of R_{gc}.

Figure 5.7 indicates that an isotropic distribution of orbits produces a larger distribution of cluster sizes than observed, particularly at large R_{gc}. While the observations suggest $\alpha = 0.14$, the model predicts $\alpha = 0.41 \pm 0.01$, in closer agreement with basic tidal theory. Therefore this "baseline" model strongly disagrees with the data, either in terms of the trend or the total scatter.

It should be noted that the assumption that all clusters are tidally filling is likely to be safest in the inner regions of the galaxy where the tidal field is strong (Alexander & Gieles, 2013). Outer clusters, for which r_t is considerably larger, are more likely to be tidally under-filling. The clear disagreement between the observations and the isotropic model suggest that either outer GCs are severely tidally under-filling, have preferentially radial orbits, or a combination of both.

5.4.2 Anisotropic Cases

We first explore how much a non-isotropic distribution of orbits can minimize both the distribution of cluster sizes and the value of α in our model cluster population. In Figure 5.8 we show the median r_h as a function of galactocentric distance for models with different values of β. Very large values of β are required in order to bring the median model cluster size down to the level of the observations. A β of 0.99, which corresponds to a mean orbital eccentricity of 0.9, produces the closest agreement. In Figure 5.9, which shows the actual distribution for $\beta = 0.99$, the scatter in the simulated data points about the median line is greatly reduced and is more comparable to the observations than the $\beta = 0$ case. However the corresponding value of α, equal to 0.21 ± 0.01, is still higher than the observed value of 0.14. Furthermore, while median cluster sizes are comparable in the mid to outer regions of M87, the $\beta = 0.99$ simulation underestimates cluster size in the inner regions of

M87. These discrepancies suggest that β likely increases with galactocentric distance. Previous observational and theoretical studies of M87 (Côté et al., 2001; Webb, Sills, & Harris, 2012), NGC 3379 and NGC 821 (Weijmans et al., 2009) , the Milky Way (Prieto & Gnedin, 2008) and dark matter halos (Zait, Hoffman, & Shlosman, 2008; Ludlow et al., 2010) draw similar conclusions, although none of the existing data are consistent with such a high mean β.

Our simulation explicitly allows for the population to have an anisotropy profile $\beta(R_{gc})$. However, in order to put constraints on the profile as was done in Webb, Sills, & Harris (2012), we first need to know the likely distribution of tidally filling and under-filling clusters in M87. Then the simulated r_h profile will represent the observed profile as opposed to being an upper limit.

5.4.3 The Effect of Tidally Under-filling Clusters

We next explore how much the existence of tidally under-filling clusters can minimize both the distribution of cluster sizes and the value of α in our model cluster population. A recent study by Alexander & Gieles (2013) demonstrated that unless all clusters form tidally filling, a present day cluster population will be made up of a mix of tidally filling and under-filling clusters. They were able to reproduce a relationship between r_h and R_{gc} similar to the Galactic GCs by assuming the population formed under-filling and then evolved in a Milky Way-like potential. Allowing clusters to be tidally under-filling would not require such high values of β as found in Section 5.4.2 or as steep an anisotropy profile. We illustrate this statement in Figure 5.10 by simulating cluster populations with the same static values of β as Figure 5.8, but with the filling parameter R_F equal to 1 (top left panel, same as Figure 5.8) ,

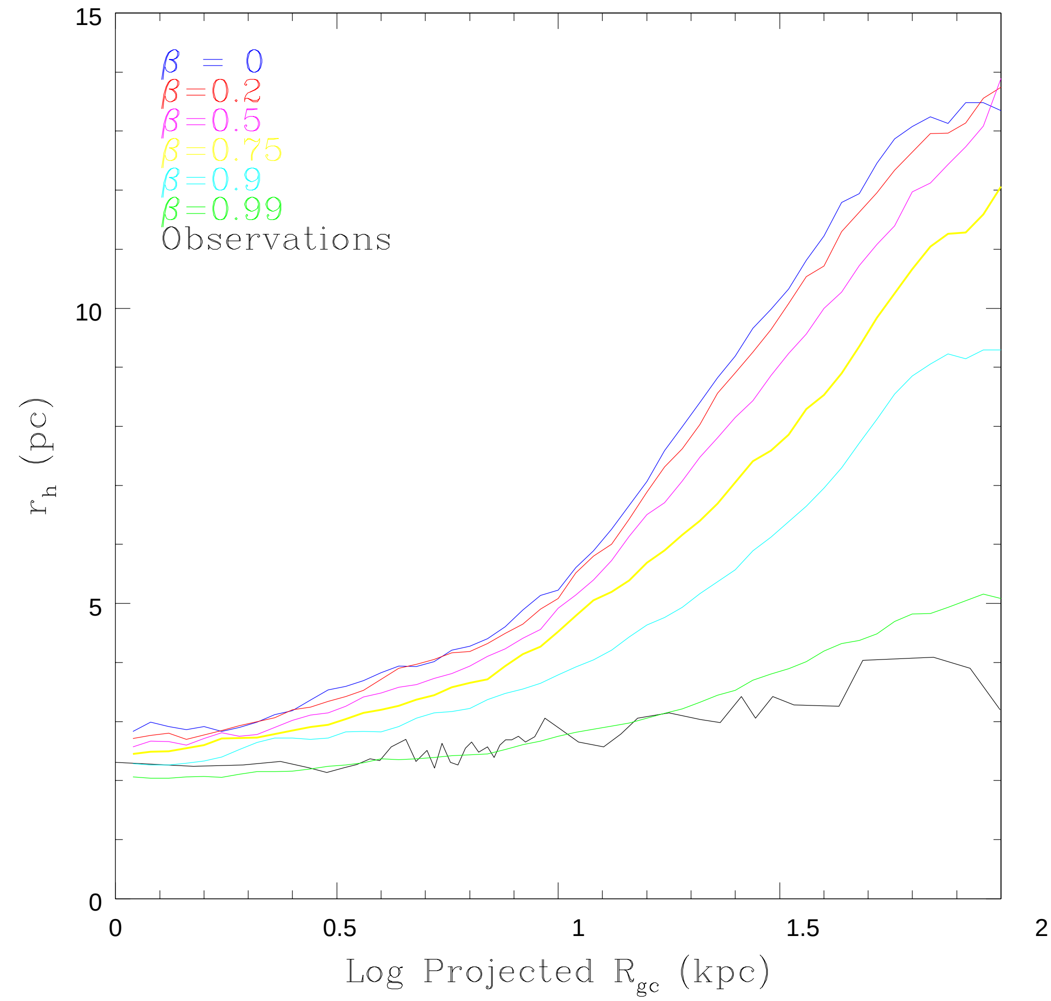

Figure 5.8 Relationship between median r_h and log R_{gc} for simulated GC populations with different values of β. Median r_h are calculated with radial bins containing 50 GCs each. The solid red line is the observed median effective radius From Figure 5.5.

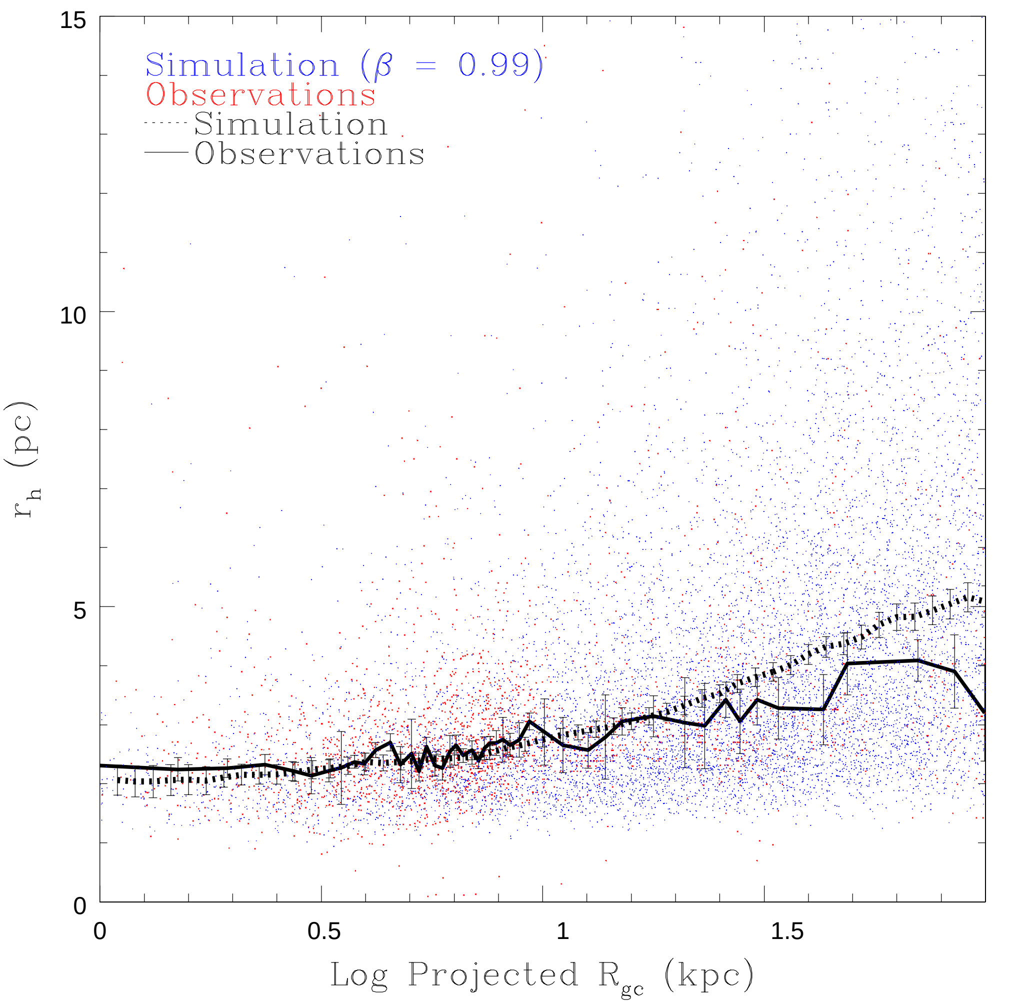

Figure 5.9 r_h and log R_{gc} of each simulated GCs (blue) for a population with $\beta = 0.99$. The dashed black line marks the median r_h calculated with radial bins containing 50 GCs each. For comparison purposes we also plot the observed clusters (red) and median (solid black line) from Figure 5.5. Error bars represent the standard error $\sigma/\sqrt(n)$ as given by Harris et al. (2010).

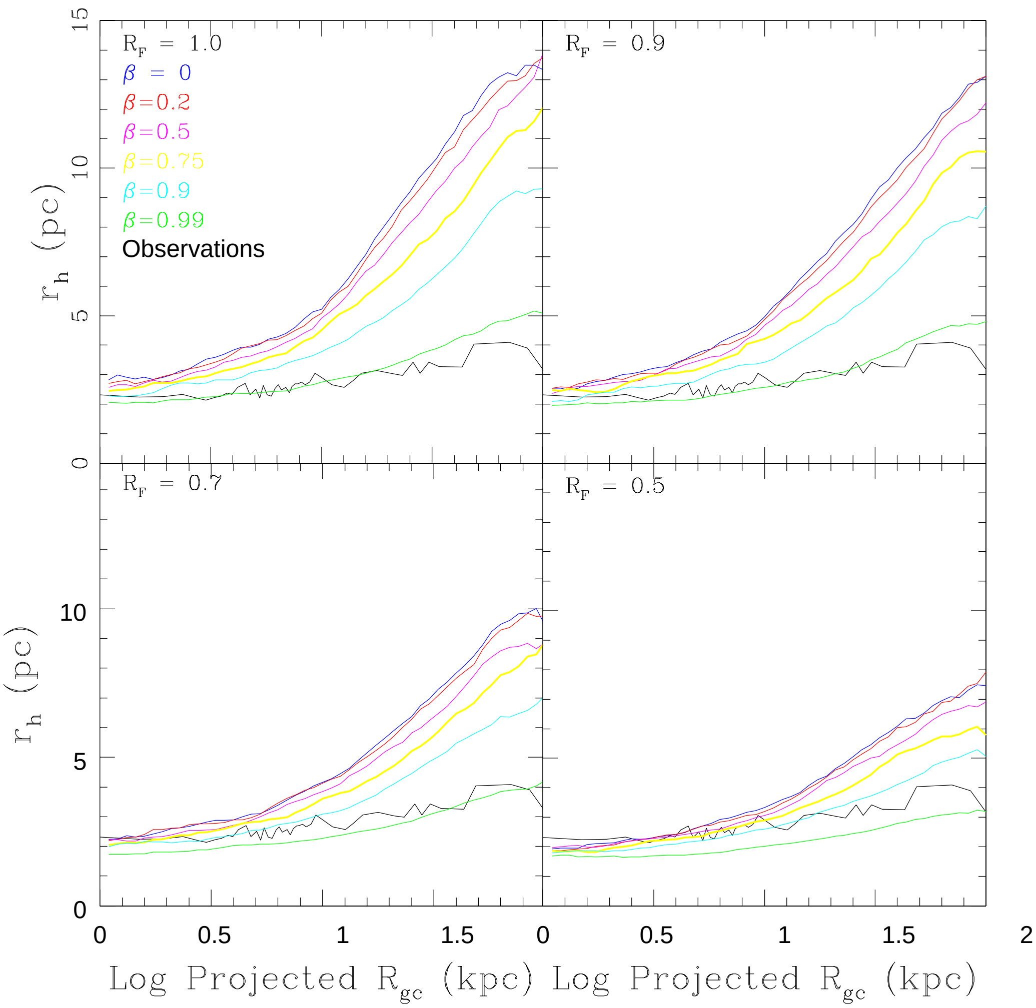

Figure 5.10 Relationship between median r_h and log R_{gc} for simulated GC populations with different values of β and $R_F = \frac{r_L}{r_t}$. Different values of β are colour coded as indicated by the top left panel. The fraction by which clusters fill their tidal radii (R_F) is indicated in each panel. Median r_h are calculated with radial bins containing 50 GCs each.

0.9 (top right panel), 0.7 (bottom left panel), and 0.5 (bottom right panel). While assuming all clusters under-fill their r_t by the same amount must be unrealistic, it serves to illustrate the effect that under-filling clusters have on the relationship between r_h and R_{gc}.

As clusters become more and more under-filling the median r_h decreases at all galactocentric distances; similar to the effect of increasing β. Additionally, decreasing R_F can also decrease the theoretical value of α. Therefore some degeneracy exists between β and R_F.

Realistically it is likely that clusters have a distribution in R_F, and that the distribution changes with R_{gc}. Alexander & Gieles (2013) found that the majority of inner clusters are tidally filling, while outer clusters range between tidally filling, near tidally filling, and tidally under-filling. The radial trend of clusters becoming tidally under-filling with R_{gc} is also in agreement with observations of Galactic GCs. Baumgardt et al. (2010) found that inner GCs ($R_{gc} < 8$ kpc) were primarily tidally filling with $0.1 < \frac{r_h}{r_t} < 0.3$ while outer GCs ($R_{gc} > 8$ kpc) can be separated into two groups of tidally filling and tidally under-filling ($\frac{r_h}{r_t} < 0.05$) clusters. We will expand on this interpretation in a following paper.

5.4.4 Red and Blue Globular Clusters

Finally, we use our simulation to search for any evidence suggesting that the red and blue GCs in M87 may differ by more than just their radial distributions and metallicities. Observational works show that blue GCs have effective radii that are on average 20% (~ 0.4 pc) larger than red GCs (e.g. Kundu & Whitmore, 1998; Kundu et al. , 1999; Larsen et al., 2001; Jordán et al., 2005; Harris , 2009a; Harris et al., 2010; Paolillo et al., 2011; Blom et al., 2012; Strader et al., 2012; Woodley, 2012; Usher et al., 2013). The size difference is also observed in our study, with mean blue cluster size being 28% (~ 1.0 pc) larger than the mean red cluster size. We suggest that the size difference we find is bigger than in other galaxies because our sample extends out to beyond

100 kpc: since clusters can reach large sizes in the outer regions of galaxy, and since the outer regions are dominated by blue clusters, the mean size difference will be larger due to the abundance of large blue clusters. Leading explanations of why this size difference exists suggest that red and blue clusters have different formation, dynamical and stellar evolution histories (e.g. Kundu & Whitmore, 1998; Jordán, 2004; Jordán et al., 2005; Harris , 2009a; Sippel et al., 2012; Schulman et al., 2012). Here we explore the possibility that the size difference may be due to different orbital anisotropy profiles.

Figure 5.11 shows the sizes of the observed blue and red GC populations in the left and right panels. The blue and red populations have the same values of α, equal to 0.11 ± 0.01 and 0.11 ± 0.02 respectively, but their r_h profiles are offset by approximately 1 pc. The size difference does not change with R_{gc}, in agreement with recent studies (Usher et al., 2013, e.g.). The different radial profiles of the red and blue clusters cause the global $\alpha \sim 0.14$ to be larger than the α's of the two sub-populations.

The identical values of α but different mean r_h between the red and blue populations cannot be explained by orbital anisotropy alone. The offset could be explained if outer red clusters are preferentially under-filling and have less eccentric orbits than outer blue clusters. If the blue population has been accreted from in-falling satellite galaxies then they should now be on highly eccentric orbits. Accreted blue clusters may also have larger r_h than red clusters if the mean tidal field they experienced as a member of the satellite galaxy is weaker than the mean field experienced by red clusters. Our future study which combines the effect of orbital anisotropy and tidally under-filling clusters will shed more light on this issue.

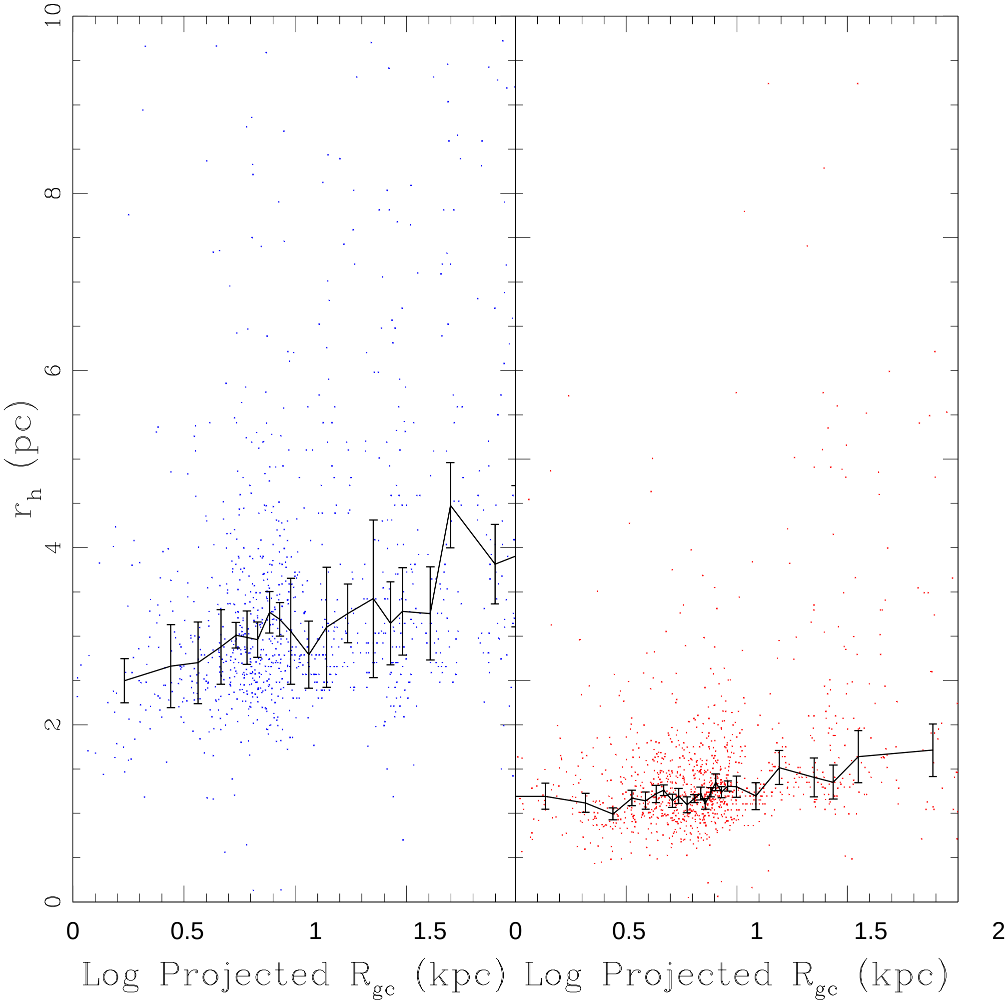

Figure 5.11 r_h versus log R_{gc} for observed blue GCs (left panel) and red GCs (right panel). The solid black lines indicate the median r_h for red and blue clusters respectively, and are calculated with radial bins containing 50 GCs each. Error bars represent the standard error $\sigma/\sqrt(n)$ as given by Harris et al. (2010).

5.5 Summary and Conclusions

We present brand new HST observations of the halo regions of M87, and perform size measurements and photometry on all identified GCs. Combining this dataset with Archive images of the central regions of M87 allow us to probe the relationship between r_h and R_{gc} out to $R_{gc} \sim 100$ kpc with over 2000 GCs. We find that r_h scales as $R_{gc}^{0.14}$, consistent with studies of most other giant E galaxies. We attempt to explain this very shallow relationship by invoking the presence of both orbital anisotropy and clusters that are tidally under-filling. To develop this interpretation we simulate many GC populations orbiting in the tidal field of M87, having a different orbital anisotropy parameter (β) or filling their tidal radii by different amounts.

Comparisons between our simulations and observations suggest that if all clusters are tidally-filling, inner clusters may have a near-isotropic distribution of orbits but outer clusters must have extremely radial orbits $\beta = 0.99$. Such high values of β are not supported in the literature.

However, allowing for the existence of tidally under-filling clusters relaxes the constraints on β as tidally under-filling clusters serve both to decrease mean cluster size and flatten the theoretical relationship between r_h and R_{gc}. We also apply these results to the red and blue cluster sub-populations separately to explain why blue clusters are on average larger than red clusters. In our observational dataset, red and blue clusters both scale as $r_h \propto R_{gc}^{0.11}$, but blue clusters are on average 1 pc larger. The only way we could theoretically reproduced this trend in our simulation is to assume outer red clusters are preferentially under-filling and have a more isotropic distribution of orbits.

Therefore, if both orbital anisotropy and the effect of tidally under-filling clusters are present in our simulation, we can reproduce the power-law proportionality between r_h and R_{gc} for both the cluster population as a whole and the red and blue cluster sub-populations. Future studies will employ the use of MCMC formalism to properly explore the degeneracy between increasing orbital anisotropy and tidally under-filling clusters, as both serve to decrease r_h. Furthermore, as previously indicated neither β or R_F are expected to be fixed values but are more likely functions of R_{gc}.

The question of why orbital anisotropy is present in the cluster population and why some clusters are tidally under-filling remain open. Issues regarding whether or not initial cluster populations are under-filling and what portion of the present day population could have been accreted make constraints on the orbital anisotropy profile and filling parameter difficult. Nevertheless, all conclude that the evolution of clusters with different initial sizes and orbits as well as the accretion of satellite galaxies and their cluster populations are key to understanding the characteristics of present day cluster populations.

5.6 Acknowledgements

We would like to thank the referee for constructive comments and suggestions regarding the presentation of the paper. JW acknowledges support from the Dawes Memorial Fellowship for Graduate Studies in Physics. AS and WEH acknowledge financial support through research grants from the Natural Sciences and Engineering Research Council of Canada.

Bibliography

Alexander, P. E. R. & Gieles, M. 2013, MNRAS, 432L, 1

Bertin, G. & Arnouts, S. 1996, å, 117, 393

Bertin, G. & Varri, A. L. 2008, ApJ, 689, 1005

Barmby, P., McLaughlin, D.E., Harris, W.E.,Harris, G.L.H., Forbes, D.A. 2007, AJ, 133, 2764

Baumgardt, H., Parmentier, G., Gieles, M., Vesperini, E. 2010, MNRAS, 401, 1832

Binney, J. & Tremaine, S. 2008, Galactic dynamics second edition (Princeton, NJ, Princeton University Press, 1987, 747 p.)

Bird, S., Harris, W. E., Blakeslee, J. P., Flynn, C. 2010, A&A, 524, 71

Blom, C., Spitler, L. R., Forbes, D. 2012, MNRAS, 420, 37

Brodie, J. P. & Strader, J. 2006, ARA&A, 44, 193

Casetti-Dinescu, D.I., Girard, T.M., Herrera, D., van Altena, W.E., López, C.E., Castillo, D.J. 2007, AJ, 134, 195

Côté, P., McLaughlin, D.E., Hanes, D.A., Bridges, T.J., Geisler, D., Merrid, D., Hesser, J.E., Harris, G.L.H., Lee, M.G., 2001, ApJ, 559, 828, 257B

Dinescu, D.I., Girard, T.M., van Altena, W.E. 1999, AJ, 117, 1792

Casetti-Dinescu, D.I., Girard, T.M., Jíková, L., van Altena, W.F., Podestá, F., López, C.E. 2013, AJ, 146, 33

Gieles, M., Baumgardt, H., Heggie , D. C., Lamers, H.J.G.L.M. 2010, MNRAS, 408, L16

Gomez, M. & Woodley, K.A. 2007, ApJ, 670, L105

Harris, W. E. 1996, AJ, 112, 1487, 2010 Edition

Harris, W.E. 2009b, ApJ, 699, 254

Harris, W.E. 2009a, ApJ, 703, 939

Harris, W.E., Spitler, L.R., Forbes, D.A., Bailin, J. 2010, MNRAS, 401, 1965

Innanen, K. A., Harris, W.E., Webbink, R.F. 1983, AJ, 88, 338

Jórdan, A. 2004, ApJ, 613, L117

Jórdan, A., Côté, P., Blakeslee, J. P., Ferrarese, L., McLaughlin, D. E. , Mei, S., Peng, E. W., Tonry, J. L., Merrit, D., Milosavljević, M., Sarazin, C. L., Sivakoff, G. R., West, M. J., 2005, ApJ, 634, 1002

King, I. R. 1962, AJ, 67, 471

Kundu, A. & Whitmore, B. C. 1998, AJ, 116, 2841

Kundu, A, Whitmore, B. C., Sparks, W. B., Macchetto, F. D., Zepf, S. E., Ashman, K. M., 1999, ApJ, 513, 733

Küpper, A. H. W, Kroupa, P, Baumgardt, H., Heggie , D. C., 2010, MNRAS, 407, 2241

Larsen, S. S. 1999, å, 139, 393

Larsen, S. S., Brodie, J. P., Huchra, J. P., Forbes, D. A., Grillmair, C. J., 2001, AJ, 121, 2974

Leigh, N., Giersz, M., Webb, J.J., Hypki, A., de Marchi, G., Kroupa, P., Sills, A. 2013, MNRAS, arXiv1309.7054

Ludlow, A. D., Navarro, J. F., Springler, V., Vogelsberger, M., Wang , J., White, S. D. M., Jenkins, A., & Frenk, C. S. 2010, MNRAS, 406, 137

Madrid, J. P., Harris, W. E., Blakeslee, J. P., Gómez, M 2009, ApJ, 705, 237

Madrid, J.P., Hurley, J.R., Sippel, A.C., 2012, ApJ, 756, 2

McLaughlin, D. E., Barmby, P., Harris, W. E., Forbes, D.A., & Harris, G.L.H. 2008, MNRAS, 384, 563

McLaughlin, D. E. & van der Marel, R. P. 2005, ApJS, 161, 304

McLaughlin, D. E. 1999, ApJ, 512, L9

Paolillo, M., Puzia, T. H., Goudfrooij, P., Zepf, S. E., Maccarone, T. J., Kundu, A., Fabbiano, G., Angelini, L. 2011, ApJ, 736, 90

Peng, E.W., Jórdan, A., Côté, P., Blakeslee, J.P., Ferrarese, L., Mei, S., West, M.J., Merritt, D., Milosavljević, M., Tonry, J.L. 2006, ApJ, 639, 95

Peng, E.W., Jórdan, A., Blakeslee, J.P., Mieske, S., Côté, P., Ferrarese, L., Harris, W.E., Madrid, J.P., Meurer, G.R. 2009, ApJ, 703, 42

Pierce, M. J., Welch, D. L., McClure, R. D., van den Bergh, S., Racine, R., & Stetson, P. B. 1994, Nature, 371, 385

Prieto, J. L. & Gnedin, O. Y. 2008, ApJ, 689, 919

Saha, Abhijit; Shaw, R.A., Claver, J.A., Dolphin, A.E. 2011, PASP, 123, 481

Schulman, R. D., Glebbeek, E., Sills, A. 2012, MNRAS, 420, 651

Sippel, A.C., Hurley, J.R., Madrid, J.P., Harris, W.E. 2012, MNRAS, 427, 167

Sirianni, M., Jee, M. J., Bentez, N., Blakeslee, J. P., Martel, A. R., Meurer, G., Clampin, M., De Marchi, G., Ford, H. C., Gilliland, R., Hartig, G. F., Illingworth, G. D., Mack, J., McCann, W. J. 2005, PASP, 117, 1049

Spitler, L.R., Larsen, S.S., Strader, J., Brodie, J.P., Forbes, D.A., Beasley, M.A. 2006, AJ, 132, 1593

Strader, J., Fabbiano, G., Luo, B., Kim, D., Brodie, J.P., Fragos, T., Gallagher, J.S., Kalogera, V., King, A., Zezas, A. 2012, ApJ, 760, 87

Tonry, J. L., Dressler, A., Blakeslee, J. P., Ajhar, E.A., Fletcher, A.B., Luppino, G.A., Metzger, M.R., Moore, C.B. 2001, ApJ, 546, 681

Usher, C., Forbes, D.A., Spitler, L.R., Brodie, J.P., Romanowsky, A.J., Strader, J., Woodley, K.A. 2013, MNRAS, arXiv1308.6585

von Hoerner, S. 1957, ApJ, 125, 451

Waters, C.Z., Zepf, S.E.., Lauer, T.R., Baltz, E.A. 2009, ApJ, 693, 463

Weijmans, A., Cappellari, M., Bacon, R., de Zeeuw, P. T., Emsellem, E., Falcon-Barroso, J., Kuntschner, H., McDermid, R. M., van den Bosch, R. C. E., and van de Ven, G., 2009, MNRAS, 398, 561

Webb, J.J., Sills, A., Harris, W.E. 2012, ApJ, 746, 93

Webb, J.J., Harris, W.E., Sills, A., Hurley, J.R. 2013, ApJ, 764, 124

Woodley, K. 2012, AAS Meeting #220, #438.07

Zait, A., Hoffman, Y. & Shlosman, I. 2008, ApJ, 682, 835

Zepf, S. E. & Ashman, K. M. 1993, MNRAS, 264, 611

Chapter 6

Globular Cluster Scale Sizes in Giant Galaxies: Orbital Anisotropy and Tidally Under-Filling Clusters in M87, NGC 1399, and NGC 5128

Jeremy J. Webb, Alison Sills, William E. Harris, Matías Gómez, Thomas H. Puzia, Maurizio Paolillo, Kristin A. Woodley

6.1 Introduction

The tidal field of a galaxy influences its globular cluster (GC) population by imposing a maximum size that each cluster can reach (e.g. von Hoerner , 1957; King , 1962; Innanen, Harris, & Webbink, 1983; Jordán et al., 2005; Binney & Tremaine, 2008; Bertin & Varri, 2008; Renaud et al., 2011). This maximum size is often referred to as the tidal radius r_t, the Jacobi radius, or the Roche lobe of the cluster. In all cases, it marks the distance from the cluster at which a star will become unbound as it feels a stronger acceleration towards the host galaxy than it will towards the GC. von Hoerner (1957) predicts that the r_t of a GC on a circular orbit at a three dimensional galactocentric distance of r_{gc} depends on the cluster's mass (M_g), and the enclosed galactic mass (M) via:

$$r_t = r_{gc}(\frac{M}{2M_g})^{1/3} \tag{6.1}$$

Under the assumption that a galaxy can be approximated by an isothermal sphere ($M_g(r_{gc}) \propto r_{gc}$) out to large distances, we expect $r_t \propto r_{gc}^{\frac{2}{3}}$. A similar relationship is also found when galaxies are modelled by a NFW profile (Navarro,Frenk & White, 1997). Taking into consideration that only the projected galactocentric distance R_{gc} can be determined for extragalactic populations, the relationship between size and distance takes the form $r_t \propto R_{gc}^{\alpha}$, where $\alpha \sim 0.4 - 0.5$ for typical radial distributions (cluster density $\propto R_{gc}^{-2}$). Since there is no observational evidence that cluster central concentration c has any dependence on either r_{gc} or R_{gc}, the mean effective (half-light) radius r_h will follow the same scaling relation as r_t.

For the Milky Way, which gives us the only cluster population for which we have three dimensional positions and solved orbits, we find $r_h \propto r_{gc}^{0.46\pm0.05}$ (positions and effective radii from Harris 1996 (2010 Edition) and orbits from Dinescu et al. (1999); Casetti-Dinescu et al. (2007, 2013)). This is a notable discrepancy from the nominal value of $\frac{2}{3}$ when three dimensional distances are known. Observations of projected cluster populations also disagree with theoretical predictions. From a study of six giant elliptical galaxies, Harris (2009a) found the combined dataset was best fit by an α of 0.11. This value is in agreement with observational studies of NGC 4594 ($\alpha = 0.19 \pm 0.03$ (Spitler et al., 2006; Harris et al., 2010a)), M87 ($\alpha = 0.14 \pm 0.01$, (Webb et al., 2013b)) and NGC 1399 ($\alpha = 0.2 \pm 0.01$ (Puzia et al., 2014)). Looking at the metal poor (blue) and metal rich (red) cluster sub-populations in NGC 5128 separately, Gómez & Woodley (2007) found $\alpha = 0.05 \pm 0.05$ for the blue clusters and $\alpha = 0.26 \pm 0.06$ for the red clusters. Only the cluster population of the giant elliptical galaxy NGC 4365 in the Virgo cluster has a measured α of 0.49 ± 0.04 that is comparable to Equation 6.1 (Blom et al., 2012), which may indicate the galaxy has a different dynamical age or has undergone a different formation scenario than the galaxies listed above.

The discrepancy between Equation 6.1 and observed values of α can be attributed to assuming that all GCs have circular orbits in a spherically symmetric tidal field and fill their theoretical r_t. The first assumption is required in order for the tidal field experienced by the cluster to be static. However it is clear that no GCs have a truly circular orbit (Dinescu et al., 1999; Casetti-Dinescu et al., 2007, 2013). Eccentric orbits are subject to tidal heating and tidal shocks which can provide outer stars enough energy to escape the cluster and energize inner stars to larger orbits (e.g. Kupper et al., 2010; Renaud et al., 2011; Webb et al., 2013a; Kennedy , 2014). Clusters on eccentric orbits are also able to re-capture temporarily un-bound stars since the cluster's instantaneous r_t is also time-dependent. N-body models of GC evolution have shown that despite spending the majority of their lifetimes at apogalacticon, clusters with eccentric orbits lose mass at a faster rate (Baumgardt & Makino, 2003) and appear smaller (Webb et al., 2013a) than clusters with circular orbits at apogalacticon. Hence incorporating the effects of orbital eccentricity on cluster evolution will reduce the discrepancy between theoretical and observed values of α. The situation will be complicated further if the cluster has an inclined orbit in a non-spherically symmetric potential (Madrid et al., 2014; Webb et al., 2014) or if the cluster has been accreted by the host galaxy via a satellite merger such that its current orbit does not reflect the tidal field in which it formed and evolved (Miholics et al., 2014; Bianchini et al., 2015; Renaud & Gieles, 2015).

The second assumption, that all clusters fill their theoretical r_t, we now understand is also unrealistic. While a GC will naturally expand due to two-body interactions (Henon, 1961), it is possible that certain clusters formed compact enough such that they have yet to expand to the point of filling their r_t. Observationally this indicates that a cluster's limiting radius r_L, the radius at which the cluster's density falls to zero, could be less than r_t. Observations of Galactic GCs show that only approximately $\frac{1}{3}$ of the population are tidally filling, in the sense that $r_L \sim r_t$ (Gieles et al., 2011). The remaining clusters in the Milky Way are still in the expansion phase and are considered to be tidally under-filling. There is also evidence of under-filling clusters in NGC 4649, where Strader et al. (2012) found no evidence for tidal truncation for clusters beyond 15 kpc and in NGC 1399, where Puzia et al. (2014) find no evidence for truncation beyond 10 kpc. Alexander & Gieles (2013) were able to reproduce the observed size distribution of Galactic GCs by assuming that all clusters form initially compact and then expand naturally via two-body interactions until they become tidally filling. After 12 Gyr of evolution, inner clusters which experience a strong tidal field and have small tidal radii have expanded to the point of being tidally filling. Outer clusters, with large tidal radii, still remain tidally under-filling after 12 Gyr. Allowing clusters to become more under-filling with increasing R_{gc} offers a second explanation as to why observed values of α are noticeably less than theoretical predictions.

Understanding how the factors discussed above can influence α allows us to use the size distribution of GC populations to constrain many properties of their host galaxy, including its mass and orbital anisotropy profiles. In two previous studies of the giant elliptical galaxy M87 (Webb et al., 2012, 2013b), we explored the effects of orbital anisotropy and tidal filling on its GC population out to 110 kpc. We found that it was possible to reproduce the observed relationship between r_h and R_{gc} in M87 by allowing cluster orbits to be preferentially radial. However the degree of radial anisotropy in the outer regions of M87 was much higher than kinematic studies suggest (Côté et al., 2001; Strader et al., 2011). We were also able to match theory and observations by allowing all clusters to be under-filling, however we only explored the effects of clusters being under-filling by the same amount at all R_{gc}. More generally, we can allow orbital anisotropy and tidal filling to be functions of R_{gc} (e.g. Côté et al., 2001; Prieto & Gnedin, 2008; Zait, Hoffman, & Shlosman, 2008; Weijmans et al., 2009; Gnedin & Prieto, 2009; Ludlow et al., 2010; Kruijssen et al., 2012; Alexander & Gieles, 2013). The next step is to incorporate these two parameters into our model as functions of R_{gc} and to apply our approach to other giant galaxies in order to compare the best-fit orbital anisotropy and tidal filling profiles.

In this study, we consider the combined effects of orbital anisotropy and tidal filling on GC populations in the giant galaxies M87, NGC 5128, and NGC 1399. Since we are focused on giant elliptical galaxies which are spherically symmetric, orbital inclination is not a contributing factor. However, inclination will have to be considered in future studies if our approach is to be applied to spiral galaxies. We also assume that all clusters in a given population have spent their entire lifetimes in the host galaxy. Miholics et al. (2014) showed that after a cluster is accreted by a host galaxy its size responds to its new potential within a few GC relaxation times and evolves as if it has always orbited in the host galaxy. The *structural* parameters (which is the focus of this study) of accreted clusters will therefore not retain a signature of the accretion process, but will instead reflect their *current* orbit in the host galaxy. The orbital distribution of a globular clusters however can provide information regarding the formation and merger history of a galaxy.

In Section 6.2 we introduce the three observational datasets used in our study and in Section 6.3 we re-introduce the theoretical model used to reproduce the observations. The best fit theoretical model for each galaxy is discussed in Section 6.4 and the results of all three galaxies are compared in Section 6.5. We summarize our findings in Section 6.6.

6.2 Observations

In the following sections, we summarize the observational GC datasets for M87, NGC 1399, and NGC 5128 used in this study. While the colour and luminosity ranges of the M87 and NGC 1399 datasets are both throughly covered, only the colour range of clusters in NGC 5128 is comparable. In NGC 5128, the dataset is incomplete for GCs fainter than the luminosity function turnover. However as we discuss in Section 6.3.3, this incompleteness is factored into our model. The main parameter extracted from each dataset is GC effective radius. Even though cluster sizes are being measured in different wave bands, many studies have found that there is minimal differences when comparing sizes measured with different filters (e.g. Harris , 2010b; Webb et al., 2013b). Hence the observational datasets are as homogeneous as possible and comparisons between GCs in each galaxy will be unaffected by any differences.

6.2.1 M87

M87 is a giant elliptical galaxy located at the centre of the Virgo cluster, with a distance modulus of $(m-M) = 30.95$ (Pierce et al., 1994; Tonry et al., 2001). Hubble Space Telescope (HST) Advanced Camera for Surveys (ACS) / Wide Field Camera (WFC) images of the central 12 kpc of M87 in the F814W (I) and F606W (V) filters are taken from program GO-10543 (PI Baltz). The more recently completed program GO-12532 (PI Harris) provided a combination of 8 ACS and WFC3 fields of view in the F814W and F475W filters of the outer regions of M87 ranging from 10 kpc to 110 kpc. See Webb et al. (2012) and Webb et al. (2013b) for a detailed description of how cluster candidates are selected and sizes are measured.

6.2.2 NGC 1399

NGC 1399 is a giant elliptical galaxy located at the centre of the Fornax cluster, with a distance modulus of $(m-M) = 31.52$ (Dunn & Jerjen, 2006; Blakeslee et al., 2009). In this study we utilize archive HST images of NGC 1399 from program GO-10129 (PI Puzia). The 3 x 3 ACS mosaic in the F606W filter covers approximately 10' x 10 ' out to a projected distance of approximately 50 kpc. A description of how cluster candidates are selected and how sizes are measured can be found in Puzia et al. (2014).

6.2.3 NGC 5128

NGC 5128 (Cen A) is a giant galaxy that is found in relative isolation, with a distance modulus of $(m - M) = 27.92$ (Harris , 2010b). We make use of Magellan/IMACS images of NGC 5128 to study its GC population out to a projected distance of approximately 40 kpc (Gómez & Woodley, 2007). A description of how cluster candidates are selected and how sizes are measured can be found in both Gómez & Woodley (2007) and Woodley & Gómez (2010a).

6.3 Model

Our model (first introduced in Webb et al. (2012) and modified in Webb et al. (2013b)) generates a mock GC population that has the same distributions in projected distance, velocity and mass as the observed dataset. The central concentration distribution and mass to light ratios of model clusters are set equal to the Milky Way cluster population (see Webb et al. (2012)). Since our model has been recently modified to be applicable to any galaxy, we will re-introduce it here.

The projected radial distribution of clusters in each galaxy is obtained by first fitting the observed number density profile ($n(R_{gc})$) with a modified two-dimensional Hubble profile:

$$n(R_{gc}) = \frac{n_0}{1.0 + (\frac{R_{gc}}{R_0})^2} \tag{6.2}$$

Equation 6.2 is then transformed to obtain a three dimensional radial distribution (Binney & Tremaine, 2008). Each model cluster is then assigned a three dimensional velocity based on the observed global line-of-site velocity dispersion. One of our two free parameters is the anisotropy parameter (β), which controls the degree of orbital anisotropy within the GC system and is defined as (Binney & Tremaine, 2008):

$$\beta = 1 - \frac{\sigma_\theta^2 + \sigma_\phi^2}{2\sigma_R^2} \tag{6.3}$$

where σ_R, σ_θ, and σ_ϕ are the velocity dispersions for each spherical coordinate. In all cases, σ_θ and σ_ϕ are assumed to be equal. The isotropic case ($\beta = 0$) means $\sigma_R = \sigma_\theta = \sigma_\phi$. If β increases from zero then σ_R increases while σ_θ and σ_ϕ decrease such that the projected σ still matches the observations and orbits become preferentially radial. The opposite occurs if β decreases from the isotropic case and orbits become preferentially circular. Model clusters are assigned masses based on the observed luminosity function of the dataset. The mass to light ratio of the model clusters is assumed to be equal to the mean value of $\frac{M}{L}_V = 2$ found by McLaughlin & van der Marel (2005) for Milky Way GCs. The central concentration (c) distribution is also assumed to be the same as Milky Way GCs (Harris , 1996), which is Gaussian with a mean of $c = 1.5$ and dispersion of 0.4.

Once each model cluster has been generated, the mass profile of the selected galaxy (see Figure 6.1 and Sections 6.3.1- 6.3.3) is used to calculate the gravitational potential field and the orbit of each individual cluster can be solved given its initial position and velocity (Binney & Tremaine, 2008). Using the formalism of Bertin & Varri (2008), we first calculate each cluster's r_t at perigalacticon R_p. For clusters with eccentric orbits we use their orbital frequency Ω at R_p to calculate r_t as opposed to $\Omega = ((d\Phi_G(R)/dR)_{R_p}/R_p)^{\frac{1}{2}}$ which assumes the cluster has a circular orbit at R (Moreno et al., 2014). We

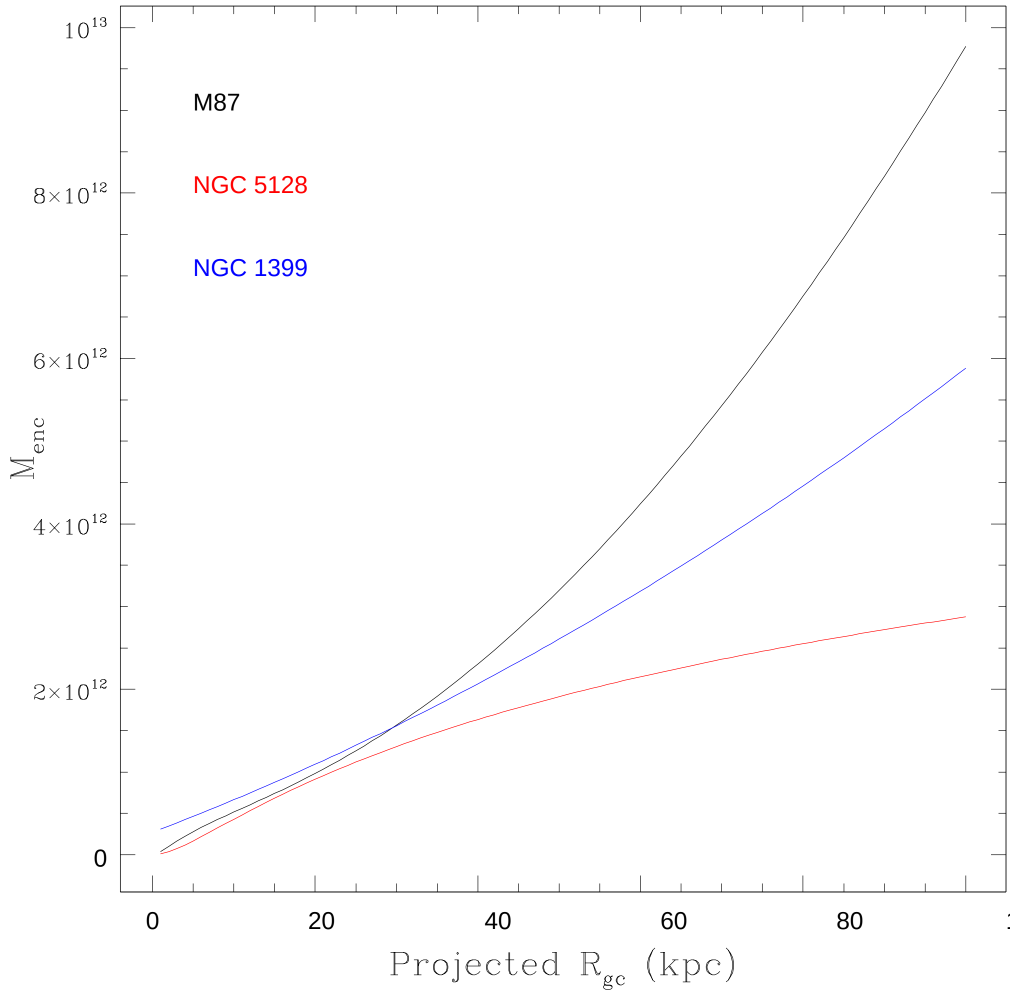

Figure 6.1 Total enclosed mass as a function of R_{gc} for M87 (black), NGC 1399 (blue), and NGC 5128 (red).

then determine r_L at R_p based on our second free parameter $R_f = \frac{r_L}{r_t}$, also known as the tidal filling parameter. R_f is a measure of how filling a cluster is at R_p, with clusters that fill only a fraction of their permitted r_t having $R_f < 1$.

We next assume that each model cluster can be represented by a King (1962) model, such that the limiting radius at R_p and the previously assigned central concentration set the cluster's surface brightness profile. However, the r_h corresponding to the surface brightness profile is only valid when the cluster it located at R_p. We therefore correct r_h values for orbital eccentricity following Webb et al. (2013a) and Webb et al. (2013b).

Finally, to best match the observed datasets, we apply magnitude and size cutoffs to the simulated dataset such that the model does not produce GCs that may exist but would not be observed. We check to make sure the simulation does not produce any clusters with evaporation or infall times due to dynamical friction less than any observed clusters. Our model also allows for metal rich and metal poor GCs to have separate radial profiles and velocity dispersions. The individual input parameters and mass profiles of each galaxy are discussed in Sections 6.3.1 - 6.3.3.

6.3.1 M87

The radial profile and luminosity function of our M87 dataset are listed in Table 6.1, along with the velocity dispersion parameters assigned to our theoretical cluster population. In a kinematic study of the GC population of M87, Côté et al. (2001) find that blue clusters have a mean velocity (minus the galaxy's systemic velocity) of -36 km/s with a dispersion of 412 km/s while red clusters have a mean velocity of 7 km/s and a dispersion of 385 km/s. They also find that the velocity dispersion increases with R_{gc}. However a more recent study by Strader et al. (2011) finds that the global velocity dispersion stays relatively constant with R_{gc}. Due to the larger dataset of Strader et al. (2011) and their more rigorous treatment of outliers, we will assume the velocity dispersion of M87 is constant at all R_{gc}.

Table 6.1: Simulated M87 Globular Cluster Population Input Parameters

Parameter	Value	Reference
Number of Clusters		
Blue	1124	
Red	1211	
Radial Distribution	Modified Hubble Profile	
Blue Population		
σ_0	37.95 arcmin^{-2}	
R_0	1.08'	
Red Population		
σ_0	95.7 arcmin^{-2}	
R_0	0.83'	
Angular Distribution	Spherically Symmetric	
Luminosity Function	Gaussian	
$\langle M_V \rangle$	-7.6	
σ_{M_V}	1.0	
Velocity Dispersion	Côté et al. (2001)	
Blue Population		
$\langle v \rangle$	-36 km/s	
σ_v	412 km/s	
Red Population		
$\langle v \rangle$	7 km/s	
σ_v	385 km/s	

The galactic potential of M87 is taken directly from McLaughlin (1999) and has the form:

$$M_{total}(r) = M_{stars}(r) + M_{dark}(r) \tag{6.4}$$

$$M_{stars}(r) = 8.10 \times 10^{11}\ M_{\odot}\ [\frac{(r/5.1kpc)}{(1 + r/5.1kpc)}]^{1.67} \tag{6.5}$$

$$M_{dark}(r) = 7.06 \times 10^{14}\ M_{\odot} \times [\ln(1 + r/560kpc) - \frac{(r/560kpc)}{(1 + r/560kpc)}] \tag{6.6}$$

The stellar mass component (Equation 6.5) was determined by fitting model mass density profiles for spherical stellar systems (Dehnen, 1993; Tremaine et al., 1994) to B-band photometry (de Vaucouleurs & Nieto, 1978), assuming the stellar mass-to-light ratio of M87 is independent of radius. The dark matter component of M87 (Equation 6.6) was determined by combining x-ray observations of hot gas in the extended M87 halo, dwarf elliptical galaxies, and early-type Virgo galaxies to generate a Navarro-Frenk-White (NFW) dark matter halo (Navarro,Frenk & White, 1997). The overall mass profile is in general agreement with the more recent kinematic study of M87 performed by Strader et al. (2011), though the latter find evidence for a larger dark matter component within 20 kpc. With the Strader et al. (2011) dataset, Agnello et al. (2014) also derive stellar and dark matter mass profiles for M87 by separating its cluster population into three sub-populations and noting their distinct radial distributions and velocity dispersions as a function of R_{gc}. The total mass of M87 as determined by Agnello et al. (2014) is comparable to McLaughlin (1999), however Agnello et al. (2014) find a more gradual increase in dark matter mass than McLaughlin (1999). As noted by Strader et al. (2011), more extensive modelling of M87 and Virgo is required in order to better constrain its dark matter halo. Considering that the differences between the mass profiles above are minimal, and the fact that our model contains two cluster sub-populations with constant velocity dispersions, we will utilize the mass profile as determined by McLaughlin (1999).

6.3.2 NGC 1399

The radial profile and luminosity function of our NGC 1399 dataset are listed in Table 6.2, along with the velocity dispersion parameters assigned to our theoretical cluster population. From the most recent kinematic dataset of the NGC 1399 GC population, Schuberth et al. (2010) found that blue clusters have a mean velocity of 11 km/s with a dispersion of 358 km/s and the red clusters have a mean velocity of 31 km/s with a dispersion of 256 km/s. To stay consistent with our model for M87, we will also assume these values remain constant with R_{gc}.

Table 6.2: Simulated NGC 1399 Globular Cluster Population Input Parameters

Parameter	Value	Reference
Number of Clusters		
Blue	558	
Red	668	
Radial Distribution	Modified Hubble Profile	
Blue Population		
σ_0	17 arcmin^{-2}	
R_0	1.1’	
Red Population		
σ_0	50 arcmin^{-2}	
R_0	0.8’	
Angular Distribution	Spherically Symmetric	

Luminosity Function	Gaussian
$\langle M_V \rangle$	-7.3
σ_{M_V}	1.3
Velocity Dispersion	Schuberth et al. (2010)
Blue Population	
$\langle v \rangle$	11 km/s
σ_v	358 km/s
Red Population	
$\langle v \rangle$	31 km/s
σ_v	256 km/s

The galactic potential of NGC 1399 was derived from ROSAT High Resolution Imager data by Paolillo et al. (2002). X-ray emission from hot gas in NGC 1399 was used to make enclosed total mass (stars and dark matter) estimates at various distances. Since we require a functional form for the mass profile of each galaxy in order to solve the orbits and calculate the size of each model cluster, and since the data does not reflect a standard NFW profile, we fit the mass profile from Paolillo et al. (2002) with a quadratic function:

$$M_{tot}(r) = 2.74 \times 10^{11}\ M_{\odot} + 3.73 \times 10^{10}\ M_{\odot} \times r + 1.87 \times 10^{8} M_{\odot} \times r^2 \quad (6.7)$$

6.3.3 NGC 5128

The radial profile and luminosity function of our NGC 5128 dataset are listed in Table 6.3. It is important to note that we have incorporated into our model the fact that our NGC 5128 cluster dataset is only 60% complete fainter than the luminosity function turnover. The velocity dispersion parameters assigned to our theoretical cluster population (also in Table 6.3) are taken from Woodley et al. (2010b). In a kinematic study of over 600 GCs, they determined that blue GCs have a mean velocity of 26 km/s with a dispersion of 149 km/s and red clusters have a mean velocity of 43 km/s with a dispersion of 156 km/s. Similar to M87 and NGC 1399, we again assume these values remain constant with R_{gc}. It is interesting to note that the velocity dispersions of the NGC 5128 cluster populations are approximately a factor of two smaller than in M87 and NGC 1399. This difference may have to do with M87 and NGC 1399 being at the centre of large galaxy clusters while NGC 5128 is more or less in isolation. We will discuss the impact of environment further in Section 6.5.

Table 6.3: Simulated NGC 5128 Globular Cluster Population Input Parameters

Parameter	Value	Reference
Number of Clusters		
Blue	278	
Red	310	
Radial Distribution	Modified Hubble Profile	
Blue Population		
σ_0	0.2 arcmin^{-2}	
R_0	3.7'	
Red Population		
σ_0	0.2 arcmin^{-2}	
R_0	4.0'	
Angular Distribution	Spherically Symmetric	
Luminosity Function	Gaussian	

$\langle M_V \rangle$	-8.0
σ_{M_V}	1.0
Velocity Dispersion	Woodley et al. (2010b)
Blue Population	
$\langle v \rangle$	26.0 km/s
σ_v	149.0 km/s
Red Population	
$\langle v \rangle$	43.0 km/s
σ_v	156.0 km/s

The galactic potential of NGC 5128 is taken from enclosed total mass estimates from Woodley et al. (2010b) based on the kinematics of the NGC 5128 cluster population. The mass profile is in agreement with previous estimates taken from studies of HI gas shells (Schiminovich et al., 1994) and other cluster datasets (Peng et al., 2004). We have fit the total mass estimates with a NFW profile (Navarro,Frenk & White, 1997):

$$M_{tot}(r) = 1.74 \times 10^{14}\ M_{\odot} \times [\ln(1 + r/8.2kpc) - \frac{(r/8.2kpc)}{(1 + r/8.2kpc)}] \tag{6.8}$$

6.4 Results

6.4.1 The Isotropic and Tidally Filling Case

We first compare our observed datasets to models generated assuming each cluster population has an isotropic distribution of orbits and that all GCs are tidally filling. In Figure 6.2 we have plotted the measured r_h of observed GCs

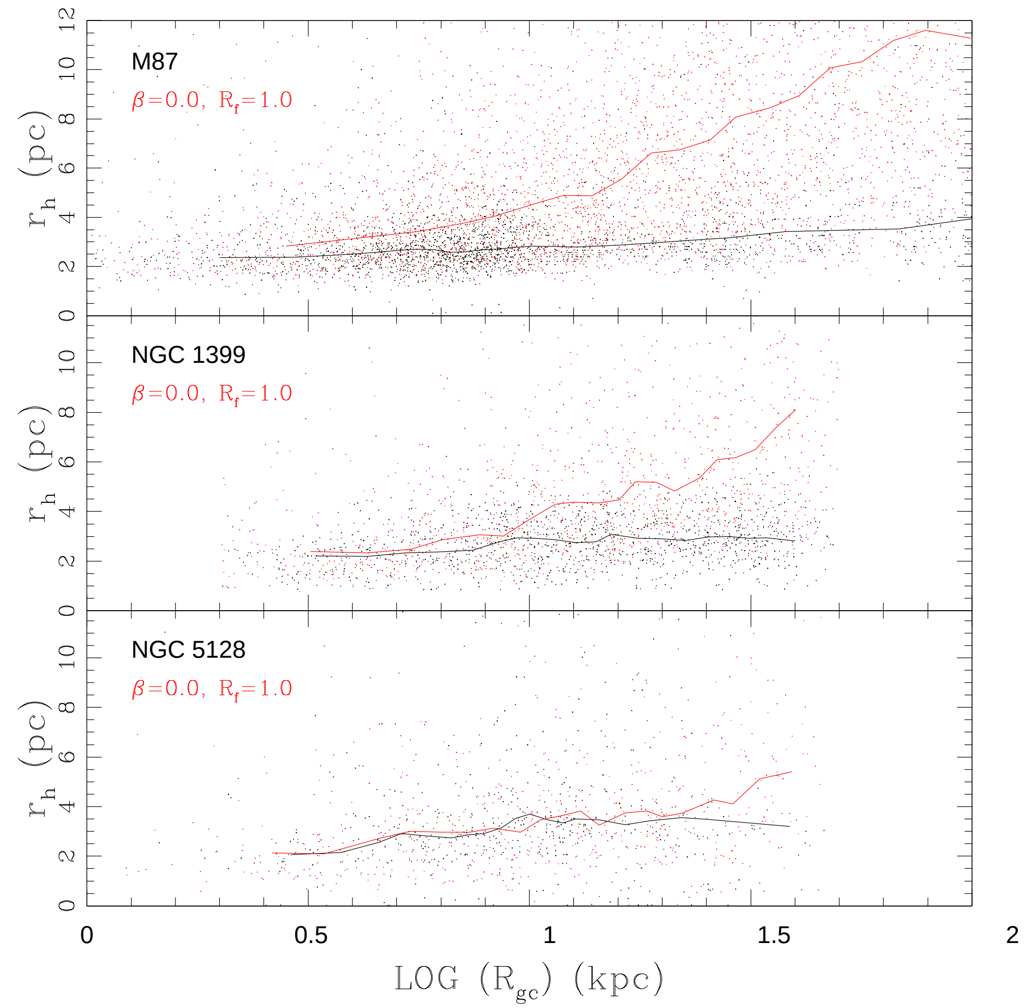

Figure 6.2 r_h vs log R_{gc} for observed globular clusters (black) and model clusters (red) in M87 (Top), NGC 1399 (Middle), and NGC 5128 (Bottom) assuming clusters have an isotropic distribution of orbits and are all tidally filling. The solid lines represent the median r_h calculated with radial bins containing 5% of the observed cluster population each.

(black) and theoretically determined r_h of model clusters (red) in all three galaxies. The solid lines show the median r_h as a function of R_{gc}.

In all three cases, by allowing clusters to have an isotropic distribution of orbits, as opposed to just circular orbits, we have pushed tidal theory closer to matching observations compared to assuming all cluster orbits are circular.

In the cases of M87 and NGC 1399, α equals 0.43 and 0.51 respectively. In the case of NGC 5128, the observations are surprisingly well matched by the isotropic case with $\alpha = 0.31$, with the model only slightly over-estimating cluster sizes at large R_{gc}. Unfortunately, especially in the cases of M87 and NGC 1399, an isotropic distribution of orbits does not fully eliminate the difference between observed and theoretically predicted vales of α. Furthermore, kinematic studies of these galaxies do not support the idea of cluster populations being isotropic. As previously discussed in this study and in Webb et al. (2013a), α can be further decreased by allowing either the anisotropy parameter β to increase or the tidal filling parameter R_f to decrease. However, in Webb et al. (2013a) we only studied the effects of static values of β and R_f on GC sizes. Studies of galaxy formation and structure suggest that cluster orbits become preferentially radial and clusters become more tidally underfilling with increasing R_{gc}. We explore the effects of these two parameters in the following sub-sections.

6.4.2 Orbital Anisotropy and Tidally Underfilling Clusters

In order to allow the values of β and R_f to be functions of R_{gc}, it is important to first establish the generic profiles. We assume the orbital anisotropy profile of a given galaxy is of the form:

$$\beta(R_{gc}) = \frac{1}{1 + (\frac{\beta_\alpha}{R_{gc}})^2} \tag{6.9}$$

where the anisotropy radius β_α replaces β as the first free parameter in our model. This form of $\beta(R_{gc})$ is in agreement with theoretical and observational studies which find that inner cluster orbits are primarily isotropic while orbits become preferentially radial with R_{gc} (e.g. Gnedin & Prieto, 2009; Ludlow et al., 2010; Kruijssen et al., 2012). While Equation 6.9 does not support negative values of β, negative values will only serve to overestimate mean cluster sizes even more than the isotropic case (Webb et al., 2012, 2013b). Similarly, the tidal filling profile is also of the form:

$$R_f(R_{gc}) = 1 - \frac{1}{1 + (\frac{R_{f\alpha}}{R_{gc}})^2} \tag{6.10}$$

where the filling radius $R_{f\alpha}$ is now our second free parameter. This form of R_f ensures clusters become less tidally filling as the tidal field becomes weaker (Alexander & Gieles, 2013).

With these two free parameters in place, we re-run our simulations for $0 < \beta_\alpha < 100$ kpc and $0 < R_{f\alpha} < 100$ kpc in search for the combination which provides the strongest agreement between our theoretical and observed cluster populations. To compare theory and observations, we first determine the median effective radius in radial bins containing 5% of the total observed cluster population. A mean effective radius is also calculated for each mock GC population using the same radial bins as the observations. To find the model which best reproduced the observed dataset, we first find the mock GC data set which minimizes χ^2:

$$\chi^2 = \sum_i^N \frac{(r_{h,obs}(R_{gc,i}) - r_{h,mod}(R_{gc,i}))^2}{r_{h,obs}(R_{gc,i})} \tag{6.11}$$

where N is the total number of bins (20), $r_{h,mod}(R_{gc,i})$ is the median effective radius of the model in the i^{th} radial bin and $r_{h,obs}(R_{gc})$ is the median effective radius of the observations in the i^{th} radial bin. For all values of χ^2 within

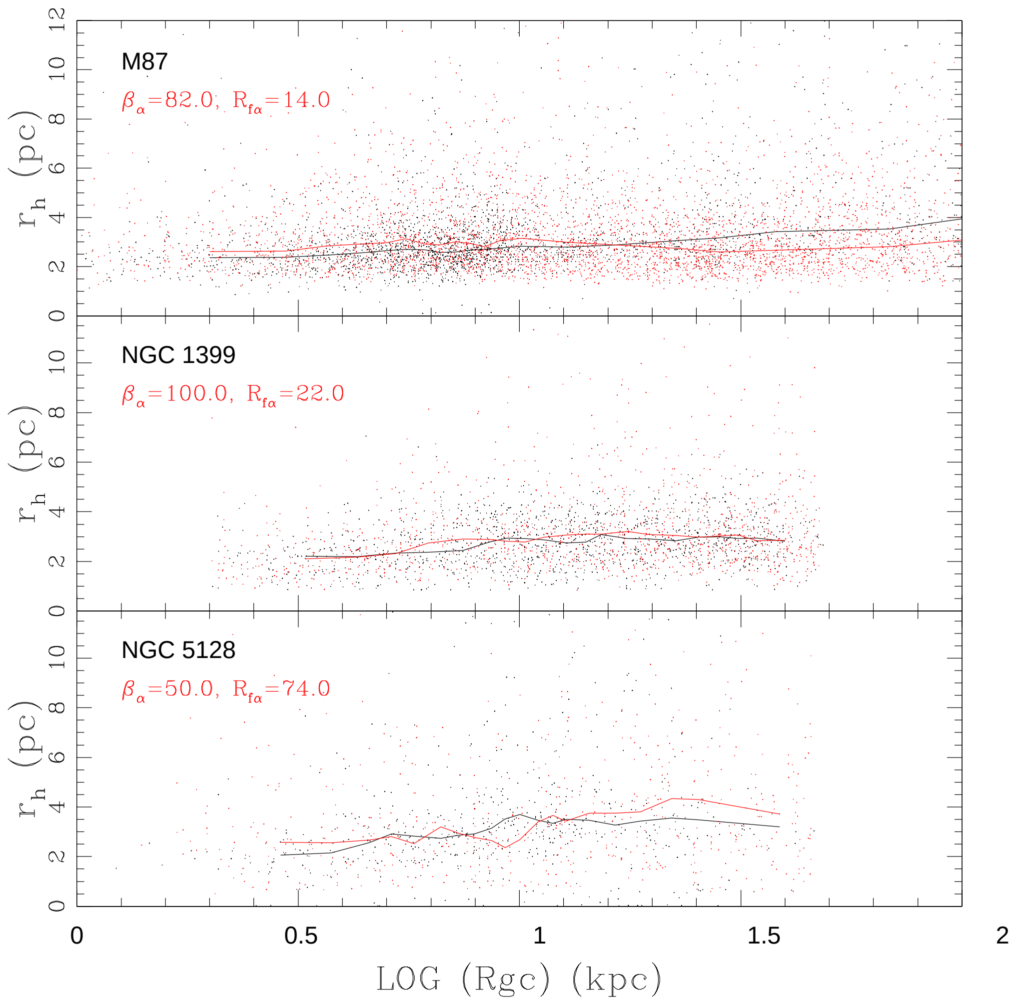

Figure 6.3 r_h vs log R_{gc} for observed globular clusters (black) and model clusters (red) in M87 (Top), NGC 1399 (Middle), and NGC 5128 (Bottom). Model clusters have anisotropy and tidal filling profiles as given by Equations 6.9 and 6.10, with the best fit values of β_α and $R_{f\alpha}$ indicated in each panel. The solid lines represent the median r_h calculated with radial bins containing 5% of the observed cluster population each.

10% of the minimum χ^2, we then search for the model with the most similar dispersion about the mean effective radius profile as the observations. The best fit models are illustrated for each galaxy in Figure 6.3.

The best fit models to M87 and NGC 1399 are very similar, with both suggesting $R_{f\alpha}$ is a more influential parameter than β_α. So while cluster orbits still become more radial with R_{gc}, it appears that the increase in β is relatively gradual, reaching values of 0.5 at 82 kpc and 100 kpc for M87 and NGC 1399 respectively. At the same time, clusters in each galaxy become 50% filling by approximately 14 kpc and 22 kpc in M87 and NGC 1399 respectively. The fact that $R_{f\alpha}$ is so small suggests that clusters must form extremely compact such that only the innermost clusters are filling their r_t while outer clusters are for the most part under-filling.

The best fit model to NGC 5128 is quite different from M87 and NGC 1399. With respect to β_α, our model suggests cluster orbits in NGC 5128 are slightly more radial than in M87 and NGC 1399. Additionally we find a much larger best fit value for $R_{f\alpha}$ (74 kpc) suggesting that the majority of cluster are tidally filling with only the outermost clusters becoming tidally under-filling. Both the best fit anisotropy radius and tidal filling radius are surprising considering how well NGC 5128 was fit by a tidally filling cluster population with an isotropic distribution of orbits. We attempt to explore this discrepancy by isolating the metal rich and metal poor sub-populations in each galaxy in the following section.

6.4.3 Separating the Metal Rich and Metal Poor Sub-Populations

In the previous section, we made the initial assumption that all clusters in a single galaxy share the same β and R_f profiles. However, it has long been known that GC populations in many types of galaxies can be divided into at least two sub-populations based on colour (e.g. Zepf & Ashman, 1993; Larsen et al., 2001; Harris , 2009b; Peng et al., 2006). Colour bimodality within cluster populations is often attributed to metallicity, with metal poor clusters being bluer than metal rich clusters (e.g. Zepf & Ashman, 1993; Brodie & Strader, 2006). Since this bimodality is observed in all but the smallest of galaxies, it is believed that the production of a two (or more) component GC population is an important step inherent to all galaxy formation and evolution mechanisms.

Galaxies form through the hierarchical merging of dwarf galaxies that combine to form a central massive galaxy(Kravtsov & Gnedin, 2005; Tonini , 2013; Li & Gnedin, 2014; Kruijssen, 2014). The first globular clusters that form will initially have low metallicities and therefore represent the blue cluster population. Once the first stars in blue clusters go supernovae and the central host galaxy has accreted enough mass, more metal rich (redder) clusters will begin to form. Once globular cluster formation ends, the central galaxy will consist of both blue and red clusters, with the blue cluster population continuing to grow in number as satellite galaxies merge with the host and their cluster populations are accreted. It should be noted that some studies suggest the bimodality is a product of non-linear colour-metallicity relations (Cantiello & Blakeslee, 2007; Cantiello et al., 2014). For the purposes of this study we assume the bimodality is due to metallicity.

Observational studies have identified many structural and kinematic differences between these two sub-populations. A common observation within GC populations (including the populations presented here) is that red GCs have effective radii that are on average 20% ($\sim$ 0.4 pc) smaller than blue GCs (e.g. Kundu & Whitmore, 1998; Kundu et al., 1999; Larsen et al., 2001; Jordán et al., 2005; Harris , 2009a; Harris et al., 2010a; Paolillo et al., 2011; Blom et al., 2012; Strader et al., 2012; Woodley, 2012; Usher et al., 2013).

The size difference is likely due to the red and blue sub-populations having different formation, dynamical and stellar evolution histories (e.g. Kundu & Whitmore, 1998; Jordán, 2004; Jordán et al., 2005; Harris , 2009a; Sippel et al., 2012; Schulman et al., 2012). And since it is known that red and blue sub-populations have noticeably different radial profiles and velocity dispersions, there is no strong reason that the sub-populations will have the same β and R_f profiles. Hence we have elected to repeat the fitting process, but with the red and blue clusters fitted separately. The final comparison between our models and observations is illustrated in Figure 6.4.

For M87, our model suggests that red clusters in M87 have a relatively isotropic distribution of orbits, but become tidally under-filling very quickly with R_{gc}. The blue cluster sub-population has a slightly higher degree of orbital anisotropy, with blue clusters also being more tidally filling than red clusters. The latter point is in agreement with observational studies that find blue clusters are on average larger than red clusters. As in M87, blue clusters in NGC 5128 have a higher degree of radial anisotropy than red clusters. However unlike M87, our models suggest that red clusters in NGC 5128 are more tidally filling than blue clusters.

The best fit models to red and blue clusters in NGC 1399 are surprisingly quite different from the total population. While the NGC 1399 models are consistent with the M87 and NGC 5128 fits in the sense that blue clusters have preferentially more radial orbits than red clusters, the best fit values of β_α are much lower for the total population fit in Figure 6.3. Furthermore, while NGC 1399 is similar to M87 in that blue clusters are more tidally filling than red clusters, the best fit $R_{f\alpha}$ is significantly higher than the total population fit. A closer look at the β_α - $R_{f\alpha}$ parameter space in the following section

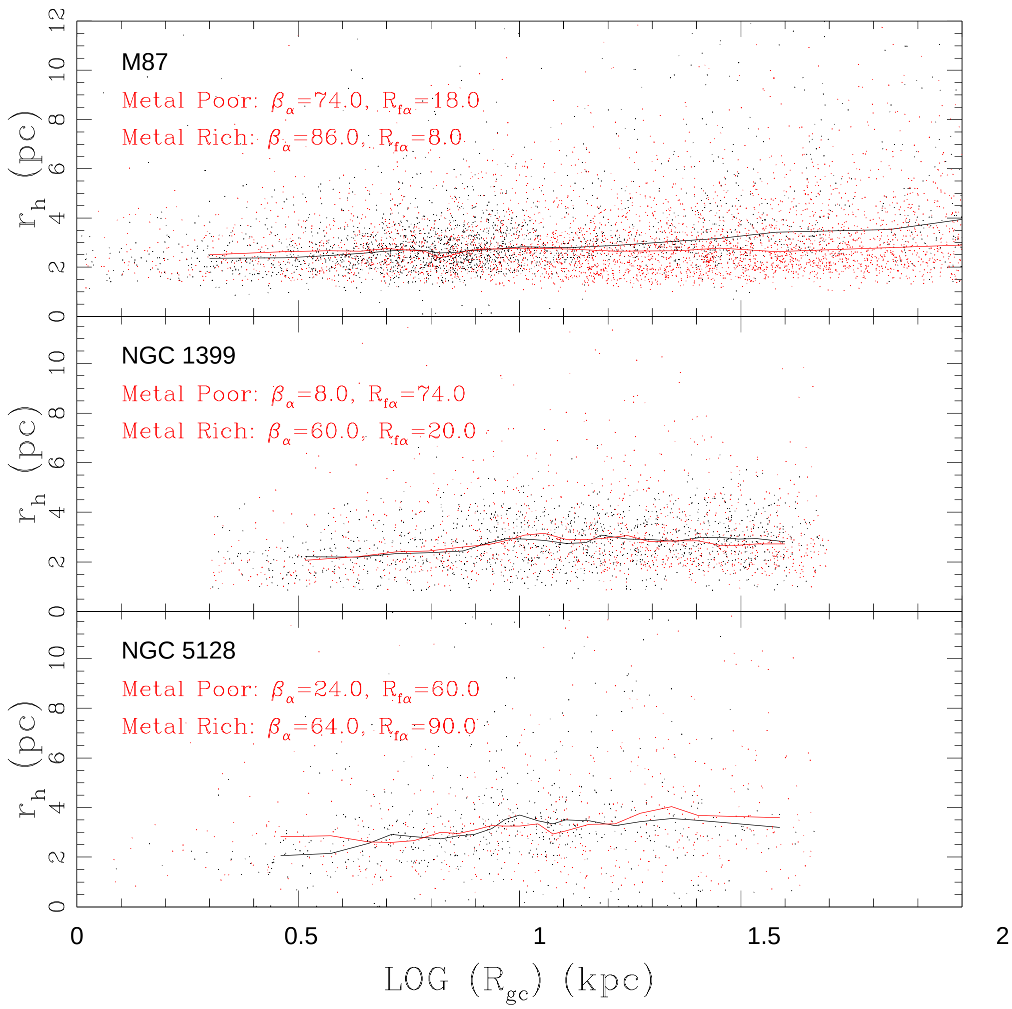

Figure 6.4 r_h vs log R_{gc} for observed globular clusters (black) and model clusters (red) in M87 (Top), NGC 1399 (Middle), and NGC 5128 (Bottom). Model clusters have anisotropy and tidal filling profiles as given by Equations 6.9 and 6.10, with the best fit values of β_α and $R_{f\alpha}$ for the metal rich and metal poor clusters indicated in each panel. The solid lines represent the median r_h calculated with radial bins containing 5% of the observed cluster population each.

will help explain this apparent discrepancy and identify the need to invoke additional observational constraints when applying our models to observational datasets.

6.4.4 Degeneracy Between β and R_f Profiles

The key issue that prevents us from putting stronger constraints on the profiles of each galaxy is the degeneracy between β and R_f. Increasing β serves to decrease cluster sizes as it results in cluster orbits being preferentially radial, bringing them deep into the galactic potential of the galaxy. Decreasing R_f results in clusters being compact and tidally under-filling, such that their observed size is less than r_t and they evolve as if they were in isolation. In Figure 6.5, the χ^2 value between our model and the observations is shown for the entire β_α and $R_{f\alpha}$ parameter space tested in Section 6.4.2.

6.4.4.1 M87

For M87, the populations can be fit by either a radially anisotropic distribution of cluster orbits or a very tidally under-filling population. In order to distinguish between possible best fits it is important to consider kinematic studies of these GC populations. As previously mentioned, Strader et al. (2011) found that the cluster population of M87 likely has a value of β equal to approximately 0.4. This result immediately rules out low values of β_α where β increases very quickly, suggesting that the best fit presented in Figure 6.3 is probable. This conclusion is also supported when model fits within 25% and 50% of the minimum value, as well as two-dimensional χ^2 tests (Rejkuba et al., 2011), are taken into consideration. Unfortunately, Strader et al. (2011) could

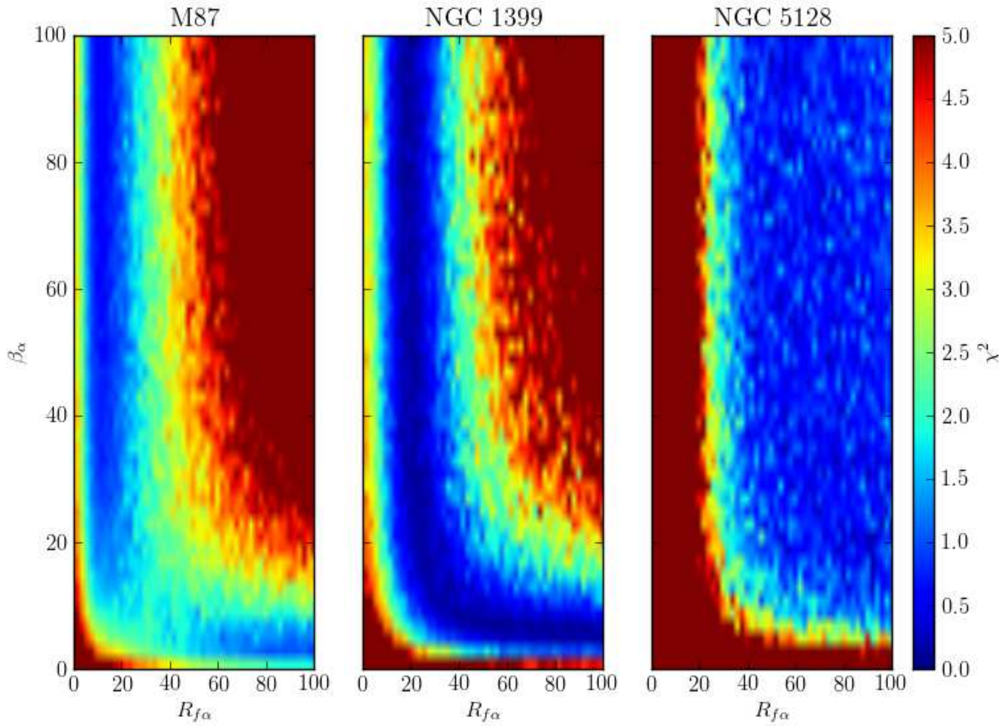

Figure 6.5 Degeneracy between β_α and $R_{f\alpha}$ for fits to the total cluster populations of M87 (left), NGC 1399 (middle) and NGC 5128 (right). The colour scale corresponds to the χ^2 between our theoretical model and observations.

not place strong constraints on the red and blue sub-populations due to the existence of an intermediate population. However, observations do not suggest that either the red and blue sub-populations have significantly different values of β indicating our fits to the sub-populations in Figure 6.4 are also the most probable.

6.4.4.2 NGC 1399

For NGC 1399, the degeneracy is larger than in M87 because the observational dataset contains almost half as many GCs and spans only $\frac{1}{3}$ the range in R_{gc}. Schuberth et al. (2010) modelled the cluster populations with β values up to and including 0.5, again ruling out the need for low values of β_α and consistent with the best fit model in Figure 6.3. These observations do however rule out the best fit models to the sub-populations in NGC 1399, especially the blue sub-population with a β_α of 8 kpc that yields an average value of β much higher than 0.5. The second best fit to the median r_h profile of blue clusters in NGC 1399, with a χ^2 only 0.015 larger than the best fit, suggests a much higher β_α of 98 kpc and a $R_{f\alpha}$ of 18 kpc, significantly closer to the fit of the total population. Similarly for the red sub-population, the next best fit to the median has a χ^2 only 0.003 larger and equals the best fit to the global population, with β_α equaling 100 kpc and $R_{f\alpha}$ equalling 22 kpc. The secondary fits are compared to the initial fits in Figure 6.6, and indicate that both sets of models produce nearly identical median r_h profiles. Unfortunately, the kinematic work of Schuberth et al. (2010) does not allow us to distinguish between these model fits any further. And since the cluster population is primarily under-filling ($R_{f\alpha}$ < 20 kpc), it is difficult to use structural parameters to trace orbital anisotropy as cluster evolution is for the most part unaffected by the surrounding tidal field.

6.4.4.3 NGC 5128

Finally, in NGC 5128 the degeneracy is less clearly defined because the cluster population is already well fit by tidally filling clusters with an isotropic distribution of orbits. Hence any combination of large values of both β_α and $R_{f\alpha}$ will provide a match between theory and observations. In a kinematic study of NGC 5128, Woodley et al. (2010b) also found that clusters could be approximated as having an isotropic distribution of orbits, with only a minor degree of radial anisotropy in the outermost regions (if at all).

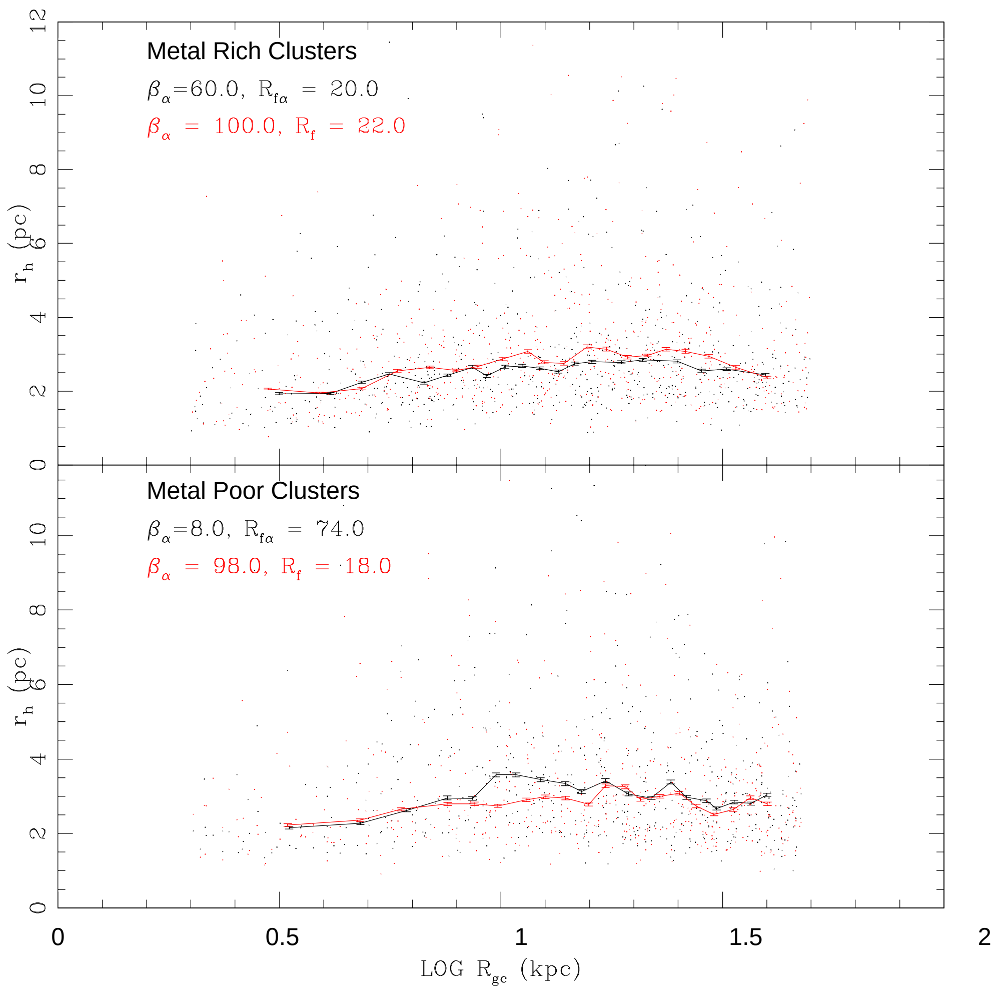

Figure 6.6 r_h vs log R_{gc} for best fit (black) and second best fit (red) models to metal rich globular clusters (top panel) and metal poor globular clusters (bottom panel) in NGC 1399. Error bars represent the standard error $\sigma/\sqrt(n)$ as given by Harris et al. (2010a).

6.5 Discussion

Our model represents a realistic GC system by allowing cluster orbits to become more radial with R_{gc}, letting clusters become less tidally filling with R_{gc}, and modelling the red and blue cluster sub-populations separately. We now discuss the best fit profiles in further detail.

6.5.1 M87

The fact that the best fit model for blue clusters suggests the population is more radially anisotropic than red clusters is in agreement with the idea that while some blue clusters form early in the small halos which eventually make up the host galaxy, most of the blue sub-population has been added via accretion of dwarf galaxies (Schuberth et al., 2010). Accreted clusters will expectedly have radial orbits, resulting in blue clusters being more radially anisotropic. Kruijssen et al. (2012) demonstrated that after a galaxy merger, the surviving cluster population will have increasing orbital anisotropy with R_{gc}. Their results find that β values can even reach 0.9 by 100 kpc. Our model also suggests that inner blue clusters are tidally filling, in agreement with the work of Miholics et al. (2014) who found that the size of accreted clusters respond to their new potential within 2-3 half-mass relaxation times. Metal rich clusters also fit this paradigm as the sub-population of clusters that formed in the original central galaxy in Virgo. One would then expect the red population to be primarily isotropic in the inner regions as it formed and evolved in a single galaxy for 12 Gyr. In order to reproduce the size-distance relationship, red clusters must also form more compact such that are still very under-filling today.

This interpretation is in agreement with the recent kinematic study of M87 performed by Strader et al. (2011). They find the GC population has preferentially radial orbits corresponding to $\beta = 0.4$, and note outer GCs (specifically metal rich ones) may have highly radial orbits in agreement with our best fit models. Furthermore, Strader et al. (2011) and Romanowsky et al. (2012) find evidence that a massive merger occurred in M87 less than 1 Gyr ago. The identification of shells, arcs, and streams of kinematically distinct GCs in M87 suggest that the outer regions of M87 have been built up via a continuous infall of material that is still ongoing today (D'Abrusco et al., 2013, 2014a,b, 2015; Longobardi et al., 2015). The authors also suggest that clusters beyond 40 kpc undergo dynamical interactions with nearby galaxies which disrupt their orbits. So while one would expect outer clusters with radial orbits to have naturally been pulled towards the centre of a galaxy, continuous disruption results in the majority of outer clusters being forced into radial orbits. Hence the outer cluster population is still in the process of assembly.

Our model slightly underestimates cluster sizes at large R_{gc}, as it predicts a flattening in the r_h - R_{gc} profile that is not observed in M87. This is likely a direct result of our choice in the functional form of the β profile in Equation 6.9 and its inability to accurately model the outskirts of M87. Since M87 is still in the process of being built up via the continuous infall of material and outer clusters are still being disrupted by nearby galaxies, the anisotropy profile of globular clusters at large R_{gc} will not be smooth. It will instead vary from region to region, as the kinematically distinct sub-populations which make up the outer halo will have a range of different β values depending on the details of how they were accreted. Evidence of kinematically separate sub-populations in M87 have even been reported by Strader et al. (2011) and

Romanowsky et al. (2012).

The functional form of our β profile is also at odds with the results of Agnello et al. (2014). In their study of M87, based on data from Strader et al. (2011), they identify three potential sub-populations in M87. The traditional red population is found to have primarily tangential orbits in the inner region of the galaxy before becoming radial at larger R_{gc}, as we find. However they suggest the blue population has mostly isotropic orbits in the inner regions and the orbits actually become preferentially tangential in the outskirts. Such a profile would reproduce the increase in cluster size at large R_{gc} that our current model does not. Agnello et al. (2014) argue that this is consistent with the adiabatic contraction of a DM halo. Assuming M87 accretes mass on slow time scales, then the outer regions should be dominated by clusters with tangential orbits as radial orbits are more efficiently pulled inwards towards the centre of the galaxy (Goodman & Binney, 1984; Lee & Goodman, 1989; Cipolina & Bertin, 1994). However Agnello et al. (2014) also identify an intermediate population between red and blue clusters that has an overall β of approximately 0.3, much closer to our best fit model to the blue sub-population. It is possible that by restricting our M87 dataset to two sub-populations we no longer recover the decreasing β profile found by Agnello et al. (2014) for blue clusters. Additionally, in their model of M87, the velocity dispersion for each sub-population changes as a function of R_{gc}. Future applications of our model will take into consideration the existence of more than two sub-populations, radially dependent velocity dispersions, and different function forms of the β profile in search for structural evidence of the Agnello et al. (2014) result.

6.5.2 NGC 1399

The initial best fit models to the red and blue sub-populations in NGC 1399 were at odds with the fit to the total cluster population. However, after taking into consideration the degeneracy between B_α and $R_{f\alpha}$ and using observational studies to constrain our model, cluster orbits in NGC 1399 are better fit by models that are more isotropic than M87. However, we still find that blue clusters have a higher degree of radial anisotropy than red clusters, consistent with blue clusters forming in dwarf galaxies before merging with a central host. The model fits are also in agreement with kinematic studies of NGC 1399 which suggest that the cluster population is closer to isotropic than M87 (Strader et al., 2011). Similar to M87, our model also predicts a flattening in the r_h-R_{gc} profile at large distances, however the observational profile of NGC 1399 also supports this trend. Since M87 and NGC 1399 are both at the center of a galaxy cluster, differences between model fits lead to the question why the anisotropy and filling profiles of red and blue clusters in the two galaxies are not more similar. Strader et al. (2011) suggests that while M87 has been built up via the continuous infall of galaxy halos, the more isotropic population of NGC 1399 could have been assembled during an initial fast accretion phase (e.g. Biviano & Poggianti, 2009). With no visual evidence for a recent merger event in NGC 1399 (Tal et al., 2009), the initial fast accretion scenario appears likely. With no recent major accretion events, any accreted clusters on plunging radial orbits will have already fallen into the galaxy centre resulting in a more isotropic distribution of cluster orbits. Furthermore, the Fornax cluster is less massive than Virgo and contains fewer galaxies, which means the outer clusters in NGC 1399 will experience fewer disruptive events resulting in a more isotropic population. Hence the anisotropy profile at large R_{gc} may still in fact be smooth, which is why our model does a better job of modelling outer clusters in NGC 1399 than in M87.

The general case of orbits becoming more radial and clusters becoming more under-filling with R_{gc} is still prevalent in both M87 and NGC 1399. The fact that both galaxies are at the centre of large clusters is likely the common factor, as neighbouring galaxies are continuously disrupting the outer cluster populations. Hence the outer regions of these galaxies cannot truly reach equilibrium. As we will see for NGC 5128 in the following section, a galaxy in isolation may in fact come closer to some sort of dynamical equilibrium.

6.5.3 NGC 5128

The degeneracy between B_α and $R_{f\alpha}$ in NGC 5128 is quite different from either M87 or NGC 1399. Differences between galaxies can be attributed to NGC 5128 having a differently shaped mass profile (as previously shown in Figure 6.1) and velocity dispersion compared to M87 and NGC 1399. A more gradual increase in enclosed mass with distance in NGC 5128 results in theoretical cluster sizes increasing at a shallower rate. A smaller velocity dispersion minimizes the chances of generating clusters with highly eccentric orbits. Hence we find that both red and blue cluster populations are primarily isotropic and tidally filling. A primarily isotropic population suggests that NGC 5128 may have also formed during an initial fast accretion phase and has undergone few recent major mergers. However, an analysis by Rejkuba et al. (2011) of the ages of stars in NGC 5128 finds that almost $\frac{1}{4}$ of the stars in the halo are 2-4 Gyr old, signifying a recent merger has occurred in the galaxy. Since our model indicates the red and blue sub-populations in NGC 5128 are nearly isotropic, it is likely that either the recent merger was a minor one that occurred on a relatively long timescale or NGC 5128 contains an intermediate cluster population. If the merger event implied by the observations of Rejkuba et al. (2011) was a singular and slow event, any accreted clusters with radial orbits would also be efficiently pulled towards the centre of the galaxy. And similar to our discussion regarding the results of Agnello et al. (2014), modelling a potentially three component population as a two component population could result in the loss or blending of the intermediate populations orbital and tidally filling characteristics.

It is also important to note that since NGC 5128 does not have any massive galaxies or satellites nearby, the outer cluster population is not being disrupted. The lack of disruption could be the main factor for NGC 5128 showing a lesser degree of orbital anisotropy. Since the halo is no longer in the process of assembling, GCs with preferentially radial orbits will have been left to naturally decay.

6.6 Conclusions and Future Work

We have successfully reproduced the distribution of GC sizes in three giant galaxies (M87, NGC 1399, and NGC 5128) by allowing cluster orbits to become more radial and clusters to become more under-filling with R_{gc}, in line with models and observations of galaxy structure and cluster populations. For M87 and NGC 1399, both galaxies that are located at the centre of a galaxy cluster, the global cluster populations have a mild degree of radial anisotropy at larger R_{gc} and are primarily under-filling beyond 15 kpc. Our findings are consistent with kinematic studies of each galaxy (e.g Côté et al., 2001; Schuberth et al., 2010; Strader et al., 2011; Woodley et al., 2010b,c), the assembly of giant galaxies via mergers and dwarf galaxy accretion (e.g Schuberth et al., 2010; Kruijssen et al., 2012), and the evolution of GC populations (Alexander & Gieles, 2013; Webb et al., 2013a). NGC 5128 on the other hand appears to be nearly isotropic and tidally filling out to large R_{gc}. Since NGC 5128 is a relatively isolated galaxy, a lack of recent major majors or nearby neighbours to disrupt outer GCs has allowed clusters on radial orbits to decay.

Separating the cluster populations of each galaxy into red and blue sub-populations reveals additional information. *In all cases we find that blue clusters have a higher degree of radial anisotropy than red clusters.* The more radial orbits of blue clusters lends credence to the idea that blue clusters are accreted via mergers with satellite galaxies and the more isotropic red clusters supports their formation within the central host. However both red and blue clusters in NGC 1399 are closer to having an isotropic distribution of orbits than cluster in M87, suggesting that despite being located at the centre of large galaxy clusters the two galaxies have undergone different formation scenarios. For example, Strader et al. (2011) suggests that M87 has likely been assembled via the continuous infall of galaxy halos and NGC 1399 likely formed via an initial fast accretion phase such that cluster sub-populations have had time to mix. This statement is supported by the fact that the Fornax cluster is less massive and contains fewer galaxies than the Virgo cluster.

The best orbital anisotropy and tidal filling profiles of NGC 5128 are much different from either M87 or NGC 1399 as they predict a nearly isotropic and tidally filling population of GCs. Similar to NGC 1399, NGC 5128 could have formed via a fast accretion phase. A fast-accretion phase, combined with the fact that NGC 5128 is an isolated galaxy with no major satellites to disrupt the outer cluster population, could result in an isotropic distribution of cluster orbits at all R_{gc}.

It is difficult to put strong constraints on the orbital anisotropy or filling profiles of either of these galaxies due to the strong degeneracy between β_α and $R_{f\alpha}$. Both parameters serve to decrease cluster size with R_{gc}. For M87 and NGC 1399, both datasets can be fit be either a low β_α - high $R_{f\alpha}$ or low $R_{f\alpha}$ - highβ_α model. Kinematic studies of both galaxies allow us to rule out the low β_α - high $R_{f\alpha}$ cases, and we can interpret both cluster populations as having orbits that become moderately radial with R_{gc} and are primarily under-filling beyond 15 kpc. Since NGC 5128 is best fit by a high β_α - high $R_{f\alpha}$ model, the degeneracy is not a factor. Unfortunately, kinematic studies of the red and blue sub-populations within each galaxy are less conclusive, and while the best fit models presented above for each galaxy are supported by past kinematic studies we cannot rule out some of the degenerate solutions.

More detailed kinematic models of cluster sub-populations, which take into consideration how velocity dispersion changes a function of R_{gc}, are required in order for us to place stronger constraints on β_α. Measuring cluster sizes and velocity over a larger range in R_{gc} will help minimize the degeneracy between β_α and $R_{f\alpha}$. In order to better constrain $R_{f\alpha}$, evolutionary models of clusters and cluster populations in giant galaxies are needed, including clusters that have been accreted via mergers.

Ultimately, what we can say with more certainty, is that best fit models to M87, NGC 1399, and NGC 5128 are telling us that giant galaxies can undergo different formation mechanisms and merger histories such that their respective GC populations evolve in significantly different environments. Initial fast accretion, continuous mergers (slow and violent), recent mergers, and neighbouring galaxies all leave an imprint on the cluster population in the form of orbital anisotropy and tidal filling profiles.

6.7 Acknowledgements

JW, WEH and AS acknowledge financial support through research grants and scholarships from the Natural Sciences and Engineering Research Council of Canada. M.P. acknowledges financial support from PRIN-INAF 2014 "Fornax Cluster Imaging and Spectroscopic Deep Survey".

Bibliography

Agnello, A., Evans, N.W., Romanowsky, A.J., Brodie, J.P. 2014, MNRAS, 442, 3299

Alexander, P. E. R. & Gieles, M. 2013, MNRAS, 432L, 1

Baumgardt H., Makino J. 2003, MNRAS, 340, 227

Bertin, G. & Varri, A. L. 2008, ApJ, 689, 1005

Bianchini, P., Renaud, F., Gieles, M., Varri, A.L. 2015, MNRAS, 447, 40

Binney, J. & Tremaine, S. 2008, Galactic dynamics second edition (Princeton, NJ, Princeton University Press, 1987, 747 p.)

Biviano, A. & Poggianti, B. M. 2009, A&A, 501, 419

Blakeslee, J. P., Jórdan, A., Mei, S., Côté, P., Ferrarese, L., Infante, L., Peng, E.W., Tonry, J.L., West, M.J. 2009, ApJ, 694, 556

Blom, C., Spitler, L. R., Forbes, D. 2012, MNRAS, 420, 37

Brodie, J. P. & Strader, J. 2006, ARAA, 44, 193

Cantiello,M. & Blakeslee, J.P. 2007, ApJ, 669, 982

Cantiello, M., Blakeslee, J.P., Raimondo, G., Chies-Santos, A.L., Jennings, Z.G., Norris, M.A.; Kuntschner, H. 2014, A&A, 564, 3

Casetti-Dinescu, D.I., Girard, T.M., Herrera, D., van Altena, W.E., López, C.E., Castillo, D.J. 2007, AJ, 134, 195

Casetti-Dinescu, D.I., Girard, T.M., Jíková, L., van Altena, W.F., Podestá, F., López, C.E. 2013, AJ, 146, 33

Cipolina, M. & Bertin, G. 1994, AA, 288, 43

Côté, P., McLaughlin, D.E., Hanes, D.A., Bridges, T.J., Geisler, D., Merrid, D., Hesser, J.E., Harris, G.L.H., Lee, M.G., 2001, ApJ, 559, 828, 257B

D'Abrusco, R., Fabbiano, G., Zezas, A. 2015, ApJ, Accepted, arXiv:1503.94819

D'Abrusco, R., Fabbiano, G., Brassington, N.J. 2014a, ApJ, 783, 19

D'Abrusco, R., Fabbiano, G., Mineo, S., Strader, J., Fragos, T., Kim, D.-W., Luo, B., Zezas, A. 2014b, ApJ, 783, 18

D'Abrusco, R., Fabbiano, G., Strader, J., Zezas, A., Mineo, S., Fragos, T., Bonfini, P., Luo, B., Kim, D.-W., King A 2013, ApJ, 773, 87

de Vaucouleurs, G., & Nieto, J.-L. 1978, ApJ, 220, 449

Dehnen, W. 1993, MNRAS, 265, 250

Dinescu, D.I., Girard, T.M., van Altena, W.E. 1999, AJ, 117, 1792

Dunn, L.P. & Jerjen, H. 2006, AJ, 132, 1384

Gieles, M., Heggie , D. C., Zhao H. 2011, MNRAS, 413, 2509

Gnedin, O. Y., & Prieto, J. L. 2009, in ESO Astrophysics Symp.: Globular Clusters-Guides to Galaxies (Berlin: Springer), 323

Gómez, M. & Woodley, K.A. 2007, ApJ, 670, L105

Goodman, J. & Binney, J.J. 1984, MNRAS, 207, 511

Harris, W. E. 1996, AJ, 112, 1487, 2010 Edition

Harris, W.E. 2009a, ApJ, 703, 939

Harris, W.E. 2009b, ApJ, 699, 254

Harris, W.E., Spitler, L.R., Forbes, D.A., Bailin, J. 2010a, MNRAS, 401, 1965

Harris, G.L.H., Rejkuba, M., Harris, W.E. 2010b, PASA, 27, 457

Henon M. 1961, Annales d'Astrophysique, 24, 369

Innanen, K. A., Harris, W.E., Webbink, R.F. 1983, AJ, 88, 338

Jórdan, A. 2004, ApJ, 613, L117

Jórdan, A., Côté, P., Blakeslee, J. P., Ferrarese, L., McLaughlin, D. E. , Mei, S., Peng, E. W., Tonry, J. L., Merrit, D., Milosavljević, M., Sarazin, C. L., Sivakoff, G. R., West, M. J., 2005, ApJ, 634, 1002

Kennedy, G.F. 2014, MNRAS, 444,3328

King, I. R. 1962, AJ, 67, 471

Kravtsov, A.V. & Gnedin, O.Y. 2005, ApJ, 623, 650

Kruijssen, J.M.D., Pelupessy, F.I., Lamers, H.J.G.L.M., Portegies Zwart, S.F., Bastian, N., Icke, V. 2012, MNRAS, 421, 1927

Kruijssen, J.M.D. 2014, Classical and Quantum Gravity, 31, 244006

Kundu, A. & Whitmore, B. C. 1998, AJ, 116, 2841

Kundu, A., Whitmore, B. C., Sparks, W. B., Macchetto, F. D., Zepf, S. E., Ashman, K. M. 1999, ApJ, 513, 733

Küpper, A. H. W, Kroupa, P, Baumgardt, H., Heggie , D. C., 2010, MNRAS, 407, 2260

Larsen, S. S., Brodie, J. P., Huchra, J. P., Forbes, D. A., Grillmair, C. J., 2001, AJ, 121, 2974

Lee, M.H. & Goodman, J. 1989, ApJ, 343, 594

Li, H. & Gnedin, O.Y. 2014, ApJ, 796, 10

Longobardi, A., Arnaboldi, M., Gerhard, O., Mihos, J. C. 2015, A&A, submitted, arXiv:1504.04369

Ludlow, A. D., Navarro, J. F., Springler, V., Vogelsberger, M., Wang , J., White, S. D. M., Jenkins, A., & Frenk, C. S. 2010, MNRAS, 406, 137

Madrid, J.P., Hurley, J.R., Martig, M., 2014, ApJ, 784, 95

McLaughlin, D. E. & van der Marel, R. P. 2005, ApJs, 161, 304

McLaughlin, D. E. 1999, ApJ, 512, L9

Miholics, M., Webb, J., Sills, A., 2014, MNRAS, 445, 2872

Moreno, E., Pichardo, B., Velázquez, H. 2014, ApJ, 793, 110

Navarro, J. F., Frenk, C. S., & White, S. D. M. 1997, ApJ, 490, 493

Paolillo, M., Fabbiano, G., Peres, G. Kim, D.-W. 2002, ApJ, 565, 883

Paolillo, M., Puzia, T. H., Goudfrooij, P., Zepf, S. E., Maccarone, T. J., Kundu, A., Fabbiano, G., Angelini, L. 2011, ApJ, 736, 90

Peng, E. W., Ford, H. C., & Freeman, K. C. 2004, ApJ, 602, 705

Peng, E.W., Jórdan, A., Côté, P., Blakeslee, S., Ferrarese, L., Mei, S., West, M. J., Merritt, D., Milosavljević, M., Tonry, J. L. 2006, ApJ, 639, 95

Pierce, M. J., Welch, D. L., McClure, R. D., van den Bergh, S., Racine, R., & Stetson, P. B. 1994, Nature, 371, 385

Prieto, J. L. & Gnedin, O. Y. 2008, ApJ, 689, 919

Puzia, T.H., Paolillo, M., Goudfrooij, P., Maccarone, T.J., Fabbiano, G., Angelini, L. 2014, ApJ, 786, 78

Rejkuba, M., Harris, W.E., Greggio, L., Harris, G.LH. 2011, A&A, 526, 123

Renaud, F., Gieles, M., Christian, M. 2011, MNRAS, 418, 759

Renaud, F. & Gieles, M. 2015, MNRAS, accepted, arXiv:1503.04815

Romanowsky, A.J., Strader, J., Brodie, J.P., Mihos, J.C., Spitler, L.R, Forbes, D.A., Foster, C., Arnold, J.A. 2012, ApJ, 748, 29

Sippel, A.C., Hurley, J.R., Madrid, J.P., Harris, W.E. 2012, MNRAS, 427, 167

Schiminovich, D., van Gorkum, J. H., van der Hulst, J. M., & Kasow, S. 1994, ApJ, 423, L101

Schuberth, Y., Richtler, T., Hilker, M., Dirsch, B., Bassin, L.P., Romanowsky, A.J., Infante, L. 2010, A&A, 512, 52

Schulman, R. D., Glebbeek, E., Sills, A. 2012, MNRAS, 420, 651

Spitler, L.R., Larsen, S.S., Strader, J., Brodie, J.P., Forbes, D.A., Beasley, M.A. 2006, AJ, 132, 1593

Strader, J., Romanowsky, A.J., Brodie, J.P., Spitler, L.R., Beasley, M.A., Arnold, J.A., Tamura, N., Sharples, R.M., Arimoto, N. 2011,APJS, 197, 33

Strader, J., Fabbiano, G., Luo, B., Kim, D., Brodie, J.P., Fragos, T., Gallagher, J.S., Kalogera, V., King, A., Zezas, A. 2012, ApJ, 760, 87

Tal, T., van Dokkum, P. G., Nelan, J., Bezanson, R. 2009, AJ, 138, 1417

Tonini, C. 2013, ApJ, 762, 39

Tonry, J. L., Dressler, A., Blakeslee, J. P., Ajhar, E.A., Fletcher, A.B., Luppino, G.A., Metzger, M.R., Moore, C.B. 2001, ApJ, 546, 681

Tremaine, S., Richstone, D.O., Byun, Y.-L., Dressler, A., Faber, S. M., Grillmair, C., Kormendy, J. and Lauer, T. R. 1994, AJ, 107, 634

Usher, C., Forbes, D.A., Spitler, L.R., Brodie, J.P., Romanowsky, A.J., Strader, J., Woodley, K.A. 2013, MNRAS, 436, 1172

von Hoerner, S. 1957, ApJ, 125, 451

Webb, J.J, Sills, A., Harris, W.E. 2012, ApJ, 746, 93

Webb, J.J., Harris, W.E., Sills, A., Hurley, J.R. 2013a, ApJ, 764, 124

Webb, J.J, Sills, A., Harris, W.E. 2013b, ApJ, 779, 94

Webb, J.J., Sills, A., Harris, W.E., Hurley, J.R. 2014, MNRAS, 445, 1048

Weijmans, A., Cappellari, M., Bacon, R., de Zeeuw, P. T., Emsellem, E., Falcon-Barroso, J., Kuntschner, H., McDermid, R. M., van den Bosch, R. C. E., and van de Ven, G., 2009, MNRAS, 398, 561

Woodley, K.A. & Gómez, M. 2010a, PASA, 27, 379

Woodley, K.A., Gómez, M., Harris, W.E., Geisler, D., Harris, G.L.H. 2010b, AJ, 139, 1871

Woodley, K.A., Harris, W.E., Puzia, T.H., Gómez, M., Harris, G.L.H., Geisler, D. 2010c, ApJ, 708, 1335

Woodley, K. 2012, AAS Meeting #220, #438.07

Zait, A., Hoffman, Y. & Shlosman, I. 2008, ApJ, 682, 835

Zepf, S. E. & Ashman, K. M. 1993, MNRAS, 264, 611

Chapter 7

Summary and Future Work

Globular clusters represent one of the key building blocks in the Universe, as they play pivotal roles in the formation of both galaxies and stars. They are found throughout the Universe and typically as members of a larger globular cluster population, ranging from just a few clusters in dwarf galaxies to tens of thousands of clusters in giant elliptical galaxies. Having formed at the same time as their host galaxy, clusters provide a window into what the Universe was like when the first galaxies began to form. Furthermore, having undergone ~ 12 Gyr of evolution within the gravitational field of a given galaxy, clusters can also provide clues as to how galaxies evolve from formation to present day. Tidally under-filling clusters, which have essentially evolved in isolation, provide insight into the conditions of the galaxy when globular clusters first form. The orbits and structural properties of tidally filling globular clusters are both sensitive to the distribution of matter in the host galaxy, with the distribution of cluster orbits likely containing information of how a galaxy was assembled. An understanding of how exactly globular clusters evolve allows for the present day properties of clusters to be used to constrain both the conditions under which globular cluster form and the dynamical history of their host galaxy. While the dynamical evolution of a globular cluster that is effectively in isolation has been long understood (Henon, 1961), the role that environment plays is still unclear. With approximately $\frac{1}{3}$ of the globular clusters in the Milky Way being found to be tidally affected (Gieles, Heggie & Zhao, 2011), environment will play a very important role in setting the global properties of a galaxy's globular cluster population. This thesis is particularly focussed on developing an understanding of how environment, primarily the tidal field of a host galaxy, affects globular cluster evolution.

Historically, theoretical studies of globular cluster evolution have focussed on idealized globular clusters which experience a static external tidal field. Many observational properties of globular cluster populations can not be explained by assuming clusters experience static tidal fields. Globular clusters in the Milky Way are all known to have non-circular orbits (Dinescu et al., 1999; Casetti-Dinescu et al., 2007, 2013), which likely applies to extragalactic populations as well. Additionally, galaxies are not spherically symmetric, consist of substructure, and grow in time via merger events. These points all illustrate that globular clusters evolve in non-static tidal fields. Computational simulations have only recently begun to directly model globular clusters in non-static tidal fields with an array of different initial conditions.

N-body simulations of star clusters with eccentric orbits in spherically symmetric potentials find orbiting in a non-static tidal field injects additional energy into a cluster, redistributing stellar orbits within a cluster and even helping some stars escape (Baumgardt & Makino, 2003; Kupper et al., 2010; Renaud et al., 2011). Prior to the work presented in this thesis, the long term effects of these processes on the dynamical evolution of globular clusters had yet to be explored. The effects of a non-spherically symmetric potential also need to be explored as there is no evidence that any galaxy is the Universe is truly spherically symmetric, including the Milky Way. Understanding how directly observable parameters evolve in a non-static tidal field will in turn give another way for globular clusters to be used to place constraints on a host galaxy. Understanding how cluster properties like r_h and r_L change as a function of their orbit allows for the radial distribution of these properties in observations of globular cluster populations to be used to constrain the distribution of cluster orbits and the distribution of matter, both baryonic and dark, within a host galaxy.

The purpose of this thesis is to extend dynamical evolution theory to a more advanced level of understanding, independent of generalizing assumptions, that can be applied to any globular cluster orbiting in any tidal field. We begin by first making use of N-body simulations of star clusters to study the effects of a non-static tidal field on globular cluster evolution. These studies are followed by an application of our theoretical results to observed globular cluster populations.

7.1 Theoretical Studies of Globular Clusters in Tidal Fields

This thesis marks the most extensive study on the effects of eccentricity and initial size on globular clusters to date, and the first systematic study of globular clusters orbiting in a Milky Way-like potential over a range of inclined orbits. In Chapter 2 we use a suite of N-body simulations which model tidally filling and under-filling clusters over a range of circular and eccentric orbits to test the historical assumption that the tidal radius of a cluster is imposed at perigalacticon. We find that the historical assumption is incorrect, and that after a perigalactic pass a cluster is able to re-capture many of the stars which were tidally stripped at perigalacticon. Furthermore, the tidal shock at perigalacticon and tidal heating over the course of the cluster's orbit are able to energize inner stars to wider orbits, effectively replacing stars that are permanently stripped at perigalacticon. We conclude that a cluster's size instead reflects its current position in a galaxy, and propose a correction factor to tidal radii calculated at perigalacticon which takes into consideration orbital eccentricity and the cluster's orbital phase.

Chapter 3 extends our study to the cluster's dynamical evolution. Our models demonstrate that compared to a cluster with a circular orbit at perigalacticon, increasing orbital eccentricity slows the dynamical evolution of a cluster because it experiences a weaker mean tidal field. However, tidal shocks at perigalacticon and tidal heating can compensate for the decreased mean tidal field by injecting additional energy into the cluster. We find that the circular orbit R_{circa} which best mirrors the evolution of a cluster on an eccentric orbit is a significantly smaller radius than the eccentric cluster's semi-major axis or time averaged galactocentric distance R_{gc}. Hence clusters which appear dynamically old at large R_{gc} are explainable by invoking a highly eccentric orbit. We illustrate how the stellar mass function of a cluster, which serves as a tracer of its dynamical age, can be used to constrain the orbits of globular clusters given their current R_{gc}.

In Chapter 4 we continue our study of clusters in non-static tidal fields by specifically focussing on the effect of orbital inclination on mass-loss rates and cluster structure. We find that a non-zero inclination leads to tidal heating and tidal shocks during disk passages that will help remove stars from a cluster, increasing the mean mass-loss rate. However, as the strength of the disk potential decreases with R_{gc}, outer clusters with inclined orbits are less affected by tidal heating and shocks, and can even have a lower mass loss rate than a cluster orbiting in the plane of the disk. Clusters with orbits that are both inclined and eccentric will be subject to increased tidal heating due to a constantly changing potential, weak tidal shocks when passing through the disk near apogalacticon, strong tidal shocks when passing through the disk near perigalacticon, and an additional tidal shock during a perigalactic pass. However, since clusters with eccentric orbits spend the majority of their lifetime near apogalacticon, the effects of orbital inclination decrease as orbital eccentricity increases since the cluster will spend more time at large R_{gc}.

In terms of cluster structure, limiting radii fluctuate wildly as a cluster with an inclined orbit travels near and through the galactic disk. We find that the limiting radius is best approximated by the tidal radius of the cluster when it is farthest from the disk, as the cluster has a significant amount of time to respond to the tidal field when at apogalacticon. Effective radii on the other hand appear to be unaffected by the additional tidal heating and shocks experienced by clusters with inclined orbits. Hence in extragalactic studies of globular cluster structure, where r_h is the only robust observable parameter, measurements of cluster size will not be sensitive to orbital inclination.

7.2 Application to Observed Globular Cluster Populations

The next step was to apply our results to observational studies of globular cluster populations. Chapters 5 and 6 represent the application of our theoretical studies to observations of globular clusters in giant galaxies. We specifically focussed on testing whether the distribution of cluster sizes in giant galaxies could be reproduced by assuming cluster populations consisted of both tidally filling and under-filling clusters with non-circular orbits.

In the first application of our work on clusters in non-static tidal fields, we aimed to reproduce the relationship between r_h and R_{gc} for clusters in the giant elliptical galaxy M87. As discussed in Chapter 5, new Hubble Space Telescope (HST) observations allowed us to study the cluster population beyond 100 kpc. While clusters in giant galaxies will not all have circular orbits, we found that the cluster population could also not be modelled with an isotropic distribution of orbits unless all clusters were severely under-filling. Instead we suggest that cluster orbits must become radially anisotropic with R_{gc} and that clusters become more tidally under-filling with R_{gc} in order to reproduce the observed r_h - R_{gc} relationship. Focussing on metal-poor and metal-rich clusters separately, we find that the size difference between red and blue clusters can be explained by both sub-populations having different anisotropy profiles. More specifically, we find evidence for blue clusters having a higher degree of radial anisotropy and being more tidally filling than red clusters.

In our culminating study, we extend our application of the evolution of clusters in non-static tidal fields in M87 to include the giant galaxies NGC 1399 and NGC 5128. When comparing all three galaxies, we find that M87 and

NGC 1399 can be modelled by clusters that quickly becoming tidally under-filling and have orbits that become moderately radial with increasing R_{gc}. NGC 5128 on the other hand is well fit by clusters that are primarily tidally filling and have an isotropic distribution of orbits. Differences between the three populations can be attributed to the differing mass profiles of their host galaxies. Further constraints can be made on the formation and merger history of each galaxy by studying the metal poor and metal rich sub-populations separately. In all cases, we find that blue clusters have a higher degree of radial anisotropy, consistent with the idea that giant galaxies form via the hierarchical assembly of smaller galaxies. While red clusters represent a sub-population that was built early by the host galaxy, blue clusters are continuously being accreted such that outer blue clusters will have preferentially radial orbits as they fall inwards. The fact that the red sub-populations of NGC 1399 and NGC 5128 are more isotropic than M87 allows us to further constrain their formation process, as an isotropic population suggests the galaxy formed via an initial fast accretion phase and clusters with the most radial orbits have since had their orbits efficiently decay via dynamic friction (Goodman & Binney, 1984; Lee & Goodman, 1989; Cipolina & Bertin, 1994). We also find that the local galaxy environment can influence cluster populations, as dynamical interactions with nearby galaxies have likely increased the degree of radial anisotropy in the outer regions of M87 and NGC 1399 by forcing outer clusters onto radial orbits. The more isolated NGC 5128 cluster population on the hand remains isotropic at large R_{gc}. However, degeneracy between the effects of orbital anisotropy and tidally under-filling clusters on the distribution of cluster sizes in a galaxy prevent us from using our best-fit models to place strong constraints on the formation conditions and present day properties of each galaxy.

These studies provide clear examples of how advancing our understanding of clusters evolution to include the effects of a non-static tidal field has allowed for observations of globular clusters to help interpret the orbital anisotropy profile, mass profile, and formation / merger history of a galaxy. Our study illustrates that differing galaxy formation and merger histories lead to globular cluster populations having different orbital distributions and structural properties from one galaxy to the next. None of this would have been possible had we been forced to assume all globular clusters have circular orbits in spherically symmetric potentials.

7.3 Future Work

Completion of this thesis has identified many potential observational and theoretical projects that will be pursued in the future. The final application of our model to the globular cluster populations of M87, NGC 1399, and NGC 5128 has revealed improvements that can be made to our model so it can be used to study additional galaxies, which include:

- Allowing for the existence of a continuum of globular cluster sub-populations

  Many studies of globular cluster populations are identifying the possible existence of three sub-populations based on colour, spatial distribution, and kinematics (Strader et al., 2011; Blom et al., 2012). Incorporating multiple sub-populations will allow for our model to better represent the observed properties of a globular cluster population.

- Allowing for velocity dispersion to change as a function of R_{gc}

  Detailed kinematic studies of globular cluster populations are finding that mean cluster velocity and velocity dispersion changes with R_{gc} (e.g. Agnello et al., 2014), our model must incorporate this factor as well.

- Placing observational constraints on our model of how cluster evolution is related to a non-static tidal field.

  The results of our studies on how cluster structure is affected by a non-static tidal field are based on knowing the mass, three dimensional position, and three dimensional velocity of each star in a cluster. These seven parameters are necessary in order to calculate whether stars are energetically bound to a cluster or not, which is not possible observationally. To better compare to observational studies, we aim to perform simulated observations of our N-body clusters to determine how our findings are reflected in observations of globular clusters.

- Adding the results of our study on the effects of orbital inclination on cluster evolution

  Our current model only allows for the study of cluster populations in spherically symmetric potentials. Hence it cannot be applied to spiral galaxies or tri-axial elliptical galaxies. With the completion of our study on the effects of orbital inclination on cluster evolution, we can incorporate the effects of a non-spherically symmetric potential into our model.

This final point will be extremely useful as we can begin to study the globular cluster population of the Milky Way, the only population for which we have three dimensional positions and are beginning to measure proper motions. With such detailed information on the Milky Way and its cluster population, the tidal field can be kept as a free parameter and our model can be used to map the distribution of matter in the Milky Way.

Perhaps the most interesting future application of our model, other than to the Milky Way, will be to galaxies which do not show the same shallow increase in r_h with R_{gc} as the galaxies presented here. Specifically NGC 4365, where Blom et al. (2012) measures that $r_h \propto R_{gc}^{0.49\pm0.04}$, is dramatically different than M87, NGC 1399, and NGC 5128. Some dwarf galaxies, despite their relatively small globular cluster populations, have also been shown to have steeper r_h profiles (Georgiev et al., 2010). Both cases may be a result of these galaxies not being subject to repeated mergers, such that clusters with initially radial orbits have decayed and the distribution of cluster orbits is either isotropic or even tangentially biased. Such a distribution of orbits will result in a steeper r_h profile since cluster orbits do not pull them deep inside the tidal field and a lack of recent mergers means their structural properties will have had sufficient time to respond to the current tidal field which they experience. Observations of these types of galaxies that provide accurate measurements of cluster size and velocity will allow for our model to be used to study their orbital anisotropy profiles, which may even reveal a tangentially anisotropic population.

Future work in theoretical globular cluster studies will focus on the final assumption made by globular cluster studies that is not addressed in this thesis. Specifically, we wish to study the evolution of globular clusters in *time* *dependent* tidal fields. While the N-body simulations presented in this thesis have significantly advanced our understanding of the dynamical evolution of globular clusters on eccentric orbits and inclined orbits in spherically symmetric and non-symmetric tidal fields, they assume the gravitational field is smooth and constant in time. They ignore that the distribution of mass within a galaxy is built up over time via the hierarchical merger of smaller galaxies (Springel et al., 2005) and that dark matter halos consist of a collection of sub-halos as opposed to being smooth isothermal halos (Stadel et al., 2009). They also ignore the possibility that some clusters have only recently been accreted by a galaxy. It is not clear whether these effects will leave a lasting mark on globular clusters such that their complete history can be inferred from present day observations. While recent studies have begun to explore these effects through simplified models (Miholics et al., 2014; Madrid et al., 2014; Bianchini et al., 2015; Renaud & Gieles, 2015), the next major step in theoretical globular cluster studies will be the combination of N-body cluster simulations with large-scale cosmological simulations. Cosmological simulations do not have the same limitations as stellar N-body codes, as they allow galaxies to form and evolve with time, and even predict the formation sites of GCs. However, in these large-scale simulations GCs appear only as point sources and their internal structure cannot be modelled. Performing N-body simulations of clusters in cosmological simulations will yield the most realistic model of globular cluster evolution to date. Such a combination will be the first step towards being able to individually model every globular cluster within a galaxy from formation to dissolution, no matter how complex its dynamical history, and truly understand how galaxies and the stars within them form and evolve.

Bibliography

Agnello, A., Evans, N.W., Romanowsky, A.J., Brodie, J.P. 2014, MNRAS, 442, 3299

Baumgardt H., Makino J. 2003, MNRAS, 340, 227

Bianchini, P., Renaud, F., Gieles, M., Varri, A.L. 2015, MNRAS, 447, 40

Blom, C., Spitler, L. R., Forbes, D. 2012, MNRAS, 420, 37

Casetti-Dinescu, D.I., Girard, T.M., Herrera, D., van Altena, W.E., López, C.E., Castillo, D.J. 2007, AJ, 134, 195

Casetti-Dinescu, D.I., Girard, T.M., Jíková, L., van Altena, W.F., Podestá, F., López, C.E. 2013, AJ, 146, 33

Cipolina, M. & Bertin, G. 1994, AA, 288, 43

Dinescu, D.I., Girard, T.M., van Altena, W.E. 1999, AJ, 117, 1792

Georgiev, I.Y., Puzia, T.H., Hilker, M., Goudfrooij, P. 2010, MNRAS, 409, 447

Gieles M., Heggie D., Zhao H. 2011, MNRAS, 413, 2509
Clusters-Guides to Galaxies (Berlin: Springer), 323

Goodman, J. & Binney, J.J. 1984, MNRAS, 207, 511

Henon M. 1961, Annales d'Astrophysique, 24, 369
Cambridge N-body Lectures. Springer-Verlag, Berlin, p.283
Cambridge N-body Lectures. Springer-Verlag, Berlin, p.321

Kupper, A. H. W, Kroupa, P, Baumgardt, H., Heggie , D. C., 2010, MNRAS, 407, 2260

Lee, M.H. & Goodman, J. 1989, ApJ, 343, 594

Madrid, J.P., Hurley, J.R., Martig, M., 2014, ApJ, 784, 95

Miholics, M., Webb, J., Sills, A., 2014, MNRAS, 445, 2872

Renaud, F., Gieles, M., Christian, M. 2011, MNRAS, 418, 759

Renaud, F. & Gieles, M. 2015, MNRAS, accepted, arXiv:1503.04815

Springel, V., White, S.D.M., Jenkins, A., Frenk, C.S., Yoshida, N., Gao, L., Navarro, J., Thacker, R., Croton, D., Helly, J., Peacock, J.A., Cole, S., Thomas, P., Couchman, H., Evrard, A., Colberg, J., Pearce, F. 2005, Nature, 435, 7042

Stadel, J., Potter, D., Moore, B., Diemand, J., Madau, P., Zemp, M., Kuhlen, M., Quilis, V. 2009, MNRAS, 398, 21

Strader, J., Romanowsky, A.J., Brodie, J.P., Spitler, L.R., Beasley, M.A., Arnold, J.A., Tamura, N., Sharples, R.M., Arimoto, N. 2011,APJS, 197, 33